

Polymer Melts Investigated by Field Cycling NMR Relaxometry: From Simple Liquid to Reptation Dynamics

Von der Universität Bayreuth
zur Erlangung des Grades eines
Doktors der Naturwissenschaften (Dr. rer. nat.)
genehmigte Abhandlung

von
Axel Herrmann
geboren am 27.08.1982 in Coburg

Tag der Einreichung: 25.09.2012
Tag des Kolloquiums: 29.11.2012

1. Gutachter: Prof. Dr. Ernst Rößler
2. Gutachter: Prof. Dr. Franz Fujara

Contents

1 Abstract	1
2 Kurzdarstellung	3
3 Extended Abstract	7
3.1 Introduction	7
3.2 From Simple Liquid to Polymer Melt	39
3.3 Universal Dynamics for Various High- M Polymers	46
3.4 Protracted Crossover to Reptation Dynamics	49
3.5 Reorientational and Translational Dynamics in Entangled Polymer Melts	54
3.6 Linear Polymers in Solution	60
4 Publications	65
Bibliography	119
Acknowledgements	131

1 Abstract

The focus of this thesis is the investigation of linear polymer melts by applying Field Cycling Nuclear Magnetic Resonance (FC NMR) relaxometry. The objective is to understand their microscopic dynamics and its dependence on the molecular mass (M) of the polymer chains. The results are the subject of five interrelated publications; one of them is concerned also with the dynamics of polymers in solution and its modifications with respect to that observed for the bulk melts.

With the commercial availability of FC NMR relaxometers, the method gained attraction for studying dynamics of soft condensed matter due to its ability to detect both the structural or α -relaxation (identified with the segmental dynamics) and slower collective dynamics. In the case of polymer melts the latter is described most often by the Rouse model for non-entangled chains and the Doi/Edwards tube-reptation model for entangled polymers. Since 2004 a commercial relaxometer by Stellar has been operated in the Rössler group. Its capability to rapidly switch between different magnetic fields allows to measure the spin-lattice relaxation time T_1 in the proton (^1H) frequency range from 10 kHz to 20 MHz. In previous works by the Rössler group polybutadienes (PB) and some low molecular liquids have been studied and the pioneering works by Kimmich and co-workers have been extended in order to combine the results of a broad temperature range: Frequency-temperature superposition is applied to construct master curves in the susceptibility representation $\chi''(\omega) = \omega/T_1$. The key benefits are: via the scaling $\chi''(\omega\tau_s)$, where τ_s denotes the time constant of segmental dynamics, an "isofrictional" representation is achieved; the accessible frequency range is significantly increased; the time constants $\tau_s(T)$ are provided and compared with those obtained by other techniques; the regimes of glassy and polymer dynamics can be easily distinguished; finally, the dipolar correlation function is obtained directly by Fourier transform.

In this thesis by employing the above approach, the dipolar correlation function $C_{\text{DD}}(t)$ of PB melts is presented and comprises – depending on M – glassy, Rouse and entanglement dynamics. The latter two relaxation regimes can be described by different power-laws $\propto t^{-\epsilon}$, which are compared to the predictions of the tube-reptation model. A good agreement is found for the Rouse regime (I). For the constrained Rouse regime (II) at long times, a highly protracted crossover to completely established reptation dynamics is discovered. That is, the exponent ϵ depends on M and reaches $\epsilon = 0.32$ only at $M = 441000$, which is in accord with Double Quantum (DQ) ^1H NMR results ($\epsilon = 0.29$) by Saalwächter and co-workers and very close to $\epsilon = 0.25$ predicted for regime II of the tube-reptation model. This is only achieved by additional relaxation experiments in cooperation with the

Fujara group at TU Darmstadt, since their home-built FC NMR relaxometer is equipped with an active stray field compensation, which allows to reach extremely low frequencies down to 200 Hz. Consequently, the frequency range is extended by two decades toward lower frequencies with respect to the commercial spectrometer and the obtained correlation function $C_{\text{DD}}(t)$ stretches over 10 decades in time and 8 in amplitude for molecular masses up to $220 \cdot M_e$. This establishes FC ^1H NMR also at long times as competitive with DQ ^1H NMR.

Furthermore, it is shown for different systems that their separated relaxation spectra of polymer dynamics are very similar, although their overall susceptibility master curves are different. By comparing selectively deuterated PB and polyisoprene, polydimethylsiloxane, and poly(propylene glycol) it is demonstrated that the polymer relaxation strength depends on the orientation of the proton pair vector with respect to the chain contour. Moreover, the characteristic molecular masses of PB are now substantiated from analyses both in the frequency- and the time-domain, i.e., the molecular mass of the Rouse unit $M_R = 500 \text{ g/mol}$ describing the onset of Rouse dynamics, and $M_e = 2000 \text{ g/mol}$ representing the molecular mass between two entanglements.

The analyses of the dipolar correlation function $C_{\text{DD}}(t)$ render a comprehensive picture of the molecular dynamics of polymers, and the coincidence between the different polymers appears support the applicability of the tube-reptation model. However, $C_{\text{DD}}(t)$ always comprises intramolecular and intermolecular contributions and up to now the dominance of the first has been assumed implicitly. Therefore, isotopic blends of high- M protonated and deuterated PB are investigated, which allows to decompose the ^1H master curves into intramolecular and intermolecular relaxation contributions. They reflect reorientational and translational dynamics, respectively. It is demonstrated that at long times or low frequencies the intermolecular contribution dominates. Consequently, the reorientational correlation function $C_2(t)$ obtained from the intramolecular part exhibits a faster decay with the long-time exponent $\epsilon = 0.49$ than $C_{\text{DD}}(t)$. This is ascertained by the FC ^2H NMR relaxation of completely deuterated PB, which detects reorientational dynamics only. The observed exponent is significantly larger than $\epsilon = 0.25$ of regime II of the tube reptation model. Concomitantly, the segmental mean square displacement $\langle \mathbf{R}^2(t) \rangle$ is attained from the intermolecular part following an approach by Kimmich and Fatkullin. The predicted power-laws of the tube-reptation model for the Rouse and constrained Rouse regimes are identified for the first time by FC NMR: a transition between the power-laws $\propto t^{0.49}$ and $\propto t^{0.19}$ is revealed, respectively. Thus, NMR relaxometry is designated as a method comparable to neutron scattering to study subdiffusion in polymer melts. In conclusion, the power-law predictions of the tube-reptation model are disclosed by the segmental mean square displacement, yet not by the reorientational correlation function, and the relation $C_2(t) \propto [\langle \mathbf{R}^2(t) \rangle]^{-1}$ as assumed by the model is not confirmed. Thus, the simple tube-reptation model does not completely describe the microscopic dynamics of polymer melts.

2 Kurzdarstellung

Den Schwerpunkt dieser Arbeit bildet die Untersuchung linearer Polymerschmelzen mithilfe der Field Cycling Nuclear Magnetic Resonance (FC NMR) Relaxometrie. Das Ziel ist es, die mikroskopische Dynamik der Polymerketten und ihre Abhängigkeit vom Molekulargewicht (M) zu verstehen. Die Ergebnisse sind Teil von fünf inhaltlich miteinander verknüpften Veröffentlichungen, von welchen sich eine auch mit der Dynamik von Polymerlösungen und den daraus resultierenden Veränderungen bezüglich der Dynamik von Schmelzen beschäftigt.

Seit der kommerziellen Verfügbarkeit von FC-NMR-Relaxometern findet die Methode erhöhte Verbreitung zum Studium der Dynamik weicher Materie, da sie in der Lage ist, sowohl die Strukturrelaxation (α -Prozess), die mit der segmentalen Dynamik identifiziert wird, als auch die langsamere kollektive Dynamik zu detektieren. Um Letztere zu beschreiben, werden im Fall von Polymerschmelzen meistens das Rouse Modell für nicht verschlaufte Ketten und das Reptationsmodell von Doi/Edwards für verschlaufte Ketten herangezogen. Seit 2004 wird in der Arbeitsgruppe Rössler ein kommerzielles Relaxometer der Firma Stelar eingesetzt. Es zeichnet sich dadurch aus, sehr schnell zwischen verschiedenen Magnetfeldern schalten zu können, und ermöglicht es, die Spin-Gitter-Relaxationszeit T_1 für Protonen (^1H) im Frequenzbereich von 10 kHz bis 20 MHz zu messen. In früheren Arbeiten der Rössler Gruppe wurden Polybutadien (PB) und einige niedermolekulare Flüssigkeiten untersucht und der ursprüngliche Ansatz von Kimmich und Mitarbeitern wurde erweitert, um auch die Ergebnisse eines sehr breiten Temperaturbereichs mit einzuschließen: Das Frequenz-Temperatur-Superpositionsprinzip wird angewandt, um Masterkurven in der Suszeptibilitätsdarstellung $\chi''(\omega) = \omega/T_1$ zu erstellen, was folgende Vorteile mit sich bringt: Durch die Skalierung $\chi''(\omega\tau_s)$, wobei τ_s die Zeitkonstante der segmentalen Bewegung bezeichnet, wird eine "isofriktionale" Darstellung erreicht; der zugängliche Frequenzbereich wird erheblich erweitert; die erhaltenen Zeitkonstanten $\tau_s(T)$ können mit jenen anderer Methoden verglichen werden; die Bereiche der Glas- und Polymerdynamik können einfach unterschieden werden; schließlich erhält man per Fourier Transformation direkt die dipolare Korrelationsfunktion.

In dieser Arbeit werden unter Verwendung des obigen Ansatzes die dipolaren Korrelationsfunktionen $C_{\text{DD}}(t)$ von PB präsentiert, die je nach M Beiträge der Glas-, Rouse- und Entanglement-Dynamik beinhalten. Die letzten beiden Relaxationsbereiche können durch verschiedene Potenzgesetze $\propto t^{-\epsilon}$ beschrieben werden, die mit den Vorhersagen des Reptationsmodells verglichen werden. Im Rouse-Bereich (I) herrscht eine gute Übereinstimmung; im constrained Rouse-Bereich (II) wird ein stark verzögerter Übergang zu vollkommen entwickelter Reptationsdynamik ent-

deckt. Dies bedeutet, dass der Exponent ϵ von M abhängt und $\epsilon = 0.32$ erst für $M = 441000$ erreicht wird, was im Einklang mit Doppelquanten (DQ) ^1H NMR Ergebnissen ($\epsilon = 0.29$) von Saalwächter und Mitarbeitern steht und dem vom Reptationsmodell vorhergesagten $\epsilon = 0.25$ sehr nahe kommt. Erreicht wird dies durch weitere Relaxationsexperimente in Kooperation mit der Arbeitsgruppe Fujara (TU Darmstadt), deren selbstkonstruiertes FC-NMR-Relaxometer mit einer aktiven Streufeldabschirmung ausgestattet ist, wodurch extrem niedrige Frequenzen bis 200 Hz erreicht werden können. Folglich wird der Frequenzbereich um zwei Dekaden zu niedrigeren Frequenzen bezüglich des kommerziellen Spektrometers erweitert und die schließlich erhaltene Korrelationsfunktion $C_{\text{DD}}(t)$ erstreckt sich über 10 Dekaden in der Zeit und 8 in der Amplitude für Molekulargewichte bis zu $220 \cdot M_e$. Dies etabliert die FC ^1H NMR auch bei langen Zeiten als konkurrenzfähige Methode zur DQ ^1H NMR.

Außerdem wird anhand verschiedener Systeme demonstriert, dass deren abgetrennter Anteil des Relaxationsspektrums, der die Polymerdynamik darstellt, sehr ähnlich ist, obwohl sich die kompletten Masterkurven voneinander unterscheiden. Der Vergleich von teildeutertem PB und Polyisopren, Polydimethylsiloxan und Polypropylenglycol zeigt, dass die Polymerrelaxationsstärke von der Orientierung des Vektors des Protonenpaares im Bezug zur Kettenkontur abhängt. Weiterhin werden die charakteristischen Molekulargewichte von PB durch Auswertungen in der Frequenz- und Zeitdomäne bestätigt, nämlich das Molekulargewicht der Rouse-Einheit $M_R = 500$ g/mol, welches das Einsetzen der Rouse-Dynamik beschreibt, sowie $M_e = 2000$ g/mol, welches das Molekulargewicht zwischen zwei Entanglements darstellt.

Die Auswertung der dipolaren Korrelationsfunktion $C_{\text{DD}}(t)$ ergibt ein umfassendes Bild der molekularen Dynamik in Polymeren und die Übereinstimmung zwischen den verschiedenen Polymeren scheint die allgemeine Anwendbarkeit des Reptationsmodells zu bekräftigen. Allerdings enthält $C_{\text{DD}}(t)$ stets intramolekulare und intermolekulare Beiträge und bislang wurden erstere implizit als dominierend angesehen. Deshalb werden Isotopenmischungen von hochmolekularem protoniertem und deutertem PB untersucht, die es ermöglichen, die ^1H Masterkurven in intra- und intermolekulare Relaxationsbeiträge zu zerlegen. Diese spiegeln entsprechend die Reorientierungs- bzw. die Translationsdynamik wider. Es wird dargelegt, dass zu langen Zeiten bzw. niedrigen Frequenzen der intermolekulare Beitrag dominiert. In Folge besitzt die Reorientierungskorrelationsfunktion $C_2(t)$, die aus dem intramolekularem Anteil gewonnen wird, mit ihrem Langzeitexponenten $\epsilon = 0.49$ einen schnelleren Abfall als $C_{\text{DD}}(t)$. Dies wird anhand der Ergebnisse für volldeutertem PB durch FC ^2H NMR belegt, wobei nur die Reorientierungsdynamik detektiert wird. Der gefundene Exponent liegt deutlich höher als $\epsilon = 0.25$ von Bereich II des Reptationsmodells. Gleichzeitig wird das segmentale mittlere Verschiebungsquadrat $\langle \mathbf{R}^2(t) \rangle$ einem Ansatz von Kimmich und Fatkullin folgend aus dem intermolekularen Anteil gewonnen. Hierbei werden die vom Reptationsmodell geforderten Potenzgesetze für den Rouse- und constrained Rouse-Bereich erstmalig mithilfe der FC-NMR identifiziert: Ein Übergang zwis-

chen den Potenzgesetzen $\propto t^{0.49}$ bzw. $\propto t^{0.19}$ ist zu beobachten. Damit ist die NMR-Relaxometrie in der Lage, auf ähnliche Weise wie die Neutronenstreuung das subdiffusive Verhalten in Polymerschmelzen zu studieren. Somit finden sich die vom Reptationsmodell vorhergesagten Potenzgesetze zwar im segmentalen mittleren Verschiebungsquadrat, nicht jedoch in der Reorientierungskorrelationsfunktion, und die Modellannahme $C_2(t) \propto [\langle \mathbf{R}^2(t) \rangle]^{-1}$ bestätigt sich nicht. Folglich ist das einfache Reptationsmodell nicht in der Lage, vollständig die mikroskopische Dynamik von Polymerschmelzen zu erfassen.

3 Extended Abstract

3.1 Introduction

Amorphous solids are a class of materials found in a variety of forms for instance as window glasses, glasses in optical instruments, mineraloids or volcanic structures, ceramic or metallic glasses, gels, colloidal or biological systems, or polymers. One possibility to create them is supercooling a liquid below its melting temperature with a sufficiently high cooling rate while avoiding crystallization. In contrast to a crystalline solid body an amorphous solid does not have a translational symmetry; its structure is liquid-like without long-range order. Yet, in terms of its dynamics it is solid, i.e., its transport coefficients like viscosity η or diffusion coefficient D^{-1} are diverging. The phenomenon is related to the glass transition, which can be considered as a continuous, however strong slowing-down of the dynamics with decreasing temperature from a fluid liquid via a viscous liquid to a glass. This process involves dynamics on many time-scales, e.g., the time constant of molecular rotation changes from 10^{-12} s at temperatures above the melting point T_m to several seconds and longer. The temperature at which the time constant equals 100 s is defined as the glass transition temperature T_g .

Glassy Dynamics in Molecular Liquids

The theoretical understanding of the glass transition is not complete yet [1, 2], although several experimental techniques have provided information on molecular dynamics. Their time windows are depicted in Figure 3.1. In the short-time regime (or at temperatures above the melting point) neutron scattering (NS) [3–6], depolarized light scattering (LS) [7–13], and optical Kerr effect (OKE) [14–16] are the important methods, while in the supercooled range photon correlation spectroscopy (PCS) [13, 17–20], nuclear magnetic resonance (NMR) [21–27], and also dielectric spectroscopy (DS) [11, 28–35] are located. Field cycling (FC) NMR [36–38] probes dynamics on intermediate time-scales ($\omega\tau \approx 1$) and is especially suited to investigate polymer chain dynamics as will be shown below.

The experimental methods in general probe directly equilibrium fluctuations, or their effect on response functions or susceptibilities. From these conclusions regarding the molecular dynamics can be drawn. In the case of a simple liquid which contains N particles at positions \mathbf{r}_i the dynamics can be characterized by density autocorrelation functions, for instance the intermediate scattering function

$$C_\rho = N^{-1} \langle \rho^*(\mathbf{q}, t) \rho(0, t) \rangle \quad (3.1)$$

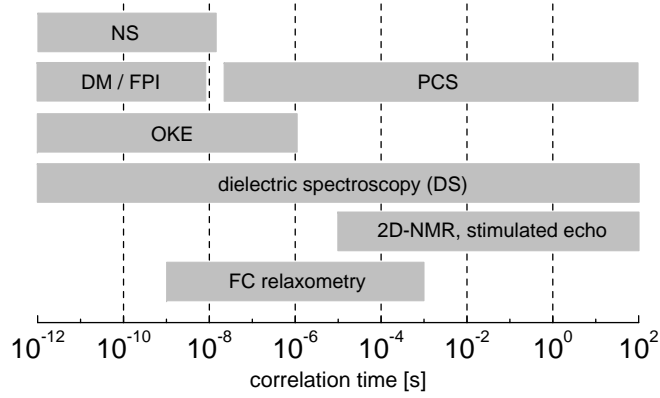


Figure 3.1: Time windows of the most important methods probing dynamics in dense molecular liquids and comparison with NMR methods: neutron scattering (NS), double monochromator/ Fabry-Perot interferometry (DM/FPI), photon correlation spectroscopy (PCS), and optical Kerr effect (OKE) (taken from [38]).

where \mathbf{q} is the scattering vector and $\rho(\mathbf{q}, t) = \sum_{i=1}^N \exp(i\mathbf{q}\mathbf{r}_i(t))$ is the density in reciprocal space. The intermediate scattering function is often examined by molecular dynamics (MD) simulations [39–41]. Its Fourier transform is known as the dynamic structure factor [42, 43] which is accessed by NS and yields information on microscopic dynamics [3, 44, 45].

A characteristic of the dynamics of molecular liquids is reorientation which is accessible by the methods mentioned above. It is described by reorientational correlation functions $g_{l,m}(t)$ of the spherical harmonics $Y_{l,m}(\vartheta, \varphi)$ of rank l [46–48]

$$g_{l,m}(t) = \langle Y_{l,m}(\vartheta(0), \varphi(0)) Y_{l,-m}(\vartheta(t), \varphi(t)) \rangle / \langle [Y_{l,m}(\vartheta(0), \varphi(0))]^2 \rangle \quad (3.2)$$

The arguments 0 and t refer to the initial and final time, respectively. In the case of vector properties, such as the molecular electric dipole moment in DS, the correlation function is of rank $l = 1$. For the tensorial molecular properties accessible, e.g., in NMR experiments rank-two correlation functions are defined. For isotropic systems the correlation functions are independent of m [36, 49]

$$g_l(t) = \langle P_l(\cos \vartheta(t)) P_l(\cos \vartheta(0)) \rangle / \langle [P_l(\cos \vartheta(0))]^2 \rangle \quad (3.3)$$

and $P_l(\cos \theta)$ is the Legendre polynomial of rank l . $g_l(t)$ is provided also by, e.g., MD simulations and is a single-particle autocorrelation function. It needs to be distinguished from a collective reorientational correlation function $C_l(t)$ [50, 51] since in most cases actually correlations of macroscopic quantities (e.g. dielectric polarization) are measured which reflect collective dynamics. Though there is no general relation between the two correlation functions, however, they are commonly assumed to be quite similar.

The Fourier transform of a correlation function provides the spectral density $J(\omega)$

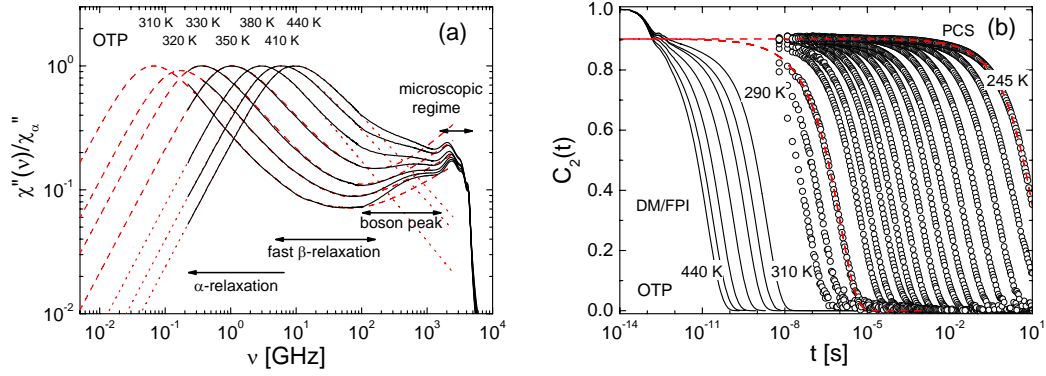


Figure 3.2: (a) Susceptibility $\chi''(\nu)$ of o-terphenyl (OTP) from depolarized light scattering (scaled on the α -peak) with relaxation regimes as indicated. Dotted and dashed lines: fit with a Cole-Davidson and a phenomenological function, respectively (adapted from [13]). (b) Correlation function $C_2(t)$ of OTP obtained from the susceptibility data of (a) by Fourier transform (solid lines). In addition, decay curves from photon correlation spectroscopy (PCS) are shown. Dashed lines: Kohlrausch fit (adapted from [13]).

(index l omitted for simplicity) or fluctuation power spectrum (Wiener-Khintchine theorem [52])

$$J(\omega) = 1/2 \int_{-\infty}^{+\infty} C(t) \exp^{-i\omega t} dt \quad (3.4)$$

It is directly obtained in, e.g., a scattering experiment or NMR relaxometry. Each spectral density or fluctuating quantity describing equilibrium fluctuations can be expressed in terms of a linear response function. This is of special interest in order to achieve a common data representation, since DS or OKE probe response functions or susceptibilities related to reorientational dynamics. The imaginary or loss part of the dynamic susceptibility $\chi''(\omega)$ is given by the fluctuation-dissipation theorem (FDT) [42, 43, 53]

$$\chi(\omega)'' = \chi_0 \frac{\omega}{k_B T} J(\omega) \quad (3.5)$$

in which χ_0 is the static susceptibility. The relation is valid in the classical limit $\hbar\omega \ll k_B T$. According to the FDT the reaction of a system to an external perturbation in the linear response regime is given by the equilibrium fluctuations, i.e., response functions are related to spontaneous, thermally driven fluctuations described by $J(\omega)$.

Typical susceptibility spectra $\chi''(\nu)$ of the glass former o-terphenyl (OTP) which were obtained by combining double monochromator- and Fabry-Perot interferometry (DM/FPI) are shown in Figure 3.2a. Within the spectral range of the technique and the temperatures applied the susceptibility exhibits features which

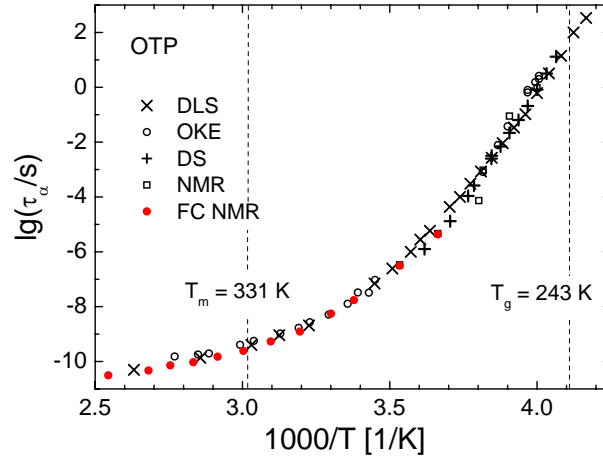


Figure 3.3: Time constants $\tau_\alpha(T^{-1})$ of molecular reorientation for OTP as revealed by different techniques. T_g and T_m denote the glass transition and the melting temperatures, respectively (adapted from [13]).

are characteristic of a glass forming liquid. At high frequencies, in the range of the boson peak and the microscopic dynamics, only weak changes with temperature are observed, while at low frequencies the spectra are strongly temperature-dependent. Here the peak reflects the main structural relaxation (α -process) and is shifted toward the boson peak while increasing temperature. The α -peak shows a non-Debye shape and can be described by a Cole-Davidson (CD) susceptibility (dotted lines) [28]. By taking into account additionally the fast β -relaxation with a power-law behavior $\propto \omega^a$ ($a > 0$), the main relaxation including the susceptibility minimum can be phenomenologically interpolated [8, 13]. Intramolecular vibrations typically detected by Raman spectroscopy are observed at frequencies above 5 THz.

Fourier transform of the DM/FPI spectra of Figure 3.2a yields the reorientational correlation function $C_2(t)$ which is displayed in Figure 3.2b at short times. At long times the data are supplemented by PCS results including temperatures down to almost $T_g = 243 \text{ K}$. While at low temperatures the two-step character of the correlation function is revealed, it almost vanishes at high temperatures. The long-time shape of $C_2(t)$ is determined by the α -relaxation and is characterized by a non-exponential decay. It can be described by a distribution of correlation times $G(\ln \tau)$ [11, 25, 28] or a stretched exponential (Kohlrausch function [54]), which is similar to the CD function used in the susceptibility representation. These features are generic for supercooled liquids and are referred to as "glassy dynamics". Note that glassy dynamics are also observed above T_m [13]. Moreover, MD simulations have disclosed very similar results for the intermediate scattering function [2, 55].

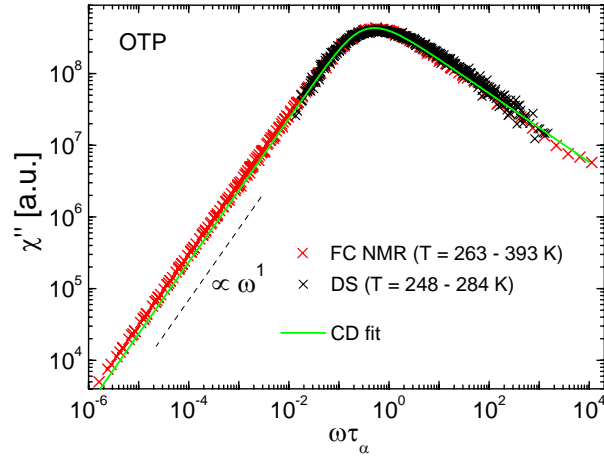


Figure 3.4: Susceptibility master curves of OTP obtained by FC NMR [56] and DS [57] in the temperature range as indicated demonstrating the applicability of frequency-temperature superposition.

The long-time decay of Figure 3.2b exhibits a uniform shape, i.e., the stretching is essentially temperature-independent and only its time constant τ_α changes. Thus, a scaling law

$$C(t)/C(0) = \hat{C}(t/\tau_\alpha) \quad (3.6)$$

or equivalently for the susceptibility

$$\chi''(\omega)/\chi''(0) = \hat{\chi}''(\omega\tau_\alpha) \quad (3.7)$$

can be introduced. As a consequence the spectra collapse in the range of the structural relaxation [13], i.e., a shift on the logarithmic time axis creates a master curve. This constitutes time-temperature or frequency-temperature superposition (FTS) and establishes an essential principle of cooperative dynamics and the analysis of the FC NMR relaxation data of viscous liquids and polymers as will be illustrated below.

Another characteristic of glassy dynamics is the super-Arrhenius temperature dependence of τ_α . Results for OTP from different techniques are compiled in Figure 3.3 as a function of the inverse temperature and are in good agreement. The correlation times stretch over more than 12 decades within a temperature interval of about 160 K. Coming from high temperatures $\lg \tau_\alpha$ increases stronger than the linear behavior predicted by the Arrhenius law. The non-Arrhenius curve is often described by the three-parameter Vogel-Fulcher-Tammann (VFT) equation [58–60]

$$\tau_\alpha = \tau_0 e^{B/(T-T_0)} \quad (3.8)$$

In Figure 3.4 master curves of the results for OTP by DS [57] and FC ^1H NMR [56] are shown to demonstrate the benefits of the representation as susceptibility

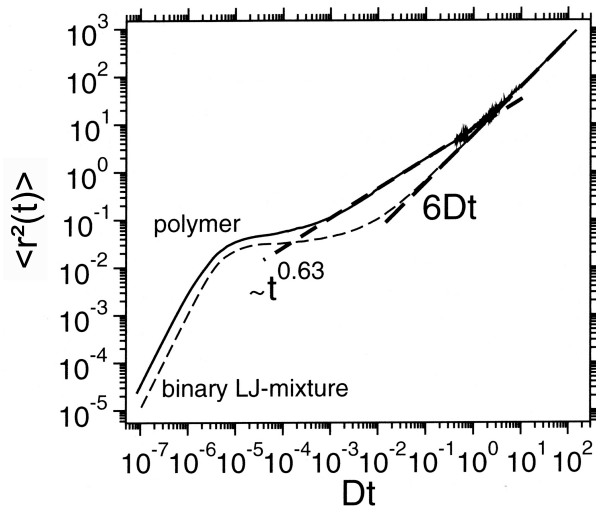


Figure 3.5: Mean square displacement $\langle r^2(t) \rangle$ of a binary Lennard-Jones (LJ) liquid (dashed line) and a polymer model (solid line) (adapted from [61]).

master curves in anticipation of a detailed explanation which follows below. The data which were measured at different temperatures are plotted as a function of the reduced frequency $\omega\tau_\alpha$ and are well described by a CD susceptibility [56]. The main structural relaxation manifests itself similarly in both methods as α -peak. Together with the agreement of the time constants τ_α (cf. Figure 3.3) this demonstrates the validity of FTS, which confirms the assumption that the spectral shape of the glassy dynamics does not change with temperature.

Some important properties of the cooperative dynamics of dense liquids are also disclosed by the time dependence of the mean square displacement $\langle r^2(t) \rangle$. Results for a binary Lennard-Jones liquid from MD simulations [62] are presented in Figure 3.5, in which three dynamical regimes can be distinguished. At short times the ballistic regime [26] with a power-law exponent 2 has been observed, where the interactions between particles are negligible and particles "fly" freely until they hit a neighboring particle. The long-time behavior is linear in time, which indicates normal diffusion. In between these two limits a plateau is present, in which the particle is confined in a cage formed by its neighbors. This "cage effect" serves as an explanation for the glass transition phenomenon.

Phenomenological Manifestation of Polymer Dynamics

First of all, an overview is provided how the dynamics of polymers manifests itself in the results of the experimental methods mentioned above, especially DS and rheology. Polymers are macromolecules which consist of several covalently bound units (monomers). There are many different kinds of topologies, compositions, and functionalities such as blends, blockcopolymers, dendrimers, polymers with functionalized side groups, micells, or nanoparticle composites in order to enhance the technically relevant properties of polymers. Their study is an attractive field for colloidal or advanced functional material research. However, the focus of this

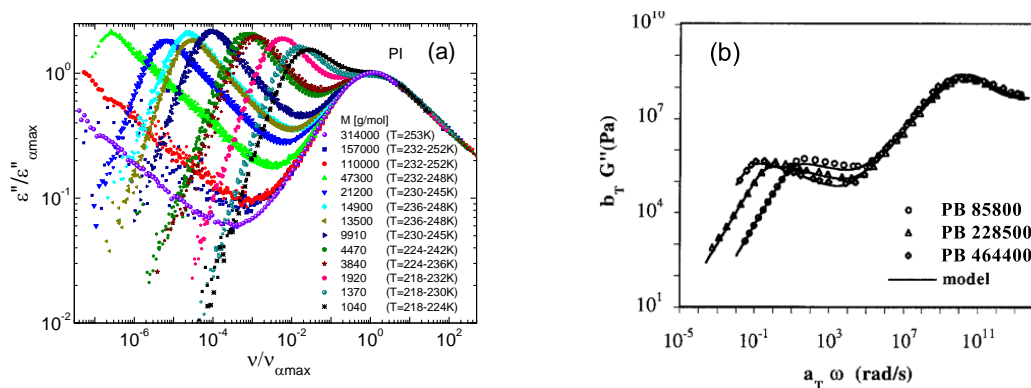


Figure 3.6: (a) Molecular weight dependence of the dielectric spectra of the different polyisoprenes investigated; dielectric permittivity ϵ'' rescaled by its α -peak height $\epsilon''_{\alpha, \max}$ displayed as a function of frequency ν rescaled by the α -peak frequency $\nu_{\alpha, \max}$ (adapted from [63]). (b) Loss modulus $G''(\omega)$ for polybutadiene (PB) of different M as obtained with a mechanical rheometer in the temperature range from 158 K to 353K (adapted from [64]).

thesis is to elucidate fundamental physical principles in melts of linear homopolymers, to which the term "polymers" refers herein.

One technique which allows to study polymer dynamics is DS. By applying an electric field to the sample, the induced polarization equals the sums of the molecular dipoles. In case of a type A polymer [65] like polyisoprene (PI) or polypropyleneglycol (PPG) a component of its monomeric dipole moment is parallel to the chain contour. This enables DS to probe in addition to the first rank correlation function $g_1(t) \propto \langle P_1(t)P_1(0) \rangle / [P_1(0)]^2$ of the segmental dynamics also a correlation function $\langle \mathbf{R}_{ee}(t)\mathbf{R}_{ee}(0) \rangle / \langle \mathbf{R}_{ee}(0)^2 \rangle$ of the end-to-end vector [30, 66]. The latter is reflected in the spectra as normal mode relaxation, which represents the M -dependent polymer dynamics. This offers an interesting possibility to study segmental and collective polymer dynamics simultaneously [63, 67]. Figure 3.6a contains spectra of PI with different M measured by DS in a wide frequency range [63]. They are scaled on the peak at high frequencies, which has been identified as the α -peak reflecting the local segmental dynamics. The peak at lower reduced frequencies represents the normal mode relaxation, i.e., polymer dynamics. It is shifted toward lower frequencies while increasing M .

In Figure 3.6b the dynamic loss modulus $G''(\omega)$ for different high- M polybutadienes (PB) obtained by rheological measurements is shown [64]. The shape of the peak at high frequencies is M -independent, while the position of the minor peak depends on M . Again the first is attributed to the glassy dynamics and the latter represents the polymer relaxation. Thus, a qualitatively similar behavior is observed as in DS, except for the fact that the weighting between the two peaks is different. Note that both in DS and rheology the presented spectra are master curves, i.e., FTS has been applied to extend the accessible frequency range.

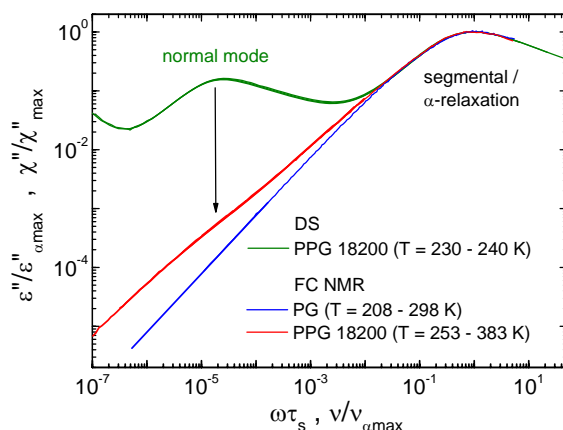


Figure 3.7: Susceptibility master curves of propylene glycol (PG) [68] obtained by FC NMR, and of poly(propylene glycol) (PPG) [69] with molecular mass $M = 18200$ compiled from FC NMR and dielectric spectroscopy (DS) in the temperature range as indicated.

In order to demonstrate the benefits of the representation as susceptibility master curves, results by DS and FC ^1H NMR are displayed as master curves in Figure 3.7 in anticipation of a detailed explanation which follows below. The main or structural relaxation (" α -peak" for simple liquids and segmental dynamics for polymers) manifests itself similarly in both methods. However, at lower frequencies specific differences are discernible. The results can be directly compared by scaling them on the amplitude and the time constant of the α -peak. Firstly, by comparing the master curves of poly(propylene glycol) (PPG) [69], a bimodal shape in case of ^1H FC NMR and a low-frequency peak ("normal-mode") in case of DS are seen. Since both features occur at low reduced frequencies, i.e., they represent dynamics slower than the (local) segmental motion, they are spectral characteristics which reflect the polymer-specific dynamics. Secondly, by comparing the NMR relaxation spectra of PPG and its monomer propylene glycol (PG) [68], an excess intensity in the first with respect to the latter is observed. Thus, this additional, low-frequency contributions in the susceptibility represent the relaxation of the polymer chains. Note that NMR relaxometry is capable to reach even lower frequencies than DS, since in the latter case dc conductivity interferes (increase at the lowest frequencies).

The applicability of FTS to the whole temperature and frequency range yields a crucial result, on which the presented analysis of NMR relaxation data relies: FTS is not only valid for the α -process alone (cf. Figure 3.4) but also for the polymer dynamics with respect to the α -process. Thus, the temperature dependence of the segmental dynamics drives that of the polymer dynamics.

Polymer Models

The tube-reptation model [70] by Doi and Edwards is most often applied to describe experimental or simulation results of the dynamics of polymer melts. It can be considered as a combination of the Rouse model [71] for non-entangled chains (with molecular mass M below the entanglement molecular mass M_e), and Doi's idea of a tube and de Gennes's reptation model [72] for $M > M_e$. It assumes a snakelike motion of a chain in a static tube which is set up by the surrounding chains and confines the dynamics of a single chain. However, on long time-scales motion along the contour and an escape from the tube is possible. This explains the transient elasticity and long-term flow. Though the tube model was originally proposed for the problem of rubber elasticity [73, 74] and can be applied to describe the dynamics of a chain in a network [72], it is also successful in explaining the properties of highly entangled polymer melts which do not form a permanent network.

In the Rouse model ($M < M_e$) a polymer chain consists of N segments ("beads") which are connected by entropic springs. The beads include a constant number of chemical bonds (or monomers) and their distribution of end-to-end distances is Gaussian. Whereas the spherical beads reflect the frictional properties due to the viscous surrounding, the entropic springs have a temperature-dependent force constant, which accounts for the polymer coil to shrink for higher temperatures. The equation of motion of the overdamped oscillator system (Langevin equation) can be solved analytically and the correlation functions of the p th Rouse normal modes $\mathbf{X}_p(t)$ can be calculated [71, 75, 76]

$$C_p(t) = \langle \mathbf{X}_p(t) \mathbf{X}_p(0) \rangle = \frac{b^2}{8N \sin^2(p\pi/2N)} \exp(-t/\tau_p); \quad p = 1, \dots, N-1 \quad (3.9)$$

where b is the effective Rouse segment length. The relaxation time of the p th mode is given by

$$\tau_p = \frac{\tau_0 \pi^2}{4 \sin^2(p\pi/2N)} \quad (3.10)$$

with $\tau_0 = b^2 \xi / (3\pi^2 k_B T)$ (ξ : friction coefficient of a bead). The relaxation time of the slowest mode ($p = 1$) is denoted as Rouse time

$$\tau_R = \tau_1 = \frac{\tau_0 \pi^2}{4 \sin^2(\pi/2N)} \quad (3.11)$$

The time constant τ_0 is referred to as the segmental time constant in polymers, i.e., $\tau_0 \approx \tau_s$. This is in turn identified with the time constant of main structural relaxation (α -process), i.e., $\tau_s \approx \tau_\alpha$, which will be explicitly demonstrated below in the context of Figure 3.21.

Eventually the quantities which are experimentally accessible can be calculated, namely for dielectric spectroscopy the permittivity [63]

$$\epsilon''(\omega) = \frac{2\Delta\epsilon_n}{N(N-1)} \sum_{p=1,3,\dots}^{N-1} \cot^2\left(\frac{p\pi}{2N}\right) \frac{\omega\tau_p}{1 + (\omega\tau_p)^2} \quad (3.12)$$

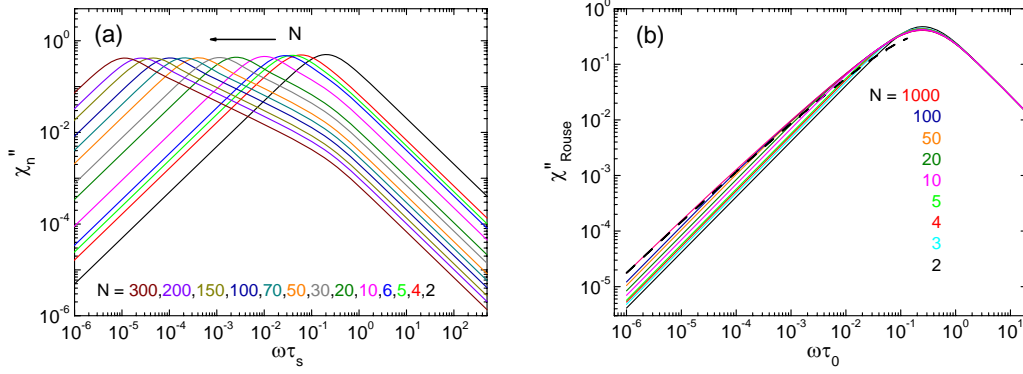


Figure 3.8: (a) Dielectric susceptibility (normal mode spectrum) calculated via the discrete Rouse model for different chain lengths N ; τ_s denotes the segmental time constant (adapted from [63]). (b) Corresponding NMR susceptibility. Dashed line: high- N limit (adapted from [77]).

and for NMR relaxation the spectral density [77]

$$J_{\text{Rouse}}(\omega) = \frac{4\tau_0}{\pi^2(N-1)^2} \sum_{p,q=1}^{N-1} \frac{\sin^2\left(\frac{p\pi}{2N}\right) + \sin^2\left(\frac{q\pi}{2N}\right)}{\frac{16}{\pi^4} \left[\sin^2\left(\frac{p\pi}{2N}\right) + \sin^2\left(\frac{q\pi}{2N}\right)\right]^2 + \omega^2\tau_0^2} \quad (3.13)$$

For the magnitude of the spectral density at $\omega = 0$ it follows

$$J_{\text{Rouse}}(0) = \frac{1}{(N-1)^2} \sum_{p,q=1}^{N-1} \frac{\tau_p\tau_q}{\tau_p + \tau_q} \quad (3.14)$$

As an illustration how the Rouse dynamics emerges with increasing chain length, Figure 3.8a shows the dielectric normal mode susceptibility $\chi''_n(\omega\tau_s) = \epsilon''(\omega\tau_s)/\Delta\epsilon_n$ (cf. eq 3.12) as calculated for different N by utilizing the discrete Rouse model [63]. With increasing N , additional low-frequency modes are accumulated, while the slowest one gives the highest intensity. A qualitatively similar picture is rendered by the normal mode spectra of Figure 3.6a. However, in the latter also effects of entanglement have to be considered for $M > M_e$.

In order to explore how polymer dynamics are probed by FC NMR relaxometry the same calculation has been performed for the spectral density J_{Rouse} (cf. eq. 3.13). In Figures 3.8b the NMR susceptibility $\chi''_{\text{Rouse}}(\omega) \propto \omega[J_{\text{Rouse}}(\omega) + 4J_{\text{Rouse}}(2\omega)]$ is presented. Analogously to the DS spectra, the increase of N provides a distribution of correlation times and additional intensity at low frequencies. However, the peak position itself is not shifted toward low frequencies, i.e., the fastest Rouse mode yields the highest intensity. This demonstrates the different weightings of the p Rouse modes for the observables of DS and NMR and is exemplified by their susceptibility for $N = 6$ in Figure 3.9 part a and b, respectively. Therein the single modes for $p = 1, \dots, 5$ calculated from eq. 3.12 and 3.13 and their sum are

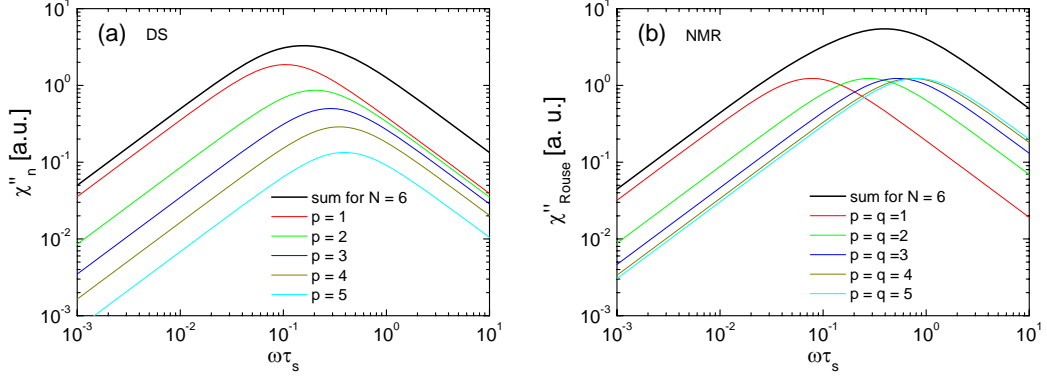


Figure 3.9: (a) Dielectric normal mode and (b) NMR susceptibility calculated via the discrete Rouse model for $N = 6$ (black line), which are composed by the sum of the individual modes with $p = 1, \dots, 5$ and $p, q = 1, \dots, 5$ (colored lines), respectively; τ_s denotes the segmental time constant.

displayed (for NMR only the modes $p = q$ are plotted for simplicity). Regarding DS, the cotangent in eq. 3.12 provides the p -dependent weighting which gives the highest amplitude for $p/N \ll 1$, i.e., $p = 1$ dominates the sum. In case of the NMR susceptibility the modes bear an equal amplitude and the maximum of the sum stems from the mode distribution in time, which is denser for the high modes. Thus, in DS the end-to-end relaxation according to the Rouse model is dominated by the slowest mode $p = 1$, and for NMR relaxometry the Rouse spectrum is governed by the fastest mode $p = N - 1$.

For long chains ($N \gg 1$) the trigonometric functions in eq. 3.9 - 3.13 are usually approximated by the first term of their series expansion ("continuous Rouse model") [66, 70]. This leads to expressions for the dielectric normal mode susceptibility [63, 66, 78], the NMR susceptibility [77], and the dynamic shear modulus [70, 79, 80]

$$\text{DS: } \chi_n''(\omega) = \frac{2}{N^2} \sum_{p=1,3,\dots}^N \cot^2\left(\frac{p\pi}{2N}\right) \frac{\omega\tau_R/p^2}{1 + (\omega\tau_R/p^2)^2} \quad (3.15)$$

$$\text{FC NMR: } \chi_{\text{Rouse}}''(\omega) = \sum_{p,q=1}^N \frac{\omega\tau_R/(p^2 + q^2)}{1 + (\omega\tau_R/(p^2 + q^2))^2} \quad (3.16)$$

$$\text{rheology: } G_{\text{Rouse}}''(\omega) \propto \sum_{p=1}^N \frac{\omega\tau_R/p^2}{1 + (\omega\tau_R/p^2)^2} \quad (3.17)$$

For the latter quantity the Rouse spectrum is similar to that of FC NMR (cf. Figure 3.9b). This can be anticipated also from the rheological results of Figure 3.6b in which the low-frequency wing of the α -peak reflects the contribution of Rouse dynamics.

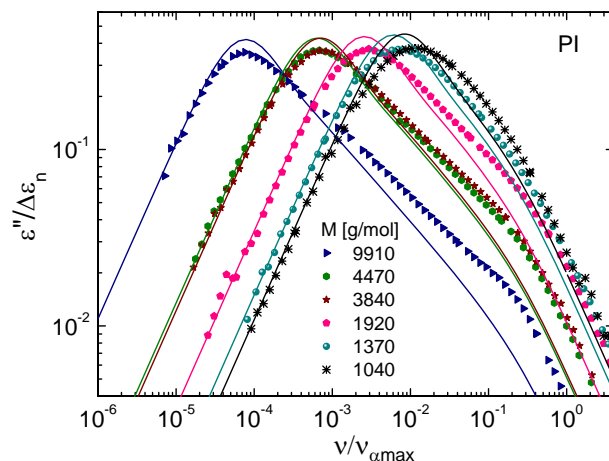


Figure 3.10: Normalized normal mode spectra for non-entangled PI ($M < 9910$) obtained from the spectra of Figure 3.6a. Lines: predictions by the Rouse theory (adapted from [63]).

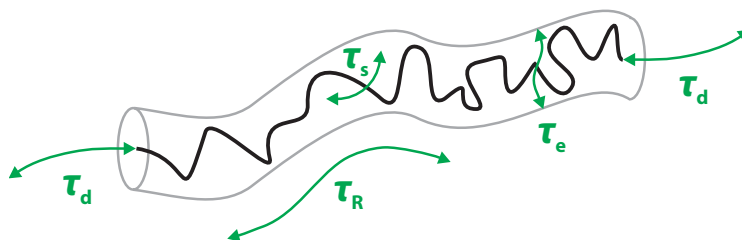


Figure 3.11: Sketch of a polymer chain in a virtual tube with the characteristic time constants of the regimes of the tube-reptation model (see text).

A direct comparison between experimental and calculated normal mode spectra is performed in Figure 3.10 for $M < M_e$ [63]. The first were attained by subtraction of the α -relaxation from the overall spectra of Figure 3.6a, while the latter were calculated from the discrete Rouse model for a corresponding number of monomers N . Both the experimental and theoretical spectra have been normalized to the same integral $\pi/2$, i.e., experiment and theory are compared on absolute scale. Though the spectral features are captured by the Rouse model, systematic deviations are recognized. The experimental normal mode spectra are broader than predicted as it is known from previous studies [67, 81]. Note that concerning the approach for decomposition, cross-relaxation terms have been assumed to be negligible.

The essentials of the tube-reptation model are illustrated in Figure 3.11 which displays a single chain within its virtual tube. For very short times the chain

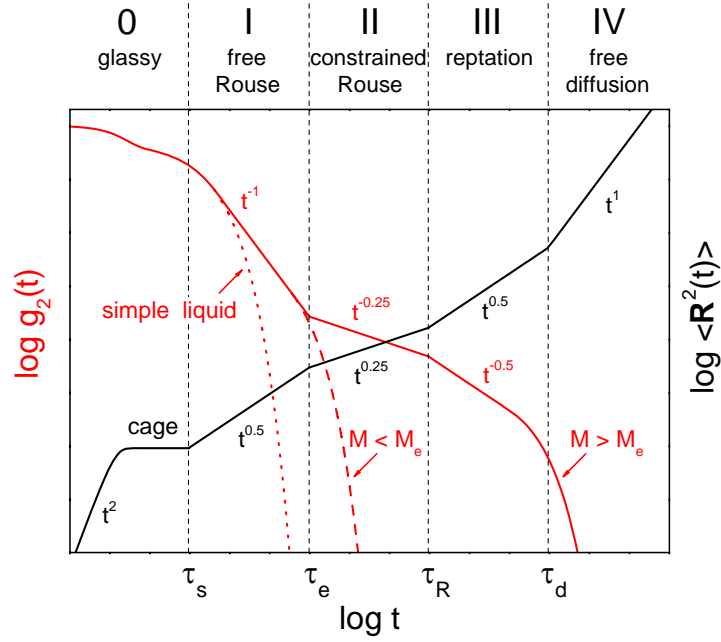


Figure 3.12: Schematic time dependence of the logarithm of the segmental reorientational correlation function $g_2(t)$ (red line) and mean square displacement $\langle \mathbf{R}^2(t) \rangle$ (black line) as a function of logarithm of time as expected from the Rouse model (non-entangled polymers, $M < M_e$) and Doi–Edwards tube–reptation model (entangled polymers, $M > M_e$) (adapted from [38]).

segments are not yet exposed to constraints of the tube. Here the segmental mean square displacement $\langle \mathbf{R}^2(t) \rangle$ as predicted by the tube-reptation model, which is displayed for an entangled polymer melt ($M > M_e$) in Figure 3.12, shows a ballistic behavior and then exhibits a plateau. This indicates the cage effect and is typical of glassy dynamics (regime 0). On the time-scales of the segmental correlation time τ_s the segments reorient and if the displacements are much smaller than the tube diameter, the chain behaves as a free Rouse chain for times on the order of the entanglement time τ_e (free Rouse dynamics, regime I). For $t \leq \tau_R$ the influence of the tube becomes effective and restricts the Rouse dynamics perpendicular to the primitive path around which the tube is constructed (constrained Rouse dynamics, regime II). Since Figure 3.11 provides a just snapshot, the primitive path can be obtained by time-averaging these motions and yields the mean positions of the chain segments, i.e., it represents a connection of the chain ends and allows for the topological constraints of the entanglements [53, 82]. For longer times the chain effectively moves along the primitive path, i.e., it performs a one-dimensional reptation-like motion in the tube taking into account that the polymer chains cannot cross each other (reptation dynamics, regime III). For the regimes of polymer dynamics (I - III) characteristic power-laws are predicted for $\langle \mathbf{R}^2(t) \rangle$ as indicated in Figure 3.12. Finally, beyond the tube disengagement time τ_d the chain leaves

the original tube and forms a new one, which leads to the free diffusion behavior $\langle \mathbf{R}^2(t) \rangle \propto t^1$ (regime IV). The characteristic times scale with the time constant of segmental motion τ_s and the number of monomers N : $\tau_e \propto \tau_s N_e^2$ (N_e : number of monomers between entanglements), $\tau_R \propto \tau_s N^2$, and $\tau_d \propto \tau_s N^3$ [70].

The reorientational correlation function $g_2(t)$ is also depicted in Figure 3.12 for a simple liquid, a non-entangled polymer melt ($M < M_e$), and an entangled melt. In regime 0 the decay at shortest times is due to fast relaxation processes and not relevant for polymer dynamics. The non-exponential decay at $t \approx \tau_s$ characterizes glassy dynamics which is a common relaxation feature in simple liquids and polymers. Note that two-step character of the correlation function (cf. also Figure 3.2b) and the plateau of $\langle \mathbf{R}^2(t) \rangle$ (cf. also Figure 3.5) appear in the same time range are due to the cage effect. For the high- M limit ($M \gg M_e$) $g_2(t)$ decays with corresponding power-laws $\propto t^{-\epsilon}$ in regimes II and III as $\langle \mathbf{R}^2(t) \rangle \propto t^\alpha$. The long-time decay in regime IV is essentially exponential [83].

The power-law exponents ϵ of $g_2(t)$ are related to those of $\langle \mathbf{R}^2(t) \rangle$. In regime I for the correlation functions of rank $l = 2, 1$ $g_2(t) = [g_1(t)]^2$ and the relation $g_2(t) \propto 1/\langle \mathbf{R}^2(t) \rangle$ hold; thus, $\epsilon = 2\alpha = 1$. In regimes II and III $g_l(t) \propto 1/\langle \mathbf{R}^2(t) \rangle$ is independent of the rank l and therefore $\epsilon = \alpha$. For deriving this relation it is assumed that within the time t the chain segment is still located in or has returned to same tube section as it was at the time $t = 0$ ("return-to-origin probability") provided that the original tube survives [47, 83].

However, deviations from the behavior predicted by the tube-reptation model have been observed, e.g., the molecular mass dependence for $M > M_e$ of the steady-state viscosity exhibits an exponent 3.4 instead of 3.0. Thus, refinements of the tube-reptation model were needed which incorporate more sophisticated topological interactions and are subject of ongoing debates [3, 40, 78, 82, 84, 85]. For example, effects of constraint release can be considered, i.e., that surrounding chains reptate by themselves and form a nonstatic tube (or matrix) [86, 87]. Also contour length fluctuations (CLF) can be taken into account, which are due to motions of the chain ends and concomitant shrinking and expanding of the chain inside of the tube [70, 88, 89]. Both mechanisms lead to a reduction of the life time of the tube and thus to a faster decay in terms of a reorientational correlation. Moreover, it is discussed especially in the simulation community whether the concept of a "continuous" tube is suitable to describe the topological constraints of "discrete" entanglements or whether a slip-spring model is more appropriate which introduces the confinements by entanglement through virtual springs loosely attached to the chains [90, 91]. Note that Graessley conjectured that that pure reptation behavior might be revealed for very high M [79], which has later been confirmed experimentally [63, 92].

Another model describing the dynamics of entangled polymer melts is the n -renormalized Rouse model, which has been introduced by Schweizer [93–95]. Its mathematical properties are very similar to the original Rouse model [71, 96], however, in order to take entanglement effects into account the relaxation times of the normal modes are modified and depend also on the entanglement molecu-

lar mass. The model has been applied by Kimmich, Fatkullin, and co-workers to explain their NMR relaxation results of the spin-lattice relaxation dispersion [47, 96, 97]. Transformed to the correlation function $g_2(t)$, two power-laws are predicted: $g_2(t) \propto (t/\tau_s)^{-0.5}$ for $\tau_s \leq t$ ("high-mode number limit") and $g_2(t) \propto (t/\tau_s)^{-0.8}$ for $\tau_e \leq t$ ("low-mode number limit", see also [47] and Pub. 1). Since these power-law exponents are different to those of the tube-reptation model (cf. Figure 3.12), the works by Kimmich and co-workers have cast doubt on the applicability of the tube-reptation model to describe the NMR relaxation results of polymer melts, which will be clarified in this thesis.

Experimental Evidence for Polymer Dynamics

The dynamics of polymers can be studied by various techniques, such as dielectric spectroscopy [30, 66, 78], neutron scattering [3, 98], and several NMR experiments [36, 99–103]. Since this thesis concentrates on field cycling NMR relaxometry [36] and aims at representing the results in a way that they can be compared [38] to those of other methods, the results of the latter and of simulations are briefly reviewed.

In Figure 3.13a results for the time dependence of the mean square displacement $g_1(t/\tau)$ as obtained by MD simulations [104] are displayed for different chain lengths N while $N_e \approx 35$. At short times all curves follow a common power-law $\propto t^{0.5}$ as predicted for the free Rouse regime (I). Above $N = 50$ and at $t > \tau_e \approx 1700$ deviations from the Rouse behavior are seen and with increasing N a power-law $\propto t^{0.25}$ clearly emerges, which is expected for the constrained Rouse regime (II) of the tube-reptation model. Note that only the five innermost monomers have been analyzed since at the chain ends fluctuations are expected due to, e.g., CLF [104, 107, 108]. However, Monte Carlo simulations [109] have revealed that the crossover to reptation dynamics is very protracted, i.e., even for $M \approx 14M_e$ the power-law of regime II of the tube-reptation model is not clearly seen. Furthermore, MD simulations [41, 61, 110] have demonstrated that for a simple liquid and a polymer the glassy dynamics (regime 0) are reflected in $\langle \mathbf{R}^2(t) \rangle$ in the same way. Yet, in the case of the polymer system, $\langle \mathbf{R}^2(t) \rangle$ exhibits between the plateau due to the cage effect and the free diffusion limit a characteristic power-law regime, which is attributed to Rouse dynamics (cf. Figure 3.5 and [61]).

Figure 3.13b presents the mean square displacement of a Neutron Spin Echo (NSE) study [98] for a polyethylene melt with $M = 190000$. NSE probes the segmental mean square displacement averaged over all monomers via the incoherent structure factor assuming a Gaussian distribution of the displacements. The time range of NSE is about 0.01 – 300 ns. At $T = 509$ K a crossover between the power-laws of regimes I and II is observed. Note that due to the high M of the samples influences of CLF have been treated as negligible. Yet, further NSE results [108] of polyethylene have revealed the relaxation contribution of CLF for intermediate M .

In Figure 3.13c the mean square displacement $\langle Z^2(t) \rangle$ of polystyrene with different

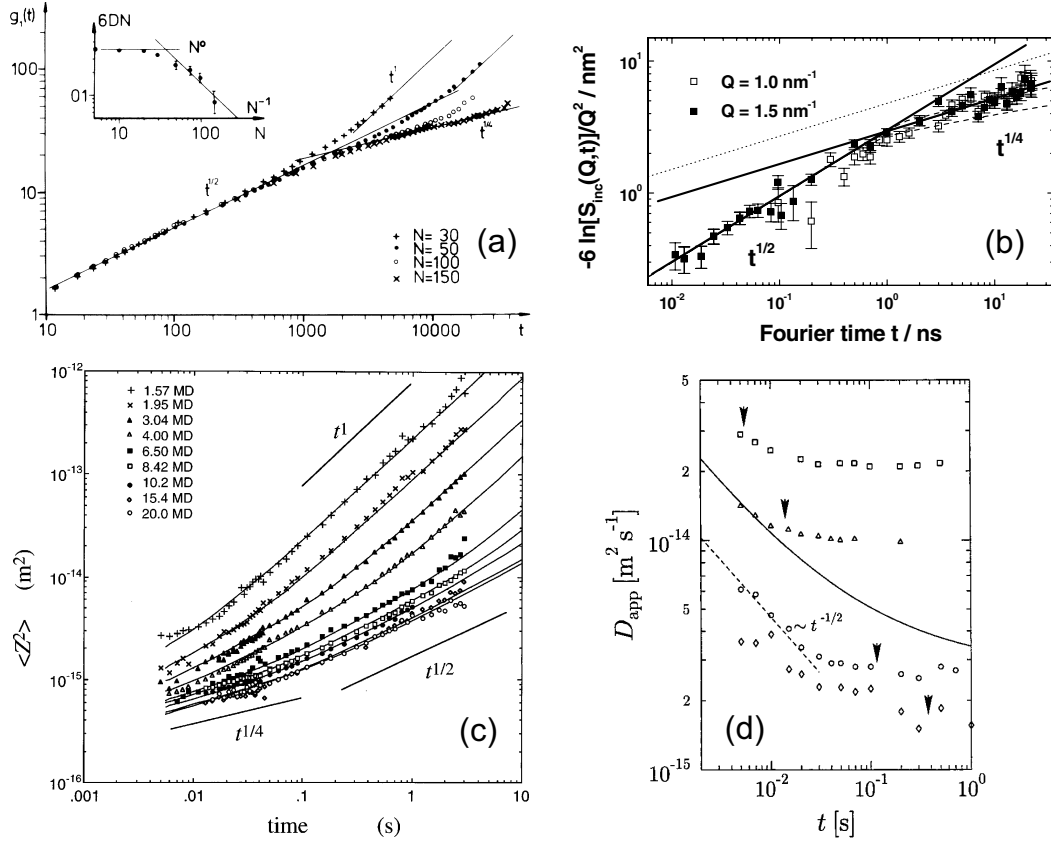


Figure 3.13: Time dependence of the mean square displacement obtained (a) by MD simulations (adapted from [104]), (b) by Neutron Spin Echo at $T = 509$ K for a polyethylene melt ($M = 190000$) (adapted from [98]), and (c) by Pulsed Gradient NMR for solutions of polystyrene with different M (as indicated in MD = 10^6 g/mol) and toluene (adapted from [105]). (d) Time-dependent self-diffusion coefficients $D_{\text{app}}(t)$ in polydimethylsiloxane melts ($M = 118000 - 716000$) measured by Field Gradient NMR; arrows indicate terminal relaxation time (adapted from [106])

M in solution investigated by Field Gradient NMR [105] is shown. By performing a spin echo experiment in a magnetic field gradient the position of the nuclear spin is encoded by the Larmor frequency. Thus, the refocused magnetization provides information about irreversible dynamical processes such as diffusion. Since the time window ranges from about 5 ms to a few seconds, semidilute polymer solutions have been measured in order to fit the dynamics into the given window. Though it has been discussed [84, 105] whether a tube model may be applied under such conditions, the mean square displacement exhibits the familiar power-law exponents of the different regimes of the tube-reptation model depending on M . For the lowest M studied the diffusive regime (IV) is observed. While increasing M at a constant temperature ($T = 290$ K) the faster dynamics are continuously shifted into the time window disclosing the regimes II and III.

In a very similar way the time dependence of the self- or the center of mass diffusion coefficient $D \propto t^{\alpha-1}$ is probed. Figure 3.13d presents the results for polydimethylsiloxane melts of different M at $T = 305$ K [106]. The time-independent D at long times indicates that normal diffusion behavior is observed for the lowest M studied. At shorter times or higher M the power law $\propto t^{-0.5}$ expected for regime III is found. Thus, coming from long times by applying NMR diffusometry the crossover from regime IV to III is explored.

To elucidate polymer dynamics several other NMR methods have been applied. ^{13}C NMR studies have found for entangled atactic polypropylene [111] and polyethylene [112] different regimes in the orientational correlation function, which also depend on M . Results for transverse relaxation have been reported for poly(ethylene oxide) [113] and deuterated polybutadiene [114], which also exhibit distinguishable Rouse and entanglement dynamics. From a combination of transverse and spin-lattice proton relaxation of polyisoprene [115] correlation functions have been constructed, which confirm the power-laws predicted by the tube-reptation model. Finally, emphasis is put on the capability of double quantum (DQ) ^1H NMR [116, 117] to directly access the correlation function in the time domain, which will be discussed in section 3.4 and Pub. 4.

In conclusion, it has been demonstrated that the short-time behavior of simple liquids is also found in polymers (regime 0). The polymer-specific dynamics show up at frequencies lower than that of the structural relaxation. Furthermore, it is a challenge to encompass the complete range of dynamics for high- M polymer melts both by experiments and simulations, and the various techniques provide data on very different and sometimes complementary time scales. In order to compare them, a uniform representation is necessary which allows also the application of FTS. This can be achieved by the susceptibility master curves, which are well suited to draw conclusions regarding the microscopic dynamics of polymers from NMR relaxation results. Technical aspects concerning the measurement of the dispersion of the spin-lattice relaxation time and the data representation in terms of susceptibility master curves are explained in the following sections. The aim is to access by FC NMR both the reorientational correlation function $g_2(t)$ and the mean square displacement $\langle \mathbf{R}^2(t) \rangle$ for polymer melts covering a wide time range.

Field Cycling NMR Relaxometry

The basic idea of FC NMR is to measure how the nuclear magnetization evolves in time toward its equilibrium in the presence of different magnetic fields B_0 . The range of B_0 is on the one hand broader and on the other hand lower than that accessible by conventional cryomagnets with static fields. Spin-lattice relaxation experiments are performed either with a mechanic or an electronic FC spectrometer [48, 118]. In the first case the sample is moved between different magnetic fields ("sample shuttle technique") which results on the one hand in a high spectral resolution and on the one other hand in transfer times on the order of 1 s [119–124]. Regarding the second method the pioneering work was done by

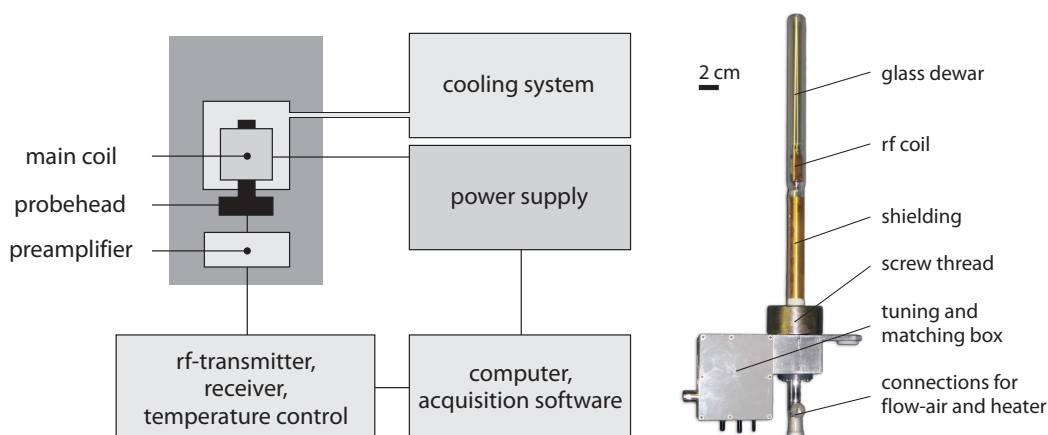


Figure 3.14: Left: schematic setup of a field cycling NMR spectrometer. Right: photo of the standard probehead by Stelar (adapted from [134]).

F. Noack [48] and R. Kimmich [36, 125]. The spectrometer is equipped with an electromagnet which allows switching electronically between different fields quite fast (≈ 1 ms, "fast field cycling") [126–130]. This capability is an advantage if the relaxation times become short, as it can be the case in viscous liquids or polymers. The latter type was used to acquire the results for this work, a commercial one in Bayreuth (Stelar Spinmaster FFC 2000 1T) [36, 37, 131] and a home-built one in Darmstadt (FC-I) [132, 133].

The most important components of an electronic FC NMR spectrometer are shown schematically in the left part of Figure 3.14. The central part is the main coil which generates the magnetic field B_0 . It is connected to bipolar MOSFET banks as computer controlled power supply and is surrounded by a refrigerant (Solvay Galden[®]) which is pumped to a heat exchanger with the lab's water cooling circuit. The standard commercial probehead (right part of Figure 3.14) with a saddle coil design for the rf-pulses can be inserted into the magnet bore from bottom, while samples can be easily changed from top. A dewar and a temperature control unit allow measurements in the temperature range from 160 K to 410 K by connecting a liquid nitrogen evaporator or heated dry air, respectively. The temperature is set with the help of a thermo sensor placed in a dummy test tube at the sample position. The accuracy of temperature measurements was better than ± 1 K, and temperature stability was better than ± 0.3 K. All relevant parameters can be set with a software provided by Stelar, which is also used for acquisition and evaluation of the data and controls the spectrometer unit (for details see [135]).

In order to measure the dispersion of the spin-lattice relaxation time $T_1(\omega)$ several cycles of polarization, relaxation, and acquisition are run as schematically depicted in Figure 3.15. The sample is polarized at high field, until an equilibrium magnetization is established. Switching to a desired different field causes relaxation and the magnetization decays toward a new equilibrium. Then after a certain time τ

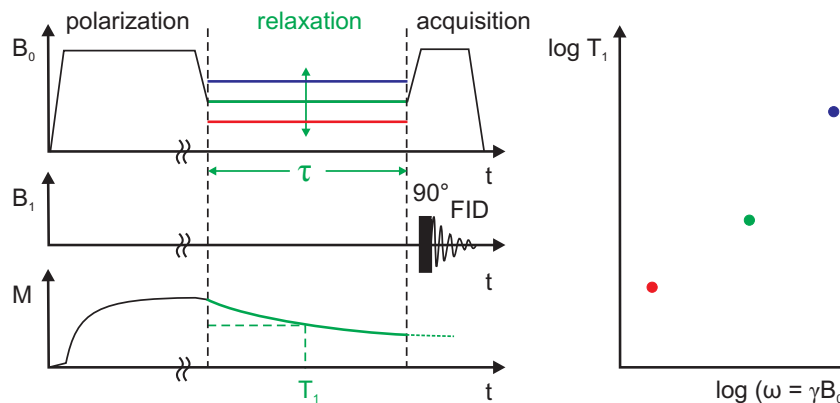


Figure 3.15: Left: schematic cycle of the magnetic fields B_0 and B_1 and the magnetization M for polarization, relaxation, and acquisition. Right: resulting spin-lattice relaxation time T_1 as a function of the Larmor frequency $\omega = \gamma B_0$.

the free induction decay (FID) is acquired at high field (signal $\propto \omega^2$) with a 90° radio frequency pulse. A magnetization curve $M(\tau)$ is measured by varying τ . In most cases the decay observed for ^1H relaxation is an exponential with the spin-lattice relaxation time T_1 as time constant. To obtain the frequency dependence $T_1(\omega)$, i.e., the dependence on the Larmor frequency $\omega = \gamma B_0$ (γ : gyromagnetic ratio of the nucleus), the magnetic field B_0 for the relaxation is changed. To obtain T_1 at lower relaxation fields (below 9 MHz in case of the Stellar relaxometer) the sample is measured without previous polarization, i.e., the build-up of magnetization $M(\tau)$ is observed.

With the commercial spectrometer $T_1(\omega)$ can be measured in the range from $\nu = \omega/(2\pi) = 10$ kHz to 20 MHz. The upper limitation is due to the capability of the cooling system to keep the temperature at the magnet constant also if relaxation times are longer than 1 s. Toward low frequencies the range is restricted by the switching time, if T_1 becomes very short, and magnetic stray fields. The switching time can be considered as a delay time until the relaxation field is stabilized (3 ms for the Stellar instrument) and is effectively a cut-off of the initial values of the magnetization curve. Stray fields stem from the earth field and in the present case from high-field magnets in the lab. By compensating them, the frequency range can be extended toward $\nu \ll 1$ kHz, which was realized with the home-built relaxometer in Darmstadt (for details see Section 3.4). Further developments regarding reaching lower frequencies are under way [136, 137].

In the case of ^1H NMR with like spins, relaxation is due to fluctuations of the homonuclear dipolar (DD) coupling between the spins of hydrogen nuclei [36, 46, 138]. Since they might be situated on the same or different molecules, the measured ^1H relaxation rate $R_1(\omega) = 1/T_1(\omega)$ comprises intramolecular and intermolecular relaxation contributions, $R_{1,\text{intra}}(\omega)$ and $R_{1,\text{inter}}(\omega)$, respectively. For each contribution a linear combination of spectral densities J is probed [139, 140].

It is a consequence of second order perturbation theory (Redfield relaxation theory [141]) and a well known result by Bloembergen, Purcell, and Pound (BPP equation) [46, 138]:

$$R_1(\omega) = K \cdot [J(\omega) + 4J(2\omega)] \quad (3.18)$$

where K is the NMR coupling constant which fulfills the condition

$$K \leq K_{\text{rigid}} = \frac{3}{10} \sum_i \left(\frac{\mu_0 \gamma^2 \hbar}{4\pi r_i^3} \right) \quad (3.19)$$

The summation includes all neighboring nuclei of the molecule and r_i refers to their distance. The limitations of the Redfield relaxation theory are discussed in more detail in Section 3.4 and [38], where extremely low frequencies are attained and the correlation times, which characterize the motion leading to relaxation, approach the relaxation times. The weighted superposition of two spectral densities at ω and 2ω is barely distinguishable from the individual spectral densities. Therefore, for a broad relaxation dispersion displayed on logarithmic scales, the relaxation rate and the spectral density are used equivalently. In summary, by measuring the dispersion of the relaxation rate, FC NMR relaxometry probes a spectral density reflecting equilibrium fluctuations, and by Fourier transform the dipolar correlation function is accessible (eq. 3.4).

Assuming the statistical independence of intramolecular and intermolecular contributions, the overall rate can be decomposed along $R_1(\omega) = R_{1,\text{intra}}(\omega) + R_{1,\text{inter}}(\omega)$ [46]. However, because of the short-range nature of the DD interaction, the main contribution is expected to stem from the nearest proton pairs belonging to the same molecular units. Consequently, it is argued that $R_1(\omega)$ is dominated by the intramolecular relaxation, i.e., segmental reorientation, and that the intermolecular coupling is relatively unimportant [36, 38, 47]. However, Kehr et al. have shown that the intermolecular contribution must not be ignored at low frequencies [142, 143].

This can be demonstrated in an isotopic dilution experiment in which blends of protonated and deuterated molecules are investigated. With increasing dilution the intermolecular contribution is reduced and the intramolecular part can be extracted. Since the intramolecular and intermolecular contributions reflect reorientational and translational dynamics, respectively, this offers a possibility to explore both motional processes in viscous liquids and polymers by NMR relaxometry. Thereby access is gained to the corresponding correlation functions (cf. eq. 3.4), especially the reorientational correlation function $g_2(t)$. Moreover, from the intermolecular part the segmental mean square displacement $\langle \mathbf{R}^2(t) \rangle$ can be attained through an approach by Fatkullin [142]. Applying also ^2H FC NMR provides the ^2H relaxation rate $R_{1,\text{Q}}(\omega)$. In this case, the relaxation is solely due to the rotational fluctuations of the quadrupolar coupling which in organic molecules like polymers is caused by the reorientational dynamics of the C- ^2H bond. Thus, directly probing segmental reorientation allows of an independent verification of the decomposed intramolecular contribution obtained by ^1H relaxation. This is

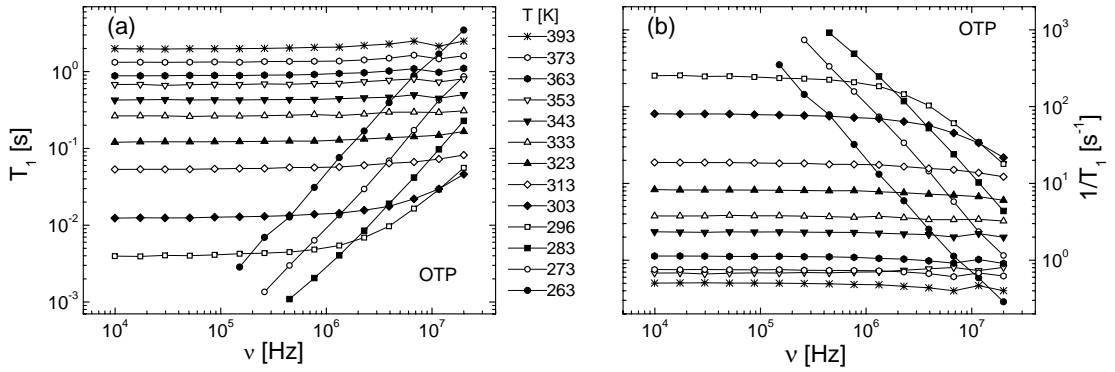


Figure 3.16: (a) Spin-lattice relaxation time T_1 of o-terphenyl (OTP) as a function of the frequency ν . Lines: guides to the eye. (adapted from [56]). (b) Relaxation rates $1/T_1(\nu)$ of the data of (a). Symbols are used correspondingly. Lines: guides to the eye.

the ultimate goal of this thesis and is examined and discussed in more detail in Section 3.5 and Pub. 4. Note that in Pub. 3 - 5 the index "DD" refers to the measured ^1H quantity in order to distinguish it from the quadrupolar and the separated intramolecular and intermolecular quantities. However, for simplicity in the following and in Pub. 1 and 2, in which no decomposition was pursued, the index will be omitted.

Figure 3.16a shows the $T_1(\nu)$ results for the glass former OTP measured in the temperature range from $T = 393$ K down to 263 K, i.e., the liquid can be super-cooled and becomes increasingly viscous. Whereas no dispersion is observed at high temperatures, at low temperatures a strong increase of T_1 with the frequency can be seen. For a given frequency the relaxation time passes through a minimum while decreasing temperature (see below). The same data are presented as relaxation rates $1/T_1(\nu)$ or spectral densities in Figure 3.16b. As expected the spectral density gets broader toward high temperatures, i.e., the correlation time τ is getting shorter. This can also be noticed at the lowest frequency, since $J(\omega = 0) = \tau$ and thus $R_1(\omega = 0) \propto \tau$ holds (cf. eq. 3.4).

The temperature dependence of T_1 at some Larmor frequencies ν is displayed in Figure 3.17 for OTP. At high temperatures T_1 is frequency-independent, whereas it exhibits a frequency-dependent minimum while cooling. These are characteristic features of the structural relaxation of the liquid being shifted from the extreme narrowing to the slow motion regime. In addition the relaxation times $T_1(T)$ for a high- M polybutadiene melt are included. While the single curves exhibit a trend similar to those of OTP, there are also clear differences: First, the minima of PB are located at lower temperatures, which is due the difference of the glass transition temperature T_g ($T_g = 243$ K for OTP and 174 K for PB 87500 [77]). Second, for the high- M polymer the extreme narrowing is not reached anymore,

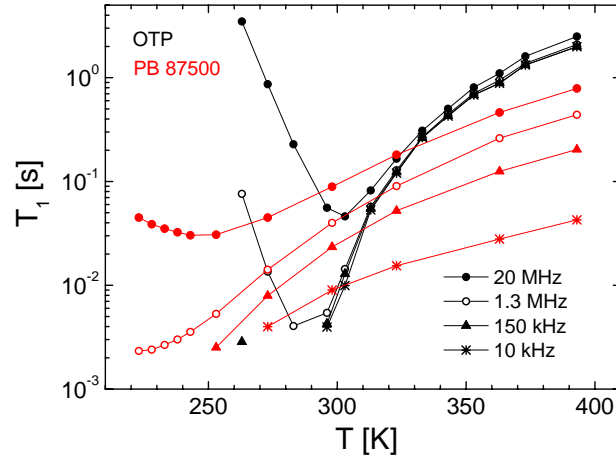


Figure 3.17: Spin-lattice relaxation time T_1 of *o*-terphenyl (OTP, black) and polybutadiene with high molecular mass $M = 87500$ (PB 87500, red) as a function of the temperature T for some Larmor frequencies ν . Lines: guides to the eye.

since the frequency-dependent polymer relaxation processes are detected on the high-temperatures wing with respect to the minimum.

Data Representation

Since polymer dynamics stretch over many decades in time or frequency [38, 47] (cf. also Figures 3.12 and 3.6), our studies aim at exploiting the dynamic range of the technique as far as possible. Besides extending the frequency range of FC NMR to about 5 decades by employing an active stray field compensation (Section 3.4), frequency-temperature superposition (FTS) is applied in order to combine the relaxation data measured in a very broad temperature range. FTS assumes that the relaxation of different applied temperatures can be shifted through the FC NMR frequency window without alteration of its spectral shape. This holds especially for the susceptibility $\chi''(\omega)$ as shown in Figure 3.2 and by eq. 3.7. The relaxation rates $1/T_1(\nu)$ (cf. eq. 3.18) are transformed to the susceptibility representation

$$\chi''(\omega) = \omega/T_1(\omega) \quad (3.20)$$

and susceptibility master curves are created by plotting χ'' as a function of the reduced frequency $\omega\tau_s$ (τ_s : time constant of segmental motion). The approach is well known from, e.g., rheology (cf. Figure 3.6b) and reflects a fundamental feature of cooperative dynamics [38]. The susceptibility representation of NMR relaxation data has also been applied by Cohen-Addad and co-workers [144, 145]. The procedure of constructing master curves is illustrated exemplarily for 1,4-polybutadiene (PB) with molecular mass $M = 87500$ g/mol for which the rates and corresponding susceptibilities are displayed in Figure 3.18a and b, respectively. A susceptibility master curve $\chi''(\omega a_T)$ (solid red line) can easily be cre-

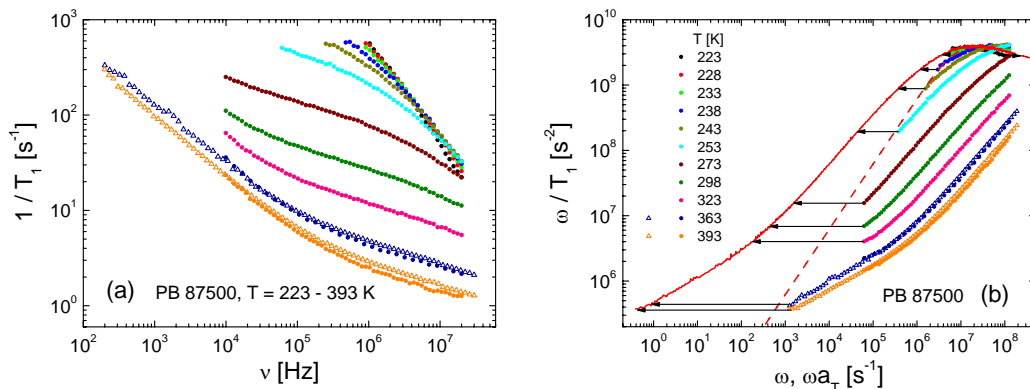


Figure 3.18: (a) Dispersion of the relaxation rate $1/T_1$ for 1,4-polybutadiene (PB) with $M = 87500$ g/mol in the temperature range as indicated measured with (open triangles) and without (circles) compensation. (b) Susceptibility representation ω/T_1 of the same data as in (a). At lowest temperatures the α -peak is discernible and fitted with a Cole-Davidson function (dashed red line). Arrows illustrate frequency-temperature superposition which is applied to create a master curve (solid red line). The color for temperatures is equivalent in both figures (adapted from Pub. 4).

ated by shifting the susceptibilities of different temperatures solely in frequency (FTS, illustrated by arrows) to achieve maximal overlap. At low temperatures the susceptibility exhibits a relaxation maximum, which reflects the main structural relaxation and from which the segmental correlation time τ_s can be extracted. The α -peak can be interpolated with an appropriate function (for instance Cole-Davidson susceptibility, dashed red line) which yields the time constant τ_s for one temperature ($T = 228$ K in Figure 3.18b). Then the temperature-dependent shift factors $a_T(T)$ can be transformed to the time constants $\tau_s(T) \approx \tau_\alpha(T)$ of segmental reorientation (see below and cf. Figure 3.21). Therefore in the following the master curves are plotted as a function of the reduced frequency $\omega\tau_s$.

Note that the construction of the susceptibility master curves presumes the applicability of FTS for both the α - and the polymer relaxation [38, 146]. That is, the susceptibility spectra of low and high temperatures, which reflect predominantly glassy and polymer dynamics, respectively, are combined to one susceptibility master curve by utilizing $\tau_s(T)$. Thus, the obtained time constants τ_s of the segmental dynamics have to be compared to those provided by other methods in order to validate the application of FTS. Moreover, the amplitudes of the α -peak for the susceptibilities of different temperatures are expected to coincide. Yet a slight reduction of the peak amplitude with decreasing temperature can be observed on a linear scale; on logarithmic scales this effect is negligible. This weak violation of FTS might result from a temperature-dependent stretching of the peak as an intrinsic property of the α -relaxation or from the emergence of a faster secondary relaxation, which is an ongoing discussion [32, 33, 147–150]. An extra part of

Section 3.2 is dedicated to an investigation of this issue.

There are several consequences and benefits of creating master curves in the susceptibility representation: First, the master curves including the relaxation data of the complete temperature interval span over about 9 decades in reduced frequency, which is a significant enhancement with respect to the results acquired for one single temperature. Second, the susceptibility master curves can be compared to spectra obtained by DS (Figures 3.6a and 3.7) or rheology (Figure 3.6b). Third, the applicability of FTS can be confirmed by comparing the obtained time constants with those of other techniques, and consequently the time constant of segmental dynamics is identified with that of the main relaxation, i.e., $\tau_s \approx \tau_\alpha$. This is fundamentally important when comparing different systems, in which the dynamics is depending on chemical structure, molecular mass, or solvent. Moreover, it is demonstrated that FC NMR is well suited to probe the slow polymer dynamics, provided that low- T_g polymers are investigated (cf. also Section 3.2). At high temperatures the rates (Figure 3.18a) are strongly increased compared to those of a simple liquid as OTP (Figure 3.16b) which reflects the polymer-specific dynamics. This manifests itself in the susceptibility (Figure 3.18b) as an excess intensity between the master curve of the polymer and the CD function representing glassy dynamics. Thus, a separation of the susceptibility into glassy and polymer dynamics is possible (see below). Finally, by Fourier transform of the master curves the dipolar correlation function is accessible over a wide time range which permits a direct comparison with the predictions of polymer models (cf. Section 3.4 and Pub. 3).

State of the Art

Many different polymer melts such as polyisobutylene (PIB), polydimethylsiloxane (PDMS), polyethyleneoxide (PEO), and 1,4-polybutadiene (PB) have been investigated by Kimmich and co-workers [36, 47] by applying FC NMR. However, only a small temperatures range and a few molecular masses without the low- M systems as a reference have been covered. As the construction of master curves has not been attempted, the frequency range has been quite limited. Neither the influence of the segmental relaxation has been explored or quantitatively estimated experimentally. A new approach has been proposed by the Rössler group yielding alternative interpretations and these preceding works are outlined in the following. A first comprehensive study of PB by S. Kariyo has included a broad range of temperatures and molecular masses from the low- M limit ($M < M_e$) to well entangled melts ($M \gg M_e$) [56, 77, 151]. Its aim has been to systematically characterize glassy and polymer dynamics and their dependency on M . Note that in the following the molecular masses M refer to the weight average molecular mass M_w , i.e., $M = M_w/(\text{g/mol})$.

At first, the results of the lowest and highest M have been compared [56]. The susceptibility master curves of PB 355, PB 466, OTP, and tristyrene are shown in Figure 3.19a. The spectra are identical for $\omega\tau_s \leq 1$, i.e., on the low-frequency

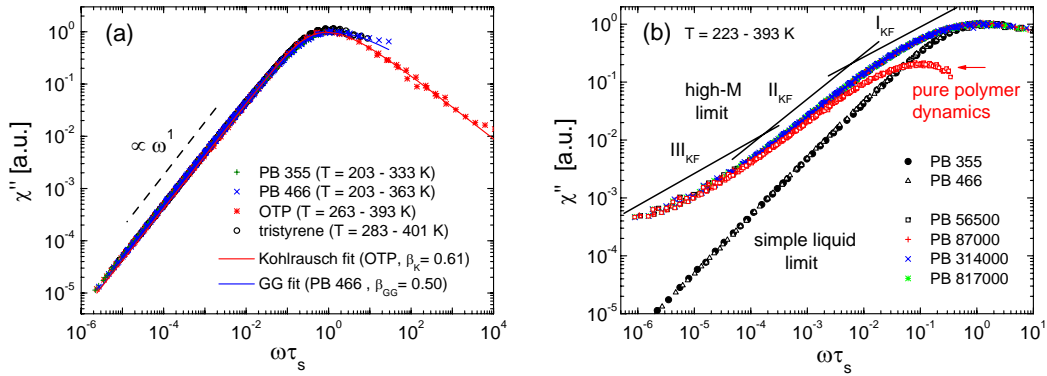


Figure 3.19: (a) Susceptibility master curves resulting from applying temperature-frequency superposition for o-terphenyl (OTP), tristyrene and the two low molecular mass 1,4-polybutadienes PB 355 and PB 466. Lines: corresponding interpolations with the generalized gamma distribution (GG) and Kohlrausch function. (adapted from [56]). (b) Susceptibility master curves for the low- M and high- M PB as indicated. The difference (red) between the high- M and low- M spectra is identified with pure polymer dynamics. Straight lines: power-law regimes (I_{KF} , II_{KF} , III_{KF}) as discussed by Kimmich, Fatkullin, and co-workers [36, 47] (adapted from [56]).

side of the main relaxation, and can be interpolated by a suitable function for the α -process with a power-law $\chi''(\omega\tau_s < 1) \propto \omega$. Explicitly, the oligomers of PB with $M = 355$ and 466 exhibit the same relaxation behavior as the glass formers OTP and tristyrene and therefore are regarded as representing the glassy dynamics of a simple liquid ("simple liquid limit"). The differences at $\omega\tau_s > 1$ are attributed to a different stretching of the α -peak of OTP and PB. Note that the master curves have been scaled to a common peak amplitude ($\chi''(\omega\tau_s \approx 1) = 1$) via division by the amplitude obtained, e.g., from a CD fit (cf. Figure 3.18b).

In Figure 3.19b the master curves of several high- M polybutadienes are displayed together with the results for the simple liquid limit. At $\omega\tau_s < 1$ an intensity in excess to that of the low- M PB is observed. This is due to polymer dynamics which is slower than the segmental dynamics. In the whole frequency range covered the susceptibilities of PB with $M = 56500 - 817000$ have the same spectral shape, i.e., the dynamics are independent of M and thus are considered to be characteristic for a well-entangled melt ("high- M limit"). The dispersion data of the high- M PB agree with those reported by Kimmich, Fatkullin, and co-workers who have claimed that the observed power-law regimes (I_{KF} , II_{KF} , III_{KF}) are universal [36, 47] and can be explained by the renormalized Rouse model [152–154]. The power-laws provide a fair approximation of the low-frequency side ($\omega\tau_s < 1$) of the master curves for high M . However, in regime I_{KF} a power-law behavior cannot be anticipated unambiguously for PB, since the curve continuously bends while approaching the relaxation maximum. Moreover, in this regime glassy dynamics

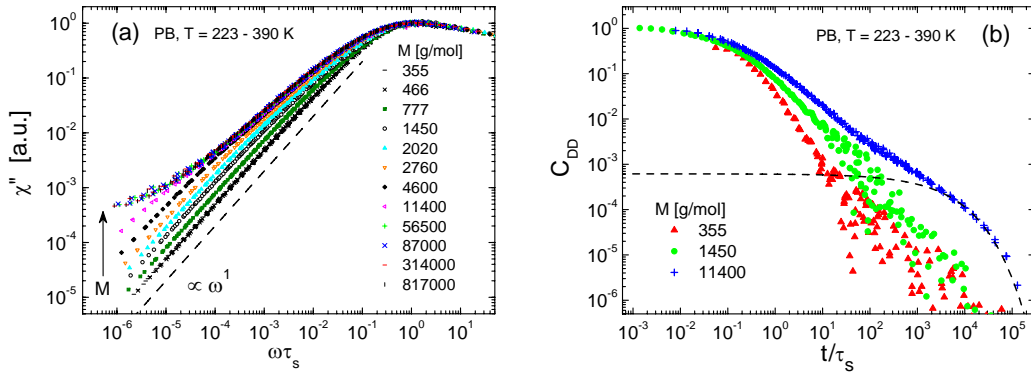


Figure 3.20: (a) Susceptibility master curves plotted as a function of the reduced frequency $\omega\tau_s$ for PB with different M as indicated (adapted from [77]). (b) Dipolar correlation function C_{DD} versus reduced time t/τ_s for three polybutadienes, obtained from selected master curves of (a). Dashed line: estimate of the plateau value associated with reptation dynamics (adapted from [77]).

is expected to influence the spectra. Thus, a separation of the master curves into contributions of glassy and polymer dynamics is necessary and can be achieved as will be described below. Note that the power-laws $I_{KF} - III_{KF}$ are not identical to those of the tube-reptation model. Thus, the works by Kimmich and Fatkullin raise doubt about the applicability of the tube-reptation model to describe the NMR relaxation behavior of polymer melts.

Furthermore, the M dependence of the dynamics between the two extreme cases of lowest and highest M has also been investigated, i.e., the crossover from glassy through Rouse to reptation dynamics [77]. The susceptibility master curves of PB with several different M are presented in Figure 3.20a. Only above $M = 466$ an excess intensity with respect to the simple liquid limit is recognized which indicates the onset of Rouse dynamics. Beginning with $M = 777$ the excess intensity at $\omega\tau_s < 1$ is increasing with M . For PB the molecular mass of the Rouse unit $M_R \approx 500$ is found. M_R is determined by the smallest possible Rouse chain. Note that here a factor 2 may be discussed [77, 151]. For higher M the crossover to terminal relaxation, which is characterized by a power-law $\chi''(\omega) \propto \omega$ ("Debye-limit", dashed line) is shifted toward lower frequencies. Thus, with higher M the distribution of polymer relaxation times ($\tau_{\text{terminal}}(M) \leq \tau < \tau_s$) is getting broader. Above $M \approx 2000$ the susceptibility master curves become bimodal which indicates the presence of an additional, slower relaxation process, i.e., entanglement dynamics. Consequently, the entanglement molecular mass of PB is identified with $M_e \approx 2000$. As mentioned before the master curves of $M \geq 56500$ are indistinguishable in the accessible frequency range (high- M limit) and M -dependent dynamics is expected to be detected only at $\omega\tau_s < 10^{-6}$, i.e., beyond the accessible frequency range.

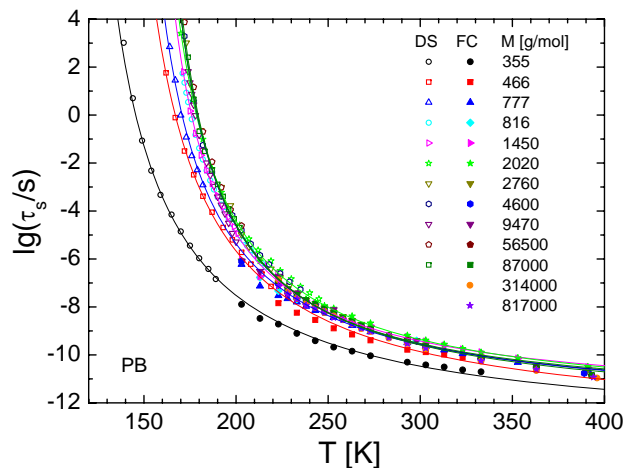


Figure 3.21: Time constants of polybutadiene (PB) as obtained by dielectric spectroscopy (DS) and FC ^1H NMR. Lines: VFT-fit of the joint data (adapted from [155]).

The dipolar correlation function $C_{\text{DD}}(t/\tau_s)$ can be obtained by Fourier transform of the master curves (eq. 3.4). Results for some M are depicted in Figure 3.20b. In analogy to $\chi''(\omega\tau_s)$ the same relaxation features are discovered. For the low- M PB the decay of the correlation function can be described by a stretched exponential, which is typical for the α -process of a simple liquid. At higher M , for the non-entangled PB 1450, the correlation decay is retarded due to Rouse dynamics, and for $M = 11400 > M_e$ the bimodal shape indicating the onset of entanglement dynamics can be clearly seen. In other words the α -process does not cause alone a complete loss of correlation; a certain residual correlation, which is referred to as polymer relaxation strength f , or the squared order parameter S^2 (see also below) survives beyond τ_s and decays on longer time-scales due to Rouse and reptation dynamics. Thus, ^1H FC NMR is able to cover three relaxation regimes: glassy, Rouse, and entanglement dynamics.

The long-time decay of PB 11400 can be fitted with a stretched exponential (dashed line in Figure 3.20b) and yields for the relaxation strength of entanglement dynamics $f_e \approx 0.0006$ which corresponds to $S_e \approx 0.025$. This emphasizes on the one hand that the amplitudes at which entanglement dynamics are disclosed in the correlation function are very low, and on the other hand the ability of NMR relaxometry to probe the correlation function on logarithmic scales, i.e., down to very low amplitudes.

By creating the master curves $\chi''(\omega\tau_s)$ (Figure 3.20a) the time constants $\tau_s(T)$ have been provided. As shown in Figure 3.21 they complement those measured by DS at low temperatures in good agreement which also verifies that the segmental correlation time is identified with time constant of the α -process, i.e., $\tau_s \approx \tau_\alpha$. The joint data of DS and FC ^1H NMR can be interpolated for each M by a VFT

function (eq. 3.8) which is a strong indication that FTS works.

The M dependence of the glass transition temperature has been obtained from the condition $T_g = T(\tau_s = 100 \text{ s})$. It has turned out that $T_g(M)$ of PB exhibits a non continuous increase (Figure 15 in [77]) as already reported by Cowie [156] for several polymers. Three linear regimes can be recognized and the crossover molecular masses can be identified with M_R and M_e [77, 157, 158]. The increase of $T_g(M)$ below M_e can be seen of course as well in Figure 3.21 for the temperatures at $\lg(\tau_s/\text{s}) = 2$. For that reason it is important to plot the master curves as a function of the reduced frequency $\omega\tau_s$. They are isofrictional spectra [159, 160] in which the dynamics of polymers with different molecular masses can be directly compared because the M dependence of the glass transition temperature T_g has been taken into account which is pronounced especially at low M [77, 157].

As mentioned the NMR relaxation of polymer melts comprises glassy (local) and polymer (collective) dynamics. One approach to extract spectra which represent solely the latter ("polymer spectra") is to decompose the susceptibility master curves [56, 77, 151]. Assuming statistical independence and time-scale separation of glassy and polymer dynamics results in multiplicative contributions, and taking into account the relaxation strength f of polymer dynamics yields [56]

$$\chi''(\omega) = (1 - f)\chi''_{\text{glassy}}(\omega) + f\chi''_{\text{polymer}}(\omega) \quad (3.21)$$

Note that a very similar approximation has been described also by Kimmich and Fatkullin [47, 125], yet it has not been employed for a decomposition. For low M , i.e., for the Rouse regime, the assumptions mentioned above are problematic, however, at least for higher M this approach can be utilized for a phenomenological description of the relaxation behavior of different polymer systems (see Section 3.3 and Pub. 2). The polymer relaxation strength f can be identified with the squared order parameter S^2 and can be determined by integrating the relative polymer contribution in the susceptibility spectra which is referred to as "excess intensity"

$$f = S^2 = \int_{-\infty}^{\infty} \chi''_{\text{polymer}}(\omega) d \ln \omega / \int_{-\infty}^{\infty} \chi''(\omega) d \ln \omega \quad (3.22)$$

Thus, the polymer spectra $\chi''_{\text{polymer}}(\omega\tau_s)$ of all $M > M_R$ can be extracted from the total spectra $\chi''(\omega\tau_s)$ by subtraction of the glassy spectrum $\chi''_{\text{glassy}}(\omega\tau_s)$ which is assumed to be given by the master curve of PB 466. Since it has been demonstrated by DS that the spectral shape of the α -peak of PB [77], PDMS [157], and polyisoprene (PI) [63] is M -independent, it is well-justified to subtract from each master curve the spectrum of the low- M reference. The resulting polymer spectra of PB can be compared to spectra calculated from the discrete Rouse model. While the number of Rouse units N can be mapped to the molecular masses M for $M < M_e$, at higher M the Rouse model does not reproduce the bimodal shape of $\chi''_{\text{polymer}}(\omega\tau_s)$. This is again a clear indication for a second relaxation process, i.e., entanglement dynamics. Furthermore, the onset of entanglement dynamics limits the number of participating Rouse units which can be supposed as the formation

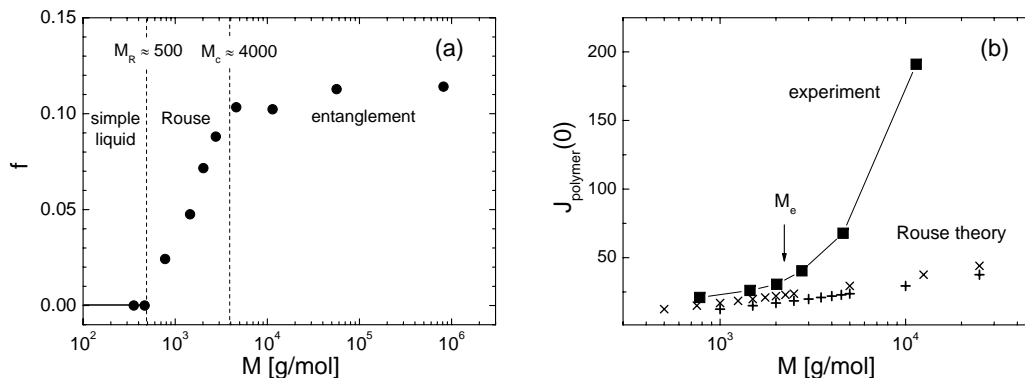


Figure 3.22: (a) Relaxation strength f of polymer dynamics as a function of molecular mass. M_R and $M_c = 2M_e$ denote the Rouse unit and entanglement molecular masses, respectively. Dynamic regimes are indicated. (adapted from [77]). (b) Spectral density of the separated polymer contribution at lowest experimentally accessed frequency as a function of M and comparison with Rouse theory. Squares: experimental data. Pluses and crosses correspond to $M_R = 500$ and 250, respectively, M_e indicates mass of onset of entanglement (adapted from [77]).

of a transient network. Note that the discrete Rouse model has to be applied, since a certain approximation cannot be used for small N , i.e., a limited number of Rouse modes [77]. Moreover, the polymer spectra need to be normalized in amplitude by their integral [161].

By inspecting the dependence of the polymer relaxation strength f on M (Figure 3.22a) again three regimes show up [77]. The transitions between the regimes mark the characteristic molecular masses M_R and M_c . M_c denotes the critical molecular mass as it is observed, e.g., for the M -dependence of the viscosity [53, 80, 86, 162], and is usually twice the entanglement molecular mass M_e [114, 163]. In the simple liquid regime $f = 0$ by definition, in the Rouse regime $f(M)$ is continuously increased, and in the entanglement regime it levels off. The maximum value of $f \approx 0.11$ is essentially determined by Rouse dynamics, although a weak increase f_e is still observed above M_c , which corresponds to that estimated from the long-time decay of the correlation function (cf. Figure 3.20b). f represents the squared order parameter S^2 [116, 164–166] and may be taken as a measure of spatial restriction of glassy dynamics. It is worthwhile to note that the quantity probed by NMR [56] is not related to structural order in the sense of long-range or static orientational order as known from, e.g., nematic liquid crystals [167]. Thus, the restriction of local segmental dynamics is a result of some segments within a single chain being pinned down between two entanglements. However, the opposite is not necessarily true, i.e., structural order may not be deduced from restricted local motion.

Moreover, an important conclusion can be drawn from f regarding the analysis of

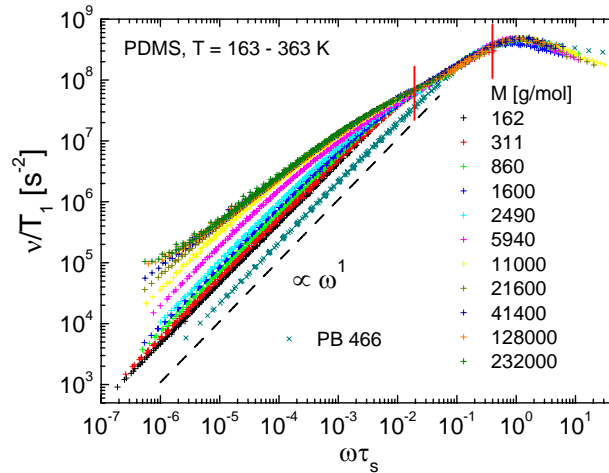


Figure 3.23: Susceptibility master curves of PDMS with M and in a temperature range as indicated. PB 466 includes as a reference for a simple liquid. Vertical lines: regime of the M -independent power-law (adapted from [155]).

the dispersion data. The susceptibility $\chi''(\omega) = \omega/T_1(\omega)$ does only reflect polymer dynamics, if $(1-f)\chi''_{\text{glassy}}(\omega) \ll f\chi''_{\text{polymer}}(\omega)$ holds (cf. eq. 3.21). In consequence especially if $f \ll 1$, e.g., for short chains exhibiting solely Rouse dynamics or for systems with a generally weak relaxation strength, the assumption of time-scale separation is not sufficient to ensure that polymer dynamics actually dominate even at $\omega\tau_s \ll 1$. This is illustrated in Figure 3.19b in which also the polymer spectrum of the high- M limit is shown. Therefore, also when evaluating dispersion data in the T_1 or $1/T_1$ representation, the fast (here: α) relaxation processes have to be taken into account [168], which is an important insight with respect to previous reports [36, 47].

An additional way to determine M_e is to directly compare the NMR relaxation results with the predictions of the Rouse model and to determine the M at which they begin to deviate from each other. In Figure 3.22b the spectral densities of the polymer contribution at the lowest accessible frequencies $\omega\tau_s \rightarrow 0$ are displayed together with those calculated from the discrete Rouse model (cf. eq. 3.14) assuming $M_R = 500$ or 250. While the lower M appear to follow the Rouse behavior $J_{\text{polymer}}(0) \propto \log M$, above a certain M the experimental spectral density increases stronger, which is due to the onset of entanglement dynamics. This transition defines $M_e \approx 2000$ and is in good agreement with literature [169].

As a second polymer PDMS has been investigated in a wide molecular mass ($M = 162 - 232000$) and temperature range ($T = 163 - 363\text{K}$) [170]. The susceptibility master curves are displayed in Figure 3.23. Concerning the polymer dynamics at $\omega\tau_s < 1$ the relaxation behavior is in general similar to that of PB. Nevertheless a clear difference between the master curves of PDMS and PB can be

recognized: Whereas in the case of PB the excess intensity due to polymer dynamics sets in at frequencies just below the main relaxation peak (cf. Figure 3.20a), for PDMS the polymer dynamics are shifted to lower frequencies and in between (marked by vertical lines) a power-law is discernible, which is a common feature for all M . This result has been explained as an anomalous α -process [170]. Yet, the effect has not been completely clarified, since possible influences of intermolecular relaxation were believed to be negligible.

In summary, the following principles set the approach of the Rössler group apart from that of Kimmich and co-workers: The measured temperature range should be as broad as possible in order to detect both the fast segmental and the slower polymer-specific dynamics. Low- M systems are investigated as a reference for the glassy spectrum which represents the segmental dynamics also for higher M . FTS is applied to create master curves in the susceptibility representation, which significantly enlarges the accessible frequency range. The master curves are Fourier transformed to the correlation function, which allows for a comparison with the results from other experimental techniques and simulations, and predictions by polymer models. As a consequence, the interpretations go far beyond what has been reported in the literature for NMR relaxation results, e.g., the emergence of polymer dynamics with M can be clearly traced and the characteristic molecular masses M_R and M_e can be determined. Recently [171] the term "molecular rheology" was coined with respect to FC and DQ ^1H NMR and their joint capability of exploring the time range from glassy dynamics to terminal relaxation in entangled polymers like "conventional" rheology. The mentioned principles are continued and enhanced in this thesis; especially lower frequencies (or longer times) will be accessed by technical means in order to experimentally ascertain as an ultimate goal the reorientational correlation function $g_2(t)$ and the mean square displacement as they are schematically rendered in Figure 3.12 over several decades.

Objectives of this Thesis

Based on the above findings more profound questions were raised which establish the principal part of this thesis. Moreover, from the studies of polymer melts the topics "polymer dynamics in confinement" and "intramolecular and intermolecular relaxation in low-molecular systems" have evolved and are continued by M. Hofmann [69] and R. Meier [172–174], respectively. The following items motivate the next sections. The sections themselves provide compact introductions and cross-relations to the corresponding publications Pub. 1 - 5 (Section 4). They also give a perspective of recent developments or further studies which are currently underway.

- Section 3.2 and Pub. 1

What can be learned from a quantitative evaluation of the correlation functions of different M and a comparison to results from simulations? When does a molecule become a polymer and can the molecular mass M_R of the Rouse unit be reliably determined?

- **Section 3.3 and Pub. 2**
Do the polymer spectra of different systems reflect universal dynamics in terms of common power-law exponents? How can the different polymer relaxation strengths observed for partially deuterated chains be understood?
- **Section 3.4 and Pub. 3**
How does the correlation function develop at longer times and is the power-law exponent of regime II of the tube-reptation model revealed? Does the correlation function evolve with M as observed by Double Quantum NMR? What happens if the Redfield limit is approached?
- **Section 3.5 and Pub. 4**
Can the frequency dependence of the intermolecular contribution to the ^1H NMR relaxation of polymers be quantified? Which conclusions can be drawn from the ^2H NMR relaxation of polymers with different M ? Can the predictions and assumptions of the tube-reptation model for the reorientational correlation function and the segmental mean square displacement be corroborated experimentally?
- **Section 3.6 and Pub. 5**
How is polymer dynamics modified in solution? How can the spectral changes upon dilution be understood with respect to other techniques?

3.2 From Simple Liquid to Polymer Melt

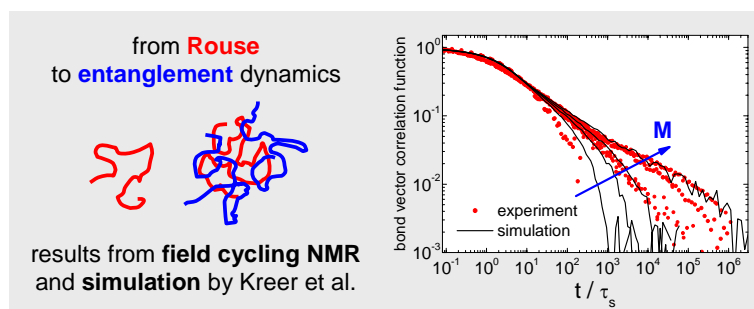


Figure 3.24: Table of Content Graphic (adapted from Pub. 1).

The question "When Does a Molecule Become a Polymer?" was the incisive title of a report by Sokolov et al. [175]. Instead of the Kuhn segment the authors have proposed the so-called molecular mass of a random step M_r to characterize the size of one bead of the polymer chain (cf. Section 3.1). Their aim has been to introduce a quantity (M_r) by which the M dependence of the glass transition temperature T_g of polystyrene and polydimethylsiloxane can be scaled in the same way. In contrast to the Kuhn segment length, for M_r the subchains, which are formed by a certain number of monomers, are not considered as completely expanded within one bead. Consequently, quite high values of M_r compared to the Kuhn segment have been obtained. Since the molecular mass of a random step M_r has been considered as an important parameter which defines the M dependence of the polymer chain dynamics [175], it has a very similar meaning as the molecular mass of the Rouse unit M_R as introduced in the preceding works of our group by Kariyo et al. (cf. Section 3.1). Therein it has been demonstrated that the characteristic molecular masses M_R and M_e can be revealed also by applying FC ^1H NMR, e.g., by distinctive kinks in the M -dependence of the polymer relaxation strength f (cf. Figure 3.22a). That is, the onset of excess intensity on the low-frequency side of the α -peak as reflected in $f(M)$ defines the molecular mass of a Rouse unit M_R neglecting sub-Rouse relaxation phenomena. Above M_R dynamics slower than that found for a simple liquid are discernible in the susceptibility master curves and the molecule can be considered as a polymer (or at least an oligomer). For PB a surprisingly high $M_R \approx 500$ has been suggested by the NMR relaxation results. The entanglement molecular mass can also be identified by extracting the polymer spectra and comparing them to the Rouse theory (cf. Figure 3.22b). The aim is now to further substantiate and quantify the conclusions by validating the transitions observed for the M dependence and analyzing the reorientational correlation functions also for $M > M_e$. In analogy to rheological studies [80, 159, 169] it is the intention to investigate how the M -dependence of polymer dynamics is probed by NMR relaxometry. In order to supplement the existing M range four new PB samples ($M = 816, 9470, 18000, 35300$) were measured with the

Stellar spectrometer at several temperatures in the range $T = 223 - 408$ K and susceptibility master curves are created. The results of the new M are combined with the existing ones and are evaluated together (see Pub. 1). Note that in Pub. 1 the same regimes 0, I, II, III, and IV as described in Section 3.1 are discussed, however, therein they are referred to as regimes I, II, III, IV, and V, respectively. In Summary, the major results are:

1. Depending on M the susceptibility master curves reflect the regimes of simple liquid, Rouse, and entanglement behavior (Figure 1 in Pub. 1). At $M = 777$ first additional intensity compared to the low- M limit of PB 466 sets in and the susceptibility of PB 816 is always slightly higher than that of PB 777. This justifies the previously determined molecular mass of the Rouse unit $M_R \approx 500$. Above M_e entanglement dynamics emerge and the shape of the master curves gets increasingly bimodal, which is not the case for the Rouse contribution. The crossover to terminal relaxation ($\propto \omega^{-1}$) is shifted toward lower frequencies. The intensity at lowest frequencies continuously increases with M until for $M \geq 56500$ the high- M limit is reached.
2. The dipolar correlation function is accessed for several $M > M_e$ up to $Z = M/M_e \approx 9$ (Figure 2 in Pub. 1) and extends over 6 decades in amplitude and 8 in time. The increasing retardation of the dynamics due to entanglement effects is clearly seen in accord with the analysis in the frequency domain. The long-time decay is interpolated by a stretched exponential which yields the longest or terminal relaxation time τ_t . Its M -dependence (Figure 3 in Pub. 1) exhibits a transition between two power-laws at $M \approx 2000$, which is identified with M_e of PB. A good agreement of $\tau_t(M > M_e)$ is also found for reanalyzed results from double quantum NMR by Graf et al. [116].
3. Two power-laws $\propto t^{-a}$ are observed for the high- M envelope of the dipolar correlation function. The first exponent $a = 0.85$ is attributed to Rouse dynamics and the one at longer times with $a = 0.5$ is associated with entanglement dynamics. However, the second exponent is at variance with the prediction of the tube-reptation model [83] and the renormalized Rouse model [47].
4. The bond vector correlation function – extracted from the dipolar correlation function under the assumption that it is given by the square root of the dipolar correlation function – can be directly compared to Monte Carlo simulation results by Kreer et al. [109] and a good agreement is found (Figure 4 in Pub. 1). Since the exponents for constraint Rouse and reptation dynamics are not revealed in both cases, the NMR results confirm that the crossover to entanglement dynamics is very protracted.

Ad 2.: The features of dipolar correlation function closely follow those obtained by simulations for PB [176, 177] as well as other NMR relaxation works [112, 115].

By direct comparison of Figure 2 of Pub. 1 with that of the preceding work (Figure 3.20b), it becomes more obvious now how the slower relaxation process attributed to entanglement dynamics emerges.

Ad 3.: Regarding the observed power-laws some comments are worthwhile. The exponent $a = 0.85$ of the first is close, yet not identical with the prediction $a = 1$ for free Rouse dynamics. It is attributed to regime I of the tube-reptation model nevertheless, though some issues need to be considered: The relaxation behavior at about 1-2 frequency decades below the α -peak still results from an interplay of glassy and Rouse dynamics, i.e., they are not well separated in time. In addition, due to the onset of entanglements there are only a limited number of active Rouse modes. Moreover, for a better resemblance to the experimental spectra a mode-dependent stretching of the Rouse modes should be introduced as revealed by MD simulations [40, 77, 109, 110, 178, 179]. At longer times the time scale separation between glassy and polymer dynamics is given and PB exhibits a strong polymer relaxation (Figure 3.22a). Yet, associating the second power-law with $a = 0.50 \pm 0.05$ with a relaxation regime of the tube-reptation model remains ambiguous at the moment. Though the value suggests regime III, this would mean at the same time that regime II and the M -dependence predicted for regime III are not observed (cf. Figure 3.12). It appears that within the accessible M range solely the terminal relaxation is depending on M . However, the twice renormalized Rouse model provides the power-law exponent $a = 0.5$ for the intersegmental correlation function [97], which represents the contribution of the intersegmental relaxation. This emphasizes that the influence of the intermolecular relaxation needs to be investigated (see Section 3.5).

Ad 4.: The bond vector correlation function $\Phi_b(t/\tau_s)$ allows a comparison between simulated and experimental curves and to directly map curves with similar M . The almost perfect coincidence at longer times ($t \gg \tau_s$), however, needs to be treated cautiously: Firstly, the intensity of the polymer-specific relaxation is related with the relaxation strength f , which reflects the weighting between glassy and polymer dynamics. Therefore the absolute agreement between the NMR results for PB and the non-atomistic simulation results might be accidental. Secondly, eq. 3 in Pub. 1 has been applied for the whole time range whereas it is theoretically valid at $t < \tau_R$ only, as has recently been pointed out by Likhtman and co-workers [180, 181].

In conclusion, analyses of the dipolar or bond vector correlation function allow a comparison with different models and other techniques. It appears that the crossover to reptation is very protracted, i.e., the power-law predictions of the tube-reptation model will only be revealed at high $M \gg M_e$. Therefore access to lower frequencies or longer times is desirable in order to clarify the attribution of relaxation regimes. Moreover, a quantitative comparison with atomistic simulations by Vogel and co-workers may become feasible [182]. Note that the data of Pub. 1 have been utilized by Saalwächter and co-workers for the analysis of their DQ NMR results [117] which is shown in more detail in Section 3.4.

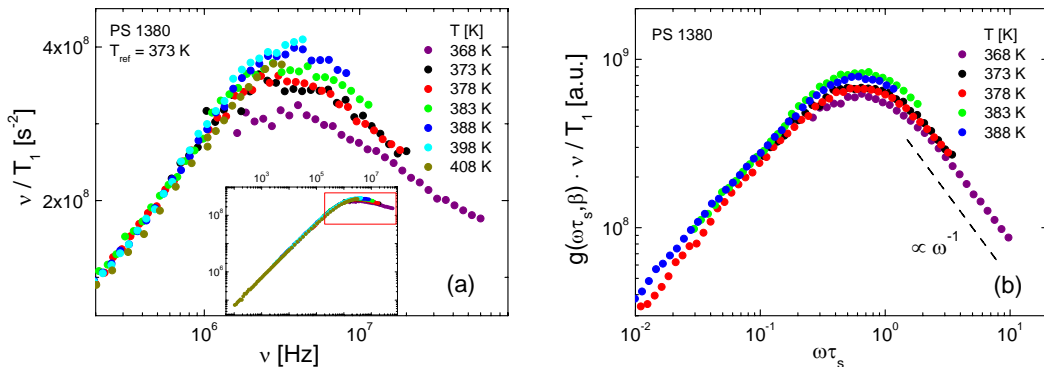


Figure 3.25: (a) Enlarged main relaxation peak of the susceptibility master curve of polystyrene (PS) with $M = 1380$ in the temperature range as indicated scaled on the relaxation data of the reference temperature. Note the linear y-axis. Inset: complete master curve in double-logarithmic representation. (b) Data of (a) which include the relaxation maximum after applying the "second scaling".

Temperature-dependent effects in the master curves

Returning to the question "When Does a Molecule Become a Polymer?" some notes are worthwhile, which have arisen from studying low- M polystyrenes (PS) and are not discussed in Pub. 1. In order to decide for which M for the first time the excess intensity exists on the low-frequency side of the α -peak, which is described, e.g., by a Cole-Davidson (CD) function, a very precise scaling on the peak time constant and amplitude is necessary (cf. Figure 3.19a). However, the master curves ("first scaling") exhibit some systematic differences in range of the relaxation maximum, which is illustrated in Figure 3.25a on a linear scale for PS with $M = 1380$; that is, creating a master curve unambiguously is not possible in this case. With decreasing temperature the peak amplitude is systematically reduced and, thus, FTS is violated. As a consequence the determination of the onset of the excess intensity with respect to a CD susceptibility is hampered. It is emphasized that in the case of PB the relaxation contribution f of polymer dynamics is relatively strong for high $M > M_e$ (cf. Figure 3.22a) and the temperature-dependent effects in the range of the relaxation maximum are small. The amplitude of the relaxation maximum depends on the NMR coupling constant (eq. 3.19) and the stretching parameter β as taken into account by, e.g., a CD function. The first can be assumed as temperature-independent in the temperature range considered here, while the latter might be a function of temperature, thus $\beta = \beta(T)$. The aim is now to convert the susceptibilities to a uniform shape by eliminating the temperature-dependent changes, i.e., to map the α -peak on a Debye curve.

As first approach the so-called "second scaling" [68] is applied by which each relaxation peak with its temperature-dependent stretching $\beta(T)$ is transformed to

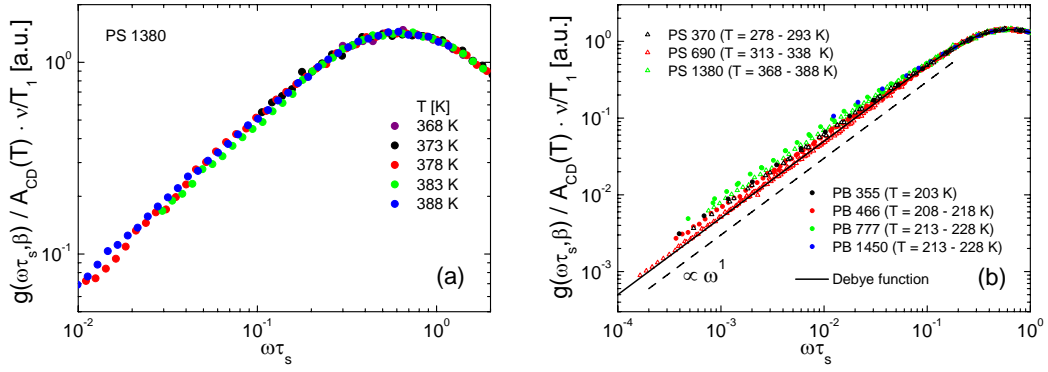


Figure 3.26: (a) Data of PS 1380 from Figure 3.25a after applying "third scaling". (b) Susceptibility master curves of PS with $M = 370, 690,$ and $1380,$ and PB with $M = 355, 466, 777,$ and 1450 in "third scaling" (PB data from [151]; for PB 355 only one dataset which exhibits the susceptibility maximum was available).

a Debye peak (with $\beta = 1$). Technically this can be achieved by interpolating the susceptibilities of each temperature with a CD function and re-plotting the data as a Debye function with the corresponding time constant τ_s , i.e., by applying for each dataset a factor

$$g(\omega\tau_s, \beta) = \frac{\chi''_{\text{Debye}}(\omega\tau_s)}{\chi''_{\text{CD}}(\omega\tau_s, \beta)} \quad (3.23)$$

where both τ_s and β are temperature-dependent. Note that only the high frequency side of the peak is fitted, since at lower frequencies polymer-specific relaxation contributions might be present which may distort the fit. The results are shown in Figure 3.25b. After applying the "second scaling" the data have a common shape in the peak range, i.e., their high-frequency wing exhibits the same power-law $\propto \omega^{-1}$. However, the amplitudes of the relaxation maxima still do not coincide. Obviously the temperature-dependent broadening of the peak alone cannot account for the the difference in amplitude observed in the original data of Figure 3.25a, and the coupling constant has to change. Note that there might also be an influence of the end groups at low M and that we have recently reported on the M -dependence of the coupling constant [155].

A "third scaling" is utilized which divides the susceptibilities by their amplitudes $A_{CD}(T)$ as determined from the individual CD fits. Thereby they are forced to agree also in amplitude, which is displayed in Figure 3.26a. These data form a master curve with a Debye-like α -peak, and this normalized representation of the master curves enables a direct comparison between different polymers.

In Figure 3.26b the susceptibility master curves of PS and PB [151] each with different low molecular masses are displayed after application of the "third scaling". In order to assess the excess intensity at $\omega\tau_s < 1$ a Debye function is also

included. Considering first the results of PS, a non-systematic trend with M is observed. The master curve of $M = 370$ already exhibits an excess intensity, whereas that of $M = 690$ clearly traces the Debye behavior. The susceptibility of PS 1380 shows a low-frequency intensity, which is larger than that of PS 370. Note that the molecular masses provided by the supplier have been confirmed by oligo-GPC (gel permeation chromatography) and MALDI-TOF (matrix-assisted laser desorption/ionization time of flight mass spectrometry) measurements. In the case of PB the effect is similar. The lowest $M = 355$ is not identical with the Debye curve, the slightly larger $M = 466$ exhibits a little lower intensity, which is yet not identical to the Debye behavior, and at higher M a stronger low-frequency contribution is noticeable. Thus, for PB the previously determined molecular mass of the Rouse unit $M_R \approx 500$ is essentially confirmed. In the case of PS, M_R is found to be higher than that of PB, say $M_R \approx 1000$. This is slightly larger than the mass of the Kuhn segment (about 8-9 monomers [175]), yet smaller than the mass of the random step $M_r \approx 5000$ reported by Sokolov and co-workers [175]. Given the currently available data, an explanation of the non-systematic behavior at very low M is rather speculative without further investigations. However, it is known from studies of low- M glass formers that an intermolecular relaxation contribution which reflects translational diffusion is always present at low frequencies ($\omega\tau_s < 1$) [68, 173, 174]. This might also be the reason for the anomaly observed for PDMS (cf. Figure 3.23). Since the intermolecular relaxation and the onset of polymer dynamics occur in the same frequency range, they are probed simultaneously by ^1H FC NMR and cannot be readily isolated. Regarding this issue more details and the extracted intermolecular relaxation contributions for PB and PDMS are presented in Section 3.5. Since at this stage this phenomenon cannot be resolved, we refrain from applying the second and third scaling, and create the master curves as described in Section 3.1, i.e., allowing minor FTS violations which are negligible on logarithmic scales (cf. inset of Figure 3.25a) and even smaller in case of PB.

In summary, presently the answer to the question "When does a molecule become a polymer?" by evaluating results of FC NMR relaxometry remains the one given above in this section. It may be refined in a future study, which explores the development of the intermolecular relaxation in oligomers with different M by isotopic dilution experiments. Thereby intermolecular and intramolecular relaxation contributions can be separated. Consequently, this would facilitate the identification of the polymer-specific relaxation as reflected in the intramolecular contribution. With increasing M , it would be expected for the intramolecular contribution that beginning at M_R the excess intensity with respect to a Debye susceptibility is discernible, while the intermolecular contribution is successively shifted toward lower reduced frequencies, as diffusion is slowed down.

Furthermore, the study of PS, whose T_g changes by more than 250 K from its monomer to high M [157], emphasizes that only low- T_g polymers can be investigated by FC NMR given the currently available temperature range of the Stellar relaxometer; of course also the temperature stability of the polymer has to be

considered. For say $T_g > 340$ K the frequency regime of the polymer relaxation can not be reached anymore at highest temperatures ($T \approx 400$ K). For example, the relaxation maximum of PS 1380 ($T_g = 314$ K [157]) is observed in the range $T = 368 - 388$ K (cf. Figure 3.25a). For the next higher M , PS 3250 with $T_g = 347$ K [157], the α -peak can be expected at temperatures $T \approx 400 - 420$ K. This underlines the necessity to access higher temperatures and also lower frequencies, which requires several hardware modifications. Note that the results of PS 1380 at $T = 408$ K (cf. inset of Figure 3.25a) have been obtained for frequencies down to 1 kHz with the FC NMR relaxometer in Darmstadt (see Section 3.4 for further details).

3.3 Universal Dynamics for Various High- M Polymers

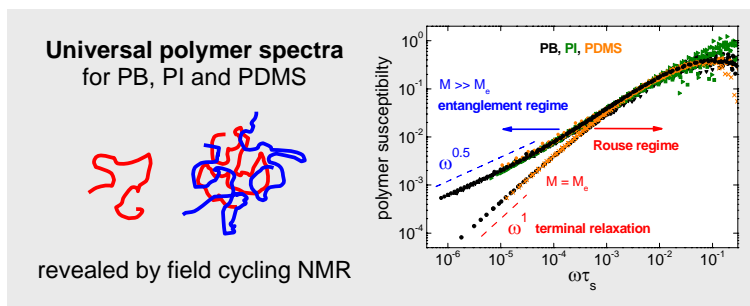


Figure 3.27: Table of Content Graphic (adapted from Pub. 2).

The emergence of polymer dynamics has been thoroughly investigated for PB in a broad range of temperatures and molecular masses by a quantitative analysis of both susceptibility master curves and the dipolar correlation functions (Pub. 1). While the glassy dynamics are intrinsic to the relaxation behavior for all M , for the high- M limit two power-laws have been observed, which have been attributed to Rouse and entanglement dynamics. However, for polymer melts the predictions for the power-law exponents of the tube-reptation model have not been confirmed by the results of the FC ^1H NMR experiments. The exponent of regime II has been discovered by Kimmich and co-workers [36, 183, 184] merely for a linear polymer confined in a solid matrix, i.e., for chain dynamics in a static tube. Yet, the authors have considered the low-frequency power-law observed for the ^1H relaxation of linear polymer melts as universal [47], although some reports show a different behavior [185].

Thus, the goal of Pub. 2 is, first, to compare the ^1H relaxation of different polymers in order to review whether the low-frequency behavior as it is reflected in the T_1 dispersion or the susceptibility is in fact universal. For that purpose high- M PI was measured and the resulting susceptibility master curve is analyzed together with the existing ones of PB and PDMS. Second, under the assumption that the entire relaxation can be separated into contributions of glassy and polymer dynamics, the polymer spectra can be extracted and the relaxation strength f can be determined (Section 3.1). Moreover, it has been discussed that the order parameter in entangled systems depends on the specific proton-proton dipolar couplings [102, 116, 165], i.e., for a high- M polymer melt f depends on the chemical structure of the monomer unit (eq. 5 of Pub. 2). Therefore partially deuterated PB and PI (the latter from [185]) were investigated and are compared with the corresponding completely protonated polymers. The central results of Pub. 2 are summarized in the following:

1. For PB, PDMS, and PI with $M > M_e$ the dispersion of T_1 (Figure 1 in Pub. 2) and consequently the susceptibility master curves (Figure 2 in

Pub. 2) do exhibit a non-universal power-law behavior at low frequencies in contrast to the claim in literature [47]. The master curves of PB have a larger excess intensity than those of PI. In the case of PDMS polymer dynamics sets in at lower frequencies than in PB and PI, and an M -independent power-law $\propto \omega^{0.5}$ is observed between polymer dynamics and the α -peak (Figure 4a in Pub. 2). A similar power-law is also seen in other low- M systems at $\omega\tau_s < 1$ (Figure 4b in Pub. 2).

2. Different selectively deuterated PB and PI show other power-laws in $T_1(\nu)$ than the corresponding completely protonated polymer chains. Concomitantly, the shape of the susceptibility master curves at $\omega\tau_s < 1$, i.e., in the range where polymer dynamics are located, is not uniform for all polymers studied.
3. A common shape for high- M PB, PDMS, PI, and the partially deuterated samples is only disclosed by taking into account the contribution of glassy dynamics along eq. 3.21. That is, at lowest frequencies their normalized polymer spectra show a common power-law $\propto \omega^{0.5}$ (Figure 3 in Pub. 2). Furthermore, at intermediate frequencies ($10^{-3} < \omega\tau_s < 1$) the high- M spectra have the same shape as those with $M \approx M_e$. This demonstrates that in the Rouse regime (I) the dynamics of non-entangled polymers with $M \approx M_e$ and entangled polymers are essentially identical. Thus, the apparent discrepancy in the overall susceptibility spectra is resolved by isolating the polymer spectra confirming the decomposition approach.
4. The relaxation strength f of polymer dynamics depends on the orientation of the internuclear vectors of the protons with respect to the chain contour (Table 2 in Pub. 2). For PB which has the highest values of f , the differently deuterated samples can be clearly distinguished: For the one with the protons at the carbon atoms of the double bond, f is higher than for the fully protonated one, whereas it is vice versa for the one with the protons at the methylene groups. In the first case the ^1H - ^1H direction is parallel to the chain contour given by the double bond. This causes just a small reduction of the order parameter of the chain. In the case of the methylene group protons, the angle between their axis and the chain contour is larger, thus the reduction is much stronger. For the completely protonated PB a value in between is found.

Ad 1.: The anomalous relaxation behavior of PDMS with the M -independent power-law ($10^{-2} < \omega\tau_s < 1$) has been outlined in Section 3.1 already. In Figure 5 of Pub. 2 it is shown explicitly that it is also found for the ^1H relaxation of the low- M glass formers glycerol and propylene glycol, and it has been attributed to an anomalous α -process. Yet, the relaxation feature does not show up in the dielectric spectra of PDMS and glycerol [186], which indicates an intermolecular origin (cf. Section 3.5). This triggered a thorough investigation of different low- M

systems [68, 172, 173, 187] with the aim to separate intramolecular and intermolecular contributions. Since the latter can be related to translational motion a quite simple way of determining the diffusion coefficient by FC NMR relaxometry has been reported [174].

Ad 3.: The power-law $\propto \omega^{0.5}$ observed in polymer spectra at lowest frequencies corresponds to the power-law $\propto t^{-0.5}$ found in the dipolar correlation function of high- M PB (Figure 2 of Pub. 1). The fact that a common power-law is revealed for all high- M systems including the selectively deuterated ones, emphasizes the importance of taking into account also the different relaxation strength of polymer dynamics. Therefore it is eminently important to study a broad temperature or frequency range, especially to access also sufficiently low temperatures including glassy dynamics. Since the glassy dynamics is a generic feature of the relaxation behavior of polymers, it is necessarily required to have a reference (τ_s) for the time scale to account for a change of τ_s , and to estimate f in order to draw conclusions from comparing different polymers. Note that an alternative approach of determining f is presented in Figure 5 in Pub. 2. Furthermore, it is demonstrated in Figure 6 in Pub. 2 that the subtraction of glassy dynamics from the total susceptibility yields essentially the same result for the polymer spectrum as a multiplicative decomposition of the dipolar correlation function.

Regarding the above mentioned results of polymer dynamics in a static confinement by Kimmich and co-workers [36, 183, 184] two comments are worthwhile. Firstly, the conclusion that the power-law of regime II of the tube-reptation model has been revealed has been drawn at first [184] from deuterated PEO in a protonated matrix, i.e., by applying FC ^2H NMR in order to detect solely the NMR signal of the confined polymer. Thereby also intermolecular relaxation contributions are excluded. Later [183] the power-law has also been confirmed by ^1H relaxometry which comprises intramolecular and intermolecular contributions. Although usually a different dispersion can be expected for ^1H and ^2H relaxation, here it appears that the intermolecular relaxation either has the same spectral shape as the intramolecular contribution or does not play a role. Secondly, from these results the corset effect has been discovered [183], i.e., that confinement effects have been observed even for confinement diameters much larger than the size of a single chain. The discussion is still ongoing [188, 189] and involves also new results by NS [190, 191] and DQ NMR [192]. However, recent FC ^1H NMR experiments for PB in nanoscopic matrices of anodic aluminum oxide by our group [69] have not shown a clear indication for the corset effect. Instead it appears that the relationship between τ_s and τ_R is changed in confinement.

Very recently we have reported [155] on a similar M -dependence of the polymer dynamics for PB, PDMS, PI, and polypropylene glycol (PPG) melts. Especially the protracted transition to full reptation dynamics has also been observed.

3.4 Protracted Crossover to Reptation Dynamics

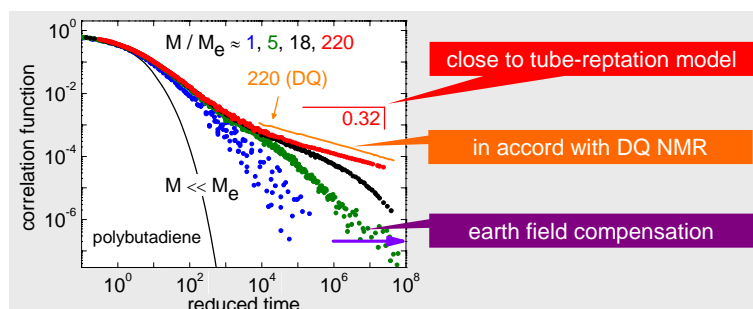


Figure 3.28: Table of Content Graphic (adapted from Pub. 3).

The previous studies [56, 77, 151, 161] and Pub. 1 and 2 have clearly shown that the most prominent features of polymer dynamics for high- M melts are revealed by FC NMR at high temperatures and low frequencies. While the Rouse regime (I) has been well covered in the master curves of PB, at lower reduced frequencies the constrained Rouse regime (II) reflecting influences of entanglements has been found to be merely in a state of development (see Figure 1 in Pub. 1). Especially the power-law exponent ϵ of regime II characterizing the long-time slope of the correlation function has not reached $\epsilon = 0.25$ as expected for $M > M_e$ by the tube-reptation model. Therefore the two limitations, highest temperature ($T \approx 410$ K) and lowest frequency ($\nu \approx 10$ kHz) which actually stem from the specifications of the Stellar spectrometer, should be reconsidered in order to further augment the accessible dynamic range of the method.

An additional increase of the temperature above $T = 408$ K (the highest T at which PB was measured in Pub. 1) is principally possible. For this purpose a home-built probehead together with a more powerful heating system could be employed which have been developed recently [134]. First test runs have indicated that higher temperatures ($T \approx 500$ K) than with the commercial equipment can be achieved while the signal-to-noise ratio of the new solenoid coil design still has to be improved. However, since the temperature dependence of the time constants $\tau_s(T)$ is very weak at such high temperatures (see Figure 3.21), the dynamics is expected to be shifted just minimally with respect to the already measured temperature, i.e., after applying FTS the master curves would be extended only insignificantly. Moreover, in the case of PB sample degradation is an issue [193], i.e., it inhibits experiments above say $T \approx 410$ K.

Thus, an enhancement toward lower frequencies ($\nu < 10$ kHz) is more promising. As the sample inside of the probehead is still exposed to the magnetic field of the earth and stray fields of the superconducting magnets in the lab which are on the scale of a few kilohertz, a feasible solution to perform relaxation experiments at defined lower fields is shielding the sample from these influences. The Stellar spectrometer offers the possibility to compensate magnetic fields along the axis

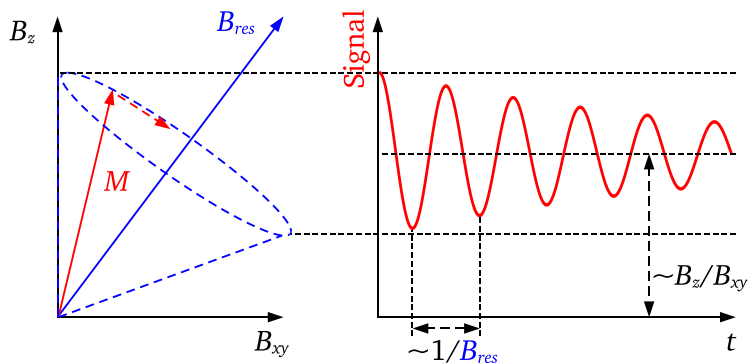


Figure 3.29: Scheme of a nutation caused by a non-compensated component of the magnetic field in the x,y -plane (adapted from [196]).

of the main coil by adjusting the offset current of the magnet with the help of a Teslameter which is inserted at the sample position before the actual relaxation experiments are started. Components of magnetic stray fields in the plane perpendicular to the axis of the main coil may be canceled out by additional coils placed around the main coil. However, it has turned out that after installing the saddle coils provided by Stelar it is still not possible to acquire reasonable magnetization curves at lower frequencies nor to successfully perform nutation experiments (see below and [194, 195]). The observation of the latter would demonstrate that the low fields are precisely controlled and stable in time.

The origin of a nutation is illustrated in Figure 3.29. If there is a component B_{xy} of the magnetic field in the x,y -plane which is not negligible compared to B_z , then the effective field \mathbf{B}_{res} is not parallel to \mathbf{z} anymore. As a result the magnetization \mathbf{M} precesses on a cone around \mathbf{B}_{res} . The acquired signal (projection on the x,y -plane) shows an oscillating exponential decay with a frequency of the Larmor frequency corresponding to B_{res} and the time constant T_1 , respectively. This allows measuring both quantities simultaneously (cf. also [133, 196]).

The fact that the nutation cannot be observed with the commercial relaxometer is due to the power supply of the magnet, since the current exhibits random spikes (some of them might be attributed to the rectified three-phase current). As a result the relaxation fields below $\nu = 10$ kHz are neither stable nor reproducible in time which leads to an unpredictable evolution of the magnetization. Thus, the drawbacks of the Stelar spectrometer are, firstly, that by construction it operates solely the single main coil for generating high (≈ 1 T), low (≈ 1 mT), and (allegedly) ultralow (≈ 10 μ T) magnetic fields and, secondly, the bipolar design of the power supply. The first requires digital-to-analog-converters which operate linearly over say five decades and the second a sophisticated compensation for leakage currents of the MOSFETs. Unfortunately up to now a solution by Stelar is lacking and relaxation experiments below $\nu = 10$ kHz are not possible with the current design of the commercial spectrometer.

The situation is more favorable in Franz Fujara's group at TU Darmstadt (Institut für Festkörperphysik). Their home-built field cycling NMR spectrometer (FC-I) [132] has been continuously upgraded during the last 10 years and in the meantime separately controls six different coils. There are three pairs of coils for compensating static fields in x -, y -, and z -direction and two B_0 -coils for the frequency ranges 30 MHz - 250 kHz and below 250 kHz. For attaining frequencies below 4 kHz there is yet another coil which is equipped with an active compensation system, i.e., the relaxation field is stabilized by simultaneously measuring the magnetic field at the sample position with a fluxgate sensor and returning this value to the PID controller. Further details are described by B. Kresse et al. in ref. [133]. Therein a reproducible nutation at very remarkable 12 Hz has been reported. Consequently, relaxation experiments at significantly lower fields than accessible with the commercial spectrometer can be reliably performed with the FC-I spectrometer and the NMR relaxation of polymers is of course an attractive area for application, which is the topic of a joint DFG project.

The goal is now to investigate the polymer dynamics on even slower time-scales than reported in Pub. 1 and 2, and to compare the obtained correlation functions to model predictions. For this purpose six PB samples with $M > M_e$ were measured both in Darmstadt and Bayreuth, and the existing master curves of three other PB samples (previously measured in Bayreuth) were supplemented by measurements in Darmstadt. The key results of Pub. 3 are:

1. The master curves now cover 10 decades in frequency (Figure 5a in Pub. 3) and are obtained by having succeeded in extending the frequency window for two decades toward lower frequencies (Figure 2 in Pub. 3).
2. The dipolar correlation functions, which now include results up to $M \approx 220M_e$, clearly reveal the protracted transition to reptation dynamics (Figure 6a in Pub. 3). This is also reflected in the very slow decrease of the M -dependent power-law exponent of regime II from $\epsilon = 0.73$ down to 0.32 (Figure 6b in Pub. 3), which however is not identical with $\epsilon = 0.25$ predicted for regime II of the tube-reptation model.
3. The FC ^1H NMR results agree well with those of DQ ^1H NMR by Vaca Chávez and Saalwächter [117, 171, 197] (Figure 7 in Pub. 3) which demonstrates that FC ^1H NMR has turned from a complementary method to DQ ^1H NMR into a competitive one.

Ad 2.: The discussed influence of constraint release and contour length fluctuations may be assessed in a forthcoming study in which "isotopic tri-block-copolymers" are investigated both by DQ and FC ^1H NMR; that is, the polymer chains have a defined number of protonated monomers in the center while the chain ends are deuterated. In this way the dynamics probed by ^1H NMR originates from the center monomers which are exposed to entanglement effects to a higher degree than the chain ends as it has been observed by simulations [104, 107, 181] and neutron

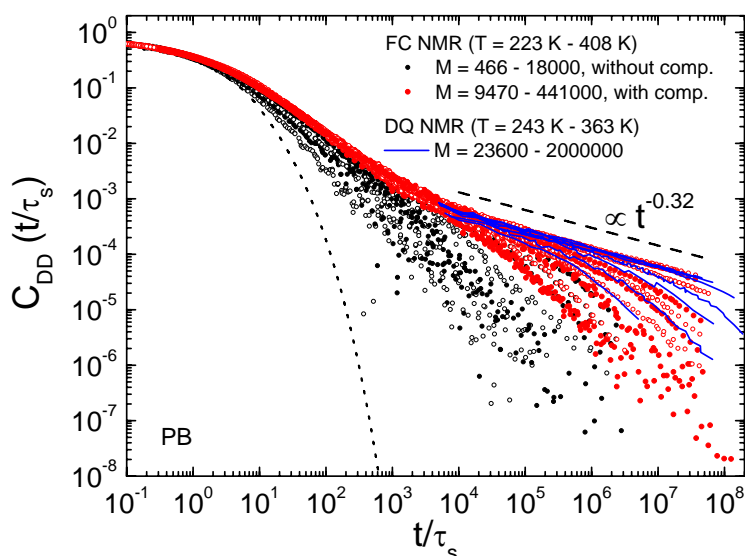


Figure 3.30: Dipolar correlation functions of PB as a function of the reduced time t/τ_s as obtained by DQ ^1H and FC ^1H NMR in the temperature and M range as specified. The DQ data are from [171]. Dotted line represents glassy dynamics. Dashed line: power-law of regime II observed for $M = 441000$.

scattering experiments [108]. It can be expected that thereby the exponent ϵ of regime II is further diminished with respect to that for completely protonated chains and comes closer to $\epsilon = 0.25$ as predicted by the tube-reptation model. In addition, blends in which the protonated and deuterated chains have different M can be investigated, e.g., to study effects of constraint release. Presumably ϵ will decrease with respect to the isotopic blend with equal M , i.e., come closer to the prediction of the tube-reptation model, if the matrix has a significantly larger M than the probe chain. However, first of all the influence of the intermolecular contribution, which is located in the same frequency range as polymer dynamics, to the total ^1H relaxation has to be investigated. This is the topic of the next Section and Pub. 4.

Ad 3.: In Figure 3.30 the dipolar correlation functions $C_{\text{DD}}(t/\tau_s)$ obtained by FC and DQ ^1H NMR for PB are compared on absolute scale. The FC data without stray field compensation correspond to Figure 2 in Pub. 1, cover about 8 decades in time, and contain molecular masses up to $M = 18000 \approx 9M_e$. They are very well complemented by the DQ data, which however begin just at $t \approx \tau_e \gg \tau_s$, to longer times and higher M . By employing the stray field compensation and including higher M , FC ^1H NMR is now able to cover also the range which was previously reserved by DQ ^1H NMR. This illustrates the strength of low-field FC ^1H NMR relaxometry: The dipolar correlation function can be traced over about 10 decades in time and 8 in amplitude, comprises also the regime of glassy dynam-

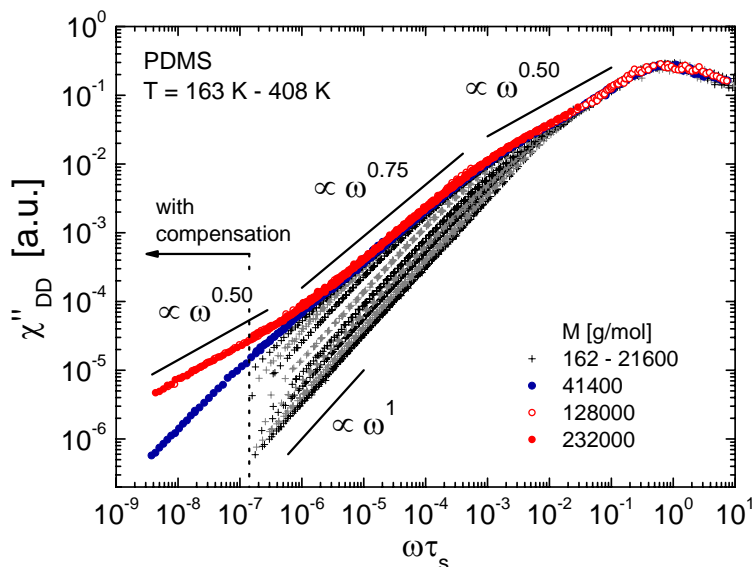


Figure 3.31: Susceptibility master curves of PDMS as a function of the reduced frequency $\omega\tau_s$ in the temperature and M range as specified. The data below $\omega\tau_s \approx 10^{-7}$ were acquired with the FC-I spectrometer in Darmstadt. Lines: observed power-laws.

ics, and, depending on M , spans all regimes of the tube-reptation model. Note that the protracted transition to reptation behavior has been disclosed also in very recent MD simulations [181] which were inspired by the joint results of FC and DQ ^1H NMR (Pub. 1, [117]).

Recently we have reported [155] a comparison of the relaxation behavior of different polymers (PB, PDMS, PI, and PPG). It remains the task of future work to study also the very low frequencies in all these systems. In perspective even lower frequencies may be accessible [133, 198]. First results for PDMS are shown in Figure 3.31. Three samples of PDMS ($M = 41400$, 128000 , and 232000) were measured with the FC-I spectrometer in Darmstadt and the corresponding master curves include about 1.5 decades below $\omega\tau_s \approx 10^{-7}$ which is the low-frequency limit in Bayreuth. While for $M = 41400$ the crossover to terminal relaxation ($\propto \omega^1$) is observed, the susceptibilities of the two samples with higher M bear the same spectral shape, i.e., they constitute the high- M envelope for PDMS in the accessible frequency range. Interestingly, they reveal a low-frequency power-law which can be only vaguely anticipated from the Bayreuth data alone (cf. Figure 4a in Pub. 2) and its power-law exponent $\epsilon = 0.50$ at low reduced frequencies is different from that of PB ($\epsilon = 0.32$) and that predicted by the tube-reptation model for regime II ($\epsilon = 0.25$). This result will be discussed in the context of the findings of the next section.

3.5 Reorientational and Translational Dynamics in Entangled Polymer Melts

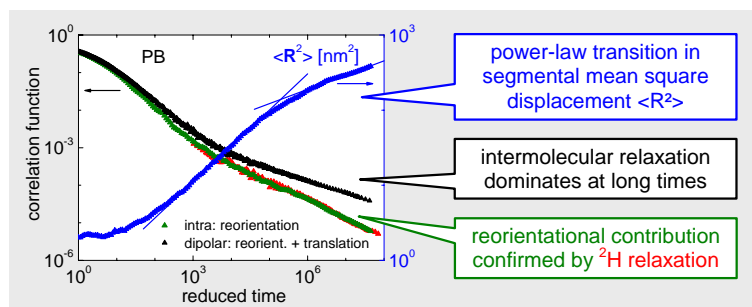


Figure 3.32: Table of Content Graphic (adapted from Pub. 4).

The analyses of FC ^1H NMR results of polymers in literature [153, 180, 185, 199], in previous works [56, 69, 77, 151, 155, 161], in Pub. 1 - 3, and also of DQ ^1H NMR results [117, 171, 197] assume that the dynamics reflected by the measured ^1H spin-lattice relaxation rate $R_{1,\text{DD}}(\omega) = 1/T_{1,\text{DD}}(\omega)$ is essentially molecular reorientation and that therefore translational contributions are negligible. Since the ^1H relaxation is caused by fluctuations of the magnetic dipole-dipole (DD) interaction and coupled spins may be situated on the same or different molecules, $R_{1,\text{DD}}(\omega)$ is a sum of intramolecular and intermolecular contributions $R_{1,\text{intra}}(\omega)$ and $R_{1,\text{inter}}(\omega)$, respectively. As a consequence these two contributions are related to reorientational and translational dynamics, respectively. However, most often the dominance of the first has been presumed, i.e., $R_{1,\text{DD}}(\omega) \approx R_{1,\text{intra}}(\omega)$, and the focus has been on interpreting the spectra in the context of model predictions which deal with reorientational dynamics only. This issue has been re-addressed by Kimmich, Fatkullin, and coworkers [36, 47, 154] who have pointed out that at low frequencies the intermolecular contribution is significant [142, 143, 154]. For DQ ^1H NMR results [117] of PB no separation has been attempted and it has been claimed that isotopic dilution does not affect the power-law of the correlation function in regime II. Note that the ^1H relaxation results of PDMS melts (cf. Figure 3.23 and [170]), which exhibit an M -independent "shoulder" on the low-frequency side of the relaxation maximum as it has been found for glycerol ([186], Pub. 2), yet not for PB or OTP, have triggered in our group also the investigation of the influence of intermolecular relaxation in low- M liquids [38, 172–174].

The objective is now to examine the effect of intermolecular contributions on the relaxation behavior of entangled polymer melts by decomposing the ^1H relaxation rate (or equivalently the susceptibility) into intramolecular and intermolecular parts. For this purpose isotopic dilution experiments were performed with PDMS and two different M of PB. That is, a protonated polymer is diluted in its deuterated counterpart with similar M , which yields blends with different molar fractions x_{H} of protons. Here the intramolecular contribution is given at infinite

dilution $x_H \rightarrow 0$ and it can be revealed experimentally by extrapolating the rates $R_{1,DD}(x_H)$ to $x_H = 0$. Another source is FC ^2H NMR relaxation with completely deuterated samples which yields $R_{1,Q}(\omega) \approx R_{1,\text{intra}}(\omega)$ and thus directly represents segmental reorientation dynamics.

While the pioneering work of Kimmich et al. [142] was restricted to just one temperature, we applied more than 10 temperatures in order to enlarge the frequency range by constructing susceptibility master curves. Finally the intramolecular relaxation rate yields the reorientational correlation function $C_2(t)$ by Fourier transform and the intermolecular contribution provides the segmental mean square displacement $\langle \mathbf{R}^2(t) \rangle$ by following an approach derived by Fatkullin [142]. Their time-dependence and mutual relationship can be compared to the predictions of the tube-reptation model.

In the case of polybutadiene, PB 24300-h₆ was dissolved in PB 22800-d₆ at four molar fractions x_H and PB 196000-h₆ was dissolved in PB 191000-d₆ at $x_H = 16\%$. The ^1H relaxation experiments were performed with the Stellar spectrometer in Bayreuth in the temperature range from 223 K to 393 K, while data at the highest temperature were also measured with the home-built relaxometer in Darmstadt to cover frequencies $\nu < 10$ kHz (see also Section 3.4). In addition the ^2H relaxation rate was measured for two temperatures in Darmstadt. Blends of PDMS 21600-h₆ with PDMS 25300-d₆ with three different x_H were investigated in the temperature range from 173 K to 408 K in Bayreuth [172] as a second system and to clarify the origin of the low-frequency shoulder. The data of the completely protonated ($x_H = 100\%$) PB and PDMS are from Pub. 3 and [170], respectively. The results were published in Pub. 4 and are summarized in the following:

1. The relaxation behavior of the PB blends essentially confirms the results by Kehr et al. [142] at one temperature: The relaxation rate is reduced while diminishing x_H (Figure 1 in Pub. 4) and for low frequencies the intermolecular contribution is dominating (Figure 3 in Pub. 4).
2. The (total) dipolar and the (separated) intramolecular and intermolecular correlations functions $C_{DD}(t/\tau_s)$, $C_{\text{intra}}(t/\tau_s)$, and $C_{\text{inter}}(t/\tau_s)$, respectively, embrace about 9 decades in time (Figure 4 in Pub. 4) and significantly differ. They clearly demonstrate the influence of the intermolecular contribution on the long-time (or low-frequency) relaxation behavior which is characterized by a power-law $t^{-\epsilon}$. In general the correlation decay of $C_{\text{intra}}(t/\tau_s)$ is faster than that of $C_{DD}(t/\tau_s)$, while that of $C_{\text{inter}}(t/\tau_s)$ is slower. Explicitly, $\epsilon = 0.49$ is found for the intramolecular part which is significantly higher than $\epsilon = 0.32$ of the total correlation function and different from $\epsilon = 0.25$ predicted for regime II of the tube-reptation model.
3. The reorientational correlation function $C_2(t/\tau_s)$ obtained by FC ^2H NMR experiments coincides well with $C_{\text{intra}}(t/\tau_s)$ determined from ^1H relaxation. The results of the separation procedure are corroborated by the ^2H relaxation results.

4. The segmental mean square displacement $\langle \mathbf{R}^2(t) \rangle$ reveals two power-law regimes t^α (Figure 5 in Pub. 4). While $\alpha = 0.49$ for both M at short times, at longer times a weaker power $\alpha = 0.19$ is observed for the higher M , and a transition toward terminal relaxation is seen for the lower M . The exponents are in accord with the predictions of the tube-reptation model for regimes I ($\alpha = 0.5$) and II ($\alpha = 0.25$), respectively, and can be compared to reports from simulations [104, 200] and neutron scattering [98].
5. By attaining $C_2(t)$ and concomitantly $\langle \mathbf{R}^2(t) \rangle$ it can be concluded that the relation $C_{\text{intra}}(t) \propto [\langle \mathbf{R}^2(t) \rangle]^{-1}$ as assumed by the tube-reptation model is not fulfilled.
6. The isotopic blends of PDMS 21600 exhibit a similar behavior than those of PB 24300 and therefore basically corroborate the results of PB. However, in PDMS the dominance of the intermolecular contribution is very strong which begins to govern the relaxation behavior already one frequency-decade below the main relaxation peak (Figure 7 in Pub. 4). Consequently, the M -independent "shoulder" observed in the master curves of the PDMS melts (cf. Figure 3.23) does not originate from an anomalous intramolecular relaxation as concluded in [155], but from the supremacy of the intermolecular part. Since distinctive entanglement effects are not established for $M \approx 2M_e$ yet, only the power-law of regime I is seen in $\langle \mathbf{R}^2(t) \rangle$. Profiting from the dominating intermolecular contribution, $\langle \mathbf{R}^2(t) \rangle$ of entangled PDMS ($M \gg M_e$) is attained from the susceptibility $\chi''_{\text{DD}}(\omega\tau_s)$ of completely protonated PDMS with $M = 232000$ and yields a crossover to a weaker power-law at long times (Figure 5 in Pub. 4).
7. An isotope effect is observed in the blends of PDMS and PB which is disclosed by the correlation times being dependent on x_{H} (Figure 8 in Pub. 4) at a given temperature. This is a crucial point since the relaxation rates $R_{1,\text{DD}}(x_{\text{H}})$ at some applied temperatures do not exhibit a linear behavior. The latter is merely achieved by constructing the susceptibility master curves (Figure 9 of Pub. 4).

Ad 1. and 7.: It is worthwhile to note that also in the isotope dilution series of PB 196000 at $T = 355\text{ K}$ of Kehr et al. [142] a nonlinear dependence of $R_{1,\text{DD}}(x_{\text{H}})$ can be found. This is shown in Figure 3.33a, in which cuts through $R_{1,\text{DD}}(\nu)$ at some frequencies are plotted. A linear extrapolation including all molar fractions would clearly lead to significant uncertainties of the intramolecular contribution ($x_{\text{H}} = 0$) which have not been discussed therein. For the PB blends with $M = 196000$ and 24300 studied in our work a similar picture emerges for $T = 393\text{ K}$ in Figure 3.33b and 3.33c, respectively. At $T = 298\text{ K}$ the relaxation rates of different x_{H} even cross each other which results in the drop of the amplitudes observed for $x_{\text{H}} = 53\%$ (Figure 3.33d).

Ad 5.: If the assumption $C_{\text{intra}}(t) \propto [\langle \mathbf{R}^2(t) \rangle]^{-1}$ is true, the product $C_{\text{intra}}(t) \cdot$

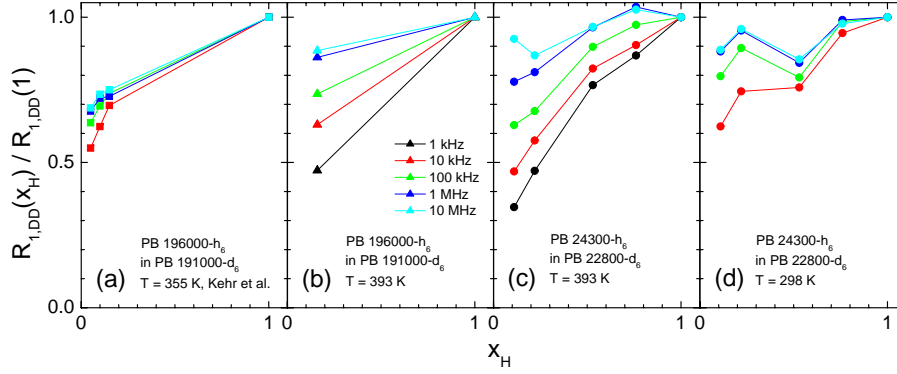


Figure 3.33: ^1H relaxation rates $R_{1,DD}(x_H)$ of the polymer blends and temperatures as indicated scaled by $R_{1,DD}(x_H = 1)$. Data in (a) are from [142]. Lines: guide for the eye.

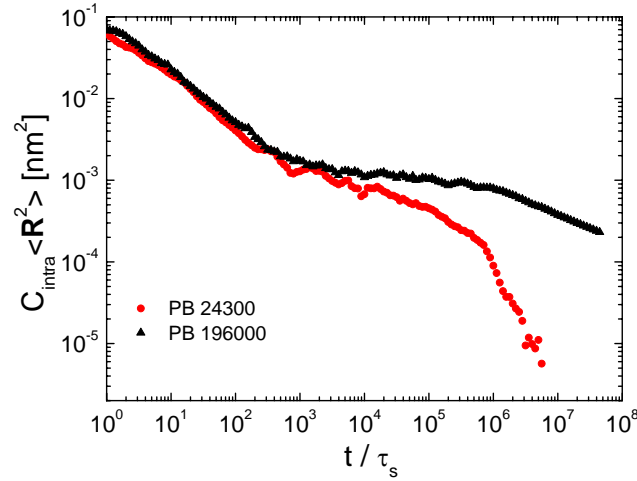


Figure 3.34: "Return to origin plot" of the PB blends with $M = 24300$ and 196000 .

$\langle \mathbf{R}^2(t) \rangle$ ("return to origin plot") yields a time-independent constant in regimes II and III, i.e., for $\tau_e < t < \tau_d$. Instead in regime II, i.e., for $t/\tau_s > 10^3$, a decaying curve with a slope reflecting the difference $\alpha - \epsilon$ of the exponents is observed (Figure 3.34). A similar behavior has been observed in simulations when constrained release was effective [181].

Ad 7.: Tentatively, the isotope effect is ascribed to a frequency-shift of the main relaxation peak with x_H at a given temperature (Figure 10 in Pub. 4), i.e., to a change of the time constant τ_s . Since this could also be caused by remaining solvent during sample preparation, it has been ensured that the solvent is completely removed by the preparation process (Figure 1a of Pub. 4). In addition the homogeneous mixing of the protonated and deuterated chains has been examined

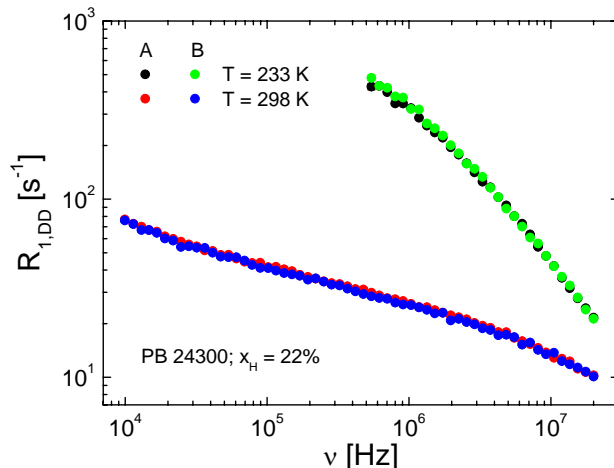


Figure 3.35: ^1H relaxation rates $R_{1,DD}(\nu)$ of PB 24300 at $x_{\text{H}} = 22\%$ for the two different temperatures as indicated. "A" and "B" denote first run and second run after repeated sample preparation, respectively.

exemplarily by dissolving the PB 24300 blend with $x_{\text{H}} = 22\%$ once more and subsequently removing the solvent again. No difference between the two measurements A (first run) and B (second run after repeated sample preparation) is observed in Figure 3.35. Thus, these well reproducible results and the fact that the same effect is found also for PDMS and in the literature [142] give confidence that the isotopic dilution was conducted correctly and emphasize again the necessity to create susceptibility master curves.

In conclusion, revisiting the idea of Kehr et al. [142, 143] and augmenting their experiments by investigating more M and a broader range of temperatures and frequencies yields results which go far beyond those reported therein. It has been demonstrated that the intramolecular contribution $\chi''_{\text{intra}}(\omega\tau_s)$ extracted from the isotope dilution experiment is identical with $\chi''_{\text{Q}}(\omega\tau_s)$ probed by FC ^2H NMR. Furthermore, for the first time FC NMR has revealed two power-law regimes for the segmental mean square displacement and it has been shown that they are associated with the regimes of free (I) and constrained Rouse dynamics (II) as predicted by the tube-reptation model. However, it is only possible to analyze the isotope dilution experiments by representing the data as susceptibility master curves – a finding eminently important for future works.

A very reliable possibility of determining the intramolecular part is investigating deuterated polymers by means of FC ^2H NMR (cf. Figure 2 in Pub. 4). Besides comparing it to $\chi''_{\text{intra}}(\omega)$ obtained from isotopic dilution results, also a discrimination between intramolecular and intrasegmental (of coupled spins within, e.g., a Rouse unit) contributions may be achieved, which has not been performed satisfactorily yet ([143], Pub. 4). Especially in the case of PDMS, firstly, low-frequency

measurements with the home-built relaxometer in Darmstadt and, secondly, a ^2H relaxation study appear to be very profitable to confirm the strong intermolecular contribution and to elucidate the shape of the intramolecular contribution in regime II for $M \gg M_e$. Since it has been proven that the susceptibility $\chi''_{\text{DD}}(\omega\tau_s < 0.1)$ is dominated by the intermolecular contribution, i.e., translational motion, the power $\epsilon = 0.50$ found at low frequencies in $\chi''_{\text{DD}}(\omega\tau_s)$ of PDMS 232000 must not be compared with the prediction in terms of reorientational dynamics for regime II of the tube-reptation model (Section 3.4). It may be expected that isotopic dilution experiments for PDMS at lower frequencies and $M \gg M_e$ will discover a second power-law of $\chi''_{\text{intra}}(\omega\tau_s)$.

Extending the time dependence of the segmental mean square displacement $\langle \mathbf{R}^2(t) \rangle$ toward longer times remains an ultimate goal. This can be attained by applying Field Gradient (FG) ^1H NMR diffusometry, which probes long-time dipolar correlations. For high- M PDMS it has been shown that the transition from regime III to IV can be accessed by inspecting the time dependence of the apparent self-diffusion coefficient obtained from stimulated echo experiments [106]. However, in entangled polymer melts it has turned out that the residual dipolar coupling is not negligible, i.e., the anisotropic segmental dynamics cause an incomplete motional averaging of dipolar correlations [201]. Therefore the measurements have to be performed in two different magnetic field gradients in order to eliminate the dipolar correlation effect which is independent of the applied gradient. It remains the challenge of future works to match $\langle \mathbf{R}^2(t) \rangle$ obtained from FC and FG ^1H NMR in regimes II or III.

3.6 Linear Polymers in Solution

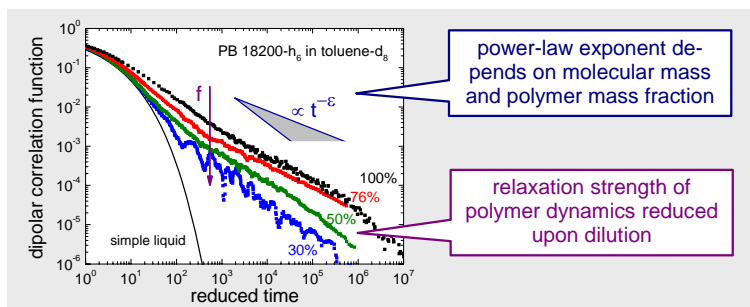


Figure 3.36: Table of Content Graphic (adapted from Pub. 5).

Up to now neat polymers have been studied by NMR relaxometry in this thesis and the results have been compared to the predictions of the tube-reptation model for high- M polymer melts. How polymer dynamics is modified upon dilution with respect to that of the melt has been subject to many studies by rheology and is now considered as textbook knowledge [80, 159, 169]. The relaxation behavior of polymers in solution has been analyzed also in reports by dielectric spectroscopy [66]. First experiments by FC NMR were performed by Kimmich and co-workers and the T_1 dispersions of PDMS diluted in CCl_4 at different concentrations have been compared [180]. The authors have claimed to observe a transition from entanglement dynamics for high M to Rouse dynamics upon dilution [36]. However, their study included results only for one temperature and the analysis did not take the concentration dependence of the time constant τ_s of segmental dynamics into account, which also drives the polymer dynamics. Preliminary own measurements [170] of PB in solution have already indicated that the polymer relaxation strength f is reduced upon dilution. That is, the low-frequency part of the master curves reflecting the relaxation contribution due to polymer dynamics is diminished. However, the PB samples studied therein had a wide distribution of molecular masses and the solvent (CCl_4) turned out to be inappropriate.

The aim is now to investigate PB with well-defined molecular masses systematically for different $M > M_e$, various concentrations, and in a broad temperature range, and to utilize the same approach for analyses which has been successfully used for bulk polymer melts. Deuterated toluene was chosen as solvent and samples with 10 different concentrations for PB 9470, three for PB 18200, and one for PB 47000 were prepared and measured with the Stellar relaxometer. Note that the given concentrations c refer to the mass fraction of the polymer. The data of the pure PB melts are from Pub. 3. The obtained relaxation data are transformed to the susceptibility representation, FTS is applied, and master curves $\chi''_{\text{DD}}(\omega\tau_s)$ are constructed. The polymer relaxation features are analyzed both in the frequency domain and in the time domain by accessing the dipolar correlation function $C_{\text{DD}}(t/\tau_s)$ via Fourier transform. Note that the master curves of the

pure PB 18200 and PB 18000 are identical in the frequency range accessible by the Stellar relaxometer – as expected due to the tiny difference in M . Since the latter sample has also been measured toward lower frequencies in Darmstadt (cf. Pub. 3) both are used equivalently. The central results are summarized in the following:

1. The susceptibility master curves $\chi''_{\text{DD}}(\omega\tau_s)$ (Figure 1 in Pub. 5) reflect the regimes of glassy, free Rouse, and entanglement dynamics as determined from the undiluted PB. The relaxation features of polymer dynamics, i.e., the excess intensity at $\omega\tau_s < 1$, are continuously diminished upon dilution. That is, the relaxation strength $f(c)$ of polymer dynamics is reduced with decreasing c in a similar way for all M (Figure 3a of Pub. 5). For high c the decay is similar to that of the plateau modulus $G_N^0(c) = G_N^0(1)c^{2.3}$, which is a comparable quantity obtained by rheology. Moreover, it appears that in the applied concentration range the intermolecular contribution is not reduced, since amplitude of the relaxation maximum which is associated with the dipolar coupling constant (cf. eq. 3.19) is not systematically changed.
2. By construction of the master curves the time constants $\tau_s(T)$ of segmental motion are provided (Figure 2 in Pub. 5) which show an acceleration of the dynamics upon dilution (plasticizer effect) due to the concentration dependence of the monomeric friction coefficient. This results in a decreased glass transition temperature $T_g(c)$ for lower polymer mass fractions.
3. Evaluating the susceptibility $\chi''_{\text{DD}}(\omega\tau_s)$ of PB 9470 in solution at lowest frequencies yields the concentration dependence of the terminal relaxation time $\tau_d(c)$ (Figure 3b in Pub. 5). It is decreased upon dilution and essentially follows the behavior $\tau_d(c) \propto c^{2.3}$ expected from rheology [159].
4. The dipolar correlation functions $C_{\text{DD}}(t/\tau_s)$ (Figure 4a in Pub. 5) obtained by Fourier transform of the master curves exhibit at long times two power-law regimes $\propto t^{-\epsilon}$, which are attributed to the regimes I and II of the tube-reptation model. In order to consider only the contribution of polymer dynamics, i.e., to remove the influence of the segmental dynamics, the separated correlation function of the polymer dynamics $C_{\text{polymer}}(t/\tau_s)$ is attained (Figure 4b in Pub. 5) and the c -dependent long-time exponent ϵ (regime II) is extracted (Figure 5 of Pub. 5). It is increased from its bulk value upon dilution up to values close to $\epsilon = 1$ as expected for the Rouse regime and thus demonstrates the diminished contribution of entanglement dynamics.
5. From the increase of ϵ it is deduced that the entanglement molecular mass $M_e(c)$ increases for lower polymer mass fractions (inset of Figure 5 of Pub. 5) as expected from rheology [169] via $M_e(c) = M_e(1)c^{-1.3}$. If $M_e(c)$ for low

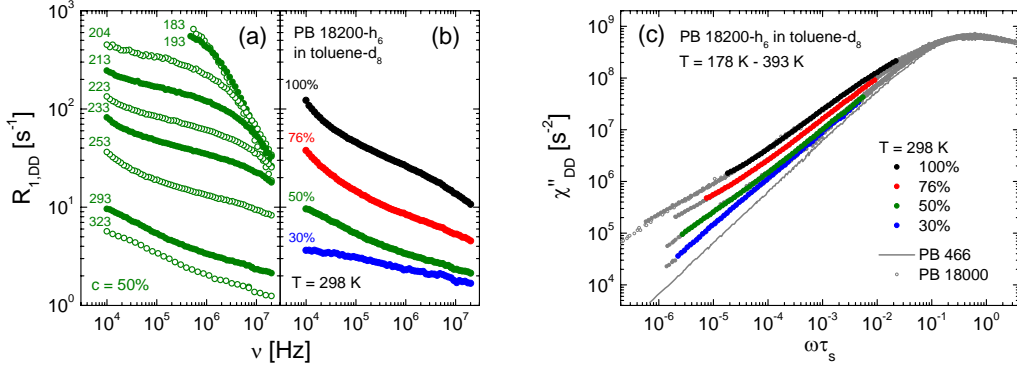


Figure 3.37: ^1H relaxation rate $R_{1,\text{DD}}(\nu) = 1/T_{1,\text{DD}}(\nu)$ of PB 18200- h_6 diluted in toluene- d_8 (a) at $c = 50\%$ polymer mass fraction and in the temperature range (in K) as indicated, and (b) for $T = 298\text{ K}$ and different concentrations. (c) Susceptibility master curves of PB 18200- h_6 including all concentrations and temperatures as indicated. The susceptibilities obtained for $T = 298\text{ K}$ are highlighted in color.

concentrations is not small compared to M anymore, the feature of entanglement dynamics, i.e., the long time shoulder, is suppressed in the polymer correlation function $C_{\text{polymer}}(t/\tau_s)$.

Ad 1.: The measured proton relaxation rates $R_{1,\text{DD}}(\nu)$ reflect features which depend on temperature, polymer mass fraction, and molecular mass. In Figure 3.37a the proton relaxation rates $R_{1,\text{DD}}(\nu)$ of PB 18200- h_6 diluted in toluene- d_8 at $c = 50\%$ for various applied temperatures are displayed. For comparison the rates at different concentrations and fixed temperature are displayed in Figure 3.37b. They reflect differently strong dispersion regimes depending on temperature and c -dependent changes of the spectral shape, respectively. Note that Kimmich and co-workers have concluded from the results [36, 180] at a single temperature that with increasing dilution the interval between segmental motion and entanglement dynamics is enlarged yielding space for Rouse dynamics. This is apparently supported by Figure 3.37b. However, the concentration dependence of the monomeric friction coefficient (or equivalently τ_s , cf. Figure 2 of Pub. 5) has to be taken into account. Therefore a representation with a reference time is needed which is achieved by the susceptibility master curves and the scaling on the segmental correlation time τ_s . In Figure 3.37c it is explicitly shown that the relaxation processes at fixed temperature ($T = 298\text{ K}$, in color) and different concentrations are differently separated from the α -process. Thus, from this representation it can be concluded that the observed changes of $R_{1,\text{DD}}(\nu)$ (Figures 3.37 a and b) are due to both a shift toward lower reduced frequencies and a diminished polymer relaxation strength.

Ad 2.: Extending the obtained time constants $\tau_s(T)$ toward lower temperatures

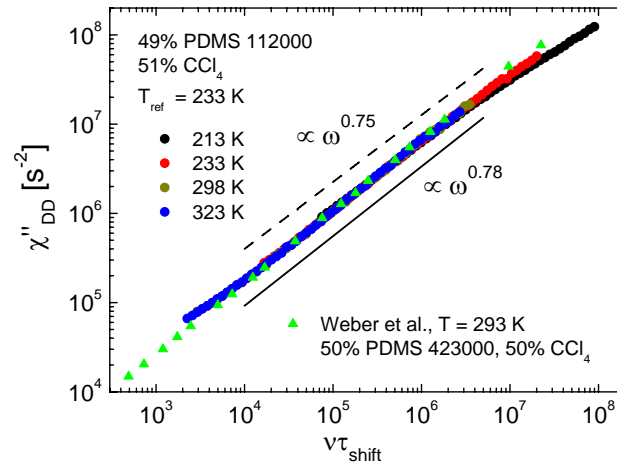


Figure 3.38: Susceptibility master curves as a function of the reduced frequency $\nu\tau_{\text{shift}}$ for PDMS with $M = 112000$ in CCl_4 at polymer mass fraction $c = 49\%$ in the temperature range as indicated. Triangles: literature data [180] for comparison. Dashed line: power-law behavior of the undiluted high- M PDMS melt. Line: power-law behavior observed for PDMS 112000 at $c = 49\%$.

with complimentary measurements by dielectric spectroscopy (DS) could, firstly, provide a verification of $\tau_s(T)$ by a different technique; secondly, it might also reveal how $\tau_s(T)$ of the lowest concentration approaches that of the pure diluent. In addition the investigation of polyisoprene (PI) in solution by broadband DS appears very attractive, as both the time constants τ_α and τ_n reflecting the segmental dynamics and the terminal relaxation time, respectively, can be extracted from the spectra (cf. Section 3.1). However, a combined study by DS and FC NMR may be hampered by the low polymer relaxation strength f of PI ([155] and Pub. 2).

Ad 4.: It appears that ϵ is reduced at higher M/M_e only for much lower polymer mass fractions. Thus, in future studies also very high M should be investigated, i.e., for which the predicted $\epsilon = 0.25$ for the bulk melt is almost reached.

A similar trend as observed for PB can be anticipated from the preliminary results of PDMS with $M = 112000$ and $c = 49\%$ in CCl_4 which are shown in Figure 3.38. Measurements below $T = 213\text{ K}$ were impeded by crystallization, i.e., it was not possible to reach the the relaxation maximum which would be expected at higher frequencies and lower temperatures. With the available relaxation data a master curve is created by applying FTS for the temperature range $T = 213\text{ K} - 323\text{ K}$ and the reference temperature $T_{\text{ref}} = 233\text{ K}$. For the reduced frequencies $10^4 < \nu\tau_{\text{shift}} < 5 \cdot 10^6$ a power-law behavior $\propto \omega^{0.78}$ is observed, which has a slightly higher exponent than the power-law $\propto \omega^{0.75}$ found for the undiluted high- M PDMS (Figure 7 in Pub. 4 and cf. Figure 3.23). A direct comparison of the master curves of undiluted and diluted PDMS in the isofrictional representa-

tion $\chi''_{\text{DD}}(\omega\tau_s)$ is unfeasible, since for the latter the the time constant τ_s could not be extracted. However, it appears that also for PDMS in solution the relaxation strength is reduced upon dilution, as the low-frequency part ($\omega\tau_s < 1$) of the master curve with diluted polymer decreases steeper than that of the pure melt. This is corroborated by the agreement with the results by Weber and Kimmich [180] for high- M PDMS with similar c at $T = 293$ K. The fact that the difference between the exponents is so small on the one hand may be explained in analogy with the finding for PB, that ϵ is significantly reduced at higher M/M_e only for much lower polymer mass fractions (cf. Figure 5 of Pub. 5). On the other hand it has been shown in Pub. 4 by an isotopic dilution experiment that the power-law $\propto \omega^{0.75}$ in the case of PDMS is due to the dominating contribution of the intermolecular relaxation, which is just reduced in amplitude yet not changed in terms of the power-law exponent in the relevant frequency range.

In conclusion, by utilizing the susceptibility representation and applying FTS, the results obtained on a microscopic level by NMR relaxometry for linear polymers in solution corroborate those of rheology which are considered as textbook knowledge. Thus, FC NMR is again proven as a competitive technique and may be referred to as "molecular rheology".

4 Publications

List of included publications as referred to in this thesis

- Pub. 1** Dipolar and Bond Vector Correlation Function of Linear Polymers Revealed by Field Cycling ^1H NMR: Crossover from Rouse to Entanglement Regime.
Herrmann, A.; Novikov, V. N.; Rössler, E. A.
Macromolecules **2009**, *42*, 2063-2068.
- Pub. 2** Universal Polymer Dynamics Revealed by Field Cycling ^1H NMR.
Herrmann, A.; Kariyo, S.; Abou Elfadl, A.; Meier, R.; Gmeiner, J.; Novikov, V. N.; Rössler, E. A.
Macromolecules **2009**, *42*, 5236-5243.
- Pub. 3** Protracted Crossover to Reptation Dynamics: A Field Cycling ^1H NMR Study Including Extremely Low Frequencies.
Herrmann, A.; Kresse, B.; Gmeiner, J.; Privalov, A. F.; Kruk, D.; Fujara, F.; Rössler, E. A.
Macromolecules **2012**, *45*, 1408-1416.
- Pub. 4** Mean square displacement and reorientational correlation function in entangled polymer melts revealed by field cycling ^1H and ^2H NMR relaxometry.
Herrmann, A.; Kresse, B.; Wohlfahrt, M.; Bauer, I.; Privalov, A. F.; Kruk, D.; Fujara, F.; Rössler, E. A.
Macromolecules **2012**, *45*, 6516-6526.
- Pub. 5** Dynamics of Linear Polybutadienes in Solution Studied by Field Cycling ^1H NMR
Herrmann, A.; Rössler, E. A.
ACS Macro Letters **2012**, *1*, 1339-1342.

Individual contributions to joint publications

- Pub. 1** I conducted all experiments for the samples listed in Table 1 therein. The other samples were measured by S. Kariyo and previously published in [77]. I performed all analyses during my Ph.D. studies.
- Pub. 2** I conducted all experiments for the samples listed in Table 1 therein as part of my preceding diploma thesis except for:
Propylene glycol was measured by R. Meier,
PB 466-h₆ and PB 2020-h₆ were measured by S. Kariyo and previously published in [151],
PB 35300-h₆ was already contained in Pub. 1,
PI 111000-h₅ and PI 127000-h₃ were measured by S. Kariyo and previously published in [185],
PI 157000-h₈ was measured by A. Abou Elfadl.
I performed all analyses during my Ph.D. studies.
- Pub. 3** I conducted all experiments with the Stellar spectrometer in Bayreuth for the samples listed in Table 1 therein. The low-frequency measurements were done by B. Kresse and me in Darmstadt. All other samples were already contained in Pub. 1. I performed all analyses during my Ph.D. studies.
- Pub. 4** I conducted all experiments with the Stellar spectrometer in Bayreuth for the PB samples. The low-frequency measurements were done by B. Kresse in Darmstadt. PB 24300-h₆ and PB 196000-h₆ were already contained in Pub. 3. The PDMS blends were measured by M. Wohlfahrt [134]. I performed all analyses during my Ph.D. studies.
- Pub. 5** I conducted all experiments. The completely protonated PB samples were already contained in Pub. 3. I performed all analyses during my Ph.D. studies.

Other publications

- From Simple Liquid to Polymer Melt. Glassy and Polymer Dynamics Studied by Fast Field Cycling NMR Relaxometry: Low and High Molecular Weight Limit.
Kariyo, S.; Brodin, A.; Gainaru, C.; Herrmann, A.; Schick, H.; Novikov, V. N.; Rössler, E. A.
Macromolecules **2008**, *41*, 5313–5321.
- From Simple Liquid to Polymer Melt. Glassy and Polymer Dynamics Studied by Fast Field Cycling NMR Relaxometry: Rouse Regime.
Kariyo, S.; Brodin, A.; Gainaru, C.; Herrmann, A.; Hintermeyer, J.; Schick, H.; Novikov, V. N.; Rössler, E. A.
Macromolecules **2008**, *41*, 5322–5332.
- Molecular Weight Dependence of Glassy Dynamics in Linear Polymers Revisited.
Hintermeyer, J.; Herrmann, A.; Kahlau, R.; Goiceanu, C.; Rössler, E. A.
Macromolecules **2008**, *41*, 9335–9344.
- Molecular Weight Dependence of Fragility in Polymers.
Abou Elfadl, A.; Herrmann, A.; Hintermeyer, J.; Petzold, N.; Novikov, V. N.; Rössler, E. A.
Macromolecules **2009**, *42*, 6816–6817.
- From Rouse to Fully Established Entanglement Dynamics: A Study of Polyisoprene by Dielectric Spectroscopy.
Abou Elfadl, A.; Kahlau, R.; Herrmann, A.; Novikov, V. N.; Rössler, E. A.
Macromolecules **2010**, *43*, 3340–3351.
- Polymer Dynamics of Polybutadiene in Nanoscopic Confinement As Revealed by Field Cycling ^1H NMR.
Hofmann, M.; Herrmann, A.; Ok, S.; Franz, C.; Kruk, D.; Saalwächter, K.; Steinhart, M.; Rössler, E. A.
Macromolecules **2011**, *44*, 4017–4021.
- Glassy, Rouse, and Entanglement Dynamics As Revealed by Field Cycling ^1H NMR Relaxometry
Hofmann, M.; Herrmann, A.; Abou Elfadl, A.; Kruk, D.; Wohlfahrt, M.; Rössler, E. A.
Macromolecules **2012**, *45*, 2390–2401.
- Field-cycling NMR relaxometry of viscous liquids and polymers.
Kruk, D.; Herrmann, A.; Rössler, E. A.
Progress in Nuclear Magnetic Resonance Spectroscopy **2012**, *63*, 33–64.

- Long-Time Diffusion in Polymer Melts Revealed by ^1H NMR Relaxometry. Meier, R.; Herrmann, A.; Kresse, B.; Privalov, A. F.; Kruk, D.; Fujara, F.; Rössler, E. A.
ACS Macro Letters **2012**, *submitted*.

Publication 1

Dipolar and Bond Vector Correlation Function of Linear Polymers Revealed by Field Cycling ^1H NMR: Crossover from Rouse to Entanglement Regime.

Herrmann, A.; Novikov, V. N.; Rössler, E. A.
Macromolecules **2009**, *42*, 2063-2068.

Copyright 2009 by The American Chemical Society
DOI: 10.1021/ma802818j

Dipolar and Bond Vector Correlation Function of Linear Polymers Revealed by Field Cycling ^1H NMR: Crossover from Rouse to Entanglement Regime

A. Herrmann,[†] V. N. Novikov,[‡] and E. A. Rössler^{*†}

Experimentalphysik II, Universität Bayreuth, 95440 Bayreuth, Germany, and IA&E, Russian Academy of Sciences, Novosibirsk, 630090, Russia

Received December 18, 2008; Revised Manuscript Received January 15, 2009

ABSTRACT: We apply field cycling NMR to study segmental reorientation dynamics in melts of linear 1,4-polybutadiene (PB) in the entanglement regime ($M \geq M_e$). Dispersion data of the spin–lattice relaxation time $T_1(\omega)$ are transformed to the susceptibility representation $\chi''(\omega) = \omega/T_1(\omega)$, and using frequency temperature superposition master curves $\chi''(\omega\tau_s)$ are constructed which reflect spectral contributions from glassy as well as polymer specific dynamics. The correlation time τ_s is determined by glassy dynamics. Transforming $\chi''(\omega\tau_s)$ into the time domain and studying the crossover from Rouse to entanglement regime, the full dipolar or segmental reorientational correlation function $F_2(t/\tau_s)$ is presented covering six decades in amplitude and 8 decades in time. Assuming $F_2(t) \cong \langle \mathbf{u}_b(t)\mathbf{u}_b(0) \rangle^2$ the bond vector correlation function $\phi_b(t) = \langle \mathbf{u}_b(t)\mathbf{u}_b(0) \rangle$ is obtained. Reaching $Z = M/M_e \cong 9$, comparison with theoretical predictions by the tube-reptation model as well as renormalized Rouse theory reveals significant discrepancies whereas good agreement is found with simulations. The crossover to entanglement dynamics appears to be very protracted.

1. Introduction

The dynamics of polymer melts comprises both polymer specific dynamics as well as glassy dynamics. Whereas “polymer dynamics” originate from collective dynamics of Rouse and reptation type,¹ glassy dynamics^{2–4} are attributed to “segmental” or “local” relaxation of the polymer chain. However, one has to keep in mind that the glass transition phenomenon itself includes cooperative motion with a dynamic correlation length presumably on the order of 1–10 nm. Regarding the interplay of polymer and glassy dynamics, detailed information is provided by molecular dynamics simulation.^{5,6} Considering the mean square displacement of an (inner) monomer in a nonentangled chain, a crossover from the initial ballistic behavior to a plateau region is identified and attributed to the cage effect, the latter being well described by the mode coupling theory of the glass transition.⁷ At longer times polymer specific subdiffusive behavior sets in which is described by Rouse theory, and finally at longest times normal diffusive behavior of the entire polymer is observed. Thus, regarding monomer relaxation only beyond the time scale of cage formation polymers and simple liquids substantially differ, and one can identify the segmental correlation time τ_s with the time scale of the α -process characterizing glassy dynamics. The latter drives the polymer dynamics via controlling the monomeric friction coefficient.

The present publication is part of a series of papers addressing the analysis of fast field cycling (FFC) NMR data for linear polymer melts.^{8,9} Preliminary results have been reported in ref 10. In the preceding work we have argued that, in order to properly access quantitative aspects of the spectral contributions due to polymer specific dynamics, the generally much stronger contribution of glassy dynamics has to be accounted for. As a first approach, assuming statistical independence and time scale separation the individual contributions to the total spectrum have been taken to be additive and “polymer spectra” have been obtained by subtracting the “glassy spectrum” from the overall spectrum. The integral over the polymer spectrum

with respect to the total spectrum then provides a measure of the polymer relaxation strength. The so obtained polymer spectra significantly differ from the overall spectra in the case of Rouse dynamics of nonentangled polymers, i.e. when moderately long chain lengths are considered. In this regime, the glass transition temperature T_g is a function of M ,¹¹ and thus the spectra have to be rescaled by τ_s to provide “iso-frictional” spectra which allow comparison among polymers with different M .^{8,9}

The separation of glassy dynamics and Rouse dynamics may be challenged as in a strict sense time scale separation leading to an additive decomposition is only partly given. The situation is less severe in the entanglement regime, i.e., above M_e , as in this case time scales of glassy and slow entanglement dynamics are well separated. Moreover, for polymers with comparably high polymer relaxation strength the situation becomes even more favorable. Here, we again have chosen polybutadiene (PB) which has turned out to exhibit strong polymer relaxation.⁹ Thus, without attempting the above-described decomposition we will analyze the full dipolar or segmental correlation function obtained from transforming the T_1 dispersion data into the time domain. Further, $T_1(\omega)$ data can be converted into the bond vector correlation function which will be compared to simulations.^{12,13} By adding further experimental data to our previous results^{8,9} for PB in the range $M > M_e$ the segmental correlation function extending up to 8 decades in time will be presented, containing now contributions from both glassy and polymer dynamics. Relying on these time domain data we will analyze the terminal relaxation for the crossover from the Rouse to the entanglement regime, an alternative approach to the one taken before by analyzing FFC NMR data in the susceptibility representation.⁹ Finally, the extracted segmental as well as the bond vector correlation function will be discussed in the light of theoretical predictions. Reaching $Z = M/M_e \cong 9$, it will turn out that standard polymer theories are inappropriate to describe our results; however, good agreement is found with simulation data.¹²

2. Theoretical Background

The spin–lattice relaxation time T_1 describes the evolution of the macroscopic nuclear magnetization toward its equilibrium

* Corresponding author.

[†] Experimentalphysik II, Universität Bayreuth.

[‡] IA&E, Russian Academy of Sciences.

Table 1. Details on the Samples

sample	M_w [g/mol]	M_w/M_n
PB816	816	1.05
PB9470	9470	1.02
PB18000	18000	1.05
PB35300	35300	1.02

value. Its frequency dependence (or dispersion) may be studied by applying the FFC technique where the external magnetic field is switched between a variable relaxation field B and a constant detection field. The angular frequency is defined by the Larmor frequency $\omega = \gamma B$ where γ denotes the gyromagnetic ratio of the nucleus. In the case of ^1H nuclei the evolution of the spin–lattice relaxation is determined by fluctuations of the dipolar interaction among the proton spins, and T_1 is dominated by intramolecular contributions but intermolecular correlation may also play a role. In the case of polymers, direct comparison of ^1H and ^2H NMR relaxation data indicate that indeed intermolecular translation dynamics may show up at very low frequencies in ^1H NMR¹⁴ (cf. also discussion part).

In order to facilitate analyses and comparisons with other techniques we rewrite the Bloembergen, Purcell, and Pound (BPP) expression¹⁵ for the relaxation rate $1/T_1$ in the susceptibility form^{8,9}

$$\omega/T_1(\omega) = C[\chi''(\omega) + 2\chi''(2\omega)] \equiv 3C\tilde{\chi}''(\omega) \quad (1)$$

where C is the NMR coupling constant, and $\chi''(\omega) = \omega J(\omega)$ the susceptibility, with the spectral density $J(\omega)$ being given in first approximation by the Fourier transform of the correlation function $F_2(t)$ and the latter by the second rank orientational correlation function of a polymer segment, more precisely of the internuclear vectors of the spin pairs in the monomer.^{9,14,15} We define a correlation function $\tilde{F}_2(t)$ given by the Fourier transform of $\tilde{\chi}''(\omega)$. As the relaxation behavior is discussed on logarithmic scales the slight difference between $\tilde{\chi}''(\omega)$ and $\chi''(\omega)$ as well as $\tilde{F}_2(t)$ and $F_2(t)$ can be neglected.

As a large temperature range is covered, glassy dynamics as well as polymer dynamics are probed, and one is able to construct master curves $\tilde{\chi}''(\omega\tau_s)$ for the NMR susceptibility assuming frequency temperature superposition (FTS). For that purpose we shift the susceptibility data of each temperature to achieve agreement with some suitable susceptibility function such as the Kohlrausch function on the high frequency side, i.e. at $\omega\tau_s \geq 1$ for which no polymer dynamics are observed. The shift factor yields the time constant τ_s of segmental motion, which may be identified with that of the α -process, the latter being the main relaxation of glass formers. For simple liquids, and oligomers with molecular weight $M < M_R$, there is no spectral contribution at $\omega\tau_s < 1$ in excess to the Debye behavior $\tilde{\chi}''(\omega) \propto \omega^1$, and their susceptibility master curves solely represent glassy dynamics (“glassy spectrum”). For samples with higher M , i.e., $M > M_R$, additional intensity on the low frequency side of the α -peak reflects polymer specific dynamics that involve time scales longer than τ_s . We therefore have identified M_R with the molecular weight of the Rouse unit, i.e. only at $M > M_R$ Rouse modes develop.^{8,9} The master curves $\tilde{\chi}''(\omega\tau_s)$ present iso-frictional spectra and allow comparing the results for different M . Alternatively, one may inspect the corresponding correlation function $\tilde{F}_2(t/\tau_s)$.

In the present contribution we refrain from separating the spectral contributions of polymer and glassy dynamics, and given that $M > M_e$, we will only assume that the long time behavior of $\tilde{F}_2(t/\tau_s)$ reflects solely polymer contributions:

$$\lim_{t \geq \tau_e \gg \tau_s} \tilde{F}_2(t/\tau_s) = \tilde{F}_{\text{polymer}}(t/\tau_s) \quad (2)$$

Here τ_e denotes the time scale beyond which entanglement effects are felt by the polymer segment. Whether eq 2 indeed

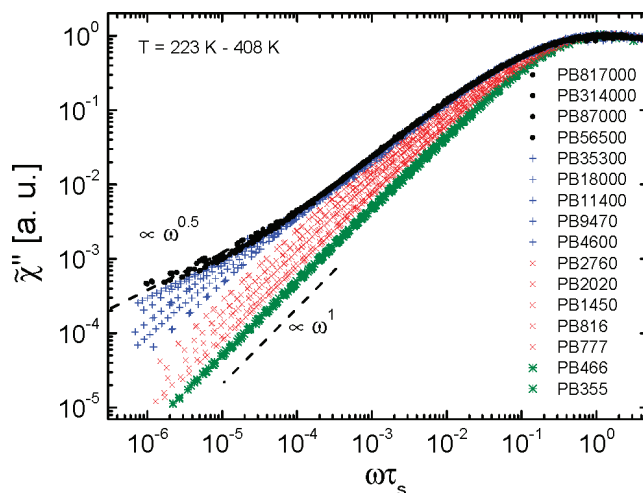


Figure 1. Susceptibility master curves for a series of polybutadienes (PB) with molecular weight (M) as indicated: (green stars) $M = 466$ represents simple liquid behavior; (red crosses) polymers showing only Rouse dynamics; (blue +) polymers showing in addition entanglement dynamics with crossover to terminal relaxation; (black circles) high M limit.

holds can be checked by comparing $\tilde{F}_2(t/\tau_s)$ with that for $M < M_R$ representing solely the contribution from glassy dynamics.

Within a coarse grained description and certain assumptions concerning the nature of the stochastic process,^{14,17} the correlation function $F_{\text{polymer}}(t)$ may be related to the square of the tangent or bond vector correlation function $\phi_b(t) = \langle \mathbf{u}_b(0)\mathbf{u}_b(t) \rangle$, i.e.,

$$F_{\text{polymer}}(t) \cong \phi_b(t)^2 \quad (3)$$

where \mathbf{u}_b is a unit vector along the contour of the polymer chain. Equation 3 offers the possibility to convert the T_1 dispersion data into the bond vector correlation function which is accessible also by simulation studies.^{12,13} This is also the route for calculating T_1 from theory like the Rouse model.^{9,14,17} We note that eq 3 has been tested for simulation vs experiment and some differences have been found.¹³

3. Experimental Section

We have investigated samples of 1,4-polybutadiene (PB) of different molecular weight M (see Table 1) in order to complete the M range of our study between the low (PB466) and the high (PB817000) M from refs 8 and 9. Note that the sample names reflect M_w (weight averaged M). The samples were purchased from Polymer Standards Service PSS, Mainz, Germany.

The dispersion of the spin–lattice relaxation time T_1 has been determined with a STELAR relaxometer FFC 2000, which allows measurements in the temperature range of 200–410 K and ^1H Larmor frequency range $\nu = 10$ kHz to 20 MHz. The accuracy of temperature measurements was better than ± 1 K, while the temperature stability was better than ± 0.3 K. We have observed simple exponential relaxation of magnetization over at least an order of magnitude in magnetization, and thus have determined the time constant T_1 by fitting to the exponential function. For further details, see refs 8 and 9.

4. Results

Susceptibility Master Curves. In Figure 1, we compile our results for the NMR susceptibility master curves $\tilde{\chi}''(\omega\tau_s)$ of PB in the molecular weight range $355 < M < 817000$ including our previous^{8,9} as well as our new data (cf. Table 1). Typical dispersion data $T_1(\omega)$ of PB have been presented in ref.^{8,9} The curves in Figure 1 are plotted as a function of the reduced frequency $\omega\tau_s$, where τ_s is the segmental correlation time which

we identify with that of the glass transition τ_α . The master curves have been constructed as described in ref 8 (cf. also Theoretical Background). Applying FTS, the master curves contain all the relaxation data for a given M measured in the temperature range 223–408 K and thereby we significantly enlarge the frequency range extending over more than 6 decades below $\omega\tau_s \cong 1$. The molecular weights chosen include the low M limit (PB355 and PB466, green stars) as well as the high M limit ($M \geq 56500$, black circles). In the latter case the dispersion of T_1 is independent of M . In this contribution we focus on the crossover from Rouse to entanglement dynamics $M > M_e$ which was not systematically covered by our previous works.^{8,9}

As demonstrated before,⁹ in the Rouse regime $M < 4600$ (red crosses in Figure 1), the dispersion data can be described by applying the discrete Rouse model with only a few Rouse modes being activated provided that the contributions of glassy and polymer dynamics are separated. The corresponding susceptibility curves at $\omega\tau_s \ll 1$ show excess intensity with respect to the spectrum of the low M limit (PB355 or PB466) which exhibits Debye behavior $\tilde{\chi}''(\omega) \propto \omega^{-1}$ typical of simple liquids.^{8,9} First polymer effects show up at $M = 777$ and the excess intensity grows until it saturates around $M = 4600$. In all cases, a Debye limit is reached at lowest frequencies indicating that the terminal relaxation can be probed in the Rouse regime.

At $4600 \leq M \leq 18000$ the master curves (blue + symbols) show discernible bimodal character which indicates the presence of entanglement dynamics. Whereas the relaxation behavior is not changed for $\omega\tau_s > 10^{-4}$ with respect to that of PB with $M < 4600$, more and more additional intensity appears at frequencies $\omega\tau_s < 10^{-4}$ signaling a further retardation of the segmental dynamics due to entanglement effects. We have explained the saturation behavior for $\omega\tau_s > 10^{-4}$ by the fact that the number of Rouse modes cannot grow any longer when M_e is reached.⁹ Note that up to $M = 18000$ a crossover to the Debye limit is still probed at lowest frequencies $\omega\tau_s = 10^{-7} - 10^{-6}$, i.e. the terminal relaxation is reached even for the onset of the entanglement regime. In the case of $M = 35300$ indication of this crossover is still discernible, however, the final Debye limit is not reached. At $M > 35300$ the crossover to the terminal relaxation is not observed at all, and the corresponding susceptibility curves display an M independent relaxation behavior (high M limit, black circles).

Reorientational Correlation Function. As an alternative way of presenting NMR data, one may Fourier transform the spectra $\tilde{\chi}''(\omega\tau_s)$ into the corresponding segmental orientational correlation functions $\tilde{F}_2(t/\tau_s)$.⁹ Such transformation is only possible for spectral data that show the limiting $\propto \omega^{-1}$ behavior at lowest frequencies, i.e. for the case that the terminal relaxation is reached. As said, for $M \leq 18000$ this condition is fulfilled, and the corresponding correlation functions are displayed in Figure 2. They are monitored over 6 decades in amplitude and up to 8 decades in reduced time t/τ_s . As we focus on the crossover from Rouse to entanglement dynamics we only show data for $M \geq 2760$. For comparison we include the corresponding correlation function for the simple liquid limit (PB466); it is interpolated by a Kohlrausch decay with a stretching parameter $\beta_K = 0.4$, a behavior typical of low molecular weight glass formers.^{3,4} As in the case of the susceptibility data in Figure 1, in going from $M = 2760$ to $M = 18000$, the correlation functions display more and more bimodal character with a distinct shoulder at long times; i.e., full reorientational relaxation of a segment is increasingly retarded due to the entanglement dynamics strongly depending on M . Although the reorientational correlation function shows a bimodal shape a clear-cut plateau region as anticipated in several works¹⁶ is not recognized. It is obvious that the correlation function of glassy dynamics given

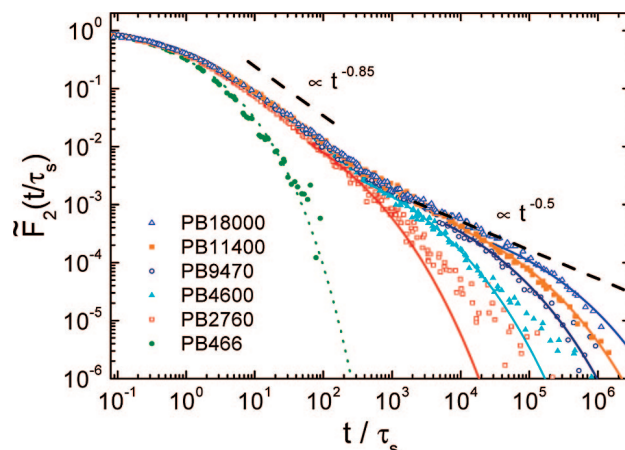


Figure 2. Dipolar or reorientational correlation functions $\tilde{F}_2(t/\tau_s)$ obtained from the data in Figure 1 via Fourier transformation for $M \geq 2760$ and for comparison $M = 466$. Dotted line: fit by Kohlrausch decay. Solid lines: estimating the terminal decay. Dashed lines: apparent power law $t^{-0.85}$ at short times, and $t^{-0.5}$ at long times for high M limit.

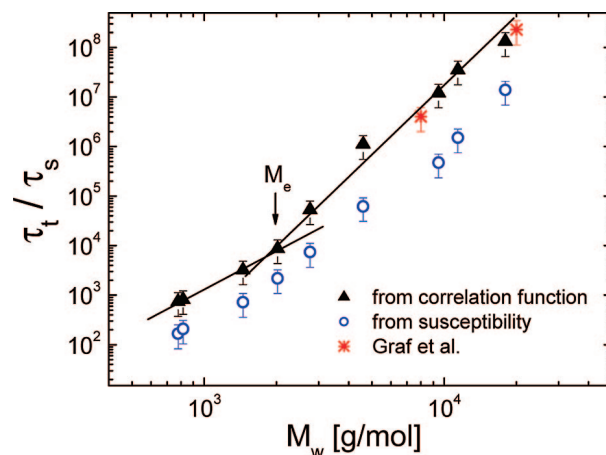


Figure 3. M dependence of the reduced terminal relaxation time τ_t/τ_s assuming a Kohlrausch decay ($\beta_K = 0.25$) at long times (black triangles) compared with corresponding data obtained from analyzing the susceptibility master curves (blue circles);⁹ data from Graf et al.¹⁶ assuming that DQ NMR probes the terminal relaxation (red stars).

by that of PB466 does not provide contributions at times $t/\tau_s > 10^2$, i.e., at time scales relevant to entanglement dynamics.

The correlation functions in Figure 2 exhibit a common behavior at times shorter than say $t/\tau_s < 3 \times 10^2$ which comprises contributions from Rouse as well as glassy dynamics and an apparent power law behavior $t^{-0.85}$ can be identified (dashed line in Figure 2). At $t/\tau_s > 3 \times 10^2$, additional contributions from entanglement dynamics set in which appear to form an M independent envelope, i.e., the higher M the later the final decay associated with the terminal relaxation and fixed by a time constant τ_t sets in. Assuming a stretched exponential terminal relaxation ($\beta_K = 0.25$) allows us to estimate the M dependence of τ_t . Technically, we determine τ_t by the time when the derivative of the correlation function becomes -1 in a double logarithmic plot. The corresponding interpolation of the decay curves are shown in Figure 2. It provides only an approximation in particular at small M for which the terminal relaxation is difficult to identify.

Figure 3 presents the time constant τ_t as a function of M , and the results for lower M (Rouse regime) are also included (black triangles). A crossover from a power law behavior $\tau_t \propto M^{2.5 \pm 0.8}$ to $\tau_t \propto M^{4.5 \pm 0.7}$ around $M \cong 2000$ emerges, which is in fair agreement with expectations for Rouse and entanglement dynamics, respectively.¹ This fixes the entanglement molecular

Table 2. Predictions of the Tube-Reptation Model for the Mean Square Segment Displacement $\langle r^2(t) \rangle$,¹ NMR Susceptibility $\chi''(\omega)$,¹⁴ Reorientational Correlation Function $F_2(t)$,²² and Bond Correlation Function $\phi_b(t)$ (assuming $F_2(t) = \phi_b^2(t)$ cf. eq 3)

regime	limit	$\langle r^2(t) \rangle$	$\chi''(\omega)$	$F_2(t)$	$\phi_b(t)$
II (free Rouse)	$\tau_s \leq t \leq \tau_e$	$M(t/\tau_R)^{0.5} \propto (t/\tau_s)^{0.5}$	$\omega\tau_s \ln(\omega\tau_s)$	$(t/\tau_s)^{-1}$	$(t/\tau_s)^{-0.5}$
III	$\tau_e \leq t \leq \tau_R$	$M(t/Z^2\tau_R)^{0.25} \propto (t/\tau_s)^{0.25}$	$(\omega\tau_s)^{0.25}$	$(t/\tau_s)^{-0.25}$	$(t/\tau_s)^{-0.125}$
IV	$\tau_R \leq t \leq \tau_d$	$M(t/\tau_d)^{0.5} \propto M^{-0.5}(t/\tau_s)^{0.5}$	$M^{+0.5}(\omega\tau_s)^{0.5}$	$M^{+0.5}(t/\tau_s)^{-0.5}$	$M^{+0.25}(t/\tau_s)^{-0.25}$
V	$\tau_d \ll t$	$M(t/\tau_d)^1 \propto M^{-2}(t/\tau_s)^1$	$(\omega\tau_s)^1$	e^{-2t/τ_d}	e^{-t/τ_d}

weight to $M_e \cong 2000$ as found before.⁹ This M value is actually by a factor of about two smaller than that value for which saturation in the frequency regime $\omega\tau_s > 10^{-4}$ (attributed to Rouse dynamics) occurs in Figure 1. The results also agree fairly well with those obtained previously from analyzing the terminal relaxation in the susceptibility representation (blue circles in Figure 3).⁹ Given this, it becomes clear from Figure 2 that up to $M = 18000$ (corresponding to $Z = M/M_e \cong 9$) a significant part of the correlation function is dominated by the terminal relaxation leading to a cutoff of the characteristic polymer relaxation. It appears that the terminal relaxation is the only M dependent feature of the correlation function. Thus, it will not be easy identifying presumably universal polymer relaxation (cf. Discussion).

5. Discussion and Conclusions

Extending our previous measurements on PB^{8–10} we constructed master curves for the susceptibility $\tilde{\chi}''(\omega\tau_s)$, and via Fourier transformation one arrives at the dipolar or segmental correlation function $\tilde{F}_2(t/\tau_s)$ of entangled polymers ($M > M_e$) monitored up to 8 decades in reduced time t/τ_s (cf. Figure 2). This function is not easily obtained by other experiments, and most simulation data do not cover sufficient time or amplitude to allow for a detailed discussion of its properties in the entanglement regime. We reiterate that the result for $\tilde{F}_2(t)$ and $\phi_b(t)$ depends only on applying FTS which is accepted as a good approximation; if deviations are reported they are small on logarithmic scales. Note also that for the discussion we can ignore the difference between $\tilde{F}_2(t)$ and $F_2(t)$ (cf. eq 1).

Testing Theoretical Predictions for Polymer Dynamics.

At first, we will discuss our result for $\tilde{F}_2(t/\tau_s)$ (cf. Figure 2) in the light of theoretical predictions within coarse grained descriptions of polymer dynamics, i.e., molecular details of the monomer are ignored.^{1,14,18–22} We only note that atomistic simulations have accessed the segmental correlation function $F_2(t)$ for PB^{23–25} as well as PI²⁶ and qualitatively similar relaxation curves have been found, in particular, the decay curves show a bimodal structure as in our experiment.

The segmental correlation function $\tilde{F}_2(t/\tau_s)$ is expected to reflect five contributions: regime I, glassy dynamics $t \leq \tau_s$; regime II, virtually free Rouse dynamics $\tau_s < t \leq \tau_e$, for which entanglement effects are not yet effective. Here, $\tau_e = \tau_s N_e^2$ denotes the entanglement time and N_e the number of Rouse units forming an entanglement unit. The time τ_e marks the crossover to dynamics governed by entanglement effects. Here, according to the tube-reptation model¹ three distinct regimes have to be further distinguished which lead to characteristic power law behavior for the mean square displacement and the dispersion of $T_1(\omega)$.^{14,18,22} At $\tau_e \leq t \leq \tau_R$, curvilinearly directed Rouse dynamics (III) occur in the fictitious tube by which a tagged polymer chain is fixed due to being entangled with other polymers. The time constant $\tau_R = \tau_s N^2$ specifies the longest Rouse time. The interval $\tau_R \leq t \leq \tau_d$ defines the diffusion process along the tube (IV) which is terminated by the tube disengagement (or disentanglement) time $\tau_d = 3\tau_s N^3/N_e$; i.e., this terminal relaxation is strongly M dependent. Finally, at $t \gg \tau_d$, translational diffusion and isotropic reorientation of the entire polymer (V) take place, and a Debye limit for the dispersion of T_1 is reached.

Table 3. Predictions of the (first) Renormalized Rouse Model for Mean Square Segment Displacement $\langle r^2(t) \rangle$,¹⁴ NMR Susceptibility $\chi''(\omega)$,¹⁴ Reorientational Correlation Function $F_2(t)$ and Bond Correlation Function $\phi_b(t)$ (assuming $F_2(t) = \phi_b^2(t)$ cf. eq 3)

regime	limit	$\langle r^2(t) \rangle$	$\chi''(\omega)$	$F_2(t)$	$\phi_b(t)$
“high-mode number limit”	$\tau_s \leq t$	$(t/\tau_s)^{0.25}$	$(\omega\tau_s)^{0.5}$	$(t/\tau_s)^{-0.5}$	$(t/\tau_s)^{-0.25}$
“low-mode number limit”	$\tau_e \leq t$	$(t/\tau_s)^{0.4}$	$(\omega\tau_s)^{0.8}$	$(t/\tau_s)^{-0.8}$	$(t/\tau_s)^{-0.4}$

Regarding the tube-reptation model, Table 2 compiles the results for the respective power law regimes of the mean square segment displacement $\langle r^2(t) \rangle$,¹ the NMR susceptibility $\chi''(\omega\tau_s)$,^{14,18} the segmental reorientational correlation function $F_2(t/\tau_s)$,²² and the bond vector correlation function $\phi_b(t/\tau_s)$ (cf. below). We emphasize that regimes I–III show no M dependence, i.e., universal envelopes are forecast for $\chi''(\omega\tau_s)$ or $F_2(t/\tau_s)$, whereas for regimes IV–V such dependence is predicted.

Referring to the free Rouse regime (II), a comment is worthwhile. As demonstrated in our previous Paper,⁹ the power law expression $\tilde{F}_2(t) \propto t^{-1}$ typical of this regime (cf. Table 1) is actually only observed in the high N limit, e.g., above $N = 10^2$. This behavior is not found in real polymers for which entanglement effects set in well before this limit is reached. Instead of testing the expected limiting behavior, one rather has to perform a discrete Rouse analysis, summing up a small number of Rouse modes.⁹ In Figure 2 we attribute the relaxation behavior at $t/\tau_s < 3 \times 10^2$ to glassy and Rouse dynamics with a few modes being active only. The behavior in this time range is essentially the same as that of the polymer with $M = 2760$ which is only slightly above M_e , thus not expected to show significant entanglement dynamics. Here, an apparent power law $\tilde{F}_2(t) \propto t^{-a}$ with $a = 0.85$ may be identified over 2 decades in time, which actually is not much different from that of the Rouse limit $a = 1$.

At $t/\tau_s > 3 \times 10^2$ the reorientational correlation function for the different $M > M_e$ follows more and more an M independent envelope. Beyond $M = 18000$, i.e., $Z \cong 9$, no full correlation function is available by Fourier transformation of the dispersion data. Instead, we include in Figure 2 the Fourier transform of the power law limit of the susceptibility (dashed line) observed at lowest frequencies in Figure 1 for $M > 18000$, i.e., for the high M limit. The corresponding exponent is $a = 0.5 \pm 0.05$. For $M \leq 18000$ the segmental correlation function is terminated by a Kohlrausch decay with a terminal time τ_d which follows the predicted M behavior (cf. Figure 3).

The results of Figure 2 are in stark contrast to the theoretical predictions of the tube-reptation model (cf. Table 2). The power law of regime III with an exponent $a = 0.25$ is not observed. The second power law of the tube-reptation model (regime IV) with an exponent $a = 0.5$ could be identified with the experimental one at longest times; however, the corresponding M dependence is missing. As said before, it appears that for the M range covered an M dependence of the segmental correlation function is only introduced by that of the terminal relaxation; i.e., for $t \ll \tau_d$, no M dependence is observed in contrast to the prediction.

As an alternative description of the dynamics of entangled polymers, the renormalized Rouse model^{20,21} is discussed by the Kimmich group.^{14,17,19} The corresponding power law predictions are compiled in Table 3. We note that a “free Rouse” regime is not expected within this approach. Before discussing

their interpretation we emphasize that the experimental T_1 dispersion data of PB compiled by us agree with those of the Kimmich group.²⁷ The authors have claimed that the two power laws of Table 3 are observed in the T_1 dispersion data (accepting an error of ± 0.05 in the exponents¹⁴). The first regime at high frequencies, the “high mode number limit”, should be described by a power law $\tilde{F}_2 \propto (t/\tau_s)^{-0.5}$ at short times. In the NMR data of Figure 2 such a behavior appears only at longest times. Regarding the second power law regime (“low mode number limit”) with $a = 0.8$, indeed, this is approximately revealed but we attribute it to the Rouse regime (cf. dashed line with $a = 0.85$). The experimentally observed behavior at longest times described by $\tilde{F}_2 \propto (t/\tau_s)^{-0.5}$, for which the contribution of glassy dynamics can safely be ignored, is attributed by Kimmich et al. to the “inter-segment interaction limit”.¹⁴ This identification has become possible by comparing ^1H and ^2H dispersion data.²⁷ The ^2H relaxation is dominated by quadrupolar interaction probing only intra segmental fluctuations whereas ^1H relaxation may contain intermolecular correlation effects, in addition (see Note Added in Proof).

We would also like to compare our results with those from double quantum (DQ) NMR experiments on PB^{16,28,29} where similar correlations are probed as in FFC NMR. The authors have analyzed their data in terms of power laws of regime III and IV of the tube-reptation model. In this study entangled PB with $Z = 4, 11, 76$ has been investigated and no terminal relaxation has been considered. In the present contribution, assuming $M_e = 2000$, we clearly identify the terminal relaxation for $Z \leq 9$ (cf. Figure 2) and cover similar time scales as the DQ NMR experiments. Thus, it may be possible that the decay curves observed in the DQ NMR experiments actually reflect the terminal relaxation instead of different power law regimes. We have interpolated the DQ NMR decay curves of ref 16 by assuming a stretched relaxation, and indeed we find for the samples with the two lowest Z values, *i.e.*, $Z = 4$ ($M = 8000$) and $Z = 11$ ($M = 20000$), a similar M dependence as in our case for the terminal relaxation in the entanglement regime (cf. Figure 3); the very slow DQ decay curve for the highest M ($Z = 76$) studied cannot be reliably interpolated. For a quantitative comparison of the FFC and DQ results one has to assume $\tau_e/\tau_s = 5 \times 10^5$, which is a reasonable value. Here, we note that in a very recent study on PB, Saalwächter and co-workers have been able to study significantly higher M values over a larger time window, and they have indeed identified the power laws of the tube-reptation model.³⁰

Bond Vector Correlation Function. As mentioned in section 2, within theoretical approaches for coarse grained polymer dynamics the correlation function $F_2(t/\tau_s)$ is given by the square of the bond vector correlation function $\phi_b(t)$ (cf. eq. 3).^{14,15,17} Therefore we plot $\phi_b(t)$ in Figure 4 obtained from the data in Figure 2. Qualitatively, the relaxation behavior does not change significantly with respect to that of $\tilde{F}_2(t)$. Of course, the corresponding exponents decrease by a factor of 2. Studying the crossover from Rouse to reptation dynamics Kreer et al.¹² have investigated the bond vector correlation function by Monte Carlo simulations. The authors have stated that the “crossover from non-entangled to entangled dynamics is very protracted”. Even for longest chains ($N = 512$) they have not found evidence of the power laws expected for tube-reptation dynamics. Moreover, no difference is observed for $N = 128$, and $N = 512 = 14N_e$; *i.e.*, the bond vector correlation function appears to be N independent over 7 decades in time. We have included in Figure 4 (solid lines) the results from the simulation study¹² (multiplied by a factor 2π in time). The curves for $N = 128$ and $N = 512$, which do not differ within the scatter of the data, exhibit high similarity compared to the FFC NMR results for highest $M = 18000$. Even the simulation data for the other N

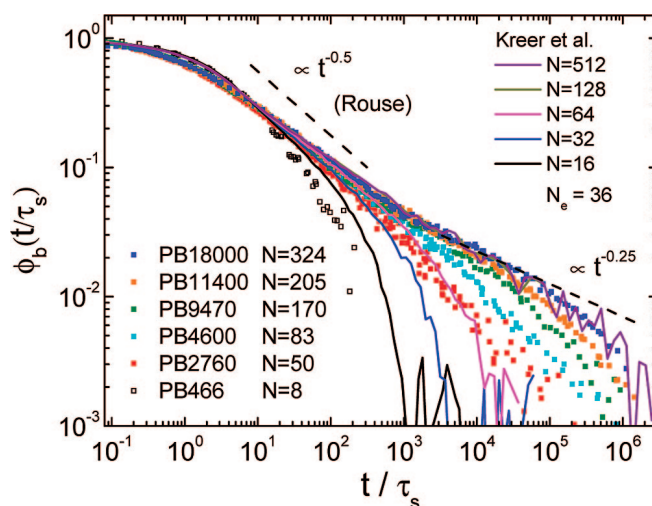


Figure 4. Bond vector correlation function $\phi_b(t/\tau_s) = F(t/\tau_s)^{1/2}$ as obtained from the T_1 dispersion data. Solid lines: data from Monte Carlo simulations by Kreer et al.;¹² given $N_e = 36$ and $M_e = 2000$, experiments and simulations are mapped onto each other; dashed lines: power law regimes.

can be mapped to the experimental ones when taking $N_e = 36$ (simulations) and $M_e = 2000$ (our experiment). Simulation as well as experiment get close to the Rouse limit $t^{-0.5}$ at times $1 < t/\tau_s < 3 \times 10^2$. At even shorter times, for which contributions from glassy dynamics dominate, small deviations between experiment and simulation are observed which, of course, are expected within coarse grained models. All in all, the similarity of both results is very striking, in particular, given that we expect also inter segmental contributions at long times,¹⁴ which are not included in the simulation. Moreover, the relaxation strength of the polymer relaxation is expected to depend on the structural details within the monomer.²⁸ Therefore, we think that the coincidence may be accidental.

Concluding, our results for the bond vector and segmental correlation function confirm the findings from simulation which do not show the crossover to the relaxation behavior predicted for these quantities by the standard polymer theories like the tube-reptation model up to values $Z \cong 9$. Of course, it may be possible that the crossover is only observed at even higher Z or M which then makes it necessary to study the dynamics up to even longer times. This view is supported by the mentioned observations in a recent DQ NMR study of PB.³⁰ As discussed, *e.g.*, by Read et al, contour length fluctuations and constraint release may play an important role.³¹ In any case, FFC NMR provides a unique opportunity for elucidating dynamics in polymer systems and indeed longer time scales may become feasible when stray field compensation is optimized.

Acknowledgment. The authors thank J. Baschnagel (Institute Charles Sadron, Strasbourg, France) for providing the simulation data, and H.W. Spiess (Mainz, Germany) and K. Saalwächter (Halle, Germany) for helpful comments on the manuscript. The authors also appreciate financial support of Deutsche Forschungsgemeinschaft (DFG) through SFB 481. V.N.N. acknowledges support by the RFBR.

Note Added in Proof. We mention that within the twice renormalized Rouse model the inter-segmental correlation function is described by a power law $t^{-0.5}$ (see ref 32) as found experimentally at longest times.

References and Notes

- (1) Doi, M.; Edwards, S. F. *The Theory of Polymer Dynamics*; Oxford Sci. Publication: Oxford, U.K., 1986.

- (2) Angell, C. A.; Ngai, K. L.; McKenna, G. B.; McMillan, P. F.; Martin, S. W. *J. Appl. Phys.* **2000**, *88*, 3113–3157.
- (3) Lunkenheimer, P.; Schneider, U.; Brand, R.; Loidl, A. *Contemp. Phys.* **2000**, *41*, 15–36.
- (4) Blochowicz, T.; Brodin, A.; Rössler, E. A. *Adv. Chem. Phys.* **2006**, *133 Part A*, 127–256.
- (5) Binder, K.; Baschnagel, J.; Paul, W. *Prog. Polym. Sci.* **2003**, *28*, 115–172.
- (6) Paul, W.; Smith, G. D. *Rep. Prog. Phys.* **2004**, *67*, 1117–1185.
- (7) Götze, W.; Sjögren, L. *Rep. Prog. Phys.* **1992**, *55*, 241–376.
- (8) Kariyo, S.; Brodin, A.; Gainaru, C.; Herrmann, A.; Schick, H.; Novikov, V. N.; Rössler, E. A. *Macromolecules* **2008**, *41*, 5313–5321.
- (9) Kariyo, S.; Brodin, A.; Gainaru, C.; Herrmann, A.; Hintermeyer, J.; Schick, H.; Novikov, V. N.; Rössler, E. A. *Macromolecules* **2008**, *41*, 5322–5332.
- (10) Kariyo, S.; Gainaru, C.; Schick, H.; Brodin, A.; Rössler, E. A. *Phys. Rev. Lett.* **2006**, *97*, 207803-1–207803-4. Erratum: Kariyo, S.; Herrmann, A.; Gainaru, C.; Schick, H.; Brodin, A.; Rössler, E. A. *Phys. Rev. Lett.* **2008**, *100*, 109901-1.
- (11) Hintermeyer, J.; A. Herrmann, A.; Kahlau, R.; Goiceanu, C.; Rössler, E. A. *Macromolecules* **2008**, *41*, 9335–9344.
- (12) Kreer, T.; Baschnagel, J.; Müller, M.; Binder, K. *Macromolecules* **2001**, *34*, 1105.
- (13) Sommer, J.-U.; Saalwächter, K. *Eur. Phys. J. E* **2005**, *18*, 167–182.
- (14) Kimmich, R.; Fatkullin, N. *Adv. Polym. Sci.* **2004**, *170*, 1–113.
- (15) Bloembergen, N.; Purcell, E. M.; Pound, R. V. *Phys. Rev.* **1948**, *73*, 679–715.
- (16) Graf, R.; Heuer, A.; Spiess, H. W. *Phys. Rev. Lett.* **1998**, *80*, 5738–5741.
- (17) Fatkullin, N.; Kimmich, R.; Weber, H. W. *Phys. Rev. E* **1993**, *47*, 4600–4603.
- (18) de Gennes, P.-G. *J. Chem. Phys.* **1971**, *55*, 572–579.
- (19) Kimmich, R.; Fatkullin, N. *J. Chem. Phys.* **1994**, *101*, 822–832.
- (20) Schweizer, K. S. *J. Chem. Phys.* **1989**, *91*, 5802–5821.
- (21) Schweizer, K. S. *J. Chem. Phys.* **1989**, *91*, 5822–5839.
- (22) Ball, R. C.; Callaghan, P. T.; Samulski, E. T. *J. Chem. Phys.* **1997**, *106*, 7352.
- (23) Faller, R.; Müller-Plathe, F.; Heuer, A. *Macromolecules* **2000**, *33*, 6602–6610.
- (24) Smith, G. D.; Borodin, O.; Bedrow, D.; Paul, W.; Qiu, X.; Ediger, M. *Macromolecules* **2001**, *34*, 5192–5199.
- (25) Smith, G. D.; Borodin, O. *J. Chem. Phys.* **2002**, *117*, 10350.
- (26) Faller, R.; Müller-Plathe, F. *Polymer* **2002**, *43*, 621–628.
- (27) Kimmich, R.; Fatkullin, N.; Seiter, R.-O.; Gille, K. *J. Phys. Chem.* **1998**, *108*, 2173–2177.
- (28) Dollase, T.; Graf, R.; Heuer, A.; Spiess, H. W. *Macromolecules* **2001**, *34*, 298–309.
- (29) Saalwächter, K. *Progr. NMR* **2007**, *51*, 1–35.
- (30) Saalwächter, K. Private communication.
- (31) Read, D. J.; Jagannathan, K.; Likhtman, A. E. *Macromolecules* **2008**, *41*, 6843–6853.
- (32) Fatkullin, N.; Kimmich, R.; Kroutieva, M. *J. Exp. Theor. Phys.* **2000**, *91*, 150–166.

MA802818J

Publication 2

Universal Polymer Dynamics Revealed by Field Cycling ^1H NMR.

Herrmann, A.; Kariyo, S.; Abou Elfadl, A.; Meier, R.;
Gmeiner, J.; Novikov, V. N.; Rössler, E. A.
Macromolecules **2009**, *42*, 5236–5243.

Copyright 2009 by The American Chemical Society
DOI: 10.1021/ma900625x

Universal Polymer Dynamics Revealed by Field Cycling ^1H NMRA. Herrmann,[†] S. Kariyo,[‡] A. Abou Elfadl,[†] R. Meier,[†] J. Gmeiner,[†] V. N. Novikov,[§] and E. A. Rössler^{*†}[†]Experimentalphysik II, Universität Bayreuth, 95440 Bayreuth, Germany, [‡]Faculty of Science and Technology, Yala Islamic University, 135/8, M.3, A. Yarang, Pattani 94169, Thailand, and [§]IA&E, Russian Academy of Sciences, Novosibirsk 630090, Russia

Received March 23, 2009; Revised Manuscript Received May 6, 2009

ABSTRACT: We apply fast field cycling ^1H NMR to study segmental reorientation dynamics in melts of linear polybutadiene, polyisoprene, and polydimethylsiloxane in the high molecular weight limit. Measuring fully protonated as well as partially deuterated polymers, we show that in contrast to previous reports the relaxation behavior at low frequencies, for which polymer-specific contributions show up, is not universal but depends on the particular internuclear vectors of the ^1H spin pairs in the monomer unit. Only after extracting the polymer specific contributions from the overall susceptibility spectra by accounting for the glassy contribution, the “polymer spectra” reveal universal behavior which can be described by two power law regimes: one attributed to free Rouse dynamics and one, at lower frequencies, to entanglement effects. Yet the predictions of the tube-reptation model are not observed.

I. Introduction

The dynamics of melts of linear polymers comprises both polymer specific dynamics and glassy dynamics. Whereas polymer dynamics originate from collective dynamics of Rouse and reptation type,^{1,2} glassy dynamics^{3–5} are attributed to “segmental” or “local” relaxation of the polymer chain. Here, one has to keep in mind that the glass transition phenomenon itself includes cooperative motion, and the segmental correlation time τ_s may be identified with that of the α -process, τ_α , characterizing glassy dynamics. The latter drives the polymer dynamics via determining the monomeric friction coefficient and is responsible for the non-Arrhenius temperature dependence of the relaxation times in polymer melts.

From an experimental point of view it is of interest whether one can separate polymer dynamics from glassy dynamics in order to test predictions by respective theories. For example, it may be possible that polymer dynamics modify glassy dynamics.⁶ In many cases one chooses experimental conditions which suggest that separation of time scales holds, and one assumes that solely polymer dynamics or solely glassy dynamics are probed as the contribution from the other relaxation is believed to be ignorable. Such an approach has also been taken in the case of fast field cycling (FFC) NMR experiments, a technique well suited to investigate the low-frequency motion in polymers.² FFC NMR monitors the dispersion of the spin–lattice relaxation time $T_1(\omega)$. To a fair approximation, the dispersion of ^1H T_1 reflects the spectrum of reorientational dynamics of a polymer segment in terms of the dipolar or second Legendre polynomial correlation function $F_2(t)$ of the spin pairs within a monomer unit. By converting the dispersion data into the time domain, the bond vector correlation function becomes accessible.⁷

Measuring at frequencies $\omega\tau_s \ll 1$, experimental results on several polymers have been reviewed by Kimmich and Fatkullin² which appear to indicate universal dispersion behavior of the spin–lattice relaxation in linear polymers. The T_1 dispersion manifests itself in characteristic power-law regimes which have been interpreted within Rouse theory (nonentangled polymers) and renormalized Rouse theory (entangled polymers).² Thus, the

experiments seem not to disclose the power laws expected for the Doi–Edwards tube-reptation model; the latter have only been observed by FFC NMR for polymers confined to tubelike pores formed by a solid matrix.⁸ However, there are reports in the literature that do not confirm such universal relaxation behavior, e.g., for the case of polyisoprene.⁹ Here, the question is whether these deviations from the presumably universal relaxation behavior at $\omega\tau_s \ll 1$ are significant and may cast doubt on the previous approach² taken to interpret the FFC NMR data. The present publication attempts to answer this question.

In a series of papers,^{7,10–12} we recently have reinvestigated the ^1H T_1 dispersion behavior of polybutadiene (PB) covering a broad range of molecular weight (M) including the low M limit; i.e., we have studied the crossover from simple liquid, to Rouse, and to entanglement dynamics. Experiments have been performed with a commercial spectrometer STELAR FFC 2000.¹³ Applying frequency–temperature superposition (FTS), we have obtained master curves covering 6 decades in frequency at $\omega\tau_s \ll 1$, and the T_1 dispersion data have been interpreted in a new fashion. The results relevant for the present context can be summarized as follows. (i) In the frequency regime attributed to Rouse dynamics the influence of the spectral contribution of the glassy dynamics cannot be ignored. (ii) The entanglement regime ($M > M_c$) manifests itself at lower frequencies or longer times than Rouse dynamics, and here the contributions from glassy dynamics can be ignored. This is the case for PB, which exhibits a comparatively strong relaxation strength of the polymer dynamics, but it may not be necessarily the case for other polymers. (iii) The bond vector correlation function shows striking similarity with those obtained from simulations;¹⁴ however, up to $Z = M/M_c \cong 9$ no indication of the power laws of the tube-reptation model can be identified, and also the renormalized Rouse theory does not fully apply. One possibility to explain these findings is to assume that the crossover to full entanglement dynamics occurs only at higher M ; i.e., the crossover is “very protracted”.^{7,14}

Investigating now different polymers by FFC ^1H NMR, the present contribution aims at demonstrating that in contrast to previous reports^{2,13} the T_1 dispersion at low frequencies in polymer melts is not universal but rather depends on the

*Corresponding author.

orientation of the internuclear vectors with respect to the contour of the chain in the particular monomer, a fact also discussed by Spiess and co-workers in the context of their high-resolution double-quantum NMR experiments.^{15–17} Only by taking into account the spectral contribution from the glassy dynamics, indeed universal polymer relaxation behavior is revealed for all the polymers investigated. These results are further substantiated by examining partially deuterated polymer samples. In particular, we will discuss results for polybutadiene (PB), polyisoprene (PI), and polydimethylsiloxane (PDMS) in the high M limit for which entanglement effects are well established and the T_1 dispersion has become M independent ($M \gg M_c$). We will show once again that the universal relaxation behavior revealed after isolating the polymer contribution is not described by current polymer theories, at least in the frequency range accessible by FFC NMR at the present time.

II. Theoretical Background

The spin–lattice relaxation time T_1 describes the evolution of the nuclear magnetization toward its equilibrium value. Its frequency dependence (or dispersion) can be studied by applying the FFC technique where the external magnetic field is switched between a variable relaxation field B and a constant detection field. The angular frequency is defined by the Larmor frequency $\omega = \gamma B$, where γ denotes the gyromagnetic ratio of the nucleus. In the case of ^1H nuclei, the spin–lattice relaxation is determined by fluctuations of the dipolar interaction of the proton spins. Usually it is argued that T_1 is dominated by intramolecular contributions.^{2,13} Accordingly, ^1H FFC NMR relaxation data are expected to reflect mainly reorientation dynamics. However, the role of intermolecular or intersegmental contributions in the case of polymers must not be ignored.²

As introduced before, we rewrite the Bloembergen–Purcell–Pound (BPP) expression¹⁸ for the relaxation rate $1/T_1$ in the susceptibility form^{7,10–12}

$$\omega/T_1 = C[\chi''(\omega) + 2\chi''(2\omega)] \equiv 3C\tilde{\chi}''(\omega) \quad (1)$$

where C is the NMR coupling constant and $\chi''(\omega) = \omega J(\omega)$ the susceptibility representation of the fluctuation spectrum, with the spectral density $J(\omega)$ being given in first approximation by the Fourier transform of the second rank orientational correlation function $F_2(t)$ of a polymer segment, more precisely of the internuclear vectors of the spin pairs in the monomer.^{2,11} The factor 3 appears in order to keep the integral over the susceptibility $\tilde{\chi}''(\omega)$ normalized to $\pi/2$ as usual.

As we cover a large temperature range, glassy dynamics as well as polymer dynamics are probed, and one is able to construct master curves $\tilde{\chi}''(\omega\tau_s)$ for the NMR susceptibility extending over many decades in time, assuming frequency–temperature superposition (FTS). For details about obtaining the master curves, the reader may consult our previous publications.^{7,10–12} The master curves $\tilde{\chi}''(\omega\tau_s)$ combine the results from a broad temperature range (say $\Delta T \cong 180$ K) and present “isofrictional” spectra which allow comparing the results for different M . For simple liquids and oligomers with low molecular weight $M < M_R$ (M_R denoting the molecular weight of the Rouse unit¹²), no spectral contribution at $\omega\tau_s < 1$ in excess to the Debye behavior $\tilde{\chi}''(\omega) \propto \omega^1$ is observable, and their susceptibility master curves solely represent glassy dynamics (“glassy spectrum”). For samples with higher M , i.e., $M > M_R$, additional intensity on the low-frequency side of the α -peak reflects polymer specific dynamics that involve time scales longer than τ_s .

As a guideline for a phenomenological decomposition of the spectral contributions from polymer and glassy dynamics, one assumes that both are statistically independent, so that their

contributions to $F_2(t)$ are multiplicative:^{2,7,10–12}

$$F_2(t) = F_{\text{glass}}(t)F_{\text{polymer}}(t) \quad (2)$$

Depending on molecular weight M , the polymer part $F_{\text{polymer}}(t)$ may contain contributions from Rouse as well as entanglement dynamics. Introducing the relative magnitude f of polymer dynamics, we write

$$F_2(t) = [(1-f)\phi_{\text{glass}}(t) + f]F_{\text{polymer}}(t) \quad (3)$$

where $\phi_{\text{glass}}(t)$ denotes the normalized correlation function describing the glassy dynamics alone.

Assuming time scale separation (cf. also ref 19), the contributions to the total susceptibility are approximately additive

$$\tilde{\chi}''(\omega\tau_s) \cong (1-f)\tilde{\chi}''_{\text{glass}}(\omega\tau_s) + f\tilde{\chi}''_{\text{polymer}}(\omega\tau_s) \quad (4)$$

Under such conditions the “polymer spectrum” $\tilde{\chi}''_{\text{polymer}}(\omega\tau_s)$ containing only the spectral contributions attributed to polymer dynamics can be extracted from the master curve $\tilde{\chi}''(\omega\tau_s)$ of each sample by subtracting the glassy spectrum $\tilde{\chi}''_{\text{glass}}(\omega\tau_s)$. Thereupon the relaxation strength $f(M)$ of polymer dynamics is obtained, which is the relative correlation loss due to polymer dynamics on time scales $t \gg \tau_s$. As found for PB, its dependence on M reflects three dynamic regimes, namely simple liquid, Rouse, and entanglement regime. Specifically, $f(M)$ strongly increases in the Rouse regime ($M_R < M < M_c$) but saturates beyond the entanglement molecular weight M_c ¹² or at $M_c \cong 2M_c$. In other words, the glassy dynamics are more and more impeded by the emerging polymer dynamics. The relaxation strength f is connected to what has been called the local order parameter $S = \sqrt{f}$.^{11,12,15,16,20} Though the applicability of eq 4 may be questioned as time scale separation may not always apply in a strict sense the results appear physically reasonable and allow a comparison of the polymer contribution for different polymers what is needed when searching for presumably universal polymer relaxation. In the Appendix we compare the results from applying eq 4 with those from eq 3. In the latter case a full deconvolution is applied, and the differences can essentially be ignored in the case of the PB data.

As discussed, for example, by Spiess and co-workers^{15,16} considering the entanglement regime, the particular value of the relaxation strength f or the order parameter S depends on the direction of the internuclear vector between a spin pair with respect to the contour of the chain. Given the order parameter of the chain S_{chain} , the order parameter S_{ij} (or f_{ij}) of a particular spin pair ij oriented with an angle ϑ_{ij} toward the contour direction is found¹⁶ by tensor calculus

$$S_{ij} = \sqrt{f_{ij}} = 1/2(3 \cos^2 \vartheta_{ij} - 1)S_{\text{chain}} \quad (5)$$

Thus, the measured order parameter S_{ij} is smaller than that of the chain. Moreover, the magnitude of spectral contribution attributed to polymer dynamics depends on the structure of the particular monomer. In other words, no universal dispersion for the overall spin–lattice relaxation time is expected. Only if the susceptibility spectra are decomposed along eq 4 the so-extracted “polymer spectra” will be expected to show universal features. As will be demonstrated, these considerations do not only hold for the entanglement regime but also for the Rouse regime. Here we add that, in contrast to double-quantum (DQ) NMR, FFC NMR usually provides only average values for f as the method cannot discriminate the contributions from different spin pairs in the monomer. However, by measuring partially deuterated polymers, the situation becomes more favorable, and this is

Table 1. Details on the Samples

sample	M_w [g/mol]	M_w/M_n	reference
propylene glycol (PG)	76		this work
PB466-h ₆	466	1.06	10
PB2020-h ₆	2020	1.07	10
PB18000-h ₄	18000	1.02	this work
PB20000-h ₂	20000	1.02	this work
PB35300-h ₆	35300	1.02	7
PI111000-h ₅	111000	1.03	9
PI127000-h ₃	127000	1.03	9
PI157000-h ₈	157000	1.01	this work
PDMS860-h ₆	860	1.41	this work
PDMS5940-h ₆	5940	1.15	this work
PDMS128000-h ₆	128000	1.13	this work

exploited in the present contribution. Still, the particular f_{ij} may depend on the configuration of the monomer unit. For example, in the case of PB samples an average over cis and trans isomers is measured. Finally, we mention that although assumed to be negligible, intermolecular coupling may still play a role. Thus, a quantitative analysis of the relaxation strength f measured by FFC ¹H NMR appears to be not straightforward.

III. Experimental Section

We investigated samples of differently deuterated as well as fully protonated 1,4-polybutadiene (PB) and 1,4-polyisoprene (PI) with $M > M_c$. The T_1 dispersion data of partially deuterated 1,4-polyisoprene (PI) from ref 9 were transformed to the susceptibility representation. Moreover, we measured samples of polydimethylsiloxane (PDMS) with different M (see Table 1). Note that the sample name of the polymers reflect the weight-average M_w and the number of proton nuclei in the monomer unit. The fully protonated samples (PB-h₆, PI-h₈, PDMS-h₆) were purchased from Polymer Standards Service PSS, Mainz, Germany, while the partially deuterated samples (PB-h₂, PB-h₄, PI-h₃, PI-h₅) were kindly provided by D. Richter and L. Willner, Institut für Festkörperforschung, Forschungszentrum Jülich, Germany. The concentration of cis, trans, and vinyl units is 51%, 42%, and 7%, respectively, for the deuterated PB samples. Propylene glycol (PG, purity $\geq 99.5\%$) was purchased from Sigma-Aldrich.

The spin–lattice relaxation time $T_1(\omega)$ was determined with a STELAR FFC 2000 relaxometer which allows measurements in the temperature range of 160–400 K and ¹H Larmor frequency range $\nu = 10$ kHz–20 MHz. For temperature control at the sample position we used a thermocouple in a test tube and inserted it into the probe. The accuracy of temperature measurements was better than ± 1 K, and temperature stability was better than ± 0.3 K. T_1 was obtained by a monoexponential fit of the magnetization curve.

IV. Results

¹H T_1 Dispersion. Figure 1 displays the dispersion of the spin–lattice relaxation time $T_1(\nu)$ for the investigated polymers PB, PI, and PDMS measured at a single temperature. The respective temperature is selected to allow the best comparison among the different polymers. As the glass transition temperature T_g increases in the order of PDMS, PB, and PI,⁶ similar temperatures with respect to T_g are chosen. In the low- M system (PB466-h₆) the dispersion profile for low frequencies ($\nu < 500$ kHz) is virtually constant, and it has been shown that the relaxation behavior (i.e., its master curve) is indistinguishable from that of a simple liquid such as *o*-terphenyl.¹¹ Thus, still no polymer specific dynamics are found for PB at $M = 466$. In contrast, the dispersion data of the polymers in the high M limit ($M \gg M_c$) can be approximated at low frequencies by a power law ν^a with $a > 0$ (as indicated in Figure 1). For the fully protonated PB (PB35300-h₆) an exponent $a = 0.23$ is

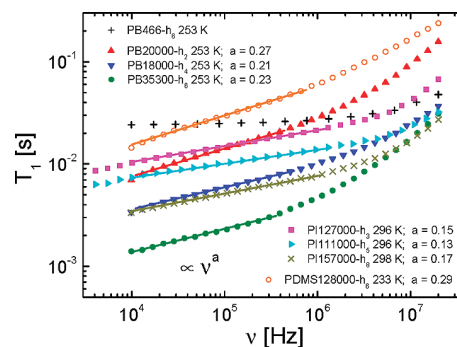


Figure 1. Dispersion of spin–lattice relaxation time $T_1(\nu)$ measured for polybutadiene (PB) at $T = 253$ K, for polyisoprene (PI) at $T = 296$ K,⁹ and $T = 298$ K and for polydimethylsiloxane (PDMS) at $T = 233$ K. Power laws ν^a with a between 0.13 and 0.29 (straight lines) at low frequencies can be observed for the polymers with $M > M_c$. The $T_1(\nu)$ curve of PB466-h₆ does not exhibit dispersion toward low frequencies (simple liquid limit).

observed. However, this power law is not found for the fully protonated PI (PI157000-h₈); instead, here $a = 0.17$. In the case of PDMS128000-h₆ a quite large exponent $a = 0.29$ is found. Moreover, for the partially deuterated PB samples (PB18000-h₄ and PB20000-h₂) power laws with $a = 0.21$ and $a = 0.27$, respectively, are obtained as shown in Figure 1. Clearly, the three differently protonated PB samples show significant variation in the exponent a . In the case of PI, partial protonation only weakly changes the exponent of the corresponding power law. Here, we emphasize that interpolation by power laws is only an approximation for specifying the differences in the relaxation behavior of the investigated polymers. Because of a different ¹H NMR coupling constant C the level of the $T_1(\nu)$ curves of the samples varies.

Since the apparent exponent a differs by a factor of about 2 among the differently protonated polymers PB, PI, and PDMS, it can be concluded that no universal dispersion is observed. Here, we note that Kimmich and co-workers^{2,13} introduced three presumably universal power law regimes (I, II, III, starting from high frequencies) for the T_1 dispersion behavior of linear polymers, and the frequency range considered in Figure 1 is that which has been called regime II with an universal exponent $a = 0.25 \pm 0.05$.² Clearly, the variation of a found in the present contribution exceeds this margin. Concerning the power laws for PI the deviations have already been recognized in refs 9 and 13. It is the goal of our contribution to understand the variation of the exponent a in the light of interplaying spectral contributions from glassy and polymer dynamics.

Susceptibility Master Curves. Measuring the T_1 dispersion in the temperature range of 223–393 K enables us to construct susceptibility master curves $\chi''(\omega\tau_s)$ for the samples of PB and PI assuming FTS. The corresponding master spectra are plotted in Figure 2 as a function of the reduced frequency $\omega\tau_s$ and are scaled by the corresponding amplitude of α -relaxation peak to account for the individual NMR coupling constant of the different polymer samples; i.e., they agree in the frequency range $\omega\tau_s \geq 1$. The susceptibility representation of the relaxation data allows to clearly distinguish between glassy and polymer specific dynamics. Whereas around the relaxation peak with $\omega\tau_s \approx 1$ contributions of glassy dynamics dominate, the excess intensity on the low-frequency side of the peak ($\omega\tau_s \ll 1$) compared to the spectrum of the simple liquid limit (PB466-h₆ or *o*-terphenyl) represents the spectral contribution for which polymer dynamics more and more dominate. The corresponding

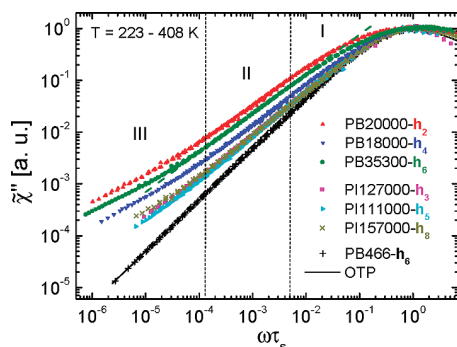


Figure 2. Master curves of the susceptibility $\chi'' = \omega/T_1$ as a function of the reduced frequency $\omega\tau_s$ for polybutadiene (PB) and polyisoprene (PI) in temperature range as indicated. Curves of PB with $M = 466$ (PB466- h_6) and *o*-terphenyl (OTP) are included as a reference for a “glassy spectrum”. Green dashed line: $\chi''(\omega) \propto \omega^{1-a}$ with $a = 0.23$ as obtained for PB35300- h_6 in regime II. Numbers and vertical dashed lines mark the different relaxation regimes according to refs 2 and 13.

amplitude is different in the entire range $\omega\tau_s < 1$ for each of the samples. In particular, the master curve of PB20000- h_2 with protons at the double bond exhibits a higher intensity than that for the fully protonated PB35300- h_6 , whereas the situation is vice versa for the spectrum of PB18000- h_4 in which only the protons of the methylene groups are present. Obviously the spectra depend on the particular proton spin pair probed in the ^1H relaxation experiment. In the case of PI, however, this effect is quite small; i.e., the excess intensity does not change strongly when partially deuterated PI is considered. We note that the different spectral intensity is not related to M since saturation is well established at $M \gg M_e$,⁹ i.e., in the high- M limit which is considered within the experimentally accessible frequency range.

The power law behavior discussed for the $T_1(\nu)$ data in Figure 1 transforms into a susceptibility behavior $\chi''(\omega) \propto \omega^{1-a}$, and the power law for regime II (discussed in Figure 1) with the corresponding exponent for PB- h_6 is included in Figure 2 (green dashed line). From this it becomes obvious that at lowest frequencies the susceptibility bends over to a weaker frequency dependence, and a second power law regime may be identified: Here, apparent exponents $a = 0.43\text{--}0.48$ and $a = 0.28\text{--}0.35$ are found for PB and PI, respectively; the values vary less than those found at higher frequencies for regime II (cf. Figure 1). Nevertheless, they again do not appear to be universal in contrast to the value $a = 0.45 \pm 0.05$ reported by Kimmich and Fatkullin for this frequency range called regime III.² For convenience, we indicate in Figure 2 the corresponding regimes according to the Kimmich and Fatkullin classification. At high frequencies close to the susceptibility maximum, it is obvious that in addition to polymer dynamics glassy dynamics contribute significantly to the relaxation. This regime has been called regime I by Kimmich and co-workers, and a power law exponent $a = 0.5 \pm 0.05$ has been claimed to be found.^{2,13} However, such an exponent cannot be clearly recognized, and as said the corresponding relaxation contributions cannot be attributed to polymer dynamics alone.

Polymer Spectra. Separating glassy and polymer spectral contributions along eq 4 by subtracting the “glassy spectrum” of PB466- h_6 from each of the total susceptibility curves $\chi''(\omega)$ of Figure 2 yields spectra reflecting only polymer dynamics (“polymer spectra”, cf. Figure 3). This allows extracting the relaxation strength f of polymer dynamics by calculating the relative integrated intensities of the individual polymer spectra (see Table 2). For PB the

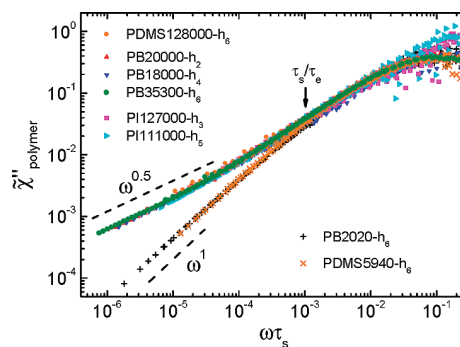


Figure 3. Normalized polymer spectra $\chi''_{\text{polymer}}(\omega\tau_s)$ obtained by subtracting the contribution of glassy dynamics (PB466- h_6 for PB and PI; PDMS860- h_6 for PDMS) from the total susceptibility spectra of Figures 2 and 4 coincide for the high- M limit. Dashed lines: power laws at low frequencies ω^1 representing terminal relaxation and $\omega^{0.5}$ for high- M polymers. Note that the polymer spectra of PDMS are shifted by a single factor in frequency (see text).

Table 2. Relaxation Strength f of Polymer Dynamics in Fully and Partially Protonated Samples of Polybutadiene (PB) and Polyisoprene (PI) as Well as Polydimethylsiloxane (PDMS) with $M > M_e$, As Obtained by Subtractive Decomposition and by Comparing Amplitudes in Figure 5

sample	f (from spectra decomposition)	f (from Figure 5)
PB20000- h_2	0.16 ± 0.02	(≈ 0.16)
PB18000- h_4	0.06 ± 0.006	0.064 ± 0.003
PB35300- h_6	0.11 ± 0.01	0.109 ± 0.003
PI127000- h_3	0.03 ± 0.01	0.031 ± 0.002
PI111000- h_5	0.02 ± 0.01	0.025 ± 0.001
PI157000- h_8	0.03 ± 0.01	0.036 ± 0.001
PDMS128000- h_6	0.02 ± 0.002	

highest value $f = 0.16$ is obtained for the sample PB20000- h_2 . As discussed before, for PB18000- h_4 f is smaller ($f = 0.06$); the fully protonated sample PB35300- h_6 is somewhat in between ($f = 0.11$). For the differently deuterated PI samples we find similarly small values ($f = 0.03$).

In Figure 3 we show the polymer spectra $\chi''_{\text{polymer}}(\omega\tau_s)$ which have been obtained by normalizing the polymer spectrum to provide an integral which equals $\pi/2$ (cf. ref 12). In this representation it is clearly seen that the high- M polymer spectra for the differently deuterated and the fully protonated PB and PI are virtually identical. In particular, power laws with the same exponents are revealed, and therefore the spectra reflect the same dynamic process, which was not evident from inspecting the total relaxation spectra. Only by accounting for the contribution of glassy dynamics universal polymer spectra are revealed. Such spectra may now be compared to predictions of polymer theories which usually exclude fast segmental dynamics. We note that at $\omega\tau_s \geq 10^{-1}$ a maximum appears in Figure 3 which signals the cutoff of the polymer spectra at high reduced frequencies.

Special Case PDMS. The susceptibility master curve of PDMS is not included in Figure 2 as particularities show up which we want to discuss separately. In Figure 4a the master curve for PDMS128000- h_6 (full circles) is displayed together with that for $M = 5940 \approx M_e = 8100$ ²¹ (open circles) and for the lowest M measured (PDMS860- h_6 ; crosses). For comparison, again the low M data for PB (PB466- h_6 ; pluses) are included. When comparing the data also with those in Figure 2 for PB or PI significant differences show up. For example, the data for PDMS860- h_6 show a different behavior to that of the low M limit for PB (PB466- h_6); specifically, the relaxation peak for PDMS860- h_6 has a shoulder at low frequencies ($\omega\tau_s \leq 1$), i.e., significant excess intensity with

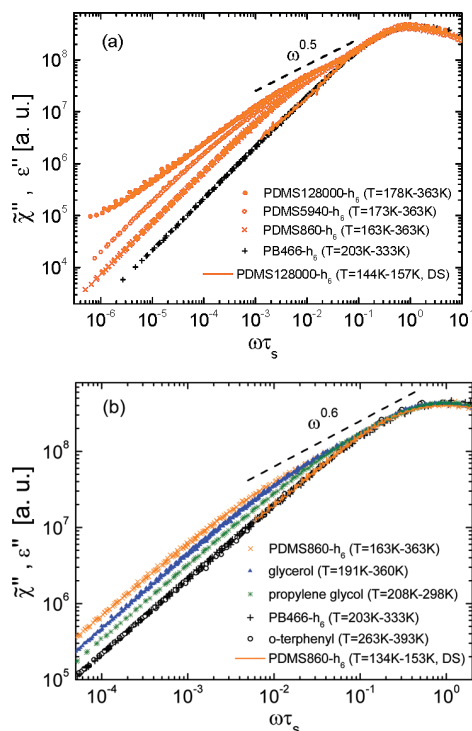


Figure 4. Master curves of the susceptibility $\chi''(\omega) = \omega/T$ as a function of the reduced frequency $\omega\tau_s$ for (a) different polydimethylsiloxanes (PDMS) as well as a master curve from dielectric studies (orange line),⁶ (b) Master curves for low- M polydimethylsiloxane (PDMS860- h_6), glycerol,²² and propylene glycol for temperature ranges as indicated: each spectra exhibits an anomaly for $\omega\tau_s \leq 1$ compared to the master curve of polybutadiene (PB466- h_6) or *o*-terphenyl as reference systems of simple liquids. Orange line: master curve for PDMS860- h_6 from dielectric spectroscopy (DS).

respect to the spectrum of PB466- h_6 . Presumably, the susceptibility data of PDMS860- h_6 show very weak contributions from polymer relaxation, if any. We have not been able to measure PDMS samples with lower M to fully check this assumption as crystallization always interferes. Inspecting all the three curves for PDMS (high and low M limit as well as M_c), this shoulder appears in all cases leading to a virtually common relaxation behavior at $10^{-2} < \omega\tau_s \leq 1$, i.e., in a frequency range for which M depending spectral contributions from polymer dynamics are already found in PB as well as in PI. This common relaxation regime is found for all investigated PDMS samples independent of M ; M -dependent contributions only appear at $\omega\tau_s < 10^{-2}$. Thus, the shoulder cannot originate from some polymer specific relaxation. We will attribute it to a particular relaxation feature already observed in the low- M limit, for which only glassy dynamics control the relaxation (cf. below).

It is worthwhile to note that a similar anomaly as for PDMS860- h_6 is also observed in the low molecular weight glass formers glycerol²² and propylene glycol (PG). In order to show this effect more clearly, we display the corresponding master curves together with those for PDMS860- h_6 , PB466- h_6 , and *o*-terphenyl (OTP) in Figure 4b. Indeed, the curves for glycerol, PG, and PDMS860- h_6 are very similar, showing in all the cases a low-frequency shoulder with respect to the data of PB466- h_6 or OTP; the latter may be taken as reference systems for FFC spectra of simple liquids.^{10,11} Interestingly, this low-frequency anomaly is only observed in the NMR data but not in the dielectric data of PDMS860- h_6 ,⁶ which is also displayed in Figure 4b (a similar behavior is observed for glycerol²²). Converting our

dielectric results for PDMS128000- h_6 ⁶ into a master curve (line), it is seen that this curve coincides very well with the dispersion data of PB466- h_6 or *o*-terphenyl (also included in Figure 4b). We emphasize that PDMS is a type B polymer;²³ thus, dielectric spectroscopy only probes glassy dynamics. Up to now this relaxation feature is not understood. We conclude that in PDMS contributions from polymer dynamics are only found at reduced frequencies lower than say $\omega\tau_s < 10^{-2}$.

In order to obtain the polymer spectrum in the case of PDMS, we have subtracted the master curve of PDMS860- h_6 from the susceptibility data of the higher M . For comparing the data with the polymer spectra of PB and PI in Figure 3, however, the polymer spectra for both PDMS128000- h_6 and PDMS5940- h_6 have been shifted in frequency by a factor of 17. This is understood by the fact that as discussed polymer dynamics set in for PDMS only at significantly lower frequencies as compared to those in PB or PI. Again, a good agreement is found. Essentially, all the polymer spectra agree after correcting for the contribution of glassy dynamics.

We note that for the high- M limit of PDMS an apparent power law behavior, $\chi''(\omega) \propto \omega^{-a}$, with $a = 0.5$ can be observed over a quite extended frequency range $10^{-3} < \omega\tau_s < 5 \times 10^{-2}$ (dashed line in Figure 4a). Thus, in the case of PDMS indeed a clear-cut power law regime is recognized as expected for regime I of the Kimmich–Fatkulkin classification scheme. However, it does not reflect solely polymer dynamics; instead, it has its origin in interplay of the contributions from (anomalous) glassy and polymer dynamics. In the case of the data for the low-molecular-weight systems displayed in Figure 4b a similar power law with an exponent $a = 0.60 \pm 0.03$ is observed (dashed line in Figure 4b). We emphasize that the experimental data for PDMS (as well as for PB) agree with those compiled by Kimmich and co-workers.^{24,25}

Comparison of Rouse and Entanglement Contribution. In order to understand the relaxation behavior of linear polymers in the limit of high M , i.e., with fully established entanglement dynamics, it is of interest to compare the polymer spectra (after subtracting the glassy spectrum from the overall relaxation spectra) with the corresponding spectrum from a sample with $M \cong M_c$ for which solely Rouse dynamics are expected and entanglement dynamics are not established yet. Therefore, we include in Figure 3 the polymer spectrum of PB2020- h_6 ¹⁰ and PDMS5940- h_6 . Clearly, a quite different behavior is observed at $\omega\tau_s \leq 10^{-3}$ between the master curves of high M and $M \cong M_c$ whereas for $\omega\tau_s > 10^{-3}$ they coincide. We attribute the much stronger amplitude below $\omega\tau_s < 10^{-3}$ of the high- M samples to contributions specific to entanglement effects; i.e., as expected, entanglement results in a significant retardation of the correlation loss which leads to a kind of bimodal relaxation. We find a power law behavior, $\chi''_{\text{polymer}}(\omega) \propto \omega^{-a}$, with an exponent $a = 0.50 \pm 0.05$ as already concluded from discussing Figure 2 for which the contribution from glassy dynamics have not yet been accounted for. In other words, at lowest frequencies the glassy contribution in $\chi''(\omega)$ can be ignored indeed.⁷

Regarding the frequency range $\omega\tau_s > 10^{-3}$ the susceptibility curves for the sample with $M = M_c$ and for the high M limit are virtually the same (cf. Figure 3). This means that the polymer dynamics of entangled polymers at such comparatively high frequencies are essentially the same as those of nonentangled polymers with $M = M_c$. As previously shown for PB,¹² the spectra of the latter can be semiquantitatively reproduced by the discrete Rouse model assuming

a few Rouse modes being activated (note $M_e/M_R = 4-5$ for PB and $9-10$ for PDMS). Within the tube-reptation model we can identify the crossover at the $\omega\tau_s \cong 10^{-3}$ reflecting the ratio τ_s/τ_e . At the entanglement time $\tau_e \cong 10^3\tau_s$ the polymer chain “feels” first entanglement effects. We note that for PB2020-h₆ and PDMS5940-h₆ the crossover to the Debye limit $\chi''(\omega) \propto \omega^1$ is observed at lowest frequencies, indicating that contributions up to the slowest (Rouse) relaxation mode are detected.^{7,12} We take the fact that the shapes of the polymer spectra of PB and PDMS for $M \cong M_e$ agree so well even at intermediate frequencies ($\omega\tau_s < 10^{-1}$) as an additional argument that indeed the additive separation of contributions from polymer and glassy dynamics is appropriate.

V. Discussion and Conclusions

Extending our previous FFC ¹H NMR measurements and analysis on PB^{7,9-12} to different polymers including partially deuterated systems and concentrating on the entanglement regime ($M \gg M_e$), it turns out that the low-frequency behavior ($\omega\tau_s < 1$) of the T_1 dispersion does not show universal power law characteristics, in contrast to what was claimed before.^{2,13} If at all power law regimes can be identified, their apparent exponents differ (cf. Figure 1). Comparing the dispersion behavior in form of the susceptibility (cf. Figure 2) to that of the low- M systems ($M < M_R$) with no polymer specific contribution but only glassy contribution, the extent of excess intensity at $\omega\tau_s < 1$ with respect to the simple liquid limit $\chi''(\omega) \propto \omega^1$ ($\omega\tau_s < 1$) is very different for the investigated polymers. It may even depend on the extent of protonation of a given monomer, i.e., on the particular spin pairs probed by ¹H NMR. In other words, the relaxation strength f in terms of eq 3 is different in the polymers. We recall that within the present definition f is a measure of the spatial restriction of glassy dynamics for a given spin pair (or groups of spin pairs) imposed by Rouse as well as entanglement dynamics. Referring in particular to the case of PDMS with its M -independent anomalous glassy dynamics in order to understand the polymer specific contribution in the T_1 dispersion data of polymers, our results emphasize the importance of including a study of the low- M limit for each polymer. However, this may not always be possible as crystallization may occur.

As discussed in section II, in the high- M limit ($M \gg M_e$) the transient entanglement network points are believed to introduce topological constraints impeding the reorientation involved in the glassy dynamics at short times ($t \leq \tau_s$), and f or the dynamic order parameter S is expected to depend on the direction of the internuclear vector between a spin pair with respect to the contour of the chain (cf. angle ϑ_{ij} in eq 5). For example, in their DQ NMR study on PB melts, Spiess and co-workers determined quite different values f_{ij} for the different spectrally resolvable spin pairs of the monomeric segment.^{15,16} Although their values of f_{ij} are significantly higher than those estimated from our FFC experiments (for a discussion of this discrepancy cf. ref 11), the same trend is observed in the present study (cf. Table 2): $f_{\text{CH}=\text{CH}}$ determining the dispersion behavior of PB-h₂ is significantly larger than f_{CH_2} , the latter essentially fixing the dispersion of PB-h₄. Qualitatively, this difference may be understood by recalling that in PB-h₂ with its protons attached to the carbon atoms at the double bond (in cis and trans configuration) the angle ϑ_{ij} with respect to the contour direction, the latter presumably fixed by the direction of the double bond, is rather small and thus leading to a small reduction of the order parameter with respect to that of the chain itself, S_{chain} . In contrast, a much stronger reduction is expected for the methylene group in PB-h₄. In the case of PI with its absence of a spin pair along the double bond, different protonation only slightly changes f (cf. Table 2).

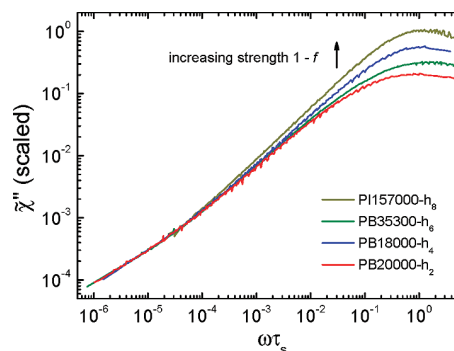


Figure 5. Susceptibility spectra for the different polymers plotted to agree at lowest frequencies.

Refraining to explain the behavior of f in detail, we rather conclude the following. (i) It appears that the considerations regarding the relative values of f hold for both the entanglement regime and the Rouse regime ($M_R < M < M_e$), and they can qualitatively explain the nonuniversal dispersion behavior of $T_1(\omega)$ in the different polymers and in selectively deuterated samples of a given polymer. (ii) Subtracting the corresponding contribution of glassy dynamics from the total dispersion via eq 4 yields universal polymer spectra (cf. Figure 3). Searching in $T_1(\omega)$ for generic polymer effects without accounting for the glass process is misleading as the latter is always a large contribution with $1 - f \gg f$. This holds especially for small M in the Rouse regime in which f decreases with decreasing M .¹²

Here two comments are worthwhile. First, subtracting the “glassy spectrum” from the total susceptibility spectrum of polymers assumes that the first does not change with M , a fact well-known from dielectric spectroscopy on type B polymers for which only the glassy transition is probed.²³ It has also been specifically tested for PB.⁶ Second, although the spectral contribution of the glassy dynamics and of Rouse dynamics are not fully separated, a simple additive separation yields universal polymer spectra. Thus, we think this separation procedure is essentially a good approximation although some distortion of the polymer spectra may be expected at $\omega\tau_s \leq 1$. In the Appendix we demonstrate that indeed the results will remain essentially unchanged if one performs a decomposition of the correlation function in the time domain instead of applying the subtraction approach of the susceptibility in the frequency domain.

As an alternative approach to the additive decomposition, one can estimate the contribution from glassy and polymer dynamics, that is f , by a simple scaling procedure. In Figure 2 the susceptibility master curves are normalized to agree in the frequency range of the glass transition. Hence, the amplitude of the susceptibility at lowest frequencies for which influence of contributions from glassy dynamics can be ignored may be taken as measure of f . Vice versa, we may plot the data in a way that they agree at lowest frequencies (cf. Figure 5). Assuming universal polymer spectra, this is nothing else than plotting $\tilde{\chi}''(\omega)/fC$ except for an unknown factor. Then, the different heights of the relaxation maximum reflect the different strength $1 - f$ of the contribution from glassy dynamics assuming similar shape of $\tilde{\chi}''_{\text{glassy}}(\omega)$. Explicitly, the maximum height in Figure 5 is a measure for $(1 - f)/f$. In order to get absolute values for f , we choose that of PB20000-h₂ obtained by the subtraction method as reference. In Table 2 we compare the results of this estimate to that of the additive separation. Very similar values are obtained, again demonstrating that the additive decomposition of the spectra yields reliable values of f . The spectra in Figure 5 agree at lowest frequencies as expected for a universal entanglement contribution (note that PDMS is excluded from this analysis due to its low-frequency anomaly of the α -process). First, deviations

from the common spectrum appear at $\omega\tau_s > 5 \times 10^{-5}$ for PI which exhibits the strongest contribution $\tilde{\chi}''_{\text{glassy}}(\omega)$. Thus, this plot directly shows the non-negligible influence from spectral contributions associated with glassy dynamics. The latter is smallest in PB- h_2 , and the corresponding spectrum reflects polymer specific contributions over the largest frequency range. This again reveals an advantage of the susceptibility representation, and it becomes obvious that extracting power law exponents in the frequency range of Rouse dynamics $\omega\tau_s > 10^{-4}$ (cf. below) without taking into account the contribution from glassy dynamics yields erroneous results.

The universal polymer spectra of entangled polymers (after separating glassy and polymer specific contributions) show two power law regimes in addition to a cutoff regime at highest frequencies (cf. Figure 3). This is in contrast to previous statements by Kimmich and co-workers, who have reported three power law regimes (I–III)^{2,13} although deviations were discussed, too.^{9,13} Their interpretation, however, suffers from the fact that glassy dynamics have not been taken explicitly into account. From the present analysis as well as from our previous works,^{7,11,12} we conclude that only two power law regimes exist for entangled polymers (at least in the currently accessible frequency range), and the crossover between them may be associated with the entanglement time τ_e . Whereas the first power law regime at high frequencies is attributed to free Rouse dynamics since it is identical with the relaxation behavior in a nonentangled polymer with $M \cong M_e$, the second one at lowest frequencies reflects contributions specific for entanglement dynamics. It is identical with regime III of the Kimmich–Fatkulin classification scheme. Since here the influence of spectral contributions from glassy dynamics can be neglected in the total dispersion spectra, the result agrees in both interpretations, i.e., a power law $\tilde{\chi}''_{\text{polymer}}(\omega) \propto \omega^{1-a}$ with $a \cong 0.5$ is recognized at lowest frequencies. Kimmich and Fatkulin attributed this dispersion regime to intersegmental relaxation.^{2,27} This has become possible by comparing ^1H and ^2H FFC NMR results for PB.²⁵ ^2H NMR does not probe intersegmental relaxation, and they have not observed regime III in this case. As the fraction of intermolecular or intersegmental relaxation is expected to depend on structural details of the monomer, it is surprising that taking this interpretation for granted this regime is found to be universal. More experimental data are needed to settle this point.

In Figure 3, at higher frequencies, the free Rouse regime is characterized by an apparent power law $\tilde{\chi}''_{\text{polymer}}(\omega) \propto \omega^{1-a}$ with $a = 0.30 \pm 0.05$, which is similar but not identical to that observed in the total dispersion for PB- h_6 and PDMS- h_6 (cf. Figures 2 and 4a), and it corresponds to regime II of the Kimmich–Fatkulin classification scheme. Both polymers show a quite large excess intensity compared to their low- M system, and consequently the difference between the total relaxation spectra and the “polymer spectra” is small. However, this is not the case for PI and PB- h_4 with their small relaxation strength (cf. Table 2). Here, the spectral contributions of the glassy dynamics cannot be ignored. Regarding the investigated polymers, regime I of the Kimmich–Fatkulin classification observed at highest frequencies in the total spectra $\chi''(\omega)$ (cf. Figure 2 or 4) clearly is dominated by spectral contribution from glassy dynamics and thus cannot be attributed to polymer specific relaxation alone.

Finally, we note that as discussed thoroughly in ref 7, the polymer specific relaxation regimes can be explained neither by the tube reptation nor by the once renormalized Rouse model. On the one hand, assuming that the spectra at lowest frequencies (regime III) are indeed dominated by intersegmental relaxation, then the twice renormalized Rouse model predicts an exponent $a = 0.5$ as experimentally observed.²⁷ On the other hand, very similar results are reported by Monte Carlo (MC) simulations,¹⁴ and as mentioned already before, it has been

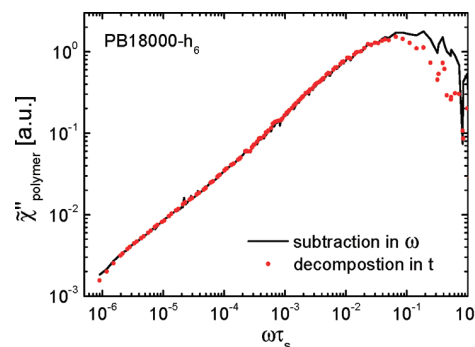


Figure 6. Polymer spectrum $\tilde{\chi}''_{\text{polymer}}(\omega\tau_s)$ of polybutadiene with $M = 18000$ (PB18000- h_6) obtained by subtracting the glassy spectrum from the total susceptibility spectrum⁷ (black line) and by decomposition of the correlation function along eq 3 (red dots).

concluded that the crossover from nonentangled to entangled dynamics with tube-reptation dynamics is “very protracted”; i.e., it may be observed at $M \gg M_e$ (for a comparison of FFC NMR and MC simulation results cf. ref 7). This is also supported by very recent results from DQ NMR.²⁸ The intriguing agreement of results from FFC NMR and simulations, again, may cast doubts on the interpretation that regime III can be attributed to intersegmental correlation effects as MC simulations do not include such correlations. In any case, FFC NMR provides a unique opportunity for elucidating dynamics in polymer systems and even lower frequencies may be accessible in the near future. The program of the Kimmich group to unravel universal polymer relaxation in chemically quite different polymers by FFC NMR appears to be indeed possible provided that the spectral contribution of the glassy dynamics is well accounted for.

Acknowledgment. The authors are grateful to D. Richter and L. Willner (Institut für Festkörperforschung, Forschungszentrum Jülich, Germany) for kindly providing the deuterated polyisoprene and polybutadiene samples. Support from Deutsche Forschungsgemeinschaft (SFB 481) is highly appreciated. We thank S. Stapf (Technische Universität Ilmenau) for valuable comments on the manuscript.

Appendix

Subtraction versus Deconvolution. Figure 6 displays the polymer spectrum $\tilde{\chi}''_{\text{polymer}}(\omega\tau_s)$ of PB18000- h_6 (data from ref 7) as obtained on the one hand (black solid line) by subtracting the glassy spectrum of PB466- h_6 from the total susceptibility master curve $\tilde{\chi}''(\omega\tau_s)$ and on the other hand (red dots) by decomposing the orientational correlation function $F_2(t)$ along eq 3. In the latter case, decomposing $F_2(t)$ by dividing out $\phi_{\text{glass}}(t)$ consisting of a Kohlrausch function with a stretching parameter $\beta_K = 0.4$ and a relaxation strength $f = 0.16$ (cf. Table 2) yields $F_{\text{polymer}}(t)$. Fourier transform back to the frequency domain again gives $\tilde{\chi}''_{\text{polymer}}(\omega\tau_s)$. As it can be concluded from Figure 6, the two approaches lead to a very similar result, in particular the shape of spectrum and consequently the apparent power laws coincide for both methods provided that $M \gg M_e$ and $\omega\tau_s < 10^{-2}$. Therefore, the additive decomposition leading to the polymer spectra reflecting a universal behavior in Figure 3 is well justified in the present context.

References and Notes

- Doi, M.; Edwards, S. F. *The Theory of Polymer Dynamics*; Oxford Sci. Publication: New York, 1986.
- Kimmich, R.; Fatkulin, N. *Adv. Polym. Sci.* **2004**, *170*, 1–113.

- (3) Angell, C. A.; Ngai, K. L.; McKenna, G. B.; McMillan, P. F.; Martin, S. W. *J. Appl. Phys.* **2000**, *88*, 3113–3157.
- (4) Lunkenheimer, P.; Schneider, U.; Brand, R.; Loidl, A. *Contemp. Phys.* **2000**, *41*, 15–36.
- (5) Blochowicz, T.; Brodin, A.; Rössler, E. A. *Adv. Chem. Phys.* **2006** *133* Part A, 127–256.
- (6) Hintermeyer, J.; Herrmann, A.; Kahlau, R.; Goiceanu, C.; Rössler, E. A. *Macromolecules* **2008**, *41*, 9335–9344.
- (7) Herrmann, A.; Novikov, V. N.; Rössler, E. A. *Macromolecules* **2009**, *42*, 2063–2068.
- (8) Fatkullin, N.; Kausik, R.; Kimmich, R. *J. Chem. Phys.* **2007**, *126*, 094904–1–094904–8.
- (9) Kariyo, S.; Stapf, S.; Blümich, B. *Macromol. Chem. Phys.* **2005**, *206*, 1292–1299.
- (10) (a) Kariyo, S.; Gainaru, C.; Schick, H.; Brodin, A.; Novikov, V. N.; Rössler, E. A. *Phys. Rev. Lett.* **2006**, *97*, 207803–1–207803–4.
(b) Erratum; Kariyo, S.; Herrmann, A.; Gainaru, C.; Schick, H.; Brodin, A.; Novikov, V. N.; Rössler, E. A. *Phys. Rev. Lett.* **2008**, *100*, 109901–1.
- (11) Kariyo, S.; Brodin, A.; Gainaru, C.; Herrmann, A.; Schick, H.; Novikov, V. N.; Rössler, E. A. *Macromolecules* **2008**, *41*, 5313–5321.
- (12) Kariyo, S.; Brodin, A.; Gainaru, C.; Herrmann, A.; Hintermeyer, J.; Schick, H.; Novikov, V. N.; Rössler, E. A. *Macromolecules* **2008**, *41*, 5322–5332.
- (13) Kimmich, R.; Anoardo, E. *Prog. NMR Spectrosc.* **2004**, *44*, 257–320.
- (14) Kreer, T.; Baschnagel, J.; Müller, M.; Binder, K. *Macromolecules* **2001**, *34*, 1105–1117.
- (15) Graf, R.; Heuer, A.; Spiess, H. W. *Phys. Rev. Lett.* **1998**, *80*, 5738–5741.
- (16) Dollase, T.; Graf, R.; Heuer, A.; Spiess, H. W. *Macromolecules* **2001**, *34*, 298–309.
- (17) Saalwächter, K. *Progr. NMR* **2007**, *51*, 1–35.
- (18) Bloembergen, N.; Purcell, E. M.; Pound, R. V. *Phys. Rev.* **1948**, *73*, 679–715.
- (19) Gubaidullin, A.; Shakirov, T.; Fatkullin, N.; Kimmich, R. *Solid State Nucl. Magn. Reson.* **2009**, *39*, 147–151.
- (20) Lipari, G.; Szabo, A. *J. Am. Chem. Soc.* **1982**, *104*, 4546–4559.
- (21) Ferry, J. D. *Viscoelastic Properties of Polymers*; Wiley: New York, 1980.
- (22) Gainaru, C.; Lips, O.; Troshagina, A.; Kahlau, R.; Brodin, A.; Fujara, F.; Rössler, E. A. *J. Chem. Phys.* **2008**, *128*, 174505–1–174505–11.
- (23) Kremer, F.; Schönhals, A., Eds. *Broadband Dielectric Spectroscopy*; Springer: Berlin, 2003.
- (24) Weber, H. W.; Kimmich, R. *Macromolecules* **1993**, *26*, 2597–2606.
- (25) Kimmich, R.; Fatkullin, N.; Seitter, R.-O.; Gille, K. *J. Chem. Phys.* **1998**, *108*, 2173–2177.
- (26) Fatkullin, N.; Kimmich, R.; Weber, H. W. *Phys. Rev. E* **1993**, *47*, 4600–4603.
- (27) Fatkullin, N.; Kimmich, R.; Kroutieva, M. *J. Exp. Theor. Phys.* **2000**, *91*, 150–166.
- (28) Chávez, F. V.; Saalwächter, K. Private communication.

Publication 3

**Protracted Crossover to Reptation Dynamics:
A Field Cycling ^1H NMR Study Including Extremely Low Frequencies.**

Herrmann, A.; Kresse, B.; Gmeiner, J.; Privalov, A. F.; Kruk, D.;
Fujara, F.; Rössler, E. A.
Macromolecules **2012**, *45*, 1408-1416.

Copyright 2012 by The American Chemical Society
DOI: 10.1021/ma202489y

Protracted Crossover to Reptation Dynamics: A Field Cycling ^1H NMR Study Including Extremely Low Frequencies

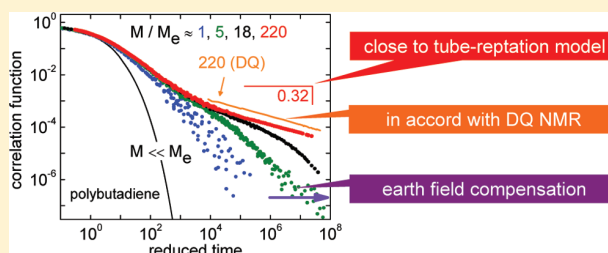
A. Herrmann,^{†,‡} B. Kresse,[‡] J. Gmeiner,[‡] A. F. Privalov,^{‡,§} D. Kruk,^{†,§} F. Fujara,[‡] and E. A. Rössler^{*,†}

[†]Experimentalphysik II, Universität Bayreuth, D-95440 Bayreuth, Germany

[‡]Institut für Festkörperphysik, TU Darmstadt, Hochschulstr. 6, 64289 Darmstadt, Germany

[§]University of Warmia & Mazury Olsztyn, Faculty of Mathematics & Computer Science, PL-10710 Olsztyn, Poland

ABSTRACT: The segmental dynamics of 1,4-polybutadiene is investigated by means of electronic field cycling ^1H NMR. The frequency dependence (dispersion) of the spin–lattice relaxation time is probed over a broad range of temperature (223–408 K), molecular mass ($355 \leq M$ (g/mol) $\leq 441\,000$), and frequency (200 Hz–30 MHz). The extremely low frequencies are accessed by employing a home-built compensation for earth and stray fields extending prior reports about 2 decades to lower frequencies. Applying frequency–temperature superposition yields master curves over 10 decades in frequency (or time), and after Fourier transform the full dipolar correlation function is traced over up to 8 decades in amplitude. Several relaxation regimes can be identified, and their power-law exponents are compared to the predictions of the Doi–Edwards tube-reptation model, namely the free Rouse (I) and the constrained Rouse regime (II). Whereas the predicted value of the power-law exponent of regime II is 0.25, we find that it depends on M and levels off at 0.32 for very high $M = 441\,000 \approx 220M_e$ (M_e : entanglement molecular mass). This is in good agreement with recent results from double quantum ^1H NMR and indicates that the actual onset of full reptation dynamics is strongly protracted.



1. INTRODUCTION

The dynamics of polymer melts is unremittingly subject to theoretical and experimental scientific research. The dynamical features are most often describable by the tube-reptation model of Doi and Edwards,¹ which can be considered as a combination of the Rouse model² for nonentangled polymer chains (with molecular mass M below the entanglement molecular mass M_e) and the essence of de Gennes' reptation model³ for $M > M_e$. The tube-reptation model is very successful in predicting semiquantitatively the M dependence of transport coefficients like viscosity and translational diffusion coefficient. In order to account for weak deviations between model predictions and experimental or simulation findings, ongoing discussions^{4–9} refine the model, e.g., by effects of contour length fluctuations (CLF)^{10,11} and constraint release (CR).^{12,13} The first ones are due to motions of the chain ends, and the latter are caused by the chains forming a nonstatic tube (or matrix). It remains an experimental challenge to probe the dynamics on a microscopic scale involving all the relaxation regimes forecast by the tube-reptation model. Important experimental techniques addressing these issues and revealing details of the dynamics on a molecular level are for example dielectric spectroscopy,^{14,15} neutron spin echo,^{16,17} and NMR,^{18–23} in particular NMR relaxometry.^{24,25}

Electronic (fast) field cycling (FC) NMR relaxometry has become an important tool for the investigation of collective dynamics in nonentangled and entangled polymers.^{24–26} It can be applied to measure the frequency dependence (dispersion)

of the spin–lattice relaxation rate $1/T_1$ over a frequency range of usually about 3 decades (10 kHz–20 MHz). In the case of ^1H NMR the technique probes the dipolar fluctuations of the proton spin pairs in the polymer melt, and they are usually assumed to be dominated by reorientational motion of the polymer segment. In a recent series of papers, we have investigated polymer dynamics of linear polybutadiene (PB) with systematically varied M .^{27–31} Frequency–temperature superposition (FTS), commonly employed in rheology of polymers,³² has been applied in order to extend the accessible frequency window of FC NMR. Thereby we have been able to monitor the dipolar correlation function of PB over more than 6 decades in amplitude and 8 decades in frequency, encompassing local segmental as well as collective polymer dynamics. In particular, the regimes I and II of the Doi–Edwards tube-reptation model¹ have been covered.

Vaca Chávez and Saalwächter have combined these results with their data from double quantum (DQ) ^1H NMR³³ which almost perfectly extend the FC ^1H NMR data up to even longer times into the reptation (III) and free-diffusion regimes (IV) of the tube-reptation model.^{33,34} Thus, for the first time the full segmental correlation function has been disclosed over more than 10 decades in time. In the light of these joint NMR results, the long-time relaxation behavior in linear polymer melts can be

Received: November 11, 2011

Revised: December 20, 2011

Published: January 24, 2012

attributed to a highly protracted transition from Rouse dynamics to almost completely established tube reptation. The latter has been reached only at $M/M_e > 200$ ($M_e \approx 2000$: entanglement molecular mass). For example, the power-law exponent ε of regime II has turned out to be M -dependent. A transition from $\varepsilon \cong 0.6$ at $M \cong M_e$ to $\varepsilon \cong 0.29$ at $M \cong 1000M_e$ has been observed. The latter exponent is quite close to the predicted value of $\varepsilon = 0.25$. In accordance with rheological^{35,36} and dielectric experiments¹⁵ as well as Monte Carlo simulations,^{37,38} we have claimed that the crossover to full tube-reptation dynamics occurs only above another characteristic molecular mass $M_r \gg M_e$.³⁰

So far, the necessary frequency (or time) window to probe the saturation behavior of the exponent ε at high M has only been accessible by DQ ^1H NMR. Yet, a field-gradient NMR study¹⁸ revealed the crossover for the self-diffusion coefficient from regime IV to regime III coming from long times. Standard FC ^1H NMR as provided by utilizing, e.g., the commercial Stellar spectrometer reaches only a low-frequency bound of, say, 10 kHz. However, especially for polymers (or soft matter in general) even lower frequencies or longer times are desirable in order to investigate their slow dynamics, i.e., tracing the correlation function over as many decades as possible with one experimental method. This can be achieved by actively compensating earth and stray fields. Already Noack and co-workers³⁹ have reported relaxation dispersion results reaching about 100 Hz. Exploiting the possibilities of a home-built FC spectrometer, very recently Kresse et al.⁴⁰ have reached down below 100 Hz. In the present contribution we will apply this technique to measure $T_1(\nu)$ of linear PB melts for different M down to 200 Hz, which is almost 2 decades lower in frequency as compared to our previous FC ^1H NMR measurements.³⁰ Thereby we considerably extend our accessible time scales to those of DQ ^1H NMR, and we will show that indeed the exponent of the regime II continuously decreases down to $\varepsilon = 0.32$ for $M = 441\,000$; i.e., even at $Z > 200$ the prediction of the power-law exponent $\varepsilon = 0.25$ is not reached. On the one hand, this well confirms the results from DQ ^1H NMR;³⁴ on the other hand, this suggests that additional relaxation mechanisms may have to be taken into consideration to describe the dynamics of entangled polymers.

2. THEORETICAL BACKGROUND

Tube-Reptation Model. As thoroughly discussed in refs 1,7,25,32, 33, and 41, the dynamics of entangled polymer chains can be attributed to five relaxation regimes (0–IV) depending on the time scale of the motion and the length of the chain. Figure 1 shows schematically the mean-square displacement $\langle r^2(t) \rangle$ and a rank-two reorientational correlation function $g^{(2)}(t)$ for a polymer segment as predicted by the Doi–Edwards tube-reptation model for a simple liquid, a nonentangled and an entangled polymer. At the shortest times, $t \leq \tau_\alpha \cong \tau_s$ (regime 0), the dynamics is governed by the glass transition phenomenon for which the long-time tail of $g^{(2)}(t)$ can be described by a stretched exponential decay, and the segmental correlation time τ_s can be identified with that of the α -process τ_α .^{24,27,33} The absence of any slower dynamics is the characteristic of a simple liquid, e.g., a molecular glass-former. In $\langle r^2(t) \rangle$ the ballistic short-time behavior ($t \ll \tau_s$) followed by a plateau signaling the cage effect is typical of glassy dynamics. Beyond the transition from oligomers to polymers at M_R (molecular mass of a Rouse unit) the chain connectivity starts to govern the segmental dynamics and is best described by the

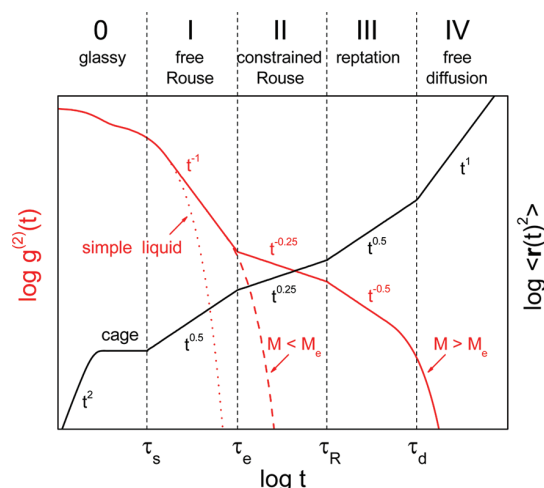


Figure 1. Schematic time dependence of the logarithm of the segmental reorientational correlation function of rank-two $g^{(2)}(t)$ (red line) and the mean-square displacement $\langle r^2(t) \rangle$ (black line) as a function of logarithm of time as expected from the Doi–Edwards tube-reptation model ($M > M_e$). For $g^{(2)}(t)$ the behavior of a simple liquid (dotted line), a nonentangled polymer ($M < M_e$, dashed line), and entangled polymers ($M > M_e$, solid line) is distinguished.

Rouse model (regime I) as reflected in the power-law behavior $g^{(2)}(t) \propto t^{-1}$ or $\langle r^2(t) \rangle \propto t^{0.5}$. Above the entanglement molecular mass M_e and between the entanglement time τ_e and the Rouse time τ_R the chain feels the constraints of its surrounding, i.e., a fictitious curved tube formed by its neighboring chains (regime II). At longer times the polymer chain diffuses along the primitive path of the tube (regime III), and finally free diffusion is reached after the terminal relaxation time ($t \gg \tau_d$: disengagement time, regime IV), leading at longest times to an essentially exponential cutoff in $g^{(2)}(t)$ or $\langle r^2(t) \rangle \propto t^1$. Note that Ball et al.⁴¹ have provided a joint analytical description for regimes III and IV. The mean-square displacement $\langle r^2(t) \rangle$ in regime II and III is proportional to the tube survival probability and $g^{(2)}(t) \propto 1/\langle r^2(t) \rangle$ holds.^{24,41} The power-laws of the individual regimes for both quantities are displayed in Figure 1, and it is a great challenge to completely identify experimentally these different relaxation regimes characterizing the microscopic dynamics of entangled polymer melts.

Field Cycling NMR, Susceptibility Representation, and Frequency–Temperature Superposition. Field cycling NMR can be applied to probe the frequency dependence of the spin–lattice relaxation time T_1 which is determined by the evolution of the nuclear magnetization toward its equilibrium value. The frequency is given by the Larmor frequency $\omega = \gamma B$ depending on the magnetic relaxation field B where γ denotes the gyromagnetic ratio of the nucleus. In the case of ^1H NMR fluctuations of the magnetic dipole–dipole (DD) interaction cause relaxation, and therefore the observed relaxation rate $R_1 = 1/T_1$ contains both intra- and intermolecular contributions.^{24,42–44} Whereas the latter one is mainly due to translational motion among molecules, the first is due to segmental, i.e. local, reorientation dynamics and is usually assumed to be the dominating part because of the short-range nature of the DD coupling. However, Kehr et al. have shown that the intermolecular contribution to R_1 must not be ignored.^{43,44}

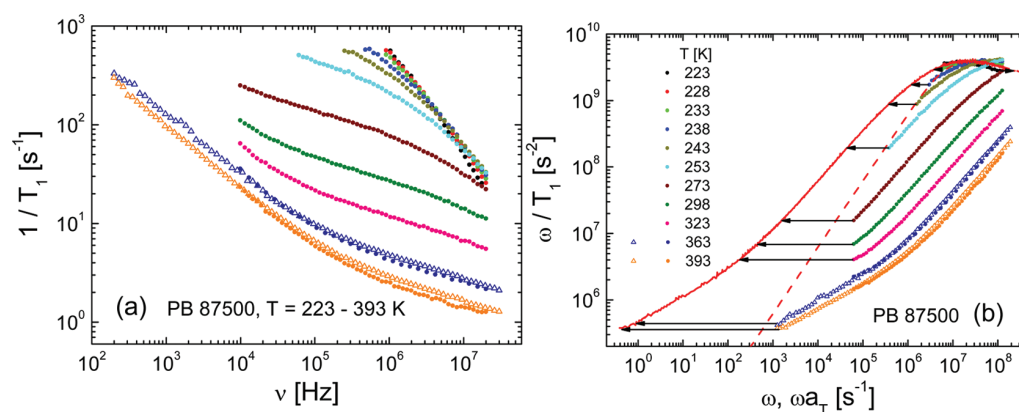


Figure 2. (a) Dispersion of the relaxation rate $1/T_1$ for 1,4-polybutadiene (PB) with $M = 87500$ g/mol in the temperature range as indicated measured with (open triangles) and without (circles) compensation. (b) Susceptibility representation ω/T_1 of the same data as in (a). At lowest temperatures the α -peak is discernible and fitted with Cole–Davidson function (dashed red line). Arrows illustrate frequency–temperature superposition which is applied to create a master curve (solid red line). The color for temperatures is equivalent in both figures.

Measurements in a large temperature interval (223–393 K) provide relaxation rates $1/T_1$ as shown in Figure 2a for 1,4-polybutadiene with molecular mass 87 500 g/mol (as an example). For each temperature a differently strong dispersion is observed. Rewriting the Bloembergen, Purcell, and Pound (BPP) expression^{42,47} for the relaxation rate

$$R_1(\omega) \propto [J(\omega) + 4J(2\omega)] \quad (1)$$

in the susceptibility representation^{25,27–31}

$$\omega/T_1(\omega) = K[\chi''(\omega) + 2\chi''(2\omega)] \equiv 3K\chi''_{\text{DD}}(\omega) \quad (2)$$

allows a direct comparison with results from other techniques. K is the NMR coupling constant, and $\chi''_{\text{DD}}(\omega)$ is subsequently called “dipolar susceptibility” probed by ^1H NMR. Although $\chi''_{\text{DD}}(\omega)$ is a weighted sum of susceptibilities $\chi''(\omega)$, both quantities are essentially indistinguishable for a broad relaxation dispersion on logarithmic scales. Via $\chi''(\omega) = \omega J(\omega)$ the normalized imaginary part of the susceptibility is associated with the spectral density $J(\omega)$ being the Fourier transform of the dipolar correlation function $C^{\text{DD}}(t)$ which, in turn, has to be distinguished from $g^{(2)}(t)$ being exclusively sensitive to rotational motion. We note that the susceptibility representation of NMR relaxation data has also been used by, for example, Cohen-Addad.⁴⁸ Applying this conversion to the relaxation data of Figure 2a yields the curves displayed in Figure 2b (colors used correspondingly), which exhibit a maximum (main relaxation or α -peak) at low temperatures or high frequencies, and obviously share a common shape but are shifted due to the applied temperatures.

In the susceptibility representation a master curve $\chi''_{\text{DD}}(\omega a_T)$ (solid red line) can easily be created by moving the individual curves solely in frequency (frequency–temperature superposition (FTS), illustrated by arrows) to achieve a good agreement. FTS is a principle commonly used, e.g., in rheology^{32,49,50} in order to extend significantly the frequency range. After interpolating the α -peak with an appropriate function (for instance, Cole–Davidson susceptibility, dashed red line) yielding the time constant τ_s for one temperature ($T = 228$ K in Figure 2b), the shift factors $a_T(T)$ can be transformed to the time constants $\tau_s(T) \approx \tau_a(T)$ of segmental reorientation.^{27–29} Therefore, in the following the master curves are plotted as a function of the reduced frequency $\omega\tau_s$ and can be regarded as “isofrictional” spectra^{50,51} in which the

dynamics of polymers with different molecular masses can be evaluated because the M dependence of the glass transition temperature T_g has been taken into account which is pronounced especially at low M .²⁹ Finally, by Fourier transform of the susceptibility master curves the dipolar correlation function $C^{\text{DD}}(t/\tau_s)$ can be obtained (cf. Figure 6a), permitting a comparison with the power-law regimes shown in Figure 1.

Relaxation at Extremely Low Frequencies. The intrinsic assumption of the polymer theories predicting the characteristic power-laws of the spin–lattice relaxation dispersion is that the ^1H spin–lattice relaxation rate $R_1(\omega)$ can be described as a combination of spectral densities (eq 1). The associated exponents have been derived within the framework of the BPP theory assuming specific forms of the spectral densities. The relaxation formula stems from the second-order perturbation theory, and in consequence, its validity regime is limited.^{52–54} There are two fundamental assumptions determining its applicability range. First, the relaxation time must not be shorter than (even comparable to) the correlation time τ of the dynamical process causing relaxation; second, the dipolar interaction has to be a small perturbation compared to the Zeeman interaction.^{42,45,55} Both conditions are potentially violated at extremely low frequencies.

On the one hand, at lower frequencies the spin–lattice relaxation rate becomes faster (T_1 becomes shorter), while on the other hand progressively slower dynamical processes are probed. When at a given frequency ν_x the relaxation dispersion still does not reach the low-frequency plateau (i.e., the extreme narrowing condition^{42,46} $2\pi\nu_x\tau \ll 1$ is not reached yet) it is obvious that $\tau \gg (2\pi\nu_x)^{-1}$. If at the same frequency the relaxation rate R_1 is larger than $2\pi\nu_x$, the condition $T_1 \gg \tau$ will be violated; such a situation is schematically depicted in Figure 3. In this regime care has to be taken when discussing the observed slopes of the apparent relaxation time in the context of the predictions of the polymer theories as the concept of the spectral density function does not apply; to describe the magnetization decay the stochastic Liouville equation (SLE) has to be employed, and this has been done up to now only for paramagnetic systems.^{53,56} The relationship $T_1 \gg \tau$ is equivalent in the low-frequency range to the Redfield condition^{42,46,52,55} $\omega_{\text{DD}}\tau \ll 1$, where ω_{DD} is the amplitude of the dipole–dipole coupling in angular frequency units. In the

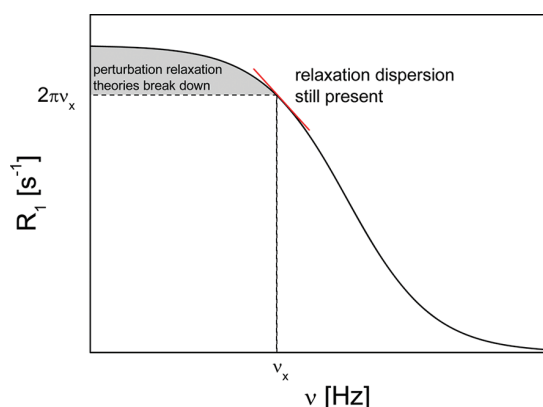


Figure 3. Schematic illustration of the validity range of the perturbation approach to relaxation. When at a frequency ν_x the relaxation rate approaches or exceeds the value of $2\pi\nu_x$, the perturbation treatment breaks down (gray area).

extreme narrowing range the relation $R_1 \propto \omega_{DD}^2 \tau = (\omega_{DD} \tau)^2 \tau^{-1}$ holds, and then $\omega_{DD} \tau \ll 1$ implies that $R_1 \ll \tau^{-1}$, i.e., $T_1 \gg \tau$.

As far as the second condition is concerned, in the low-field range ω_{DD} can approach or even exceed the Zeeman splitting frequency ω , and then the dipolar interaction which is responsible for the relaxation cannot be treated as a small perturbation of the Zeeman interactions. Then the classical relaxation formulae break down, and the SLE approach has to be applied as well.^{52,53} It can also happen that residual dipolar interactions (a part of the dipolar coupling which does not vanish due to motional averaging) become comparable with the Zeeman interaction, thereby considerably altering the proton energy level structure. In such a case one can still apply the perturbation relaxation theory (if other conditions are not violated), but the resulting relaxation expressions are different from the “classical” ones^{52,54,57} (eq 1) which is not taken into account in the theoretical predictions for the characteristic polymer relaxation slopes. This is a typical situation in polymer melts where a residual coupling exists due to the slow anisotropic dynamics of entangled chains. We will return to these issues in the discussion part, however, a satisfactory consideration will remain the task of future theoretical work.

3. EXPERIMENTAL SECTION

Samples of linear 1,4-polybutadiene (PB) with a narrow molecular mass distribution have been investigated over a large range of molecular masses (M). The polymers have been purchased from Polymer Standards Service, Mainz, Germany, thoroughly degassed in 5 and 10 mm NMR tubes and sealed under vacuum. Table 1 gives an

Table 1. Details on the Samples^a

sample	M_w [g/mol]	M_w/M_n
PB 24300	24300	1.01
PB 47000	47000	1.04
PB 87500	87500	1.05
PB 143000	143000	1.02
PB 196000	196000	1.02
PB 441000	441000	1.07

^aThe sample name reflects the molecular mass M_w .

overview over molecular masses and polydispersities M_w/M_n in addition to those M already studied in ref 30.

¹H NMR spin–lattice relaxation experiments have been performed with two different electronic field cycling (FC) relaxometers: a commercial one (Stelar Spinmaster FFC2000) at Bayreuth University and a home-built one at Darmstadt University. In Bayreuth, experiments were performed at temperatures from 223 up to 408 K; in Darmstadt, temperatures from 355 up to 393 K were measured.

Let us, at this point, mention the most important characteristics and the specific differences between the two FC relaxometers: The Bayreuth Stelar relaxometer covers a ¹H frequency range from $\nu = \omega/2\pi = 10$ kHz up to 20 MHz. Times of about or less than 3 ms are achieved for switching from a high polarization field to any desired evolution field, thereby avoiding undershoots or strong field oscillations. Lower ¹H frequencies can only be reached at the home-built Darmstadt relaxometer⁵⁸ which, since about 10 years, has been continuously upgraded. For the present project, frequencies down to 200 Hz and up to 30 MHz have been reached. The low frequencies can be attained by utilizing a three-dimensional resistive coil arrangement for compensating for the earth field and other magnetic stray fields. For stabilizing fields corresponding to ¹H frequencies below 1 kHz an active field drift and fluctuation compensation tool is activated. Field switching is performed in a controlled way reaching switching times of about 3 ms if the active compensation tool is not used (above 1 kHz) and 6 ms if the compensation tool is used (below 1 kHz). For technical details the reader is referred to ref 40, where it is demonstrated that in favorable cases ¹H frequencies down to 12 Hz can be reached.

Spin–lattice relaxation times—especially for high- M polymers at very low fields, yet at a temperature far above T_g —may eventually become even shorter than the switching time of the employed relaxometer. As long as the magnetization decay is monoexponential, this does not cause a conflict with the finite switching time except for a corresponding signal reduction. Exemplifying magnetization decay curves are shown in Figure 4 for a couple of ¹H frequencies. For each

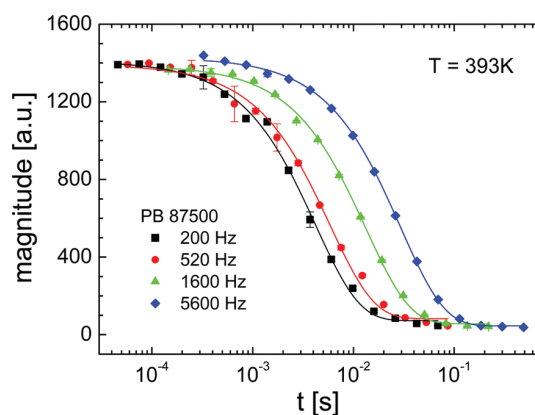


Figure 4. Magnetization decay curves of PB 87500 at $T = 393$ K in various relaxation fields as indicated. Solid lines: corresponding monoexponential fit.

relaxation field the magnetization decays exponentially characterized by the spin–lattice relaxation time T_1 . Note that the abscissa assignment of the variable time starts from a point safely after the field switching has been done.

A comparison of the relaxation rate $1/T_1(\nu)$ and susceptibility $\chi''_{DD} = \omega/T_1$ measured with both the Stelar and the home-built spectrometer is shown in Figures 2a and 2b, respectively, for PB 87500 at $T = 363$ and 393 K. The curves coincide well for the two temperatures, indicating also that the temperature control agrees for both instruments. Furthermore, it demonstrates the benefit of a compensation for stray fields: almost 2 decades can be gained at low frequencies, and consequently the relaxation rate dispersion covers more than 5 decades.

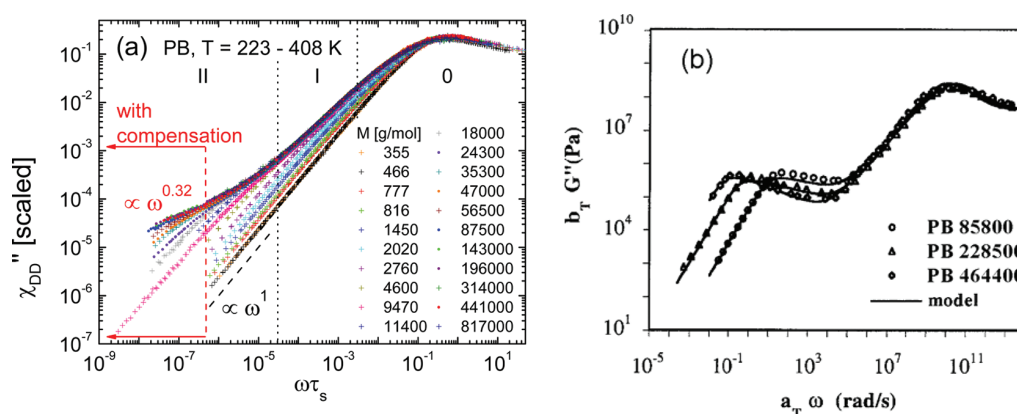


Figure 5. (a) Susceptibility master curves as a function of the reduced frequency $\omega\tau_s$ for all investigated M of PB in the temperature range as indicated. The frequency range in which T_1 has been acquired while employing the compensation for stray fields is marked by arrows. Vertical dotted lines: relaxation regimes 0, I, and II, i.e., glassy dynamics, Rouse and entanglement dynamics, respectively. (b) Loss modulus $G''(\omega)$ for PB (with M as indicated) as obtained with a mechanical rheometer and applying FTS (figure adapted with permission from ref 60).

As outlined in section 2, Fourier transform is applied to obtain the dipolar correlation function. Since many decades in frequency are involved, instead of fast Fourier transform, we utilize an algorithm based on the Filon algorithm.⁵⁹ When at low frequencies the terminal relaxation, i.e., the crossover to $\chi''_{DD} \propto \omega^1$, is reached, the susceptibility master curve can be transformed as it is. For the master curves with $M \geq 35\,300$, for which the terminal relaxation is beyond the experimentally accessible frequency window, it is essential to extend the susceptibility with the corresponding power-law $\omega^{\epsilon(M)}$ over some decades. Otherwise, truncation errors of the algorithm would cause a misleading decay of the correlation function at longest times, which can be avoided by the described extension and subsequently discarding the previously added points. This, in contrast, is not necessary for the evaluation of the DQ ^1H NMR experiments measuring dipolar couplings directly in the time domain,^{19,33,34} however, being able to probe the correlation function only for $t > \tau_e$. We will demonstrate that low-field FC NMR adds 2 decades to our prior results³⁰ in $C^{DD}(t/\tau_e)$ and also allows investigating higher M , in total providing a mutual verification of the results of both NMR techniques.

4. RESULTS

According to the procedure outlined in section 2, the T_1 dispersion data have been converted to the susceptibility representation $\chi''_{DD} = \omega/T_1$, and by merging the data of the different temperatures, a master curve of the reduced frequency $\omega\tau_s$ has been created for each M (Figure 5a). The scaling by the segmental correlation time τ_s as said yields “isofrictional” spectra and provides a common peak at $\omega\tau_s \approx 1$ representing the primary α -relaxation governed by the glass transition. At $\omega\tau_s \geq 1$ the spectral shape of the peak is independent of M . With increasing M a continuously rising excess intensity on the low-frequency side of the peak ($\omega\tau_s < 1$) is discernible which is due to the slower, M -dependent polymer dynamics. For the high- M ($M > M_e \approx 2000$) master curves three different relaxation regimes (0, I, II) can be distinguished and are phenomenologically in accordance with those from Kimmich’s classification.²⁴ Below we will attribute them to glassy (0), Rouse (I), and constrained Rouse (II) dynamics of the Doi–Edwards tube-reptation model which is however different from Kimmich’s interpretation.^{24,25,30,31} At lowest frequencies in regime II, especially in the range in which the compensation tool has been employed (arrows in Figure 5a), M -dependent power-laws can be identified.

The susceptibility master curves (Figure 5a) reflect segmental (“local”) as well as collective polymer dynamics

and will be described in the following by going from high to low reduced frequencies. While a simple liquid (PB with $M = 466$) only exhibits glassy dynamics in form of the α -peak with a power-law ω^1 at $\omega\tau_s < 1$, at $M = 777$ the contribution of polymer dynamics begins to increase with M in regime 0 and saturates around $M = 4600$. Yet, since for frequencies $\omega\tau_s > 3 \times 10^{-3}$ and around the relaxation maximum glassy dynamics still contributes, regime 0 is designated as glassy dynamics (cf. Figure 1). Note that the frequency position of the lines separating the regimes in Figure 5a differs slightly from our previous works.^{25,31} In the frequency range $3 \times 10^{-5} < \omega\tau_s < 3 \times 10^{-3}$ the susceptibility of $M = 4600 \approx 2M_e$ represents an envelope with a power-law ω^ϵ even for the high- M ($M \gg M_e$) systems, indicating that the dynamics remains unchanged if M is increased beyond M_e . In this regime the dispersion data can be well described by applying the Rouse model;²⁹ therefore, it is attributed to free Rouse dynamics (regime I). Approaching lower frequencies ($\omega\tau_s < 3 \times 10^{-5}$, regime II), a crossover to a second power-law $\omega^{\epsilon(M)}$ with $\epsilon < \alpha$ is observed. While increasing M the master curves progressively approach the enveloping shape constituted by the highest M . Whereas for $M \leq 11\,400$ a crossover to the power-law ω^1 (Debye limit) characterizing terminal relaxation is accessible in the frequency range of the Stellar spectrometer ($\omega\tau_s \geq 5 \times 10^{-7}$), for larger M the slowest relaxation mode is more and more shifted to lower frequencies. Together with the fact that the power-laws of the tube-reptation model (regimes II and III) are expected to be very protracted, i.e., to be disclosed only for very high M ($M > 100M_e = 200\,000$),^{15,34,37} this rendered the need for low-field relaxation experiments.

Within the frequency range marked by the arrows in Figure 5a ($\omega\tau_s < 5 \times 10^{-7}$) the relaxation data have been obtained with the home-built spectrometer equipped with the active compensation system. Two limiting power-laws can be distinguished in the susceptibility of PB with different M : For $M \leq 35\,300$ the power-law ω^1 indicates that the terminal relaxation has been detected (in a $1/T_1$ plot such as Figure 2a this would manifest itself in a horizontal line, i.e., ω^0), and for $M = 441\,000$ a power-law $\omega^{0.32}$ is revealed extending over more than 1 decade at lowest frequencies. In between the power-law exponent continuously decreases for increasing M , which will be evaluated and discussed below (see also Figure 6b).

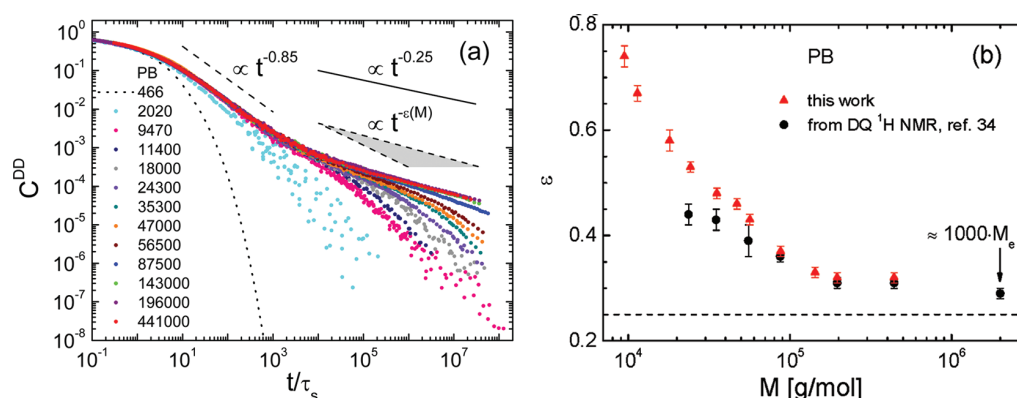


Figure 6. (a) Dipolar correlation function $C^{DD}(t/\tau_s)$ of PB for various M obtained by Fourier transforming the susceptibility master curves of Figure 5a. Dotted curve: low- M system representing glassy dynamics. Dashed lines: observed power-laws of regime I and II. Gray area illustrates variation of power-law exponent ϵ of regime II for $24\,300 \leq M \leq 441\,000$. Solid line: predicted power-law of regime II by tube-reptation model. (b) Power-law exponent ϵ as a function of M obtained in the time domain. For comparison, DQ ^1H NMR results³⁴ are included. Even at $M \approx 2\,000\,000$ the prediction of the tube-reptation model $\epsilon = 0.25$ (dashed line) is not fully approached yet.

However, this already shows that the dynamics in regime II is dependent on M even if $M \gg M_e$.

For comparison, Figure 5b contains master curves of the dynamic loss modulus $G''(\omega)$ for different high- M PB from rheological measurements.⁶⁰ In that study a mechanical spectrometer with cone–plate and torsional configuration was used in the temperature range from 158 to 353 K, and FTS has been applied as well, thereby increasing the accessible frequency range from 3 (as in FC NMR using the Stellar relaxometer) to 17 decades. The master curves of different M exhibit a common high-frequency peak and an M -dependent minor peak at lower frequencies. The first is attributed to the glassy dynamics, and the latter represents the slowest relaxation mode. Since a low-frequency peak as in the rheological data is not observed in the FC ^1H NMR master curves, obviously the relaxation mode spectrum is weighted differently for the two techniques. However, the susceptibility representation offers the possibility to directly compare the results from FC ^1H NMR (Figure 5a) and rheology (Figure 5b), i.e., microscopic and macroscopic dynamics as reflected in the $T_1(\omega)$ and $G''(\omega)$ measurements, respectively. Recently,³⁴ the term “molecular rheology” was coined with respect to FC and DQ ^1H NMR and their capability of exploring the time range from glassy dynamics to terminal relaxation in entangled polymers like “conventional” rheology.

Fourier-transforming the susceptibility master curves $\chi''_{DD}(\omega\tau_s)$ of Figure 5a allows displaying them as the full dipolar correlation function $C^{DD}(t/\tau_s)$ in Figure 6a (cf. Experimental Section). While the low- M system (PB 466, dotted line) exhibits a stretched exponential (Kohlrausch) decay typical of a simple liquid, for higher M the relaxation becomes increasingly retarded as already discussed in ref 30. Depending on M characteristic power-laws t^α can be identified with their exponents (above M_e) having the same absolute value than in the frequency domain (Figure 5a). In the time range up to $t/\tau_s < 10^3$ a common envelope with $\alpha = 0.85$ is found which is not altered at high M similarly to the susceptibility representation. This is close to $\alpha = 1$ predicted by the Rouse theory (cf. Figure 1), and therefore it can be regarded as the high- M envelope for the free Rouse dynamics (regime I). First, the free Rouse dynamics leads to a distribution of correlation times in the range $\tau_s < \tau < \tau_e$, and then above M_e entanglement dynamics provides relaxation on

increasingly slower time scales $t > \tau_e$ (regime II), leading to a bimodal shape. Here, particularly the M -dependent power-law $t^{\epsilon(M)}$ is recognized. Analogous to Figure 5a, ϵ is reduced with growing M as indicated by the gray sector (for $24\,300 \leq M \leq 441\,000$) in Figure 6a.

This dependence $\epsilon(M)$ is plotted in Figure 6b. From the correlation functions (Figure 6a) the minimum slope ϵ has been determined for each M by a linear fit in the double-logarithmic representation over at least 1 decade in time. A continuous decrease of ϵ from 0.73 to 0.32 can be noted in the M range between 9470 and 441 000. Note that our previous data³⁰ were restricted to $M = 18\,000$ or $\epsilon > 0.5$, and now the M range in the time domain is extended by a factor of about 25. The new high- M results obtained by low-field FC ^1H NMR agree well with those from DQ ^1H NMR,³⁴ which are included in Figure 6b for comparison. This demonstrates that low-field FC ^1H NMR is capable to cover the full M dependence of ϵ . For the highest M the power ϵ determined by FC and DQ ^1H NMR is slightly larger, yet close to the prediction $\epsilon = 0.25$ of the tube-reptation model for regime II (cf. Figure 1). Since this theoretically expected value is still not yet reached with both NMR techniques and could possibly be attained only for $M > 2\,000\,000$, it can be concluded that the crossover to full reptation dynamics is very protracted.

Figure 7 shows a direct comparison of the correlation function for several high- M PB measured by FC and DQ ^1H NMR plotted in a way to further test the relaxation behavior in regime II. It displays the long-time end of the FC data of Figure 6a focusing on the time window of the DQ data which have been inserted from ref 34. Samples with comparable M are displayed in the same color. The amplitude is divided by the predicted power-law $t^{0.25}$ for regime II of the tube-reptation model illustrating how the theoretically expected behavior (horizontal line) is approached with increasing M , yet not completely attained. Whereas in the correlation function of PB with $M = 9470 \approx 5M_e$ no indication for the power-law of regime II can be seen; above $M = 24\,300$ the curves come closer to the model prediction and trace the envelope shape of the highest $M = 441\,000$ continuously longer with higher M before bending away at long times. Moreover, a good agreement among the FC and DQ ^1H NMR data can be observed. In order to achieve the best match among them, the DQ data have been scaled by a factor of 0.5 in amplitude. Vaca

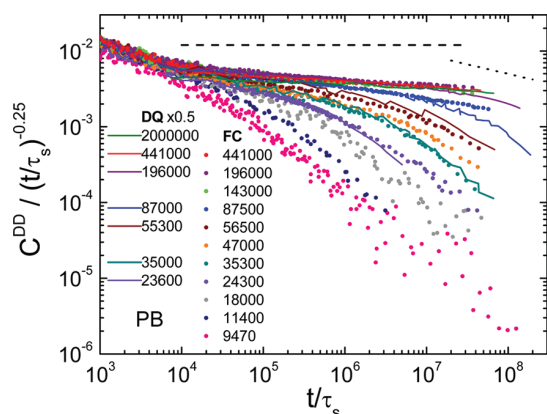


Figure 7. Correlation function for PB with M as indicated measured by FC and DQ ^1H NMR³⁴ (dots and lines, respectively) divided by the power-law $t^{-0.25}$. Dashed horizontal line and dotted line: expectation for regimes II and III of the tube-reptation model, respectively.

Chávez and Saalwächter⁶¹ applied a factor of 0.7, ascribing it to shortcomings of their model determining the absolute value of the correlation function. We note that the investigated polymers were obtained from the same supplier and in the case of PB with $M = 196\,000$ and $441\,000$ the identical polymer was examined by both NMR methods.

5. DISCUSSION

In Figure 7, a second power-law regime (II) can be clearly identified extending over 3 decades in time for $M \geq 143\,000$. While increasing M the protracted transition to almost completely established reptation dynamics is characterized by the very slow approach of the exponent ε toward $\varepsilon = 0.25$ predicted by the tube-reptation model (Figure 6b). The latter has been reported for the mean-square displacement by, e.g., neutron spin echo (NSE)¹⁷ and simulations.^{4,37,38} The observed exponent $\varepsilon(441\,000) = 0.32$ corresponds in the $1/T_1$ representation to -0.68 , which is larger than the value -0.42 found by Kimmich et al.⁶² for PB with $M = 65\,500$ at $T = 313\text{ K}$. This difference is due to the larger M investigated at both higher temperatures and lower frequencies in the present study. Concerning the identification of regime III of the tube-reptation model, the situation is less convincing. For PB with $M \leq 56\,500$ the correlation function exhibits just a smooth transition to terminal relaxation, and the predicted power-law $t^{-0.5}$ (cf. dotted line in Figure 7) may merely be assumed over 1 decade. Therefore, according to our current results, it cannot be decided whether the dynamic range of regime III is quite narrow, resulting in a smooth transition to regime IV (as observed in the DQ ^1H NMR study³⁴), whether there is an interplay between the dynamics of different regimes, or whether the power-law would be more pronounced for higher M and at yet longer times beyond our experimentally accessible range. The first is corroborated by a theoretical work⁴¹ yielding an analytical expression for regimes III and IV together. However, the direct comparison of the correlation functions from both NMR methods demonstrates that FC ^1H NMR is indeed capable of reaching the time scales which formerly have been restricted to DQ ^1H NMR. We emphasize the agreement among the results of DQ and FC ^1H NMR, since the theoretical concepts involved in these methods are quite different, i.e., coherent spin-evolution measuring dipolar

correlations in the time domain and longitudinal relaxation probing a spectral density in the frequency domain, respectively.

Regarding the limitations of the perturbation-based relaxation theories (cf. Theoretical Background), we are aware that our experimental results collected at lowest frequencies need to be treated cautiously. For the high- M polymers one sees from Figure 2a that the relaxation rate still grows up at low frequencies even though it has already reached $(3\text{ ms})^{-1}$ at $\nu = 200\text{ Hz}$. Consequently with $\tau = (2\pi\nu)^{-1} = 0.8\text{ ms}$ the condition $T_1 \gg \tau$ is not strictly fulfilled anymore. Even more, since a relaxation dispersion is still observed the condition will be violated further as frequency decreases. In order to provide exact theoretical predictions for the characteristic polymer relaxation, a treatment based on a full (nonperturbative) solution the stochastic Liouville equation should be adopted. To our knowledge, such a general description has not been formulated yet. Therefore, we base our analysis on the second-order perturbation theory, even though we are aware of its limitation. We note that the Larmor frequencies are still above the typical residual dipolar coupling of about 100 Hz observed for high- M polymer melts which was the second condition to be fulfilled (see above).^{34,63} Together with the consistency between FC and DQ ^1H NMR data (Figures 6b and 7) this provides some confidence that our results are still unaffected by low-frequency effects exceeding second-order perturbation theory.

When comparing the observed power-law exponents to the predicted ones, we underline that the dipolar correlation function $C^{\text{DD}}(t)$ probed by FC ^1H NMR does not need to be identical to the rank-two reorientational correlation function $g^{(2)}(t)$ of a polymer segment. A common assumption in the analysis of FC ^1H NMR experiments is that the intramolecular contribution to relaxation dominates, and therefore the influence of intermolecular relaxation can be neglected.^{26,27,30,34} As mentioned, results by Kehr et al.^{43,44} indicate that this is not necessarily the case at low frequencies, suggesting that ε might also be sensitive to influences of the intermolecular relaxation. However, DQ ^1H NMR results for isotopic dilution of PB $196\,000$ with deuterated PB of the same M and thereby suppressing the intermolecular interaction have shown³³ that the value of ε remains the same as in the pure PB though the absolute values of $C^{\text{DD}}(t)$ are different. Very recent own measurements point into the same direction.

The ε values in Figure 6b are notably higher than 0.25 predicted by the tube-reptation model. This may be caused by the early onset of terminal relaxation for $M \leq 56\,500$ or by additional relaxation mechanisms. Even at highest $M = 441\,000 \gg M_e$ the theoretical exponent is not reached. In other words, although $M \gg M_e$ a static tube appears to be not formed yet. All approaches to refine the Doi–Edwards model such as constraint release (CR) or contour length fluctuations (CLF) cause additional correlation loss, i.e., a steeper decay which results in ε being higher than expected from the original tube-reptation model, and are candidates for interpreting our findings. We note that the (twice) renormalized Rouse theory has been used by Kimmich and Fatkullin to describe the experimentally observed power-laws.^{24,62} In the light of the recent DQ ^1H NMR results together with our data measuring a large frequency and temperature range and exploiting FTS, the applicability of the renormalized Rouse model as proposed in ref 24 can be ruled out, especially in the low-frequency range.^{25,44}

The protracted transition to full reptation dynamics has also been observed in Monte Carlo simulations by Kreer et al.³⁷ and Paul.³⁸ Actually, Kreer et al. seem to be the first ones to discuss this phenomenon; however, such a delayed crossover has not been recognized by more recent simulation work.⁶⁴ A possible explanation may be due to the fact that the NMR signal is averaged over all segments in the chain. Whereas the chain ends participate in forming a new tube, the inner monomers are exposed to the topological confinement of the tube to a higher degree. Therefore, their reorientation is more hindered, which is closer to the model picture of a static tube. Kremer et al.^{65,66} already pointed out by means of MD simulations that the outer monomers fluctuate stronger, and in order to observe actual entanglement effects, one should inspect the innermost monomers. Zamponi et al.⁶⁷ have concluded from a NSE study of polyethylene (PE) with $M = 25\,000$ that the dynamic structure factor of a completely protonated chain differs from that of a partially deuterated chain with protons only at the inner part due to CLF. Effects of CR were believed to be negligible.

Yet, complementing the NSE experiments, Vaca Chávez and Saalwächter³³ directly proved that ε is influenced indeed by CR effects, since diluting PB with $M = 55\,000$ in a deuterated PB matrix with both lower and higher M changes ε . Because diluting PB with $M = 196\,000$ in the same deuterated M does not modify ε , an influence of intermolecular relaxation on ε for the highest M can be excluded. However, a very recent study⁶⁸ combining viscoelastic and dielectric relaxation spectra claims to have proven that the dielectric spectra are determined by reptation and CLF motion only and not by CR contributions. Thus, for a final interpretation additional evidence addressing the relevance of CR, CLF, and NMR specific intermolecular relaxation effects is needed and part of ongoing work.

Whereas the above discussion implies a continuous transition to full reptation, there are several indications for a discontinuous change of the dynamics at another characteristic molecular mass $M_r \gg M_e$. For PB Colby et al.⁵⁰ disclosed at $M_r \approx 200M_e$ a departure from the viscosity power-law $\eta(M) \sim M^{3.4}$ to $M^{3.0}$, for PE Vega et al.³⁵ found $M_r \approx 440M_e$, and for polyisoprene (PI) Abdel-Goad et al.³⁶ discovered $M_r \approx 44M_e$. Therefore, the relation M_r/M_e is not constant for different polymers.⁶⁹ In a recent study¹⁵ by dielectric spectroscopy on PI we reported a saturation behavior at $M_r \approx 20M_e$ both from the shape and time constant of the dielectric normal mode.

6. CONCLUSIONS

We have investigated the dynamics of PB melts in a series of different M by FC ^1H NMR focusing on the low-frequency behavior for $M > M_e$. The frequency window provided by the commercially available Stelar FC spectrometer has been extended significantly for 2 decades toward lower frequencies (Figure 2) with the aid of a home-built spectrometer⁴⁰ in order to explore polymer dynamics on even slower time scales than in our previous study.³⁰ The susceptibility representation of the relaxation dispersion offers a comparison with rheological data (Figures 5a and 5b). As a result of applying FTS, the susceptibility master curves and the corresponding dipolar correlation functions (Figure 5a and 6a, respectively) embrace over 10 decades in frequency or time and can be analyzed in a range which before was restricted to DQ ^1H NMR experiments.³³ Consequently, for all M studied FC ^1H NMR is now able to cover the relaxation regimes 0, I, and II (glassy, free Rouse, and constrained Rouse dynamics, respectively; cf. Figure

1) and for $M \leq 56\,500$ also regimes III and IV (reptation dynamics and free diffusion, respectively) of the tube-reptation model.

The particular goal of this contribution has been to study the transition from Rouse to fully established reptation dynamics at $M \gg M_e$. From the slow decrease of the power-law exponent $\varepsilon(M)$ in regime II from 0.73 to 0.32 with increasing M toward the predicted $\varepsilon = 0.25$, it can be concluded that only for very high M the characteristic dynamics of the tube-reptation model is disclosed. The M dependence of ε is very similar to the values reported by DQ ^1H NMR³⁴ for high M (Figure 6b), and a direct comparison of the correlation functions obtained by FC and DQ ^1H NMR shows a good agreement (Figure 7). Hence, FC NMR has turned from a complementary method to DQ NMR into a competitive one. Moreover, we anticipate that a further enhancement of the stray field compensation tool will contribute 1 more decade at low frequencies. This could further illuminate the reptation dynamics of regime III and provide the basis for a joint description of dielectric, viscoelastic, and NMR relaxometric data.

AUTHOR INFORMATION

Corresponding Author

*E-mail: ernst.roessler@uni-bayreuth.de.

ACKNOWLEDGMENTS

The financial support of Deutsche Forschungsgemeinschaft (DFG) through priority program SPP 1369 "Polymer-Solid Contacts: Interfaces and Interphases" (RO 907/16) and grant FU 308/14 is acknowledged. The authors thank F. Vaca Chávez and K. Saalwächter for valuable discussions and providing their data for Figure 7.

REFERENCES

- (1) Doi, M.; Edwards, S. F. *The Theory of Polymer Dynamics*; Oxford Science Publications: Oxford, 1986.
- (2) Rouse, P. E. *J. Chem. Phys.* **1953**, *21*, 1272–1280.
- (3) de Gennes, P. G. *J. Chem. Phys.* **1971**, *55*, 572–579.
- (4) Kremer, K.; Grest, G. S. *J. Chem. Phys.* **1990**, *92*, 5057–5086.
- (5) Lodge, T. P.; Rotstein, N. A.; Prager, S. *Adv. Chem. Phys.* **1990**, *79*, 1–132.
- (6) Watanabe, H. *Prog. Polym. Sci.* **1999**, *24*, 1253–1403.
- (7) Binder, K.; Baschnagel, J.; Paul, W. *Prog. Polym. Sci.* **2003**, *28*, 115–172.
- (8) Richter, D.; Monkenbusch, M.; Arbe, A.; Colmenero, J. *Neutron Spin Echo in Polymer Systems*; Springer: Berlin, 2005.
- (9) Read, D. J.; Jagannathan, K.; Likhtman, A. E. *Macromolecules* **2008**, *41*, 6843–6853.
- (10) Doi, M. *J. Polym. Sci., Polym. Lett. Ed.* **1981**, *19*, 265–273.
- (11) Milner, S. T.; McLeish, T. C. B. *Phys. Rev. Lett.* **1998**, *81*, 725–728.
- (12) Rubinstein, M.; Colby, R. H. *J. Chem. Phys.* **1988**, *89*, 5291–5306.
- (13) Likhtman, A. E.; McLeish, T. C. B. *Macromolecules* **2002**, *35*, 6332–6343.
- (14) Adachi, K.; Wada, T.; Kawamoto, T.; Kotaka, T. *Macromolecules* **1995**, *28*, 3588–3596.
- (15) Abou Elfadl, A.; Kahlau, R.; Herrmann, A.; Novikov, V. N.; Rössler, E. A. *Macromolecules* **2010**, *43*, 3340–3351.
- (16) Zamponi, M.; Wischniewski, A.; Monkenbusch, M.; Willner, L.; Richter, D.; Likhtman, A. E.; Kali, G.; Farago, B. *Phys. Rev. Lett.* **2006**, *96*, 238302.
- (17) Richter, D.; Butera, R.; Fetters, L. J.; Huang, J. S.; Farago, B.; Ewen, B. *Macromolecules* **1992**, *25*, 6156–6164.

- (18) Pahl, S.; Fleischer, G.; Fujara, F.; Geil, B. *Macromolecules* **1997**, *30*, 1414–1418.
- (19) Graf, R.; Heuer, A.; Spiess, H. W. *Phys. Rev. Lett.* **1998**, *80*, 5738–5741.
- (20) Pearson, D. S.; Fetters, L. J.; Graessley, W. W.; Ver Strate, G.; von Meerwall, E. *Macromolecules* **1994**, *27*, 711–719.
- (21) Komlosh, M. E.; Callaghan, P. T. *J. Chem. Phys.* **1998**, *109*, 10053–10067.
- (22) Klein, P. G.; Adams, C. H.; Brereton, M. G.; Ries, M. E.; Nicholson, T. M.; Hutchings, L. R.; Richards, R. W. *Macromolecules* **1998**, *31*, 8871–8877.
- (23) Chernov, V. M.; Krasnopol'skii, G. S. *J. Exp. Theor. Phys.* **2008**, *107*, 320–312.
- (24) Kimmich, R.; N. Fatkullin, N. *Adv. Polym. Sci.* **2004**, *170*, 1–113.
- (25) Kruk, D.; Herrmann, A.; Rössler, E. A. *Prog. Nucl. Magn. Reson. Spectrosc.* **2011**, DOI: 10.1016/j.pnmrs.2011.08.001.
- (26) Kimmich, R.; Anordo, E. *Prog. Nucl. Magn. Reson. Spectrosc.* **2004**, *44*, 257–320.
- (27) Kariyo, S.; Gainaru, C.; Schick, H.; Brodin, A.; Novikov, V. N.; Rössler, E. A. *Phys. Rev. Lett.* **2006**, *97*, 207803. Erratum: Kariyo, S.; Herrmann, A.; Gainaru, C.; Schick, H.; Brodin, A.; Novikov, V. N.; Rössler, E. A. *Phys. Rev. Lett.* **2008**, *100*, 109901.
- (28) Kariyo, S.; Brodin, A.; Gainaru, C.; Herrmann, A.; Schick, H.; Novikov, V. N.; Rössler, E. A. *Macromolecules* **2008**, *41*, 5313–5321.
- (29) Kariyo, S.; Brodin, A.; Gainaru, C.; Herrmann, A.; Hintermeyer, J.; Schick, H.; Novikov, V. N.; Rössler, E. A. *Macromolecules* **2008**, *41*, 5322–5332.
- (30) Herrmann, A.; Novikov, V. N.; Rössler, E. A. *Macromolecules* **2009**, *42*, 2063–2068.
- (31) Herrmann, A.; Kariyo, S.; Abou Elfadl, A.; Meier, R.; Gmeiner, J.; Novikov, V. N.; Rössler, E. A. *Macromolecules* **2009**, *42*, 5236–5243.
- (32) Strobl, G. *The Physics of Polymers*; Springer: Berlin, 1996.
- (33) Vaca Chávez, F.; Saalwächter, K. *Phys. Rev. Lett.* **2010**, *104*, 198305.
- (34) Vaca Chávez, F.; Saalwächter, K. *Macromolecules* **2011**, *44*, 1549–1559.
- (35) Vega, J. F.; Rastogi, S.; Peters, G. W. M.; Meijer, H. E. H. *J. Rheol.* **2004**, *48*, 663–678.
- (36) Abdel-Goad, M.; Pyckhout-Hintzen, W.; Kahle, S.; Allgaier, J.; Richter, D.; Fetters, L. J. *Macromolecules* **2004**, *37*, 8135–8144.
- (37) Kreer, T.; Baschnagel, J.; Müller, M.; Binder, K. *Macromolecules* **2001**, *34*, 1105–1117.
- (38) Paul, W. *Chem. Phys.* **2002**, *284*, 59–66.
- (39) Noack, F. *Prog. NMR Spectrosc.* **1986**, *18*, 171–276.
- (40) Kresse, B.; Privalov, A. F.; Fujara, F. *Solid State Nucl. Magn. Reson.* **2011**, *40*, 134–137.
- (41) Ball, R. C.; Callaghan, P. T.; Samulski, E. T. *J. Chem. Phys.* **1997**, *106*, 7252–7361.
- (42) Abragam, A. *The Principles of Nuclear Magnetism*; Clarendon Press: Oxford, 1961.
- (43) Kehr, M.; Fatkullin, N.; Kimmich, R. *J. Chem. Phys.* **2007**, *126*, 094903-1–094903-8.
- (44) Kehr, M.; Fatkullin, N.; Kimmich, R. *J. Chem. Phys.* **2007**, *127*, 084911-1–084911-7.
- (45) Solomon, I.; Bloembergen, N. *J. Chem. Phys.* **1956**, *25*, 261–266.
- (46) Slichter, C. P. *Principles of Magnetic Resonance*; Springer: Berlin, 1990.
- (47) Bloembergen, N.; Purcell, E. M.; Pound, R. V. *Phys. Rev.* **1948**, *73*, 679–715.
- (48) Guillermo, A.; Dupeyre, R.; Cohen-Addad, J. P. *Macromolecules* **1990**, *23*, 1291–1297.
- (49) Ferry, J. D. *Viscoelastic Properties of Polymers*; J. Wiley: New York, 1980.
- (50) Rubinstein, M.; Colby, R. H. *Polymer Physics*; Oxford University Press: Oxford, 2003.
- (51) Colby, R. H.; Fetters, L. J.; Graessley, W. W. *Macromolecules* **1987**, *20*, 2226–2237.
- (52) Kruk, D. *Theory of Evolution and Relaxation of Multi-Spin Systems*; Arima: Bury St. Edmunds, 2007.
- (53) Kruk, D.; Kowalewski, J. *J. Magn. Reson.* **2003**, *162*, 229–240.
- (54) Kruk, D.; Fujara, F.; Gumann, P.; Medycki, W.; Tacke, Ch. *Solid State Nucl. Magn. Reson.* **2009**, *35*, 152–163.
- (55) Redfield, A. G. In *Encyclopedia of Nuclear Magnetic Resonance*; Grant, D. M., Harris, R. K., Eds.; Wiley: Chichester, 1996; p 4085.
- (56) Freed, J. H. In *Spin Labeling Theory and Applications*, 53rd ed.; Berliner, L. J., Ed.; Academic Press: New York, 1976.
- (57) Kruk, D.; Nilsson, T.; Kowalewski, J. *Phys. Chem. Chem. Phys.* **2001**, *3*, 4907–4917.
- (58) Lips, O.; Privalov, A.; Dvinskikh, S.; Fujara, F. *J. Magn. Reson.* **2001**, *149*, 22–28.
- (59) Filon, L. N. G. *Proc. R. Soc. Edinburgh* **1929**, *49*, 38–47.
- (60) Palade, L.; Verney, V.; Attané, P. *Rheol. Acta* **1996**, *35*, 265–273.
- (61) Vaca Chávez, F.; Saalwächter, K. *Macromolecules* **2011**, *44*, 1560–1569.
- (62) Kimmich, R.; Fatkullin, N.; Seitter, R.-O.; Gille, K. *J. Chem. Phys.* **1998**, *108*, 2173–2177.
- (63) Cohen Addad, J. P. *Prog. NMR Spectrosc.* **1993**, *25*, 1–316.
- (64) Meyer, H. Private communication.
- (65) Kremer, K. *Macromolecules* **1983**, *16*, 1632–1638.
- (66) Kremer, K.; Grest, G. S.; Carmesin, I. *Phys. Rev. Lett.* **1988**, *61*, 566–569.
- (67) Zamponi, M.; Monkenbusch, M.; Willner, L.; Wischnewski, A.; Farago, B.; Richter, D. *Europhys. Lett.* **2005**, *72*, 1039–1044.
- (68) Glomann, T.; Schneider, G. J.; Brás, A. R.; Pyckhout-Hintzen, W.; Wischnewski, A.; Zorn, R.; Allgaier, J.; Richter, D. *Macromolecules* **2011**, *44*, 7430–7437.
- (69) Fetters, L. J.; Lohse, D. J.; Milner, S. T.; Graessley, W. W. *Macromolecules* **1999**, *32*, 6847–6851.

Publication 4

Mean Square Displacement and Reorientational Correlation Function in Entangled Polymer Melts Revealed by Field Cycling ^1H and ^2H NMR Relaxometry.

Herrmann, A.; Kresse, B.; Wohlfahrt, M.; Bauer, I.; Privalov, A. F.; Kruk, D.; Fatkullin, N.; Fujara, F.; Rössler, E. A.
Macromolecules **2012**, *45*, 6516–6526.

Copyright 2012 by The American Chemical Society
DOI: 10.1021/ma301099h

Mean Square Displacement and Reorientational Correlation Function in Entangled Polymer Melts Revealed by Field Cycling ^1H and ^2H NMR Relaxometry

A. Herrmann,[†] B. Kresse,[‡] M. Wohlfahrt,[†] I. Bauer,[†] A. F. Privalov,[‡] D. Kruk,[§] N. Fatkullin,^{||} F. Fujara,[‡] and E. A. Rössler^{†,*}

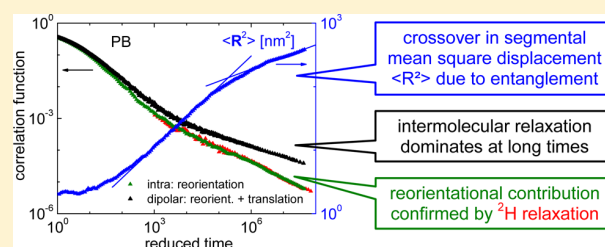
[†]Experimentalphysik II, Universität Bayreuth, 95440 Bayreuth, Germany

[‡]Institut für Festkörperphysik, TU Darmstadt, Hochschulstrasse 6, 64289 Darmstadt, Germany

[§]Faculty of Mathematics & Computer Science, University of Warmia & Mazury Olsztyn, Sloneczna 54, 10710 Olsztyn, Poland

^{||}Institute of Physics, Kazan Federal University, Kazan 420008, Tatarstan, Russia

ABSTRACT: Mixtures of protonated and deuterated polybutadiene and polydimethylsiloxane are studied by means of field-cycling (FC) ^1H NMR relaxometry in order to analyze the intra- and intermolecular contributions to spin–lattice relaxation. They reflect reorientational and translational dynamics, respectively. Master curves in the susceptibility representation $\chi''(\omega\tau_s)$ are constructed by employing frequency–temperature superposition with τ_s denoting the segmental correlation time. The intermolecular contribution is dominating at low frequencies and allows extracting the segmental mean square displacement $\langle R^2(t) \rangle$, which reveals two power-law regimes. The one at short times agrees with $t^{0.5}$ predicted for the free Rouse regime and at long times a lower exponent is observed in fair agreement with $t^{0.25}$ expected for the constrained Rouse regime of the tube-reptation model. Concomitantly the reorientational rank-two correlation function $C_2(t/\tau_s)$ is obtained from the intramolecular part. Again two power-law regimes $t^{-\varepsilon}$ are identified for polybutadiene. The first agrees with t^{-1} of free Rouse dynamics whereas at long times $\varepsilon = 0.49$ is obtained. The latter is corroborated by the ^2H relaxation of deuterated polybutadiene, yet, it does not agree with $\varepsilon = 0.25$ predicted for constrained Rouse dynamics. Thus, the relation $C_2(t) \propto \langle R^2(t) \rangle^{-1}$ as assumed by the tube-reptation model is not confirmed.



1. INTRODUCTION

The commonly accepted model for the dynamics of entangled polymers is referred as the tube-reptation model,¹ which is a combination of the Rouse model² for nonentangled chains (with molecular mass M below the entanglement mass M_e) and de Gennes' reptation idea³ for $M > M_e$. The model predicts four different power-law regimes (I–IV) for the time dependence of the mean square displacement $\langle R^2(t) \rangle$ of a polymer-segment. Regarding the short-time dynamics MD simulations^{4–6} as well as neutron scattering experiments⁷ have essentially confirmed the model by identifying a crossover from $\langle R^2(t) \rangle \propto t^{0.5}$ to $\langle R^2(t) \rangle \propto t^{0.25}$ forecast for the transition from free Rouse (regime I) to constrained Rouse dynamics (or incoherent reptation dynamics, regime II). On long time scales the final crossover from $\langle R^2(t) \rangle \propto t^{0.5}$ typical of reptation (regime III) to $\langle R^2(t) \rangle \propto t$ of the terminal regime of free diffusion (regime IV) has been observed in polymer melts^{8,9} as well as polymer solutions¹⁰ by field gradient NMR. Another regime (regime 0) which is usually not included in polymer theories reflects 'glassy dynamics' at very short times, i.e., local motions connected with fluctuations of intrasegmental degrees of freedom on the time scale of the segmental correlation time τ_s .

Regarding the time correlation function characterizing the segmental reorientations a corresponding set of power-laws is provided by the tube-reptation model. In regime II and III the reorientational correlation function $C_l(t)$ is given by $C_l(t) \propto \langle R^2(t) \rangle^{-1}$ independently of its rank l , whereas in regime I $C_l(t)$ is l -dependent with $C_2(t) = [C_1(t)]^2 \propto t^{-1}$ and $C_1(t) \propto \langle R^2(t) \rangle^{-1}$. The argument used for deriving the power-laws for regime II and III follows the idea that the correlation function $C_l(t)$ reflects the probability that at time t the chain segment has not left the original tube segment and thus is given by the return-to-origin probability which is provided by $\langle R^2(t) \rangle^{-1}$. We note that alternative models for describing the dynamics of entangled polymers, namely the (n)-renormalized Rouse model and the more complicated polymer-mode-coupling model,^{11–15} end up with different relationships between the reorientational correlation functions and the mean square displacement (cf. Discussion).¹⁶ Thus, the experimental investigation of the power-law behavior of correlation functions of different ranks

Received: May 30, 2012

Revised: July 17, 2012

Published: August 2, 2012

together with the mean square displacement provides the chance to validate the different theoretical approaches.

Field-cycling (FC) NMR relaxometry detects polymer dynamics by measuring the frequency dependence (dispersion) of the spin–lattice relaxation time T_1 . The frequency given by the Larmor frequency $\omega = \gamma B_0$ (γ : gyromagnetic ratio) is a variable depending on the magnetic relaxation field B_0 which can be electronically controlled over 4–5 decades.¹⁷ The relaxation rate $R_1(\omega) = 1/T_1(\omega)$ is related to the spectral density of the motion causing the relaxation and the spectral density is given as the Fourier transform of a corresponding time correlation function.¹⁸

In the case of FC ^1H NMR the relaxation originates from fluctuations of magnetic dipole–dipole (DD) interactions between proton spin pairs. Since the interacting nuclei may be situated on the same or different molecules, the measured $R_{1,\text{DD}}(\omega)$ is a sum of intra- and intermolecular contributions, $R_{1,\text{intra}}(\omega)$ and $R_{1,\text{inter}}(\omega)$, respectively. $R_{1,\text{inter}}(\omega)$ reflects mainly the relative translational motions of chain segments from different molecules, and can be utilized to attain the segmental mean square displacement $\langle R^2(t) \rangle$.¹⁹ $R_{1,\text{intra}}(\omega)$ is associated with segmental reorientation dynamics described by $C_2(t)$ and is usually assumed to be dominating. However, it has been shown that in polymer systems especially at low frequencies intermolecular relaxation may contribute significantly.^{19–22} Thus, in order to disentangle reorientational and translational dynamics the two contributions, $R_{1,\text{intra}}(\omega)$ and $R_{1,\text{inter}}(\omega)$ have to be separated, and FC NMR relaxometry offers the unique possibility to determine both quantities independently. Following the pioneering work of Kimmich and co-workers^{19,22} it is the objective of the present work to demonstrate that FC NMR relaxometry is able to trace both $\langle R^2(t) \rangle$ and $C_2(t)$ through different regimes of polymer dynamics which allows explicitly examining the relationship between $\langle R^2(t) \rangle$ and $C_2(t)$ assumed, e.g., within the tube-reptation model.

Another source of information is provided by the ^2H relaxation rate $R_{1,\text{Q}}(\omega)$ which is predominantly of quadrupolar origin. The relaxation is caused solely by rotational fluctuations of the quadrupolar coupling which in organic molecules like polymers is due to the reorientational dynamics of the C– ^2H bond. Thereby one directly probes the segmental reorientation, and the spectral density is expected to be essentially of the same shape as that obtained from $R_{1,\text{intra}}(\omega)$ via ^1H NMR. Here, one has to note that in polymer systems the spectral shapes of $R_{1,\text{intra}}(\omega)$ and $R_{1,\text{Q}}(\omega)$ do not need to be identical necessarily. In principle, $R_{1,\text{intra}}(\omega)$ also probes fluctuations of spin pairs sitting on different segments of the same molecule, however, this contribution is expected to be small.^{16,22} Consequently, we will in addition present results for $R_{1,\text{Q}}(\omega)$.

Polymer dynamics stretches over many decades in time or frequency. We combine relaxation data of 1,4-polybutadienes (PB) and polydimethylsiloxane (PDMS) obtained from a commercial Stellar FC spectrometer^{17,23} and a home-built FC relaxometer.²⁴ The frequency range of the latter is extended toward lower frequencies by compensating earth and stray fields.²⁵ In order to further augment the dynamic range and cover the different regimes of polymer dynamics we apply frequency–temperature superposition (FTS) which assumes that the polymer relaxation can be shifted through the FC NMR frequency window by changing temperature over a large interval without alteration of its spectral shape. Explicitly, the relaxation data $R_1(\omega)$ measured at different temperatures are

transformed to the susceptibility representation $\chi''(\omega) = \omega/T_1(\omega)$ and the susceptibility is plotted as a function of the reduced frequency $\omega\tau_s$.^{23,26} The approach is well-known from, e.g., rheology and reflects a fundamental feature of cooperative dynamics.²⁵

In our previous FC ^1H NMR works no separation in intra- and intermolecular contribution was attempted, and the total dipolar correlation function $C_{\text{DD}}(t/\tau_s)$ (comprising both intra- and intermolecular contributions) of PB obtained from $\chi''_{\text{DD}}(\omega\tau_s)$ has been presented covering 10 decades in time and eight decades in amplitude.^{23,26} In addition to local dynamics determined by the glass transition phenomenon, two power-laws have been observed for the correlation function reflecting free Rouse (I) and constrained Rouse dynamics (II). Yet, assuming implicitly that $C_{\text{DD}}(t/\tau_s)$ is dominated by intramolecular contributions the theoretically predicted power-law exponent ε for the regime II has not been reached even for the highest M ; $\varepsilon = 0.32 \pm 0.02$ has been found, still above $\varepsilon = 0.25$ which is forecast by the tube-reptation model. This highly protracted transition to full reptation has also been observed by double quantum ^1H NMR experiments²⁷ and to some extent in simulations.^{28,29} However, both NMR techniques so far have not investigated the role of intermolecular relaxation systematically.

In the present work, we decompose the total relaxation rate $R_{1,\text{DD}}(\omega\tau_s)$ into the contributions $R_{1,\text{intra}}(\omega\tau_s)$ and $R_{1,\text{inter}}(\omega\tau_s)$ for PDMS and two different M of PB by utilizing the isotope dilution technique.^{30–35} Preliminary results without attaining the decomposition have already been published.^{23,36} In order to validate this decomposition we compare the shape of the extracted ^1H intramolecular relaxation dispersion with the results obtained from FC ^2H NMR. As will be demonstrated our results for $\langle R^2(t/\tau_s) \rangle$ confirm the findings from neutron scattering, so far the only experimental method which allows probing dynamics of entangled polymers at short times. Yet, regarding the reorientational correlation function $C_2(t/\tau_s)$ our results are at variance with the prediction of the tube-reptation model. We will clearly show that at low frequencies the spin–lattice relaxation in fully protonated polymer melts is—as in the case of simple liquids like glycerol^{37,38}—dominated by intermolecular relaxation.

2. THEORETICAL BACKGROUND

We briefly outline the procedure of determining the segmental mean square displacement from the intermolecular relaxation rate $R_{1,\text{inter}}(\omega)$ discussed in detail by Kimmich and co-workers.^{19,20} By definition the intermolecular correlation function $C_{\text{inter}}(t)$ for isotropic systems is given as^{18,39}

$$C_{\text{inter}}(t) = \frac{4\pi}{5} \int \int \frac{P_2(\theta_t)}{r_t^3} \frac{P_2(\theta_0)}{r_0^3} W(\mathbf{r}_t - \mathbf{r}_0, t) \rho(\mathbf{r}_0) \, d\mathbf{r}_t \, d\mathbf{r}_0 \quad (1)$$

where \mathbf{r}_t and \mathbf{r}_0 are the spatial vectors connecting two nuclei of different molecules at times t and $t = 0$, respectively, and $P_2(\theta_t)$ and $P_2(\theta_0)$ are the corresponding rank-two Legendre polynomials of the angle θ with respect to some reference frame. The propagator $W(\mathbf{r}=\mathbf{r}_t-\mathbf{r}_0, t)$ denotes the probability that the molecule of interest changes its position from \mathbf{r}_0 to \mathbf{r}_t during the time t while $\rho(\mathbf{r}_0)$ is the equilibrium distribution. For a uniform distribution $\rho(\mathbf{r}_0)$ beyond a distance on the order of the molecular size (so-called distance of closest approach) and a Gaussian propagator $W(\mathbf{r}, t)$, the correlation function $C_{\text{inter}}(t)$

can be expressed by the *relative* mean square displacement $\langle \mathbf{r}^2(t) \rangle$ ^{19,20}

$$C_{\text{inter}}(t) \propto \langle \mathbf{r}^2(t) \rangle^{-3/2} \quad (2)$$

Under the condition that the molecules move independently the mean square displacement is given by $\langle \mathbf{R}^2(t) \rangle = 1/2 \langle \mathbf{r}^2(t) \rangle$. The relaxation rate $R_{1,\text{inter}} = 1/T_{1,\text{inter}}$ is connected to the Fourier transform of $C_{\text{inter}}(t)$ via the standard Bloembergen, Purcell, and Pound (BPP) expression⁴⁰

$$1/T_1 \propto \int_0^\infty \langle \mathbf{r}^2(t) \rangle^{-3/2} [\cos \omega t + 4 \cos 2\omega t] dt \quad (3)$$

Explicitly, assuming a subdiffusive power-law $\langle \mathbf{r}^2(t) \rangle \propto t^\alpha$ for the segmental motion of a polymer chain with $\alpha < 2/3$ at $t \gg \tau_s$, the segmental mean square displacement can be derived from the relaxation rate $R_{1,\text{inter}}(\omega)$ along^{19,20}

$$\langle \mathbf{r}^2(t = \omega^{-1}) \rangle = N^{2/3} \left(\frac{\mu_0}{4\pi} \gamma_{\text{H}}^2 \hbar \right)^{4/3} g(\alpha) (\omega R_{1,\text{inter}}(\omega))^{-2/3} \quad (4)$$

The parameter γ_{H} denotes the gyromagnetic ratio of the proton and N is the spin density. The Fourier transform depends on the actual value of the exponent α , and the factor $g(\alpha)$ reads

$$g(\alpha) = \left(\sqrt{\frac{6\pi^3}{25}} \frac{1 + 2^{3\alpha/2+1}}{\cos(3\pi\alpha/4)\Gamma(3\alpha/2)} \right)^{2/3} \quad (5)$$

Thus, in order to evaluate $\langle \mathbf{R}^2(t) \rangle$ quantitatively one has to know the value of α . For $0.25 < \alpha < 0.5$, as expected by the tube-reptation model (cf. Introduction), $g(\alpha)$ varies by a factor of 3 which is actually not significant when logarithmic scales are considered. Moreover, $g(\alpha)$ is constant for a given power-law regime and a different α leads only to a rescaling of the amplitude of $\langle \mathbf{R}^2(t) \rangle$ without altering the power-law itself. Following Kehr et al.¹⁹ we choose $\alpha = 1/3$ which yields for the gamma function $\Gamma(3\alpha/2) = \sqrt{\pi}$.

3. EXPERIMENTAL SECTION

Blends of monodisperse 1,4-polybutadienes (PB, PDI ≤ 1.03 , purchased from PSS, Mainz, Germany) with different molar fractions of protonated (PB- h_6) and deuterated (PB- d_6) chains were prepared by thoroughly dissolving the different mole fractions with chloroform (Fisher Scientific, Loughborough, U.K., 99.97%, used without further purification) to achieve homogeneous mixing. After 3 days of rotating and shaking the solvent was removed by freeze-drying and the sample was kept under vacuum for several days until no change in mass was observable any longer. The isotopic mixtures of polydimethylsiloxane (PDMS, PDI ≤ 1.12 , purchased from PSS) were set up in the same way with *n*-hexane (purchased from VWR, Fontenay-sous-Bois, France, 98.9%, used without further purification) as solvent. The corresponding weight-average molecular masses $M = M_w$ of protonated and deuterated polymers vary negligibly and are listed in Table 1. The isotope dilution series of PB comprise the proton molar fractions $x_{\text{H}} = 100\%$, 76%, 53%, 22%, and 11% for PB 24300- h_6 with PB 22800- d_6 , and 100% and 16% for PB 196000- h_6 with PB 191000- d_6 . For PDMS blends with $x_{\text{H}} = 100\%$, 75%, 47%, and 24% for PDMS 21600- h_6 with PDMS 25300- d_6 were measured. The data of the fully protonated PB and PDMS are from refs 26 and 36, respectively. In the following the blends are referred to by providing M and x_{H} of the protonated polymer.

The ^1H NMR spin–lattice relaxation experiments were performed with two different electronic field cycling (FC) relaxometers, a commercial one (Stelar Spinmaster FFC2000) at Bayreuth University and a home-built one at Darmstadt University. With the first one experiments were performed at temperatures from 173 K to 408 K;

Table 1. Details on the Samples^a

sample	M_w [g/mol]	M_w/M_n
PB 24300- h_6	24 300	1.01
PB 22800- d_6	22 800	1.02
PB 196000- h_6	196 000	1.02
PB 191000- d_6	191 000	1.03
PDMS 21600- h_6	21 600	1.04
PDMS 25300- d_6	25 300	1.12

^aThe sample name reflects the molecular mass M_w ; the index denotes the number of protons or deuterons per monomer.

with the second ^1H and ^2H NMR spin–lattice relaxation experiments at temperatures from 355 K up to 408 K were measured. The temperature interval applied for the ^2H relaxation experiments was smaller than in the case of FC ^1H NMR, as in the first case the spin–lattice relaxation time is much shorter and its determination at low temperatures is limited by the switching time of the relaxometer. The Stelar relaxometer covers a ^1H frequency range from $\nu = \omega/2\pi = 10$ kHz to 20 MHz while the switching time from high polarization field to relaxation field was 3 ms. Lower ^1H frequencies can only be reached at the home-built relaxometer²⁴ at which frequencies down to 400 Hz and up to 30 MHz were accomplished for the present project. The low frequencies were attained by utilizing a three-dimensional resistive coil arrangement for compensating the earth field, other magnetic stray fields, and field drifts. Switching times of 3 or 6 ms were achieved when the compensation system is not used ($\nu > 1$ kHz) or when it is employed ($\nu \leq 1$ kHz), respectively. For technical details the reader is referred to ref 25, where it is demonstrated that in favorable cases ^1H frequencies down to 12 Hz can be reached.

The relaxation time T_1 was determined by an exponential fit of the magnetization decay curve. We note that a decomposition of the homogeneous isotopic blends can be excluded, since no trend of an explicitly biexponential magnetization decay was observed nor a time dependence of T_1 , i.e., T_1 measured at a certain temperature remains constant even if in the meantime the sample was kept at a lower temperature for a longer time. In order to ensure that the solvent was completely removed, in Figure 1a two T_1 dispersions obtained in

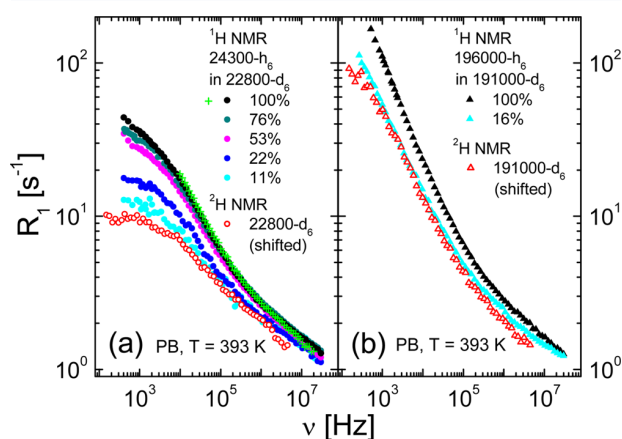


Figure 1. ^1H spin–lattice relaxation rate $R_{1,\text{DD}}(\nu)$ at $T = 393$ K for blends of protonated and deuterated 1,4-polybutadiene (PB) of molecular mass $M = 24300$ (a) and 196000 (b) with proton molar fractions x_{H} as indicated and obtained using the home-built relaxometer. The spectral shape of the ^2H relaxation rates $R_{1,\text{Q}}(\nu)$ of the fully deuterated PB- d_6 (shifted) is similar to that of the ^1H spectra at the lowest x_{H} . Green crosses in (a): PB sample with $M = 24300$ and $x_{\text{H}} = 100\%$, for which chloroform was added and later removed again, measured with the commercial spectrometer (see Experimental Section).

different ways for the fully protonated ($x_H = 100\%$) sample of PB with $M = 24300$ at $T = 393$ K are compared exemplarily: First, the pure melt was measured as it is (black circles), and second, it was treated as described above (green crosses); i.e., chloroform was added and subsequently removed again. Within the experimental error the two $T_1(\nu)$ curves coincide very well. This indicates also that the temperature control agrees for both instruments, since the second sample was measured with the commercial relaxometer. Furthermore, the enhanced frequency range of the home-built relaxometer is illustrated.

The isotope dilution technique^{30–35} is a well established method of ^1H NMR to separate intra- and intermolecular relaxation contributions. By diluting a protonated polymer in a deuterated matrix (“invisible” for ^1H NMR), the intermolecular relaxation is successively reduced when x_H is decreased. Thus, for infinite dilution ($x_H \rightarrow 0$) in absence of intermolecular dipolar interactions (the negligible influence of proton-deuteron coupling can be omitted) the dipolar relaxation rate $R_{1,DD}(\omega)$ is given by the intramolecular contribution $R_{1,intra}(\omega)$. Therefore, $R_{1,intra}(\omega)$ can be determined by linearly extrapolating $R_{1,DD}(\omega)$ as a function of x_H (at a given frequency) and the intermolecular part is given by $R_{1,inter}(\omega) = R_{1,DD}(\omega) - R_{1,intra}(\omega)$. This holds equivalently in the susceptibility representation $\chi''_{DD}(\omega) = \omega/T_{1,DD}(\omega)$. However, it turns out that for both PB and PDMS this linear behavior is revealed experimentally only in the master curves, i.e., by inspecting $\chi''_{DD}(\omega\tau_s)$ as a function of the reduced frequency $\omega\tau_s$, and not in the susceptibilities $\chi''_{DD}(\omega)$ for a given temperature. As it will be shown indications of an isotope effect are observed, i.e., the relaxation data bear slightly different correlation times τ_s depending on x_H , which is eliminated by inspecting the “isofrictional” master curves. This will be discussed in detail in Appendix B. Regarding details about constructing the susceptibility master curves $\chi''(\omega\tau_s)$ the reader is referred to our previous publications.^{23,26}

4. RESULTS

Polybutadiene. In Figure 1a and 1b the ^1H relaxation rate $R_{1,DD}(\nu)$ at $T = 393$ K for different molar fractions x_H is displayed for the isotope dilution series of PB with $M = 24300$ and 196000 , respectively. In the latter case only a single dilution is applied ($x_H = 16\%$). The data of the fully protonated samples are taken from ref 26. For both M the relaxation rates $R_{1,DD}(\nu)$ decrease in amplitude with decreasing x_H , as expected. At low frequencies $R_{1,DD}(\nu)$ is more diminished than at high frequencies, and for $M = 24300$ this reduction is stronger than for $M = 196000$. This finding already indicates that the intermolecular contribution to the total relaxation becomes larger while decreasing the frequency, which confirms the results of Kehr et al.^{19,22} For comparison the ^2H relaxation dispersion $R_{1,Q}(\nu)$ of the two fully deuterated PB- d_6 at $T = 393$ K are shown (the low-frequency limit of $\nu \approx 400$ Hz for protons corresponds to $\nu \approx 150$ Hz for deuterons). Their shape is quite similar to the one of the ^1H relaxation rates for the lowest molar fraction as for $x_H \ll 1$ the latter is indeed dominated by the intramolecular contribution. Note that for a direct comparison $R_{1,Q}(\nu)$ has been shifted in amplitude (cf. also description of Figure 2) to take into account the different coupling constants of ^1H and ^2H NMR. Our ^1H results for PB 196000- h_6 at $T = 355$ K perfectly reproduce those measured by Kimmich and co-workers.¹⁹ In the ^2H relaxation rates of PB 191000- d_6 increased scatter is seen below 3 kHz,²² which will be discussed in Appendix A.

While Figure 1 shows relaxation data at a single temperature, the application of FTS allows constructing master curves by combining data measured at ten different temperatures (223 K to 393 K). Figure 2 presents the susceptibility master curves $\chi''_{DD}(\omega\tau_s)$ for the isotopic blends of PB with the two molar masses. The frequency range is now significantly extended with respect to Figure 1. The susceptibility data for each temperature

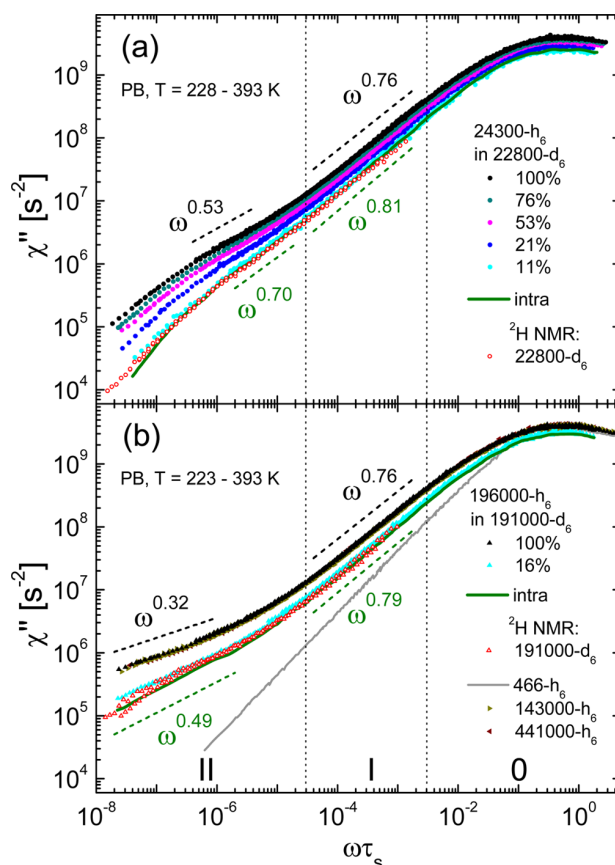


Figure 2. ^1H susceptibility master curves as a function of the reduced frequency $\omega\tau_s$ for the PB blends with $M = 24300$ (a) and 196000 (b) in the temperature range as indicated, corresponding intramolecular contributions (see text), and ^2H master curves ($T = 355$ K and 393 K) of the deuterated polymers. Dotted vertical lines: relaxation regimes 0, I, and II, i.e., glassy, Rouse, and constrained Rouse dynamics, respectively. Dashed lines: power-laws observed for fully protonated sample and intramolecular contribution. In part b the master curves of low- M PB- h_6 ($M = 466$, reference for a simple liquid) and high- M PB- h_6 ($M = 143000$ and 441000 with the same spectral shape as that of $M = 196000$) are also included.²⁶

were shifted solely along the frequency axis to achieve maximal overlap. Since at low temperatures the susceptibility exhibits a relaxation maximum at which $\omega\tau_s \approx 0.6$ holds, the shift factors can be identified with the time constants $\tau_s(T)$ which are displayed in Figure 9a (Appendix B). As expected, the correlation times are quite similar, yet, it appears that a weak isotope effect is observed which will be discussed in the Appendix B.

In the susceptibility master curves (Figure 2) a peak at high (reduced) frequencies is present which reflects the “local” segmental dynamics (or α -process, i.e., regime 0). The master curves of the polymers exhibit at $\omega\tau_s < 1$ an intensity in excess to that of a simple liquid which is signaled by $\chi''_{DD}(\omega\tau_s) \propto \omega^\epsilon$ with $\epsilon < 1$, whereas in simple liquids $\chi''_{DD}(\omega\tau_s) \propto \omega$ is found (PB 466- h_6 as low- M limit in Figure 2b).²³ Two relaxation regimes with characteristic power-law exponents ϵ are recognized and can be identified with the Rouse (I) and tentatively with the constrained Rouse (II) regimes.²⁶ The different amplitudes of the master curves reflect the decreasing intermolecular contribution while the molar fraction x_H becomes smaller.

As shown in Figure 10a (Appendix B) the susceptibility master curves are reduced linearly with x_H , as expected. This linear behavior has been carefully checked and used for extrapolation to $x_H = 0$ to reveal the spectral shape of the intramolecular contribution $\chi''_{\text{intra}}(\omega\tau_s)$ (see Experimental Section) which is included in Figure 2 for both PB samples.

Considering $\chi''_{\text{DD}}(\omega\tau_s)$ of $x_H = 100\%$ and the extracted intramolecular contribution $\chi''_{\text{intra}}(\omega\tau_s)$ only a slight change of ε is observed in regime I, whereas in regime II ε depends on M and x_H . In Figure 2a for $M = 24300 \approx 12M_e$ ($M_e \approx 2000$, ref 41) the manifestation of the power-law in regime II is restricted due to the terminal relaxation observed at lowest frequencies. However, it appears that the terminal relaxation time is shortened with lower x_H . This is actually expected as the terminal intermolecular relaxation follows a power-law $\propto t^{-3/2}$ which decays slower than the corresponding exponential decay of the intramolecular contribution. Still, ε is increased when the intermolecular contribution is successively diminished. This effect becomes more evident in Figure 2b for the master curve of PB- h_6 with $M = 196000 \approx 98M_e$ which perfectly coincides with those of $M = 143000$ and 441000 (from ref 26) and consequently can be regarded as representing the spectral shape of highest M . Here the terminal relaxation is beyond the lowest accessible frequencies and does not affect ε in regime II. It increases from $\varepsilon = 0.32 \pm 0.02$ for $x_H = 100\%$ to $\varepsilon = 0.49 \pm 0.05$ for the intramolecular contribution. The latter is rather high and does not agree with the prediction $\varepsilon = 0.25$ of the tube-reptation model. The fact that at low frequencies for both M the intramolecular contribution decreases stronger than $\chi''_{\text{DD}}(\omega)$ of $x_H = 100\%$ is due to the more dominating intermolecular contribution. The intra- and intermolecular contributions are explicitly compared in Figure 3.

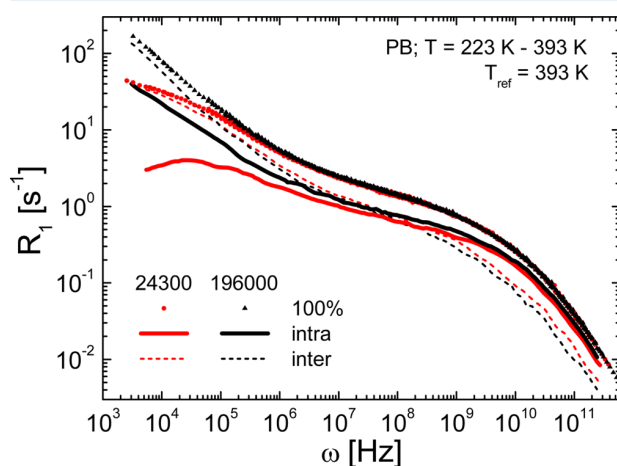


Figure 3. Relaxation rates $R_{1,DD}(\omega)$ for PB with $M = 24300$ (a) and 196000 (b) with $x_H = 100\%$ and corresponding intra- and intermolecular contributions as obtained from the susceptibility master curves of Figure 2 for the reference temperature 393 K.

The ^2H master curves $\chi''_Q(\omega\tau_s)$ included in Figure 2 for PB- d_6 with $M = 22800$ and 191000 coincide well with the corresponding intramolecular contributions $\chi''_Q(\omega\tau_s)$. We note that in the case of the FC ^2H NMR data ($T = 355$ K and 393 K), it is not possible to construct master curves comprising also the segmental relaxation peak nor to obtain τ_s , since the ^2H spin–lattice relaxation time become significantly shorter than the switching time of the FC spectrometer while approaching

lower temperatures. As a consequence the time constants acquired for the corresponding PB blend with the lowest x_H (cf. Figure 9a in Appendix B) were applied to the ^2H NMR susceptibilities in order to provide the ^2H master curves as a function of $\omega\tau_s$. Afterward $\chi''_Q(\omega\tau_s)$ was scaled in amplitude taking into account the different coupling constants of ^1H and ^2H NMR and to compare its spectral shape with $\chi''_{\text{intra}}(\omega\tau_s)$. Indeed a satisfactory agreement is found over the entire frequency range. We conclude that $\chi''_{\text{intra}}(\omega\tau_s)$ and $\chi''_Q(\omega\tau_s)$ are essentially the same, and dipolar interactions between protons on different segments of the same molecule (referred to as “intra chain contribution” in ref 22) are negligible which again confirms the results by Kehr et al.²²

In Figure 3 for both M the relaxation rates $R_{1,DD}(\omega)$, $R_{1,\text{intra}}(\omega)$, and $R_{1,\text{inter}}(\omega)$ are presented at the reference temperature $T_{\text{ref}} = 393$ K obtained from the susceptibility master curves and thus containing the combined results of the entire temperature range. Benefiting from having applied FTS, this representation complements the rates measured at $T = 393$ K toward higher frequencies (cf. Figure 1). In other words it displays the results in a way as they are expected to be measured in a relaxation experiment at a single temperature (T_{ref}) but with a much broader frequency range. This has been achieved by choosing $u = \omega\tau_s$ as in the master curves (Figure 2) and plotting $(\chi''(u)/u) \cdot \tau_s(393 \text{ K})$ as a function of $u/(\tau_s(393 \text{ K}))$, which is identical to $R_1(\omega)$ at $T = 393$ K. Now, intra- and intermolecular relaxation contributions can be compared directly with regard to their dependence on frequency and molecular mass. Whereas $R_{1,\text{intra}}(\omega)$ is the dominating contribution at high ω , it is vice versa for $R_{1,\text{inter}}(\omega)$, and for both M they cross between $\omega = 10^7$ Hz and 10^8 Hz. For $M = 24300$, the ratio $R_{1,\text{intra}}(\omega)/R_{1,DD}(\omega)$ is about 1/10 and 1/2 at the lowest and highest frequencies, respectively, and for $M = 196000$, these ratios are larger especially at lowest frequencies. Comparing the influence of the different M the shapes of $R_{1,\text{intra}}(\omega)$ and $R_{1,\text{inter}}(\omega)$ begin to differ below $\omega \approx 10^6$ Hz and $\omega \approx 10^5$ Hz, respectively, while for $R_{1,DD}(\omega)$ this occurs in between. In the case of PB 24300 the intramolecular part shows a weak maximum at lowest frequencies which, of course, is unphysical and which is attributed to uncertainties in the $x_H \rightarrow 0$ extrapolation procedure. In particular, when the intramolecular contribution is rather small with respect to the total relaxation rate the relative error of $R_{1,\text{intra}}(\omega)$ may become quite large. Nevertheless, the supremacy of the intermolecular contribution at low frequencies is obvious and at lowest frequencies the amplitude of $R_{1,\text{inter}}(\omega)$ almost approaches that of $R_{1,DD}(\omega)$.

In Figure 4 the normalized correlation functions $C_{\text{DD}}(t/\tau_s)$, $C_{\text{intra}}(t/\tau_s)$, $C_{\text{inter}}(t/\tau_s)$, and $C_Q(t/\tau_s)$ (from ^2H NMR) as obtained by Fourier transform of the corresponding susceptibility master curves are displayed for both M . Again, the three relaxation regimes 0, I, and II can be identified and the exponent ε of the susceptibility representation reappears in the power-law behavior $t^{-\varepsilon}$. At short times (regime 0) all correlation functions agree which signals that they similarly reflect the segmental (local) dynamics. In regime I only weak differences among the correlation functions are observed which become, however, significant in regime II, i.e., at long times. In the case of PB with $M = 24300$ the correlation functions show an essentially exponential cutoff at longest times typical of the terminal relaxation. Whereas the power-law exponents of $C_{\text{inter}}(t/\tau_s)$ (given in Figure 4) are always lower than the corresponding ones of $C_{\text{DD}}(t/\tau_s)$ those of $C_{\text{intra}}(t/\tau_s)$ are always higher. Moreover, for both M the reorientational correlation

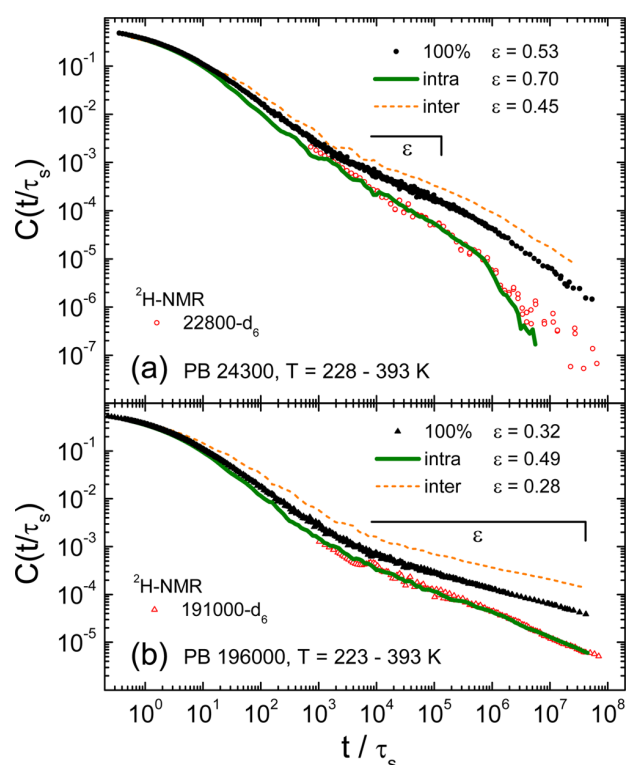


Figure 4. Dipolar correlation function $C_{DD}(t/\tau_s)$ for PB with $M = 24300$ (a) and 196000 (b) comprising intra- and intermolecular contributions, and correlation functions $C_{intra}(t/\tau_s)$ and $C_{inter}(t/\tau_s)$ reflecting solely reorientational or translational dynamics, respectively. For regime II, their power-law exponents ε are indicated. $C_{intra}(t/\tau_s)$ is determined from the isotope dilution series while $C_Q(t/\tau_s)$ is obtained by FC ^2H NMR.

function $C_{intra}(t/\tau_s)$ obtained from the intramolecular contribution agrees well with $C_Q(t/\tau_s)$ from ^2H relaxation, thus $C_Q(t/\tau_s) \approx C_{intra}(t/\tau_s) \approx C_2(t/\tau_s)$ holds for $t/\tau_s \gg 1$.

In Figure 5a the mean square displacement $\langle R^2(t/\tau_s) \rangle$ for PB with $M = 24300$ and 196000 calculated from $\chi''_{inter}(\omega\tau_s)$ via eq 4 is shown and embraces about 7 decades in time. The covered time span has been enlarged significantly compared to that reported by Kehr et al.¹⁹ We applied the following parameters: $\alpha = 1/3$ (see Theoretical Background) and 0.876 g/cm^3 as mass density⁴² of PB. Clearly two regimes are recognized. The first one, at short times, yields a power-law $t^{0.49 \pm 0.03}$ for both M in accordance with the Rouse model prediction of $t^{0.5}$. At long times a power-law $t^{0.19 \pm 0.03}$ is observed for the high- M PB which is close to $t^{0.25}$ expected for the constrained Rouse dynamics (regime II), while PB 24300 shows a tendency to crossover to a similar behavior but free diffusion interferes at longest times. As will be shown in the following, comparable results are found for PDMS (cf. Figure 5b). We note that the results agree well with those reported previously¹⁹ for a single temperature. Thus, for the first time the mean square displacement determined by results of FC NMR yields clearly distinguishable power-law regimes which can be related to the regimes I and II of tube-reptation model.

For comparison Figure 5c shows results of $\langle R^2(t) \rangle$ from neutron spin-echo measurements⁷ for a polyethylene (PE) melt with $M = 190000$ at a single temperature. The behavior expected by the tube-reptation model has been observed also therein, i.e., the transition of the power-law exponent from

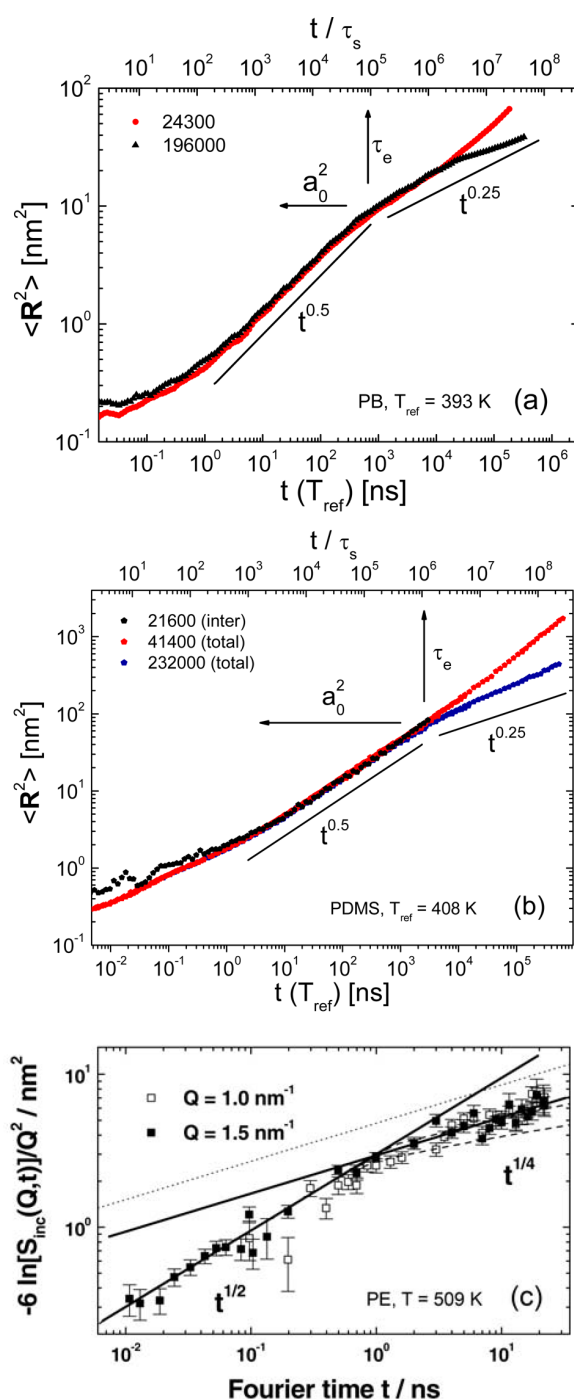


Figure 5. (a) Segmental mean squared displacement $\langle R^2(t/\tau_s) \rangle$ for PB with $M = 24300$ and 196000 calculated from $\chi''_{inter}(\omega\tau_s)$ according to eq 4. Upper axis: reduced time. Lower axis: time t at the reference temperature $T_{ref} = 393$ K. (b) Corresponding representation of $\langle R^2(t/\tau_s) \rangle$ for PDMS with $M = 21600$. For $M = 41400$ and 232000 , $\langle R^2(t/\tau_s) \rangle$ is obtained from $\chi''_{BD}(\omega\tau_s)$ (see text). Lower axis: time t at $T_{ref} = 408$ K. (c) $\langle R^2(t) \rangle$ for polyethylene (PE) with $M = 190000$ measured by neutron spin-echo at $T = 509$ K (Figure reprinted with permission from ref 7. Copyright 2003 American Physical Society). Lines: power-laws $t^{0.5}$ and $t^{0.25}$ as expected for the Rouse (I) and the constrained Rouse regime (II), respectively.

0.5 to 0.25. Note that the ordinate is identical with $\langle R^2(t) \rangle$ as long as the diffusive displacement probability distribution is assumed to have Gaussian shape,⁷ an assumption also included in deriving $\langle R^2(t) \rangle$ from the intermolecular correlation function (cf. Theoretical Background).

Polydimethylsiloxane. Figure 6 shows the susceptibility master curves $\chi''_{DD}(\omega\tau_s)$ of the isotopic dilution series of PDMS

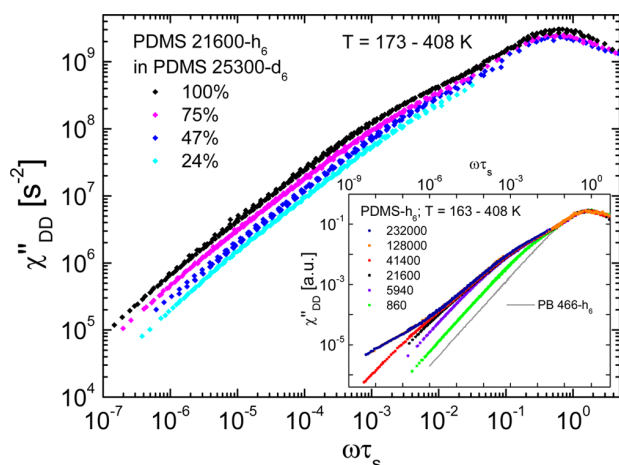


Figure 6. ^1H susceptibility master curves $\chi''_{DD}(\omega\tau_s)$ for the PDMS blends with $M = 21600$ for the proton molar fractions x_{H} and in the temperature range as indicated. Inset: master curves $\chi''_{DD}(\omega\tau_s)$ for PDMS with different M ($\omega\tau_s > 10^{-7}$, data from ref 36; $\omega\tau_s \leq 10^{-7}$, present work with the home-built relaxometer) and for PB 466- h_6 (reference for a simple liquid²⁶).

21600- h_6 with PDMS 25300- d_6 for four different molar fractions x_{H} , which have been obtained by ^1H FC NMR experiments in the temperature range from 173 K up to 408 K with the commercial spectrometer (cf. also ref 36). Qualitatively the same effects as in the case of PB 24300 (cf. Figure 2a) are observed: the relaxation maximum at $\omega\tau_s \approx 1$, power-law regimes for $\omega\tau_s < 1$ which are characteristic of polymer dynamics, the approaching crossover to terminal relaxation at lowest reduced frequencies, and most importantly the amplitude of $\chi''_{DD}(\omega\tau_s)$ is reduced while decreasing x_{H} . However, as discussed previously^{43,36} the ^1H FC NMR results of PDMS show particularities which are well recognizable in the master curves of PDMS for different M (inset of Figure 6, from ref 36): first, polymer dynamics sets in only below $\omega\tau_s \approx 10^{-2}$ in contrast to PB for which the onset appears close to $\omega\tau_s \approx 1$ and, second, with respect to the low- M limit of PB (from ref 26) an excess intensity is observed for all M (including also the low- M limit) in the range $10^{-2} < \omega\tau_s < 1$. By separating the intra- and intermolecular relaxation contributions the nature of this “shoulder” will be clarified.

The time constants $\tau_s(T)$ as yielded from creating the master curves of the PDMS blends are displayed in Figure 9b in Appendix B. An isotope effect can be seen as in the case of PB (for details see Appendix B). The amplitude of the susceptibilities is reduced linearly with decreasing x_{H} (see Figure 10b in Appendix B). The intramolecular and intermolecular contributions $\chi''_{\text{intra}}(\omega\tau_s)$ and $\chi''_{\text{inter}}(\omega\tau_s)$, respectively, are extracted by linearly extrapolating $\chi''_{DD}(x_{\text{H}})$ as described above for PB. The isolated spectra are presented together with the total susceptibility $\chi''_{DD}(\omega\tau_s)$ of PDMS 21600 with $x_{\text{H}} = 100\%$ in Figure 7. The most noticeable difference compared to PB is the

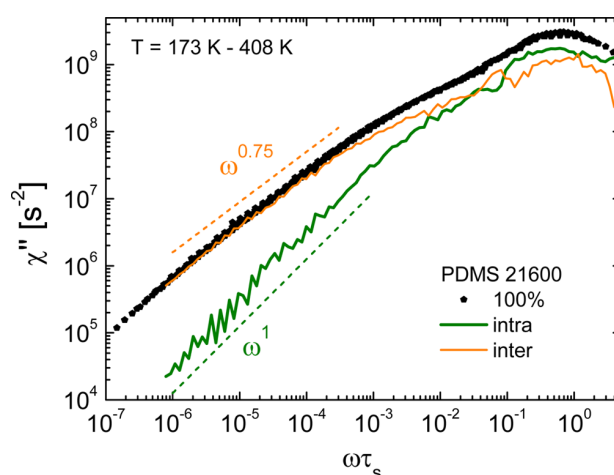


Figure 7. Susceptibility master curve for PDMS with $M = 21600$ with $x_{\text{H}} = 100\%$ and corresponding intra- and intermolecular contributions obtained by means of the isotope dilution experiment. Dashed lines: power-laws observed for the intra- and intermolecular contributions.

dominance of $\chi''_{\text{inter}}(\omega\tau_s)$ which begins already about one decade below the relaxation peak and within the frequency regime of the excess intensity exhibiting the “shoulder”. For lower $\omega\tau_s$ the intermolecular part approaches $\chi''_{DD}(\omega\tau_s)$ and they reach essentially the same amplitude at $\omega\tau_s \leq 10^{-4}$. In contrast, $\chi''_{\text{intra}}(\omega\tau_s)$ decays sharply and the power-law behavior of terminal relaxation is found at $\omega\tau_s \leq 10^{-3}$. Only one power-law regime with $\varepsilon = 0.75 \pm 0.03$ is found in $\chi''_{\text{inter}}(\omega\tau_s)$ of PDMS 21600, and it represents the main contribution to the total relaxation as reflected in $\chi''_{DD}(\omega\tau_s)$. At lowest frequencies, $\chi''_{DD}(\omega\tau_s)$ decays more steeply which indicates that also in the intermolecular part a crossover to terminal relaxation is observed. Given that $M_c \approx 2M_e \approx 24000$ ⁴² no strong entanglement effects are observed.

The segmental mean square displacement $\langle R^2(t/\tau_s) \rangle$ for PDMS with $M = 21600$ is calculated from $\chi''_{\text{inter}}(\omega\tau_s)$ via eq 4 and is displayed in Figure 5b. Again $\alpha = 1/3$ and 0.895 g/cm^3 as mass density⁴² were used. For the longest times which were accessible in the isotope dilution series a power-law $t^{0.49 \pm 0.03}$ is recognizable which agrees with the prediction of $t^{0.5}$ for regime I. No crossover to regime II is recognized because M is still too small. Since in PDMS $\chi''_{\text{inter}}(\omega\tau_s)$ is dominating in the regimes of polymer dynamics ($\omega\tau_s \ll 1$), it can be approximated by $\chi''_{\text{inter}}(\omega\tau_s \ll 1) \approx \chi''_{DD}(\omega\tau_s \ll 1)$. Therefore, the susceptibilities $\chi''_{DD}(\omega\tau_s)$ of the completely protonated PDMS- h_6 with $M = 41400$ and 232000 which have been investigated at lower frequencies with the home-built relaxometer (cf. inset of Figure 6) are used to obtain $\langle R^2(t/\tau_s) \rangle$ also for higher M (cf. Figure 5b). The data of the first essentially reproduce $\langle R^2(t/\tau_s) \rangle$ of $M = 21600$ determined from $\chi''_{\text{inter}}(\omega\tau_s)$ in regime I. At longer times they increase with a higher exponent which indicates the approach of free diffusion. Solely minor deviations are seen at $t/\tau_s < 10^3$, which are due to the influence of the intramolecular contribution which is negligible at longer times as shown before. For $\langle R^2(t/\tau_s) \rangle$ of $M = 232000 \gg M_e$ a transition to a weaker power-law regime is discovered at longest times. Its exponent $\alpha = 0.34 \pm 0.03$ is larger than $\alpha = 0.25$ expected for regime II of the tube-reptation model. However, a similar picture as found for PB (cf. Figure 5a) is rendered.

5. DISCUSSION

We have separated the intra- and intermolecular relaxation contribution to the total ^1H relaxation for PB and PDMS. This has been corroborated in the case of PB by comparing the spectral shape of the intramolecular ^1H relaxation contribution with that of ^2H . No significant difference is observed. It has been shown clearly that the intermolecular relaxation contribution is dominating at low frequencies. As already emphasized^{19–22} it is not possible to ignore this contribution. However, benefiting from the strong intermolecular contribution the segmental mean square displacement $\langle \mathbf{R}^2(t/\tau_s) \rangle$ has been calculated from $\chi''_{\text{inter}}(\omega\tau_s)$. For PB as well as PDMS two power-law regimes are found. The one at short times (regime I) agrees with the prediction $t^{0.5}$ of the Rouse model while the one at long times exhibits a significantly lower exponent in fair agreement with $\alpha = 0.25$ forecast by the tube-reptation model for constrained Rouse dynamics (regime II). We find $\alpha = 0.19 \pm 0.03$ for PB and $\alpha = 0.34 \pm 0.03$ for PDMS.

Because of the strong intermolecular contribution, the intramolecular part of PB significantly changes with respect to the total relaxation. It is found that the exponent of $C_2(t/\tau_s)$ in regime II is rather high and does not agree with the prediction $\varepsilon = 0.25$ of the tube-reptation model. Explicitly, while the long-time exponent in the total dipolar correlation $C_{\text{DD}}(t)$ is $\varepsilon = 0.32 \pm 0.02$ it becomes $\varepsilon = 0.49 \pm 0.05$ for $C_2(t/\tau_s)$. We emphasize that the exponent agrees with the one extracted from the ^2H relaxation results which demonstrates the reliability of the separation procedure via the isotope dilution technique. A similar trend is observed in very recent DQ ^1H NMR results by Saalwächter and co-workers.⁴⁴

Next we compare the results for $C_2(t/\tau_s)$ and $\langle \mathbf{R}^2(t/\tau_s) \rangle$. Since the shape of the susceptibilities for high- M PB is considered to be M independent and representatively described by $M = 196000$ (cf. Figure 2b), we will restrict further discussion to those results. As said, the reorientational correlation function yields $C_2(t/\tau_s) \propto t^{-0.49 \pm 0.05}$ for regime II. Together with the result for the segmental mean square displacement, explicitly $\langle \mathbf{R}^2(t/\tau_s) \rangle \propto t^{0.19 \pm 0.03}$ (following essentially the tube-reptation model), it can be concluded that in regime II the fundamental assumption of the tube-reptation model $C_l(t) \propto \langle \mathbf{R}^2(t) \rangle^{-1}$ for $t > \tau_e$ is not fulfilled (τ_e is the entanglement time). This is confirmed by recent MD simulations by Meyer et al.⁴⁵ which have shown that in regime II the slopes of the reorientational correlation functions of different rank l are neither identical: $C_1(t) \propto t^{-0.25}$ and $C_2(t) \propto t^{-0.34}$ have been observed in a regime where $\langle \mathbf{R}^2(t) \rangle \propto t^{0.25}$ is well identified. In other words, the presumed relation only holds for $l = 1$, explicitly $C_1(t) \propto \langle \mathbf{R}^2(t) \rangle^{-1}$. However, recent simulations by Wang et al.²⁹ have shown a power-law relationship of $C_2(t) \propto [C_1(t)]^m$ for $m = 2$ and 1 in the regimes I, and II, respectively, i.e., they essentially have confirmed the tube-reptation model. In contrast to the results of the tube-reptation model the experimentally observed relation between $C_l(t)$ and $\langle \mathbf{R}^2(t) \rangle$ suggests an l -dependence as forecast by the (n)-renormalized Rouse model and the polymer-mode-coupling model,^{11–16} and a relation $C_2(t) \propto [C_1(t)]^2 \propto \langle \mathbf{R}^2(t) \rangle^{-2}$ is predicted. The present results seem to suggest $C_2(t) \propto \langle \mathbf{R}^2(t) \rangle^{-2}$ which is, however, at variance with the result of the MD simulations of Meyer et al.⁴⁵ Regarding the Rouse regime (I) the prediction $C_2(t) \propto C_1(t)^2 \propto t^{-1}$ (at $\tau_s < t < \tau_e$) is in good agreement with our experiments. Simulations have shown that it is important to average only over the innermost monomers⁴ in order to reveal

the power-laws of the tube-reptation model. This remains a future experimental task in order to thoroughly examine also effects constraint release or contour length fluctuations.^{27,29}

As shown in Figure 5 where the NMR results are compared to those from neutron scattering a very similar behavior is observed for $\langle \mathbf{R}^2(t/\tau_s) \rangle$ which demonstrates the potential of FC ^1H NMR. In other words, NMR relaxometry has become the second method to probe subdiffusive translational motion in polymer melts. The entanglement time τ_e and the tube diameter $a_0 = (\langle \mathbf{R}^2(t = \tau_e) \rangle)^{1/2}$ can be estimated by following the mean square displacement until at $t = \tau_e$ the slope departs from the initial power-law regime.¹ From the intersection (arrows in Figures 5a and 5b) of the power-laws we find for PB $\tau_e/\tau_s \approx 10^5$ and $a_0 \approx 3$ nm, and for PDMS $\tau_e/\tau_s \approx 10^6$ and $a_0 \approx 8$ nm. Introducing a reference temperature ($T_{\text{ref}} = 393$ and 408 K) and using the corresponding τ_s yields $\tau_e(T_{\text{ref}}) \approx 0.8$ μs and 2 μs for PB and PDMS, respectively. From rheological experiments⁴² at $T = 413$ K, the tube diameters $a_0 = 4.4$ nm and 7.9 nm have been determined for PB and PDMS, respectively. A neutron spin echo study⁴⁶ found for PB $a_0 = 4.4$ nm and $\tau_e = 5$ ns at $T = 509$ K, and also a recent study⁴⁷ analyzing atomistic MD simulations of PB with $M \approx 11000$ has reported very similar values $a_0 \approx 3$ nm.

We emphasize that our conclusions rely on the low-frequency relaxation results (cf. Appendix A) and the possibility to extract intramolecular and intermolecular relaxation contributions from the overall relaxation by isotopic dilution. The demonstrated coincidence between the shapes of $\chi''_{\text{intra}}(\omega\tau_s)$ and $\chi''_{\text{Q}}(\omega\tau_s)$ determined by ^1H and ^2H relaxation, respectively, and the fact that latest results⁴⁴ by ^1H DQ NMR indicate a similar trend for ε make the results even more trustworthy. We assume cross-relaxation terms to be negligible, since an exponential magnetization decay is observed and the intermolecular proton–deuteron coupling is below 5% of the intermolecular proton–proton coupling.¹⁹

The evaluation of $\langle \mathbf{R}^2(t/\tau_s) \rangle$ presumes a Gaussian probability distribution to link the intermolecular relaxation rate with the relative mean-squared displacement. Gaussian statistics is a

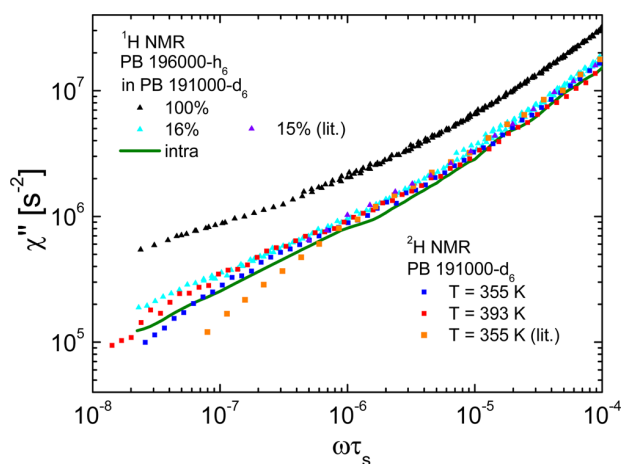


Figure 8. Zoom into Figure 2b with the ^1H master curves of the PB 196000 with $x_{\text{H}} = 100\%$ and 16% and the corresponding intra-molecular contribution. The ^2H susceptibilities at $T = 355$ and 393 K of PB 191000- d_6 are displayed in different colors. Literature data for PB 191000- d_6 (from ref 22) and PB 196000 with $x_{\text{H}} = 15\%$ (from ref 19), both at at $T = 355$ K, are included for comparison.

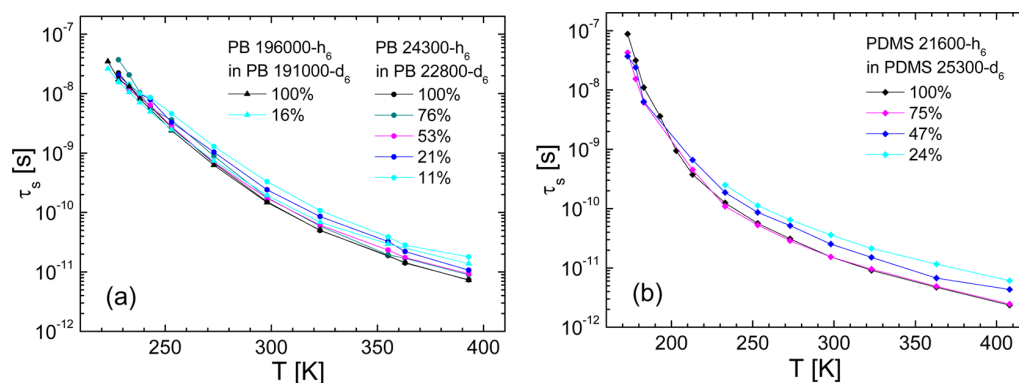


Figure 9. Correlation times $\tau_s(T)$ for the PB blends with $M = 24300$ and 196000 (a) and the PDMS blends with $M = 21600$ (b) of different molar fractions x_H . Lines: guide for the eye.

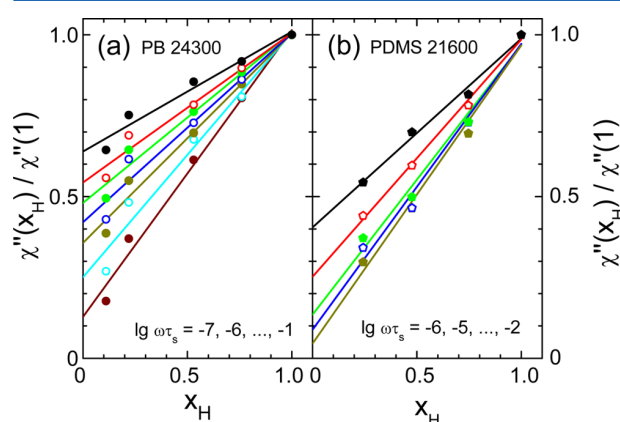


Figure 10. Dependence of the ^1H susceptibility on the molar fraction x_H at some reduced frequencies $\omega\tau_s$ for the PB 24300 blends (a) and the PDMS 21600 blends (b). Lines: linear extrapolation to determine the intramolecular contribution at $x_H = 0$.

reasonable assumption for describing relative displacements of segments from different molecules in first approximation¹⁶ at least for $t > \tau_s$ and has also been used in the analysis of the NS data.⁷ Yet, non-Gaussian statistics may apply for describing the ordinary segmental, i.e., not relative, displacements as assumed by the tube-reptation model.^{1,7,16,21,29,48} Note that the application of Gaussian statistics is only important for a numerical coefficient in eq 4. For any reasonable model of polymer dynamics at $t > \tau_s$, eq 2 holds, because very general arguments without using Gaussian statistics yield $C_{\text{inter}}(t) \propto W(\mathbf{r}=0, t)$,^{16,19} i.e., the probability density of a pair of spins of different molecules to recover in the time t their initial spatial separation. It follows from scaling arguments that this quantity decays $\propto \langle r^2(t) \rangle^{-3/2}$, as $\langle r^2(t) \rangle^{1/2}$ is the only important characteristic length for the relative displacements during the time t .

Concerning the particularities of PDMS they are attributed to a strong intermolecular contribution dominating already at comparatively high frequencies. In our previous publication,³⁶ in which we presented results without the decomposition into intra- and intermolecular contributions, we concluded that this M -independent effect originates from a particularity of the intramolecular relaxation contribution. Given the results from the decomposition into intra- and intermolecular parts we have to revise this interpretation. Although at the moment we do not understand the reason for the extremely strong intermolecular

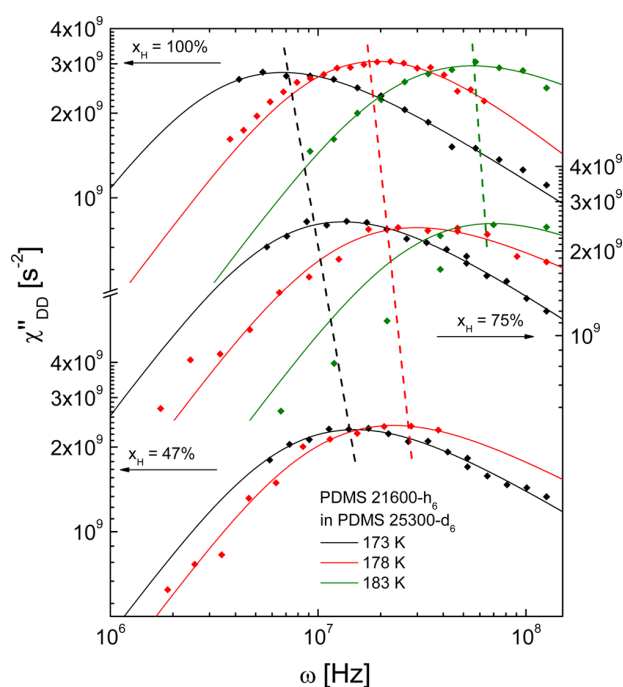


Figure 11. ^1H susceptibility $\chi''_{\text{DD}}(\omega) = \omega/T_1(\omega)$ of the PDMS 21600 blends with molar fractions $x_H = 100\%$ and 47% (left axis) and $x_H = 75\%$ (right axis) for the temperatures indicated. Lines: fits of the α -peak with a Cole–Davidson function. Dashed lines illustrate the shift of the peak position at a constant temperature due to different x_H .

contribution in PDMS, the finding once again emphasizes that the intermolecular relaxation contribution must be taken into account when analyzing FC ^1H NMR results.

Finally, a note regarding the application of the isotope dilution technique is necessary. When testing for given temperatures the linearity of the relaxation rate $R_{1,\text{DD}}(x_H)$ (or equivalently the susceptibility) no satisfactory results are observed (cf. also ref 33), which we attribute to an isotope effect. The segmental time constant τ_s of the protonated polymer is slightly changed by dilution with deuterated polymer (Figure 9 in Appendix B). Although the effect is rather small it renders the construction of susceptibility master curves $\chi''_{\text{DD}}(\omega\tau_s)$ obligatory to allow the extrapolation to $x_H \rightarrow 0$ and to reveal the linearity in x_H (Figure 10 in Appendix B).

6. CONCLUSIONS

By applying the isotope dilution technique we have separated the relaxation contributions from reorientational and translational dynamics in entangled melts of PB (Figure 2 and 3) and PDMS (Figure 7). For PB, we have provided the corresponding time correlation functions (Figure 4). Because of an isotope effect (Figures 9 and 11) the isotope dilution technique can only be applied in combination with employing susceptibility master curves. The shape of the reorientational correlation function as obtained from the isotope dilution series is reproduced by the ^2H relaxation results. Its long-time power-law exponent is higher than that of the dipolar correlation function and that forecast by the tube-reptation model due to the dominating influence of intermolecular relaxation. The time-dependence of the segmental mean square displacement (Figure 5) determined from the intermolecular contribution yields power-laws, which essentially accord with the predictions for regime I and II establishing FC ^1H NMR as a competitive technique to probe also translational dynamics of polymers. From the fact that for PB in regime II the power-law exponents $\varepsilon = 0.49 \pm 0.05$ and $\alpha = 0.19 \pm 0.03$ are found for the reorientational correlation function and the mean square displacement, respectively, it can be concluded that also the relation $C_2(t) \propto \langle R^2(t) \rangle^{-1}$ as assumed for the tube-reptation model does not hold.

APPENDIX

A. ^2H Relaxation at Low Frequencies

As discussed in context of Figure 2b, the ^2H master curve of PB 191000- d_6 exhibits increased scatter at low frequencies and therefore we compare it to literature data. An enlargement of the results of Figure 2b is displayed in Figure 8. By inspecting the susceptibilities (red and blue) which constitute the ^2H master curve of PB 191000- d_6 it can be seen that the data of the two temperatures do not exactly coincide at $\omega\tau_s < 10^{-7}$. Moreover, the ^2H data by Kehr et al.²² (orange) deviate at $\omega\tau_s < 5 \times 10^{-7}$ from both our ^2H data and the intramolecular contribution obtained from ^1H relaxation. At such high M and low frequencies the following situation has to be considered: The ^2H spin–lattice relaxation time is on the order of the switching time of the relaxometer (which is not the case for PB 22800- d_6 , cf. Figure 1) and below $\nu = 1$ kHz the ^2H magnetization curves feature a discernible non-exponential decay. In addition it has been already pointed out by Kehr et al.²² that in this frequency range the correlation times approach the relaxation times, i.e., the Redfield condition might be violated. This contradicts the fundamental assumption of the relaxation theory: one can express the relaxation rates in terms of spectral densities only if the motion leading to the relaxation (or the inverse resonance frequency) is much faster than the relaxation time itself.¹⁸ In the low frequency range, this requirement limits the validity of the relaxation theory and is equivalent to the Redfield condition $\omega_{\text{DD}}\tau_c \ll 1$ where ω_{DD} is the amplitude of the dipole–dipole interaction in angular frequency units and τ_c is the correlation time. Furthermore, at low frequencies the quadrupolar coupling becomes comparable with the Zeeman interaction and that changes the quantization axis of the proton magnetization.⁴⁹ The standard relaxation theory is only valid if the Zeeman interaction dominates (cf. also ref 26). As a consequence the last decade of the ^2H relaxation at low frequencies needs to be treated cautiously. Both the literature and our ^2H results bend away from the

expected power-law behavior, yet for our data this occurs about one decade lower in frequency than for the data by Kehr et al. Therefore, we have confidence in our data at least down to $\omega\tau_s \approx 10^{-7}$. However, future investigations are necessary to elucidate these issues when such low frequencies are approached by state-of-the-art equipment.

B. Isotope Effect

The correlation times $\tau_s(T)$ of the PB and PDMS blends for the different molar fractions x_{H} are shown in Figure 9, parts a and b, respectively, as obtained by the construction of the susceptibility master curves. For a given temperature $\tau_s(T)$ is quite similar, however, a small trend depending on x_{H} can be seen, which is in the case of PB more distinctive for $M = 24300$. At high temperatures $\tau_s(T)$ is increased by a factor of 3 while reducing x_{H} . This isotope effect is observed for both PB and PDMS; i.e., it appears that the dynamics of the polymer melt is somewhat altered by the addition of deuterated polymer. As the molecular masses of the protonated and deuterated samples are similar, i.e., the glass transition temperature $T_g(M)$ has reached its saturation value for high M , and it has been ensured that the solvent is completely removed (cf. Experimental Section and Figure 1a) we can neglect an influence from this side. It is well known that mixtures of protonated and deuterated polymers may phase separate. Although we do not see any indication for such phase separation, e.g., a non-exponential spin–lattice relaxation, still there may be small changes of the intrinsic friction coefficient caused by, e.g., changes of the coil dimensions. It may be this isotope effect which renders the necessary linearity of $R_{\text{I,DD}} = R_{\text{I,DD}}(x_{\text{H}})$ at a given frequency to be not fully satisfactory; however, in the master curves $\chi''_{\text{DD}}(\omega\tau_s)$ the linearity with x_{H} is restored (Figure 10).

The shift of the time constant can be directly recognized in Figure 11 in which the “raw” data of different x_{H} are displayed as susceptibility $\chi''_{\text{DD}}(\omega) = \omega/T_1(\omega)$ for some applied temperatures at which the relaxation maximum is observed. As a guide for the eye the dashed lines mark the frequency shifts of the main relaxation peaks at constant temperatures between different x_{H} , which of course translates into the time constants τ_s describing the peak position.

AUTHOR INFORMATION

Corresponding Author

*E-mail: ernst.roessler@uni-bayreuth.de.

Notes

The authors declare no competing financial interest.

ACKNOWLEDGMENTS

We would like to thank Deutsche Forschungsgemeinschaft (DFG) for funding through grants FU 308/14 and RO 907/16 (SPP 1369) and Russian Foundation for Basic Research (RFBR) for support through Fund 10-03-00739-a. We are very grateful to R. Kimmich, Universität Ulm, for valuable discussions and cooperation, and N. Popp, Inorganic Chemistry III, Universität Bayreuth, for help with sample preparation.

REFERENCES

- (1) Doi, M.; Edwards, S. F. *The Theory of Polymer Dynamics*; Oxford Sci. Publications: Oxford, 1986.
- (2) Rouse, P. E. *J. Chem. Phys.* **1953**, *21*, 1272–1280.
- (3) de Gennes, P. G. *J. Chem. Phys.* **1971**, *55*, 572–579.
- (4) Kremer, K.; Grest, G. S.; Carmesin, I. *Phys. Rev. Lett.* **1988**, *61*, 566–569.
- (5) Paul, W.; Smith, G. D. *Rep. Prog. Phys.* **2004**, *67*, 1117–1185.

- (6) Barrat, J.-L.; Baschnagel, J.; Lyulin, A. *Soft Matter* **2010**, *6*, 3430–3446.
- (7) Wischniewski, A.; Monkenbusch, M.; Willner, L.; Richter, D.; Kali, G. *Phys. Rev. Lett.* **2003**, *90*, 058302.
- (8) Pahl, S.; Fleischer, G.; Fujara, F.; Geil, B. *Macromolecules* **1997**, *30*, 1414–1418.
- (9) Fischer, E.; Kimmich, R.; Fatkullin, N.; Yatsenko, G. *Phys. Rev. E* **2000**, *62*, 775–782.
- (10) Komlosh, M. E.; Callaghan, P. T. *J. Chem. Phys.* **1998**, *109*, 10053–10067.
- (11) Schweizer, K. S. *J. Chem. Phys.* **1989**, *91*, 5802–5821.
- (12) Schweizer, K. S. *J. Chem. Phys.* **1989**, *91*, 5822–5839.
- (13) Schweizer, K. S.; Fuchs, M.; Szamel, G.; Guenza, M.; Tang, H. *Macromol. Theory Simul.* **1997**, *6*, 1037–1117.
- (14) Fatkullin, N. F.; Kimmich, R.; Kroutieva, M. *J. Exp. Theor. Phys.* **2000**, *91*, 150–166.
- (15) Krutyeva, M. A.; Fatkullin, N. F.; Kimmich, R. *Polym. Sci., Ser. A* **2005**, *47*, 1022–1031.
- (16) Fatkullin, N.; Gubaidullin, A.; Stapf, S. *J. Chem. Phys.* **2010**, *132*, 094903.
- (17) Kimmich, R.; Anardo, E. *Prog. Nucl. Magn. Reson. Spectrosc.* **2004**, *44*, 257–320.
- (18) Abragam, A. *The Principles of Nuclear Magnetism*; Clarendon Press: Oxford, U.K., 1961.
- (19) Kehr, M.; Fatkullin, N.; Kimmich, R. *J. Chem. Phys.* **2007**, *126*, 094903.
- (20) Kimmich, R.; Fatkullin, N.; Seitter, R.-O.; Gille, K. *J. Chem. Phys.* **1998**, *108*, 2173–2177.
- (21) Kimmich, R.; Fatkullin, N. *Adv. Polym. Sci.* **2004**, *170*, 1–113.
- (22) Kehr, M.; Fatkullin, N.; Kimmich, R. *J. Chem. Phys.* **2007**, *127*, 084911.
- (23) Kruk, D.; Herrmann, A.; Rössler, E. A. *Prog. Nucl. Magn. Reson. Spectrosc.* **2012**, *63*, 33–64.
- (24) Lips, O.; Privalov, A.; Dvinskikh, S.; Fujara, F. *J. Magn. Reson.* **2001**, *149*, 22–28.
- (25) Kresse, B.; Privalov, A. F.; Fujara, F. *Solid State Nucl. Magn. Reson.* **2011**, *40*, 134–137.
- (26) Herrmann, A.; Kresse, B.; Gmeiner, J.; Privalov, A. F.; Kruk, D.; Fujara, F.; Rössler, E. A. *Macromolecules* **2012**, *45*, 1408–1416.
- (27) Vaca-Chávez, F.; Saalwächter, K. *Phys. Rev. Lett.* **2010**, *104*, 198305.
- (28) Kreer, T.; Baschnagel, J.; Müller, M.; Binder, K. *Macromolecules* **2001**, *34*, 1105–1117.
- (29) Wang, Z.; Likhtman, A. E.; Larson, R. G. *Macromolecules* **2012**, *45*, 3557–3570.
- (30) Bonera, G.; Rigamonti, A. *J. Chem. Phys.* **1965**, *42*, 171–174.
- (31) Zeidler, M. D. *Ber. Bunsen-Ges. Phys. Chem.* **1965**, *69*, 659–668.
- (32) Kintzinger, J. P.; Zeidler, M. D. *Ber. Bunsen-Ges. Phys. Chem.* **1972**, *77*, 98–103.
- (33) Morita, M.; Ando, I.; Nishioka, A.; Sato, K.; Kato, Y.; Suzuki, S. *Polym. Sci., Polym. Lett. Ed.* **1980**, *18*, 109–113.
- (34) Collignon, J.; Sillescu, H. *J. Polym. Sci., Polym. Lett. Ed.* **1980**, *18*, 669–672.
- (35) Lindner, P.; Rössler, E.; Sillescu, H. *Makromol. Chem.* **1981**, *182*, 3652–3669.
- (36) Hofmann, M.; Herrmann, A.; Abou Elfadl, A.; Kruk, D.; Wohlfahrt, M.; Rössler, E. A. *Macromolecules* **2012**, *45*, 2390–2401.
- (37) Meier, R.; Kruk, D.; Gmeiner, J.; Rössler, E. A. *J. Chem. Phys.* **2012**, *136*, 034508.
- (38) Kruk, D.; Meier, R.; Rössler, E. A. *Phys. Rev. E* **2012**, *85*, 020201.
- (39) Hwang, L. P.; Freed, J. H. *J. Chem. Phys.* **1975**, *63*, 4017–4025.
- (40) Bloembergen, N.; Purcell, E. M.; Pound, R. V. *Phys. Rev.* **1948**, *73*, 679–715.
- (41) Graessley, W. W. *Polymeric Liquids & Networks: Dynamics and Rheology*; Taylor & Francis Group: New York, 2008.
- (42) Fetters, L. J.; Lohse, D. J.; Richter, D.; Witten, T. A.; Zirkel, A. *Macromolecules* **1994**, *27*, 4639–4647.
- (43) Herrmann, A.; Kariyo, S.; Abou Elfadl, A.; Meier, R.; Gmeiner, J.; Novikov, V. N.; Rössler, E. A. *Macromolecules* **2009**, *42*, 5236–5243.
- (44) Saalwächter, K. *Private communication*.
- (45) Meyer, H. *Private communication*.
- (46) Richter, D.; Butera, R.; Fetters, L. J.; Huang, J. S.; Farago, B.; Ewen, B. *Macromolecules* **1992**, *25*, 6156–6164.
- (47) Stephanou, P. S.; Baig, C.; Mavrantzas, G. *Soft Matter* **2011**, *7*, 380–395.
- (48) Fatkullin, N.; Kimmich, R. *Phys. Rev. E* **1995**, *52*, 3273–3276.
- (49) Kruk, D.; Kowalewski, J. *Mol. Phys.* **2003**, *101*, 2861–2874.

Publication 5

Dynamics of Linear Polybutadienes in Solution Studied by Field Cycling ^1H NMR.

Herrmann, A.; Rössler, E. A.
ACS Macro Letters **2012**, *1*, 1339–1342.

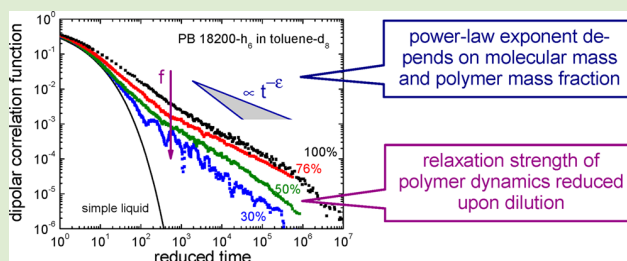
Copyright 2012 by The American Chemical Society
DOI: 10.1021/mz3004924

Dynamics of Linear Polybutadienes in Solution Studied by Field Cycling ^1H NMR

Axel Herrmann and Ernst A. Rössler*

Experimentalphysik II, Universität Bayreuth, 95440 Bayreuth, Germany

ABSTRACT: Field cycling ^1H NMR relaxometry is utilized to investigate dynamics in solutions of monodisperse polybutadienes of different molecular mass (M) and deuterated toluene. Broad temperature and polymer mass fraction ranges ($c = 5\text{--}100\%$) are studied. By applying frequency–temperature superposition, susceptibility master curves $\chi''_{\text{DD}}(\omega\tau_s)$ are constructed. They cover the segmental relaxation and polymer chain dynamics, and provide the concentration dependence of the segmental time constant $\tau_s(T)$. The relaxation strength of polymer dynamics is reduced similarly for all M with decreasing c ; for the lowest c , almost no polymer dynamics shows up, that is, the dipolar correlation function obtained via Fourier transform decays almost completely due to segmental dynamics. The dipolar correlation function is decomposed into contributions of segmental and polymer dynamics. Its long-time power-law exponent associated with entanglement dynamics is increased from its bulk value with reduced c . This is interpreted as a continuous increase of the effective entanglement molecular mass.



The dynamics of polymer melts is most often described by the tube-reptation model,¹ which yields predictions for the subdiffusive behavior of a chain segment. For polymers in concentrated and semidilute solution, modifications with respect to the bulk behavior have been reported, for example, by rheology^{2–4} or analyses of the dielectric normal mode spectrum.⁵ Expected are, for example, a concentration dependence of the monomeric friction coefficient ζ_0 and of friction-insensitive properties, for example, the plateau modulus G_N^0 , a shift of the terminal relaxation time τ_d toward shorter times and an increase in the entanglement spacing M_e . Pioneering works of field cycling (FC) NMR relaxometry by Kimmich and co-workers have qualitatively disclosed a transition from entanglement dynamics for a high M melt to Rouse-like behavior for high dilution.^{6,7}

FC NMR relaxometry has been established as a powerful technique to probe the microscopic dynamics of polymers.^{7,8} By electronically controlling the magnetic relaxation field B , the dispersion of the spin–lattice relaxation time T_1 is measured over 3–5 decades in frequency, which is given by the Larmor frequency $\omega = \gamma B$ (γ : gyromagnetic ratio). A very helpful concept in analyzing the NMR relaxation dispersion is the construction of master curves in the susceptibility representation:⁸ first, the measured relaxation rate $R_1(\omega) = 1/T_1(\omega)$ is transformed to the susceptibility representation $\chi''_{\text{DD}}(\omega) = \omega/T_1(\omega)$, which at low temperatures allows to extract the time constant τ_s of segmental motion. Second, by applying frequency–temperature superposition (FTS), the susceptibility is shifted solely in frequency to finally provide a master curve as a function of the reduced frequency $\omega\tau_s$. Thereby, the frequency window of the technique is significantly extended. FTS is well-known from, for example, rheology and reflects a

fundamental feature of cooperative dynamics in condensed matter.⁸ The master curves $\chi''_{\text{DD}}(\omega\tau_s)$ (“NMR susceptibility” in the following) exhibit a peak at $\omega\tau_s \approx 1$, which is identified with the segmental or local dynamics governed by the α -process of the glass transition. For polymers at $\omega\tau_s < 1$, an excess intensity with respect to the spectrum of a simple liquid is observed, which is due to the slower, M -dependent polymer dynamics. Its integral is a measure for the polymer relaxation strength f , that is, the residual correlation that relaxes at $t > \tau_s$ due to Rouse and entanglement dynamics.⁸ It is dominated by the Rouse contribution and is an analog to G_N^0 obtained by rheology; the latter, however, is determined solely by the terminal relaxation caused by entanglement dynamics.

Our previous studies^{8–11} have focused on understanding the NMR relaxation of simple liquids, nonentangled and entangled polymer melts, that is, the emergence of polymer dynamics with M . The dipolar correlation functions $C_{\text{DD}}(t/\tau_s)$ have been extracted by Fourier transform of the NMR susceptibility, cover 10 decades in time, and exhibit different power-law regimes, which have been compared to the predictions of the tube-reptation model.

The aim of this Letter is to investigate how the addition of a low- M diluent to a linear polymer melt (polybutadiene with $M > M_e$) is probed by ^1H FC NMR. As a reference for the behavior of bulk melts the previous results¹⁰ are used. A comprehensive picture is rendered by employing the above approach for the first time to polymers in solution, because the susceptibility master curves $\chi''_{\text{DD}}(\omega\tau_s)$ reflect the spectral

Received: October 9, 2012

Accepted: October 26, 2012

changes upon dilution in a similar way as those of rheology. A large temperature range is studied and FTS is applied in order to include both the (fast) segmental and the (slow) chain dynamics in the master curves.

The monodisperse 1,4-polybutadienes (PB, PDI \leq 1.04) were purchased from PSS, Mainz, Germany, and $M = M_w$ in g/mol denotes their mass average molecular mass. Solutions of PB- h_6 and deuterated toluene (Sigma-Aldrich, degree of deuteration above 99.96%, used without further purification) were prepared by degassing both components, dissolving different mass ratios, and flame sealing the glass tube with the frozen compound under vacuum. The given concentration c is the mass fraction of the polymer, which is very similar to the volume fraction, because the mass densities are rather equal. The volume fraction associated with the critical concentration at the overlap limit can be estimated by $c^* < N_m^{-4/5}$, where N_m is the number of monomers per chain.¹³ For the PB samples, this yields values $c^* < 0.02$ (for $M = 9470$), thus, the regimes of concentrated and semidilute solutions are covered. The samples were measured with a commercial Stellar FC spectrometer in the frequency range $\nu = \omega/(2\pi) = 10$ kHz to 20 MHz and T_1 was determined by an exponential fit of the magnetization curve. Note that by applying ^1H FC NMR only the dynamics of the protonated PB is probed.

In Figure 1a–c, the master curves $\chi''_{\text{DD}}(\omega\tau_s)$ in the susceptibility representation are compiled by applying FTS for PB with $M = 9470$, 18200, and 47000, respectively, and different polymer mass fractions c . A temperature range of $T = 168$ –393 K has been covered depending on c in order to create the master curves. The relaxation regimes of glassy (0), free Rouse (I), and constrained Rouse (II) dynamics are indicated as obtained for the undiluted melts (black curves).¹⁰ Regime 0, in fact, contains an interplay of segmental (glassy) and Rouse dynamics. Note that the master curves are an isofrictional representation, as changes in the time scale due to a concentration-dependent friction coefficient are scaled out by plotting the data as a function of the reduced frequency $\omega\tau_s$. This allows of monitoring the concentration dependence of the spectral shape of $\chi''_{\text{DD}}(\omega\tau_s)$: The segmental dynamics is represented by the α -peak at $\omega\tau_s \approx 1$. At $\omega\tau_s < 1$ the excess intensity reflecting the polymer relaxation contribution with respect to the simple liquid (PB 466) is diminished for all M with decreasing concentration c . For the lowest concentration of PB 9470, the susceptibility almost approaches that of the simple liquid, that is, the polymer character as probed by ^1H relaxation gets lost as the dipolar correlations are relaxed almost completely by the segmental dynamics.

Upon addition of a deuterated diluent it is expected on the one hand that the polymer dynamics is modified; on the other hand for ^1H NMR the dipolar coupling of the protons which comprises intramolecular and intermolecular contributions is reduced due to the latter. Isotope dilution experiments by ^1H FC NMR, that is, blending protonated and deuterated polymers with similar M , allow attaining both relaxation contributions. Thereby, it has been demonstrated^{11,12} that, while the intermolecular part dominates at low reduced frequencies ($\omega\tau_s \ll 1$), also in the frequency range of the α -peak ($\omega\tau_s \approx 1$) the amplitude is reduced. However, this is surprisingly not observed in the present case (cf. Figure 1).

The segmental time constants $\tau_s(T)$ are displayed in Figure 2 for the dilution series of PB 9470 with different c as yielded from the construction of the susceptibility master curves. The curves can be interpolated with a Vogel–Fulcher–Tammann

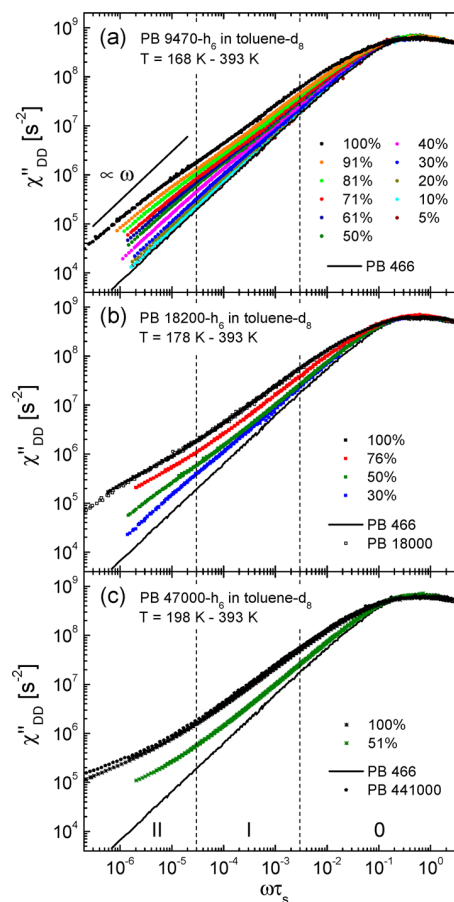


Figure 1. Susceptibility master curves $\chi''_{\text{DD}}(\omega\tau_s)$ of PB- h_6 with $M = 9470$ (a), 18200 (b), and 47000 (c) diluted in toluene- d_8 for the polymer mass fractions and in the temperature range as indicated. PB 466 and PB 441000: reference for the simple liquid and undiluted high- M limit, respectively.¹⁰ Dashed lines: regimes of glassy (0), free Rouse (I), and constrained Rouse (II) dynamics. The undiluted PB samples have been measured also toward lower frequencies,¹⁰ where the susceptibility of PB 18000 perfectly extends that of PB 18200.

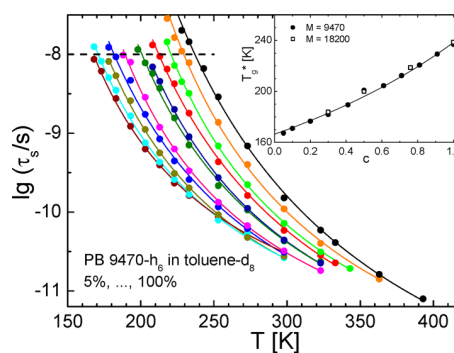


Figure 2. Time constants $\tau_s(T)$ of segmental motion for PB 9470 with different concentrations. Lines: VFT interpolations. Inset: glass transition temperature T_g^* as a function of concentration; line: fit with Fox eq ($1/T_g^* = c/T_{g,\text{polymer}} + (1-c)/T_{g,\text{solvent}}$).

(VFT) function⁸ and are shifted toward lower temperatures with decreasing c . This indicates the well-known plasticizer effect, that is, the segmental dynamics of the polymer gets faster by addition of the solvent. The glass transition temperature is usually defined as $T_g = T(\tau_s = 100 \text{ s})$. Because FC NMR detects

dynamics on much faster time scales, we define $T_g^* = T(\lg(\tau_s/s = -8))$. The corresponding dependence $T_g^*(c)$ is shown in the inset of Figure 2 for PB with $M = 9470$ and 18200 . A continuous decrease of about 70 K with reduced c is observed that follows the Fox equation.²

In Figure 3a the relaxation strength f of polymer dynamics is plotted as a function of c . It is given by the difference between

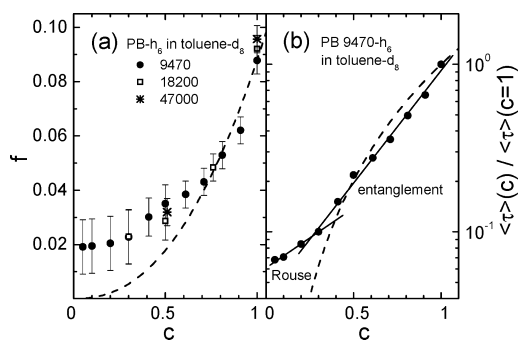


Figure 3. (a) Relaxation strength f of polymer dynamics as a function of polymer mass fraction c for PB with different M . Dashed line: expectation for $G_N^0(c)$. (b) Ratio $\langle \tau \rangle(c) / \langle \tau \rangle(c = 1)$ of PB 9470 obtained from the susceptibility at lowest frequencies. Dashed line: expectation for $\tau_d(c)$ from rheology.

the integrated susceptibilities of the polymer and the simple liquid (e.g., PB 466). With decreasing concentration, f is reduced similarly for all M . This demonstrates that for lower c less correlation survives beyond glassy dynamics, that is, on time scales $t > \tau_s$. Obviously due to the enhanced segmental mobility at lower c , the α -process is more efficient at the expense of the relaxation contribution of polymer dynamics. As noted, in FC NMR f is dominated by Rouse dynamics (regime I, cf. Figure 1). The plateau modulus G_N^0 of rheology is expected^{3,4} to be decreased upon dilution along $G_N^0(c) = G_N^0(c = 1)c^{2.3}$, which is included in Figure 3a (dashed line). A similar trend is observed at high c for f and G_N^0 . However, the latter is determined solely by the integral of the terminal relaxation spectrum associated with entanglement dynamics.

For PB 9470 the NMR susceptibility $\chi''_{DD}(\omega\tau_s)$ exhibits a behavior close to $\propto \omega$ at lowest reduced frequencies (Figure 1a), that is, the slowest or terminal relaxation process is detected. This is equivalent to an essentially constant dipolar spectral density $J_{DD}(\omega)$, as $\chi''_{DD}(\omega) = \omega J_{DD}(\omega)$ holds.⁸ Therefore, at lowest frequencies, the mean correlation time $\langle \tau \rangle$ of polymer dynamics is provided, that is, $\langle \tau \rangle = J_{DD}(0) \propto \chi''_{DD}(\omega\tau_s = 2 \times 10^{-6})$. The mean correlation time comprises a weighted sum of the individual correlation times of the different Rouse and entanglement modes and, for $M > M_e$, its slowest contribution is given by the terminal relaxation time τ_d . In Figure 3b the ratio $\langle \tau \rangle(c) / \langle \tau \rangle(c = 1)$ is depicted. It decreases with lower c , as expected⁴ by rheology for the terminal relaxation time $\tau_d(c) \propto c^{2.3}$ (dashed line). A crossover (solid lines) to a weaker c -dependence can be anticipated below $c = 40\%$, which we interpret as a transition from Rouse and entanglement dynamics to solely Rouse-like relaxation (see also below).

The dipolar correlation function $C_{DD}(t/\tau_s)$ obtained by Fourier transform of the susceptibility master curves (Figure 1) is presented in Figure 4a for PB 18200 with different c . As a reference for the bulk melt behavior, which is discussed first, $C_{DD}(t/\tau_s)$ of undiluted PB with different M (black symbols)

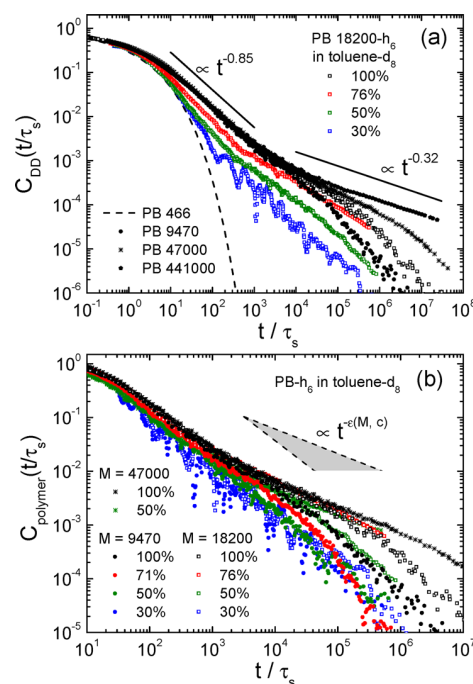


Figure 4. (a) Dipolar correlation functions $C_{DD}(t/\tau_s)$ of PB 18200 with different c and undiluted PB with different M , as indicated. Lines: power laws observed for the free Rouse (I) and constrained Rouse (II) regime of the tube-reptation model for high $M = 441000$.¹⁰ (b) Correlation function $C_{polymer}(t/\tau_s)$ of the polymer relaxation contribution of PB with $M = 9470, 18200$, and 47000 at some c . $\epsilon(M,c)$ denotes the power-law exponent of regime II.

including PB 466¹⁰ as the low- M system and PB 441000¹⁰ for $M \gg M_e = 2000$ is presented. Analogously to the susceptibility representation, $C_{DD}(t/\tau_s)$ reflects segmental, free Rouse, and entanglement dynamics.¹⁰ The latter two can be described by power-laws $\propto t^{-\epsilon}$, which exhibit the exponents $\epsilon = 0.85$ and $\epsilon = 0.32$ ($M \gg M_e$) for the regimes I and II, respectively. In regime II, ϵ depends on M , and only for very high M the prediction $\epsilon = 0.25$ of the tube-reptation model is almost approached, which indicates a highly protracted transition to reptation dynamics.¹⁰ For the decay of $C_{DD}(t/\tau_s)$ of PB 18200 with different c , a similar effect is observed: the exponents ϵ depend on c . Its origin cannot be unambiguously clarified due to the interplay of segmental and polymer relaxation contributions which is difficult to interpret.

To eliminate the influence of the segmental dynamics, Figure 4b shows the correlation functions $C_{polymer}(t/\tau_s)$, which contain only the polymer relaxation contribution of PB with different M and comparable c . Statistical independence between segmental and polymer dynamics, that is, a multiplicative approach $C_{DD}(t) = C_{segmental}(t) \cdot C_{polymer}(t)$, is assumed and the polymer relaxation strength f (cf. Figure 3a) is introduced. Finally, $C_{polymer}(t/\tau_s)$ is obtained by dividing each $C_{DD}(t/\tau_s)$ by the contribution $C_{segmental}(t/\tau_s)$ of the segmental dynamics, as given by PB 466, explicitly: $C_{polymer}(t/\tau_s) = C_{DD}(t/\tau_s) / [(1-f)\phi_{segmental}(t/\tau_s) + f]$, where $\phi_{segmental}(t/\tau_s)$ denotes the normalized segmental correlation function. While ϵ remains essentially unchanged in the Rouse regime (I), effects on dilution are observed for the entanglement dynamics at long times; in regime II, ϵ is increasing with lower c for $M = 9470$ and 18200 . The values $\epsilon(c)$ obtained by a power-law fit are displayed in Figure 5 together with $\epsilon(c = 1)$ of the undiluted PB melts with different

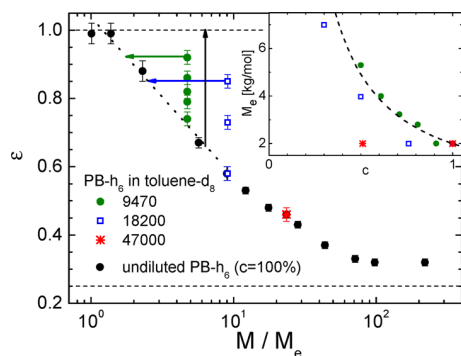


Figure 5. Exponent ε as a function of reduced molecular mass M/M_e (black symbols) and polymer mass fraction c (colored symbols). The black arrow indicates lower c . Dashed lines: predictions for the free Rouse and constrained Rouse regime of the tube-reptation model. Data of undiluted PB from ref 10. Inset: Dependence of the entanglement molecular mass M_e on c . Dashed line: $M_e(c) = M_e(c = 1) c^{-1.3}$.

M .¹⁰ While decreasing c , the exponent is increased with respect to its bulk value (black symbols). We interpret this as an effect due to a changed entanglement molecular mass M_e upon dilution. As a result, the exponent is increased toward $\varepsilon = 1$ of the free Rouse regime. The entanglement molecular mass M_e as a function of c is estimated by mapping (cf. green and blue arrows in Figure 5) $\varepsilon(M, c)$ on the curve $\varepsilon(M, c = 1)$. This reveals that M_e is continuously enlarged upon dilution (inset of Figure 5) as expected^{3,4} from rheology by $M_e(c) = M_e(c = 1) c^{-1.3}$ (dashed line). It appears that for higher M much lower concentrations c are needed to cause an increase of ε (or M_e), because ε remains unchanged with respect to the bulk in the case of PB 47000 with $c = 50\%$.

In conclusion, the feature of entanglement dynamics, that is, the “shoulder” at long times in $C_{\text{polymer}}(t/\tau_s)$ (Figure 4b) continuously disappears and a transition from entanglement to Rouse behavior is observed for decreasing c , similar to that for decreasing M in neat PB (Figure 4a).¹⁰ This conclusion is also supported by prior reports⁷ of FC NMR relaxometry by Kimmich and co-workers. At longest times, the faster decay upon dilution may reflect the shortening of the terminal relaxation time τ_d , as displayed in Figure 3b. We note that, at longest times, effects of a reduced intermolecular relaxation for lower c may contribute.¹¹

In summary, we have demonstrated that FC NMR relaxometry is well suited to investigate and quantitatively characterize the dynamics of polymers also in solution. The NMR susceptibility representation, the application of FTS, and the transformation to the dipolar correlation function allows of analyses of relaxation features, depending on temperature, molecular mass, and polymer mass fraction. Explicitly, we observe the disappearance of the entanglement dynamics upon dilution as it is indicated by the increase of the power-law exponent of the constrained Rouse regime of the tube-reptation model. The well established results of rheology are reflected by the master curves of NMR relaxation; this representation goes significantly beyond literature reports⁷ and may render FC NMR as “molecular rheology”.

AUTHOR INFORMATION

Corresponding Author

*E-mail: ernst.roessler@uni-bayreuth.de.

Notes

The authors declare no competing financial interest.

ACKNOWLEDGMENTS

The financial support of Deutsche Forschungsgemeinschaft (DFG) through priority program SPP 1369 “Polymer-Solid Contacts: Interfaces and Interphases” (RO 907/16) and Grant FU 308/14 are acknowledged.

REFERENCES

- (1) Doi, M.; Edwards, S. F. *The Theory of Polymer Dynamics*; Oxford Sci. Publications: Oxford, 1986.
- (2) Ferry, J. D. *Viscoelastic Properties of Polymers*; Wiley: New York, 1980.
- (3) Graessley, W. W. *Polymeric Liquids & Networks: Dynamics and Rheology*; Taylor and Francis: New York, 2008.
- (4) Rubinstein, M.; Colby, R. H.; *Polymer Physics*; Oxford University Press: New York, 2008.
- (5) Watanabe, H. *Macromol. Rapid Commun.* **2001**, *22*, 127–175.
- (6) Kimmich, R.; Schnur, G.; Köpf, M. *Adv. Polym. Sci.* **1988**, *20*, 385–421.
- (7) Kimmich, R.; Fatkullin, N. *Adv. Polym. Sci.* **2004**, *170*, 1–113.
- (8) Kruk, D.; Herrmann, A.; Rössler, E. A. *Prog. Nucl. Magn. Reson. Spectrosc.* **2012**, *63*, 33–64.
- (9) Meier, R.; Kruk, D.; Gmeiner, J.; Rössler, E. A. *J. Chem. Phys.* **2012**, *136*, 034508.
- (10) Herrmann, A.; Kresse, B.; Gmeiner, J.; Privalov, A. F.; Kruk, D.; Fujara, F.; Rössler, E. A. *Macromolecules* **2012**, *45*, 1408–1416.
- (11) Herrmann, A.; Kresse, B.; Wohlfahrt, M.; Bauer, I.; Privalov, A. F.; Kruk, D.; Fatkullin, N.; Fujara, F.; Rössler, E. A. *Macromolecules* **2012**, *45*, 6516–6526.
- (12) Kehr, M.; Fatkullin, N.; Kimmich, R. *J. Chem. Phys.* **2007**, *127*, 084911.
- (13) Strobl, R. *The Physics of Polymers*; Springer: Berlin, 1996.

Bibliography

- [1] Götze, W. *Journal of Physics Condensed Matter* **1999**, *11*, A1–A45.
- [2] Götze, W. *Complex Dynamics in Glass-Forming Liquids*; Oxford University Press: Oxford, 2009.
- [3] Richter, D.; Monkenbusch, M.; Arbe, A.; Colmenero, J. *Advances in Polymer Science* **2005**, *174*, 1–221.
- [4] Bartsch, E.; Fujara, F.; Geil, B.; Kiebel, M.; Petry, W.; Schnauss, W.; Sillescu, H.; Wuttke, J. *Physica A* **1993**, *201*, 223–236.
- [5] Petry, W.; Wuttke, J. *Transport Theory and Statistical Physics* **1995**, *24*, 1075–195.
- [6] Tölle, A. *Reports on Progress in Physics* **2001**, *64*, 1473–1532.
- [7] Berne, B. J.; Pecora, R. *Dynamic Light Scattering*; Wiley: New York, 1976.
- [8] Li, G.; Du, W. M.; Chen, X. K.; Cummins, H. Z.; Tao, N. J. *Physical Review A* **1992**, *45*, 3867–3879.
- [9] Cummins, H.; Li, G.; Hwang, Y.; Shen, G.; Du, W.; Hernandez, J.; Tao, N. *Zeitschrift für Physik B* **1997**, *103*, 501–519.
- [10] Adichtchev, S.; Benkhof, S.; Blochowicz, T.; Novikov, V. N.; Rössler, E.; Tschirwitz, C.; ; Wiedersich, J. *Physical Review Letters* **2002**, *88*, 055703.
- [11] Blochowicz, T.; Brodin, A.; Rössler, E. A. *Advances in Chemical Physics, Part A* **2006**, *133*, 127–256.
- [12] Brodin, A.; Rössler, E. A. *Journal of Chemical Physics* **2007**, *126*, 244508.
- [13] Petzold, N.; Rössler, E. A. *Journal of Chemical Physics* **2010**, *133*, 124512.
- [14] Torre, R.; Bartolini, P.; Pick, R. M. *Physical Review E* **1998**, *57*, 1912–1920.
- [15] Hinze, G.; Brace, D. D.; Gottke, S. D.; Fayer, M. D. *Journal of Chemical Physics* **2000**, *113*, 3723–3733.
- [16] Cang, H.; Novikov, V. N.; Fayer, M. D. *Journal of Chemical Physics* **2003**, *118*, 2800–2807.

- [17] Fytas, G.; Dorfmueller, T.; Wang, C. H. *Journal of Physical Chemistry* **1983**, *87*, 5041–5045.
- [18] Meier, G.; Gerharz, B.; Boese, D.; Fischer, E. W. *Journal of Chemical Physics* **1991**, *94*, 3050–3059.
- [19] Patkowski, A.; Steffen, W.; Nilgens, H.; Fischer, E. W.; Pecora, R. *Journal of Chemical Physics* **1997**, *106*, 8401–8408.
- [20] Brodin, A.; Bergman, R.; Mattsson, J.; Rössler, E. A. *European Physical Journal B* **2003**, *36*, 349–357.
- [21] Schmidt-Rohr, K.; Spiess, H. W. *Multidimensional Solid State NMR and Polymers*; Academic Press: London, 1994.
- [22] Böhmer, R.; Hinze, G.; Diezemann, G.; Geil, B.; Sillescu, H. *Physical Review E* **1996**, *36*, 55–60.
- [23] Geil, B.; Fujara, F.; Sillescu, H. *Journal of Magnetic Resonance* **1998**, *130*, 18–26.
- [24] Hinze, G. *Physical Review E* **1998**, *57*, 2010–2018.
- [25] Böhmer, R.; Diezemann, G.; Hinze, G.; Rössler, E. *Progress in Nuclear Magnetic Resonance Spectroscopy* **2001**, *39*, 191–267.
- [26] Böhmer, R.; Diezemann, G. In *Broadband Dielectric Spectroscopy*; Kremer, F., Schönhals, A., Eds.; Springer: Berlin, 2003; p 265.
- [27] Vogel, M.; Medick, P.; Rössler, E. A. *Annual Reports on NMR Spectroscopy* **2005**, *56*, 231–299.
- [28] Böttcher, C. J. F.; Bordewijk, P. *Theory of Electric Polarization, Vol. 2*; Elsevier: Amsterdam, 1973.
- [29] Williams, G. *Journal of Non-Crystalline Solids* **1991**, *131-133 Part 1*, 1–12.
- [30] Kremer, F.; Schönhals, A. *Broadband Dielectric Spectroscopy*; Springer: Berlin, 2003.
- [31] Dixon, P. K.; Wu, L.; Nagel, S. R.; Williams, B. D.; Carini, J. P. *Physical Review Letters* **1990**, *65*, 1108–1111.
- [32] Kudlik, A.; Benkhof, S.; Blochowicz, T.; Tschirwitz, C.; Rössler, E. *Journal of Molecular Structure* **1999**, *479*, 201–218.
- [33] Lunkenheimer, P.; Schneider, U.; Brand, R.; Loidl, A. *Contemporary Physics* **2000**, *41*, 15–36.

- [34] Blochowicz, T.; Tschirwitz, C.; Benkhof, S.; Rössler, E. A. *Journal of Chemical Physics* **2003**, *118*, 7544–7555.
- [35] Blochowicz, T.; Gainaru, C.; Medick, P.; Tschirwitz, C.; Rössler, E. A. *Journal of Chemical Physics* **2006**, *124*, 134503.
- [36] Kimmich, R.; Anardo, E. *Progress in Nuclear Magnetic Resonance Spectroscopy* **2004**, *44*, 257–320.
- [37] Ferrante, G.; Sykora, S. *Advances in Inorganic Chemistry* **2005**, *57*, 405–470.
- [38] Kruk, D.; Herrmann, A.; Rössler, E. A. *Progress in Nuclear Magnetic Resonance Spectroscopy* **2012**, *63*, 33–64.
- [39] Kob, W. In *Slow Relaxations and Nonequilibrium Dynamics in Condensed Matter, Vol. 77, Les Houches*; Barrat, J.-L., Feigelman, M. V., Kurchan, J., Eds.; Springer: Berlin, 2003; p 199.
- [40] Binder, K.; Baschnagel, J.; Paul, W. *Progress in Polymer Science* **2003**, *28*, 115–172.
- [41] Barrat, J.-L.; Baschnagel, J.; Lyulin, A. *Soft Matter* **2010**, *6*, 3430–3446.
- [42] Balucani, U.; Zoppi, M. *Dynamics of the Liquid State*, 3rd ed.; Clarendon Press: Oxford, 1994.
- [43] Hansen, J. P.; McDonald, I. R. *Theory of Simple Liquids*; Academic Press: London, 2006.
- [44] Bée, M. *Quasielastic Neutron Scattering*; Adam Hilger: Bristol, 1988.
- [45] Lovesey, S. W. *Theory of Neutron Scattering in Condensed Matter*; Oxford University Press: New York, 1994.
- [46] Abragam, D. *Principles of Nuclear Magnetism*; Oxford University Press: Oxford, 1983.
- [47] Kimmich, R.; Fatkullin, N. *Advances in Polymer Science* **2004**, *170*, 1–113.
- [48] Noack, F. *Progress in Nuclear Magnetic Resonance Spectroscopy* **1986**, *18*, 171–276.
- [49] Blochowicz, T.; Kudlik, A.; Benkhof, S.; Senker, J.; Rössler, E.; Hinze, G. *Journal of Chemical Physics* **1999**, *110*, 12011–12022.
- [50] Madden, P.; Kivelson, D. *Advances in Chemical Physics* **1984**, *56*, 467–566.
- [51] Madden, P. A. In *Proc. Les Houches Summer School*; Hansen, J. P., Levesque, D., Zinn-Justin, J., Eds.; Elsevier: New York, 1991; p 547.

- [52] Khintchine, A. *Mathematische Annalen* **1934**, *109*, 604–615.
- [53] Strobl, G. R. *The physics of polymers*; 2. corr. ed.; Springer-Verlag: Berlin, 1997.
- [54] Kohlrausch, R. *Annalen der Physik (Leipzig)* **1847**, *12*, 393.
- [55] Aichele, M.; Baschnagel, J. *European Physics Journal E* **2001**, *5*, 245–256.
- [56] Kariyo, S.; Brodin, A.; Gainaru, C.; Herrmann, A.; Schick, H.; Novikov, V. N.; Rössler, E. A. *Macromolecules* **2008**, *41*, 5313–5321.
- [57] Richert, R. *Journal of Chemical Physics* **2005**, *123*, 154502.
- [58] Vogel, H. *Physikalische Zeitschrift* **1921**, *22*, 645–646.
- [59] Fulcher, G. S. *Journal of the American Ceramic Society* **1925**, *6*, 339–355.
- [60] Tammann, G.; Hesse, W. Z. *Zeitschrift für anorganische und allgemeine Chemie* **1926**, *156*, 245–257.
- [61] Baschnagel, J.; Bennemann, C.; Paul, W.; Binder, K. *Journal of Physics: Condensed Matter* **2000**, *12*, 6365–6374.
- [62] Kob, W.; Andersen, H. C. *Physical Review E* **1995**, *51*, 4626–4641.
- [63] Abou Elfadl, A.; Kahlau, R.; Herrmann, A.; Novikov, V. N.; Rössler, E. A. *Macromolecules* **2010**, *43*, 3340–3351.
- [64] Palade, L.-I.; Yerney, V.; Attan, P. *Rheologica Acta* **1996**, *35*, 265–273.
- [65] Stockmayer, W. H. *Pure and Applied Chemistry* **1967**, *15*, 539–554.
- [66] Watanabe, H. *Macromolecular Rapid Communications* **2001**, *22*, 127–175.
- [67] Imanishi, Y.; Adachi, K.; Kotaka, T. *Journal of Chemical Physics* **1988**, *89*, 7585–7592.
- [68] Meier, R.; Kahlau, R.; Kruk, D.; Rössler, E. A. *Journal of Physical Chemistry A* **2010**, *114*, 7847–7855.
- [69] Hofmann, M.; Herrmann, A.; Ok, S.; Franz, C.; Kruk, D.; Saalwächter, K.; Steinhart, M.; Rössler, E. A. *Macromolecules* **2011**, *44*, 4017–4021.
- [70] Doi, M.; Edwards, S. F. *The theory of polymer dynamics*; Clarendon Press: Oxford, 1986.
- [71] Rouse, P. E. *Journal of Chemical Physics* **1953**, *21*, 1272–1280.
- [72] de Gennes, P. G. *Journal of Chemical Physics* **1971**, *55*, 572–579.

- [73] Edwards, S. F. *Proceedings of the Physical Society* **1967**, *92*, 9–16.
- [74] Treloar, L. R. G. *The Physics of Rubber Elasticity*, 3rd ed.; Clarendon Press: Oxford, 1975.
- [75] Bueche, F. *Journal of Chemical Physics* **1953**, *22*, 603–609.
- [76] Verdier, P. H. *Journal of Chemical Physics* **1966**, *45*, 2118–2121.
- [77] Kariyo, S.; Brodin, A.; Gainaru, C.; Herrmann, A.; Hintermeyer, J.; Schick, H.; Novikov, V. N.; Rössler, E. A. *Macromolecules* **2008**, *41*, 5322–5332.
- [78] Watanabe, H. *Progress in Polymer Science* **1999**, *24*, 1253–1403.
- [79] Graessley, W. W. *Journal of Polymer Science: Polymer Physics Edition* **1980**, *18*, 27–34.
- [80] Ferry, J. D. *Viscoelastic Properties of Polymers*, 3rd edition; Wiley: New York, 1980.
- [81] Boese, D.; Kremer, F. *Macromolecules* **1990**, *23*, 829–835.
- [82] Kremer, K.; Grest, G. S. *Journal of Chemical Physics* **1990**, *92*, 5057–5086.
- [83] Ball, R. C.; Callaghan, P. T.; Samulski, E. T. *Journal of Chemical Physics* **1997**, *106*, 7352–7361.
- [84] Lodge, T. P.; Rotstein, N. A.; Prager, S. *Advances in Chemical Physics* **1990**, *79*, 1–132.
- [85] Likhtman, A. Viscoelasticity and molecular rheology. <http://www.personal.reading.ac.uk/~sms06al2/book/molrel.pdf>, 2011; Preprint for 2nd ed. of "Comprehensive Polymer Science".
- [86] Rubinstein, M.; Colby, R. H. *Journal of Chemical Physics* **1988**, *89*, 5291–5306.
- [87] Likhtman, A. E.; McLeish, T. C. B. *Macromolecules* **2002**, *35*, 6332–6343.
- [88] Doi, M. *Journal of Polymer Science: Polymer Letters Edition* **1981**, *19*, 265–273.
- [89] Milner, S. T.; McLeish, T. C. B. *Physical Review Letters* **1998**, *81*, 725–728.
- [90] Read, D. J.; Jagannathan, K.; Likhtman, A. E. *Macromolecules* **2008**, *41*, 6843–6853.
- [91] Sukumaran, S. K.; Likhtman, A. E. *Macromolecules* **2009**, *42*, 4300–4309.

- [92] Abdel-Goad, M.; Pyckhout-Hintzen, W.; Kahle, S.; Allgaier, J.; Richter, D.; Fetters, L. J. *Macromolecules* **2004**, *37*, 8135–8144.
- [93] Schweizer, K. S. *Journal of Chemical Physics* **1989**, *91*, 5802–5821.
- [94] Schweizer, K. S. *Journal of Chemical Physics* **1989**, *91*, 5822–5839.
- [95] Schweizer, K. S. *Macromolecular Theory and Simulations* **1997**, *6*, 1037–1117.
- [96] Fatkullin, N.; Gubaidullin, A.; Stapf, S. *Journal of Chemical Physics* **2010**, *132*, 094903.
- [97] Fatkullin, N. F.; Kimmich, R.; Kroutieva, M. *Journal of Experimental and Theoretical Physics* **2000**, *91*, 150–166.
- [98] Wischnewski, A.; Monkenbusch, M.; Willner, L.; Richter, D.; Kali, G. *Physical Review Letters* **2003**, *90*, 058302.
- [99] Kimmich, R. *NMR: Tomography, Diffusometry, Relaxometry*; Springer-Verlag: Berlin, 1997.
- [100] Cohen-Addad, C. P. *Progress in Nuclear Magnetic Resonance Spectroscopy* **1993**, *25*, 1–316.
- [101] Klein, P. G.; Ries, M. E. *Progress in Nuclear Magnetic Resonance Spectroscopy* **2003**, *42*, 31–52.
- [102] Saalwächter, K. *Progress in Nuclear Magnetic Resonance Spectroscopy* **2007**, *51*, 1–35.
- [103] Spiess, H. W. *Macromolecules* **2010**, *43*, 5479–5491.
- [104] Kremer, K.; Grest, G. S.; Carmesin, I. *Physical Review Letters* **1988**, *61*, 566–569.
- [105] Komlosh, M. E.; Callaghan, P. T. *Journal of Chemical Physics* **1998**, *109*, 10053–10067.
- [106] Pahl, S.; Fleischer, G.; Fujara, F.; Geil, B. *Macromolecules* **1997**, *30*, 1414–1418.
- [107] Kremer, K. *Macromolecules* **1983**, *16*, 1632–1638.
- [108] Zamponi, M.; Monkenbusch, M.; Willner, L.; Wischnewski, A.; Farago, B.; Richter, D. *Europhysics Letters* **2005**, *72*, 1039–1044.
- [109] Kreer, T.; Baschnagel, J.; Müller, M.; Binder, K. *Macromolecules* **2001**, *34*, 1105–1117.

- [110] Paul, W.; Smith, G. D. *Reports on Progress in Physics* **2004**, *67*, 1117–1185.
- [111] Qiu, X.; Moe, N. E.; Ediger, M. D.; Fetters, L. J. *Journal of Chemical Physics* **2000**, *113*, 2918–2926.
- [112] Qiu, X.; Ediger, M. D. *Macromolecules* **2002**, *35*, 1692–1698.
- [113] Ries, M. E.; Brereton, M. G.; Cruickshank, J. M.; Klein, P. G.; Ward, I. M. *Macromolecules* **1995**, *28*, 3282–3289.
- [114] Klein, P. G.; Adams, C. H.; Brereton, M. G.; Ries, M. E.; Nicholson, T. M.; Hutchings, L. R.; Richards, R. W. *Macromolecules* **1998**, *31*, 8871–8877.
- [115] Chernov, V. M.; Krasnopol'skii, G. S. *Journal of Experimental and Theoretical Physics* **2008**, *107*, 302–312.
- [116] Graf, R.; Heuer, A.; Spiess, H. W. *Physical Review Letters* **1998**, *80*, 5738–5741.
- [117] Vaca Chávez, F.; Saalwächter, K. *Physical Review Letters* **2010**, *104*, 198305.
- [118] Kimmich, R.; Noack, F. *Journal of Physics E: Scientific Instruments* **1987**, *20*, 43–46.
- [119] Weitekamp, D. P.; Bielecki, A.; Zax, D.; Zilm, K.; Pines, A. *Physical Review Letters* **1983**, *53*, 1807–1810.
- [120] Kerwood, D. J.; Bolton, P. H. *Journal of Magnetic Resonance* **1969**, *75*, 142–146.
- [121] Wu, D.; Johnson, C. S. *Journal of Magnetic Resonance* **1995**, *116*, 270–272.
- [122] Wagner, S.; Dinesen, T.; Rayner, T.; Bryant, R. *Journal of Magnetic Resonance* **1999**, *140*, 172–178.
- [123] Redfield, A. G. *Magnetic Resonance in Chemistry* **1999**, *41*, 753–768.
- [124] Grosse, S.; Gubaydullin, F.; Scheelken, H.; Vieth, H.-M.; Yurkovskaya, A. V. *Applied Magnetic Resonance* **1999**, *17*, 211–225.
- [125] Kimmich, R.; Schnur, G.; Köpf, M. *Progress in Nuclear Magnetic Resonance Spectroscopy* **1988**, *20*, 385–421.
- [126] Redfield, A. G.; Fite, W.; Bleich, H. E. *Review of Scientific Instruments* **1968**, *39*, 710–715.
- [127] Kimmich, R.; Noack, F. *Zeitschrift für Angewandte Physik* **1970**, *49*, 248.

- [128] Blanz, M.; Rayner, T. J.; Smith, J. A. S. *Measurement Science and Technology* **1993**, *4*, 48–59.
- [129] Terekhov, M.; Dvinskikh, S. *Instruments and Experimental Techniques* **1996**, *39*, 452–457.
- [130] Seitter, R.-O.; Kimmich, R. In *Encyclopedia of Spectroscopy and Spectrometry*; Lindona, J., Tranter, G., Holmes, J., Eds.; Academic Press: London, 1999; pp 2000–2008.
- [131] Anoardo, E.; Galli, G.; Ferrante, G. *Solid State Nuclear Magnetic Resonance* **2001**, *20*, 365–404.
- [132] Lips, O.; Privalov, A. F.; Dvinskikh, S. V.; Fujara, F. *Journal of Magnetic Resonance* **2001**, *149*, 22–28.
- [133] Kresse, B.; Privalov, A. F.; Fujara, F. *Solid State Nuclear Magnetic Resonance* **2012**, *40*, 134–137.
- [134] Wohlfahrt, M. Field-Cycling (FC) NMR: Untersuchung von Polymer-schmelzen, Konstruktion eines FC-NMR Probenkopfs. Diplomarbeit, Universität Bayreuth, 2012.
- [135] Spinmaster FFC - 2000 Fast Field Cycling NMR Relaxometer Reference Manual. Stelar s.r.l.: via E.Fermi, 4. 27035 Mede (PV). Italy, 2001.
- [136] Sousa, D. M.; Marques, G. D.; Cascais, J. M.; Sebastiao, P. J. *Solid State Nuclear Magnetic Resonance* **2010**, *38*, 36–43.
- [137] Spinscope, <http://www.spinscope.com>, 2012.
- [138] Bloembergen, N.; Purcell, E. M.; Pound, R. V. *Phys. Rev.* **1948**, *73*, 679–712.
- [139] Slichter, C. P. *Principles of Magnetic Resonance*; Springer: New York, 1990.
- [140] Fukushima, E.; Roeder, S. *Experimental Pulse NMR: A Nuts and Bolts Approach*; Addison-Wesley: Reading, 1993.
- [141] Redfield, A. G. In *Encyclopedia of Nuclear Magnetic Resonance*; Grant, D. M. ., Harris, R. K., Eds.; Wiley: Chichester, 1996; p 4085.
- [142] Kehr, M.; Fatkullin, N.; Kimmich, R. *Journal of Chemical Physics* **2007**, *126*, 094903.
- [143] Kehr, M.; Fatkullin, N.; Kimmich, R. *Journal of Chemical Physics* **2007**, *127*, 084911.
- [144] Cohen-Addad, J. P.; Messa, J. P. *Journal de Physique* **1976**, *37*, L193–L196.

- [145] Lartigue, C.; Guillermo, A.; Cohen-Addad, J. P. *Journal of Polymer Science Part B: Polymer Physics* **1997**, *35*, 1095–1105.
- [146] Ding, Y.; Sokolov, A. P. *Macromolecules* **2006**, *39*, 3322–3326.
- [147] Brodin, A.; Gainaru, C.; Porokhonsky, V.; Rössler, E. A. *Journal of Physics: Condensed Matter* **2007**, *19*, 205104.
- [148] Gainaru, C.; Kahlau, R.; Rössler, E. A.; Böhmer, R. *Journal of Chemical Physics* **2009**, *131*, 184510.
- [149] Ngai, K. L.; Paluch, M. *Journal of Chemical Physics* **2004**, *120*, 857.
- [150] Johari, G. P.; Goldstein, M. *Journal of Chemical Physics* **1970**, *53*, 2372–2388.
- [151] Kariyo, S.; Gainaru, C.; Schick, H.; Brodin, A.; Novikov, V. N.; Rössler, E. A. *Physical Review Letters* **2006**, *97*, 207803.
- [152] Fatkullin, N.; Kimmich, R. *Journal of Chemical Physics* **1994**, *101*, 822–832.
- [153] Kimmich, R.; Gille, K.; Fatkullin, N.; Seitter, R.; Hafner, S.; Müller, M. *Journal of Chemical Physics* **1997**, *107*, 5973–5978.
- [154] Kimmich, R.; Fatkullin, N.; Seitter, R.-O.; Gille, K. *Journal of Chemical Physics* **1998**, *108*, 2173–2177.
- [155] Hofmann, M.; Herrmann, A.; Abou Elfadl, A.; Kruk, D.; Wohlfahrt, M.; Rössler, E. A. *Macromolecules* **2012**, *45*, 2390–2401.
- [156] Cowie, J. M. G. *European Polymer Journal* **1975**, *11*, 297–300.
- [157] Hintermeyer, J.; Herrmann, A.; Kahlau, R.; Goiceanu, C.; Rössler, E. A. *Macromolecules* **2008**, *41*, 9335–9341.
- [158] Abou Elfadl, A.; Herrmann, A.; Hintermeyer, J.; Petzold, N.; Novikov, V. N.; Rössler, E. A. *Macromolecules* **2009**, *42*, 6816–6817.
- [159] Rubinstein, M.; Colby, R. H. *Polymer Physics*; Oxford University Press: Oxford, 2003.
- [160] Colby, R. H.; Fetters, L. J.; Graessley, W. W. *Macromolecules* **1987**, *20*, 2226–2237.
- [161] Kariyo, S.; Herrmann, A.; Gainaru, C.; Schick, H.; Brodin, A.; Novikov, V. N.; Rössler, E. A. *Physical Review Letters* **2008**, *100*, 109901.
- [162] Berry, G. C.; Fox, T. *Advances in Polymer Science* **1968**, *5*, 261–357.

- [163] Liu, C.; He, J.; Keunings, R.; Bailly, C. *Macromolecules* **2006**, *39*, 3093–3097.
- [164] Cohen-Addad, C. P. *Journal of Chemical Physics* **1975**, *63*, 4880–4885.
- [165] Dollase, T.; Graf, R.; Heuer, A.; Spiess, H. W. *Macromolecules* **2001**, *34*, 298–309.
- [166] Callaghan, P. T.; Samulski, E. T. *Macromolecules* **2000**, *33*, 3795–3802.
- [167] Demus, D., Goodby, J., Gray, G. W., Spiess, H. W., Vill, V., Eds. *Handbook of Liquid Crystals*; Wiley VCH: New York, 1998.
- [168] Levitz, P.; Korb, J.; Petit, D. *European Physical Journal E* **2003**, *12*, 29–33.
- [169] Graessley, W. W. *Polymeric Liquids & Networks: Dynamics and Rheology*; Taylor & Francis Group: New York, 2008.
- [170] Herrmann, A. NMR-Relaxometrische Untersuchungen von Schmelzen linearer Polymere. Diplomarbeit, Universität Bayreuth, 2007.
- [171] Vaca Chávez, F.; Saalwächter, K. *Macromolecules* **2011**, *44*, 1549–1559.
- [172] Meier, R. Untersuchung niederfrequenter Anomalien in molekularen Glasbildnern durch Fast Field Cycling ¹H-NMR. Diplomarbeit, Universität Bayreuth, 2009.
- [173] Meier, R.; Kruk, D.; Gmeiner, J.; Rössler, E. A. *Journal of Chemical Physics* **2012**, *136*, 034508.
- [174] Meier, R.; Kruk, D.; Rössler, E. A. *Physical Review E* **2012**, *85*, 020201.
- [175] Ding, Y.; Kisliuk, A.; Sokolov, A. *Macromolecules* **2004**, *37*, 161–166.
- [176] Faller, R.; Müller-Plathe, F.; Heuer, A. *Macromolecules* **2000**, *33*, 6602–6610.
- [177] Smith, G. D.; Borodin, O.; Bedrov, D.; Paul, W.; Qiu, X.; Ediger, M. D. *Macromolecules* **2001**, *34*, 5192–5199.
- [178] Bennemann, C.; Baschnagel, J.; Paul, W.; Binder, K. *Computational and Theoretical Polymer Science* **1999**, *9*, 217–226.
- [179] Padding, J. T.; Briels, W. J. *Journal of Chemical Physics* **2001**, *114*, 8685–8693.
- [180] Weber, H. W.; Kimmich, R. *Macromolecules* **1993**, *26*, 2597–2606.
- [181] Wang, Z.; Likhtman, A. E.; Larson, R. G. *Macromolecules* **2012**, *45*, 3557–3570.

- [182] Bormuth, A.; Henritzi, P.; Vogel, M. *Macromolecules* **2010**, *43*, 8985–8992.
- [183] Mattea, C.; Fatkullin, N.; Fischer, E.; Beginn, U.; Anoardo, E.; Kroutieva, M.; Kimmich, R. *Applied Magnetic Resonance* **2004**, *27*, 371–381.
- [184] Kimmich, R.; Seitter, R.-O.; Beginn, U.; Möller, M.; Fatkullin, N. *Chemical Physics Letters* **1999**, *307*, 147–152.
- [185] Kariyo, S.; Stapf, S.; Blümich, B. *Macromolecular Chemistry and Physics* **2005**, *206*, 1292–1299.
- [186] Gainaru, C.; Lips, O.; Troshagina, A.; Kahlau, R.; Brodin, A.; Fujara, F.; Rössler, E. A. *Journal of Chemical Physics* **2008**, *128*, 174505.
- [187] Kruk, D.; Meier, R.; Rössler, E. A. *Journal of Physical Chemistry B* **2011**, *114*, 951–957.
- [188] Kimmich, R.; Fatkullin, N. *Macromolecules* **2010**, *43*, 9821–9827.
- [189] Kimmich, R.; Fatkullin, N. *Journal of Chemical Physics* **2011**, *134*, 057101.
- [190] Krutyeva, M.; Martin, J.; Arbe, A.; Colmenero, J.; Mijangos, C.; Schneider, G.; Unruh, T.; Su, Y.; Richter, D. *Journal of Chemical Physics* **2009**, *131*, 174901.
- [191] Martín, J.; Krutyeva, M.; Monkenbusch, M.; Arbe, A.; Allgaier, J.; Radulescu, A.; Falus, P.; Maiz, J.; Mijangos, C.; Colmenero, J.; Richter, D. *Physical Review Letters* **2010**, *104*, 197801.
- [192] Ok, S.; Steinhart, M.; Şerbescu, A.; Franz, C.; Vaca Chávez, F.; Saalwächter, K. *Macromolecules* **2010**, *43*, 4429–4434.
- [193] Luda, M. P.; Guaita, M.; Chiantore, O. *Makromol. Chem.* **1992**, *193*, 113–121.
- [194] Anoardo, E.; Ferrante, G. M. *Applied Magnetic Resonance* **2003**, *24*, 85–96.
- [195] Carty, D. Extending the NMR FFC2000 Spinmaster Field Range down to Low Field. Stelar s.r.l.: via E.Fermi, 4. 27035 Mede (PV). Italy, 2005.
- [196] Kresse, B. Weiterentwicklung der Field-Cycling-Relaxometrie zu kleinen Larmorfrequenzen. Master-Thesis, Technische Universität Darmstadt, 2010.
- [197] Vaca Chávez, F.; Saalwächter, K. *Macromolecules* **2011**, *44*, 1560–1569.
- [198] Burghoff, M.; Hartwig, S.; Trahms, L.; Bernarding, J. *Applied Physics Letters* **2005**, *87*, 054103.

- [199] Kariyo, S.; Stapf, S. *Macromolecules* **2002**, *35*, 9253–9255.
- [200] Stephanou, P. S.; Baig, C.; Mavrantzas, V. G. *Soft Matter* **2011**, *7*, 380–395.
- [201] Kimmich, R.; Fischer, E.; Callaghan, P.; Fatkullin, N. *Journal of Magnetic Resonance Series A* **1995**, *117*, 53–61.

Acknowledgements

First I would like to thank my supervisor Ernst Rössler for his constructive suggestions, kindness, and inspirations. By providing the freedom to organize one's work for oneself and through his open-door policy, he created a very pleasant atmosphere.

I am indebted to Franz Fujara for the opportunity to work in his lab in Darmstadt, and for his valuable advises and enthusiasm throughout the project. The most significant interpretations were suggested by the low-frequency Darmstadt relaxation data.

I am also very grateful to Alexei Privalov and Benjamin Kresse for introducing me to the Darmstadt FC I relaxometer and the Damaris software, and the repetitive adjustment of the compensation system. Their outstanding technical knowledge made the "50 Her(t)z project" become a reality.

Many thanks to Irene Bauer and Herrn Jürgen Gmeiner for their help with preparing the – in most cases highly viscous – samples.